USAID FROM THE AMERICAN PEOPLE | LEBANON

LEBANON LITANI RIVER BASIN MANAGEMENT SUPPORT PROGRAM

SEISMIC DEFORMATION ANALYSIS OF QARAOUN DAM

2012 February
This report was prepared by AMEC under subcontract with International Resources Group (IRG) for the Lebanon LRBMS Program.

LEBANON LITANI RIVER BASIN MANAGEMENT SUPPORT PROGRAM

SEISMIC DEFORMATION ANALYSIS OF QARAOUN DAM

Contract No.: EPP-I-00-04-00024-00

2012 February

DISCLAIMER
The author's views expressed in this publication do not necessarily reflect the views of the United States Agency for International Development or the United States Government

FOREWORD

This Seismic Deformation Analysis was prepared by AMEC under subcontract with IRG, the main contractor for the Litani River Basin Management Support (LRBMS) Program, a USAID-funded program in Lebanon (Contract EPP-I-00-04-00024-00 Task Order No. 7 under the Integrated Water and Coastal Resources Management Indefinite Quantity Contract (IQC) II).

TABLE OF CONTENTS

1. INTRODUCTION 1-1
1.1. Purpose 1-1
1.2. Report Organization 1-1
1.3. Project Team and Acknowledgements 1-2

2. PROJECT AND FACILITY DESCRIPTION 2-1

3. PROBABILISTIC SEISMIC HAZARD ANALYSIS 3-1
3.1. Techtonic Setting and Seismicity 3-1
3.1.1. Tectonic Setting 3-1
3.1.2. Seismicity 3-2
3.2. Source Characterization 3-3
3.2.1. Source Characterization 3-3
3.3. Earthquake Ground Motions 3-7
3.3.1. Earthquake Catalog 3-7
3.3.2. Maximum Earthquake Magnitudes 3-8
3.3.3. Earthquake Recurrence 3-8
3.3.4. Attenuation Relationships 3-9
3.4. Ground Motion Hazard Analysis 3-10
3.4.1. Calculations of Frequency of Exceedance 3-10
3.4.2. Probabilities of Exceedance 3-11
3.4.3. Uniform Hazard Response Spectra 3-12
3.4.4. Near Fault Directivity Effects 3-13
3.4.5. Comparison of Results with Other Studies 3-13
3.5. Development of Acceleration Time Histories 3-14
3.5.1. Selection of Seed Time Histories 3-14
3.5.2. Development of Spectrum-Compatible time histories 3-14
3.6. Recommended Earthquake Scenarios for Deformation Analyses 3-15

4. NONLINEAR DEFORMATION ANALYSIS 4-1
4.1. Approach and Methodology 4-1
4.2. Static Stresses and Static Properties 4-2
4.3. Nonlinear Soil Model and Parameters 4-4
4.4. Structural and Interface Elements 4-6
4.5. Analysis Results using Postulated Ground motions 4-6
4.5.1. 100-year event (Dayhook record) 4-7
4.5.2. 2,475-year event (Tabas record) 4-7
4.5.3. Results using additional Developed Acceleration Time Histories 4-8
4.6. Sensitivity Analysis Using Mohr-Coulomb Model 4-8
4.7. Performance of Embankments during Past Earthquakes 4-9
4.8. Overall Estimate Of Deformation Potential 4-10

5. SUMMARY AND CONCLUSIONS 5-1

6. BASIS FOR ANALYSES AND CONCLUSIONS 6-1

7. REFERENCES 7-1

ACRONYMS

AMEC	AMEC Environment & Infrastructure, Inc.
CENA	Central and Eastern North America
CFRD	Concrete-faced rockfill dam
Global CMT	Global Centroid Moment Tensor
IRG	International Resources Group
LRBMSP	Litani River Basin Management Support Program
MPa	Megapascals
NEHRP	National Earthquake Hazards Reduction Program
NGA	Next Generation Attenuation
Pa	Pascals
PEER	Pacific Earthquake Engineering Research Center
PGA	Peak Ground Acceleration
PSHA	Probabilistic Seismic Hazard Analysis
psi	Pounds per square inch
S_a	Spectral Acceleration
UHRS	Uniform Hazard Response Spectrum
USNGDC	United States National Geophysical Data Center

EXECUTIVE SUMMARY

Qaraoun Dam is a 60 m high concrete-faced rockfill embankment built in 1960 and located at the southern end of the Bekaa valley in central Lebanon. Lebanon, which is situated near the tectonic boundary of the African and Arabian plates, is within a seismically-active region of the Dead Sea fault system that includes many complex fault structures with a history of producing high levels of earthquake shaking in the region. Large earthquake events that tend to occur in Lebanon, typically every few hundred years, have the potential to cause significant and possibly catastrophic damage to man-made structures not designed for such high levels of ground shaking. Therefore, it is important to evaluate the response of such structures, particularly ones whose integrity is critical to the prevention of loss of life and property, to these frequent (and less frequent, more damaging) earthquakes.

The scope of this study includes:

1. estimating the level of shaking at the Qaraoun Dam site from potential seismic sources in the vicinity, and developing representative earthquake ground motions, and
2. performing analyses to estimate the seismic response and deformation of the dam embankment resulting from the postulated earthquake shaking.

Probabilistic Seismic Hazard Analysis

The process by which the ground shaking levels were estimated at the dam site is known as a probabilistic seismic hazard analysis (PSHA). The results of the PSHA are presented in terms of peak ground acceleration and response spectral values for various specified annual frequencies of exceedance, or return periods. The return period, in years, is defined as the inverse of the annual frequency of exceedance.

A PSHA begins with a detailed study of the tectonic setting and historical seismicity of the region where all known earthquakes have occurred. Sources of those earthquakes are identified as either: a) active crustal faults (i.e., well-defined fault structures that have generated earthquakes within the past 35,000 years and that are manifested at the ground by surface rupture); or b) areal seismic source zones (i.e., regions where earthquakes have been observed to originate that are not attributed to a specific mapped fault). Each of the fault sources was characterized by its proximity to the site, type of faulting, maximum length of faulting, maximum thickness of rupture, dip, annual slip rate, and maximum potential for energy release (M_{MAX}). Each of the areal seismic zones is characterized by its proximity to the site, type of faulting, maximum thickness of rupture, dip, and M_{MAX}. Once all sources are identified and characterized, subjective weighting factors are applied to each characteristic value to represent the probability of occurrence for that particular value. A probabilistic model is then developed to represent a finite number of individual earthquake scenarios in the vicinity of the analyzed site. For Qaraoun Dam, six active crustal faults, and eight areal seismic source zones were identified as potential seismic sources.

All 14 seismic sources were considered to contribute to the seismic hazard at the dam with varying levels of activity and maximum energy release. The **Yammouneh fault**, located approximately 2.4 km west of Qaraoun Dam, was calculated to contribute the most to the seismic hazard due to its close proximity to the dam and its relatively high annual slip rate. However, for the development of the overall seismic hazard, each source was evaluated for its potential to release an amount of energy that would lead to a specific level of shaking (measured as acceleration) at the dam site. The overall annual probability of the dam to experience (or exceed) a particular level of acceleration is the sum of the annual probabilities from all seismic sources to that level of acceleration.

Development of Earthquake Ground Motions

The scope of work for this study required the development of ground shaking levels for 100-year, and 10,000-year return period "scenario earthquakes." A ground shaking level for the 100-year return period has a one percent chance of being exceeded in one year, or about a 40 percent chance of being exceeded in 50 years. The 10,000-year return period ground motion has approximately 0.5 percent chance of being exceeded in 50 years. Ground motions were also developed for a two percent chance of being exceeded in 50 years to be consistent with estimates of ground motions from a maximum magnitude earthquake on the nearby active Yammouneh fault. The two percent chance of being exceeded in 50 years corresponds to a 2,475-year return period.

The results of this study indicate that the **peak ground acceleration at the dam site for the 100-year return period is about 0.15g** (where g is the acceleration due to gravity). This level of computed acceleration may be considered similar to what might have been experienced in the vicinity of the epicentral region of the magnitude 5.8 earthquake that occurred in the area in 1956. The estimated **peak ground acceleration for the 2,475-year return period is about 0.78g**. The dominant source for this level of shaking is a magnitude 7.0 to 7.5 earthquake on the Yammouneh fault about 2.4 km from the dam site. This level of ground shaking is considered similar to what might have been experienced in the epicentral region of the magnitude 7.4 earthquake that occurred in the Bekaa Valley in 1759. The estimated **peak ground acceleration for the 10,000-year return period is about 1.2g**.

Uniform hazard response spectra, UHRS, (spectral accelerations at various structural periods of vibration) were developed from the PSHA to represent the frequency content and level of shaking for the 100-year, 475-year, 975-year, 2475-year, and 10,000-year return period earthquake scenarios. The UHRS were then used to develop scenario acceleration time histories for the 100-year and 10,000-year events using the following approach:

1. select a recorded (seed) acceleration time history from the historical record that closely represents the distance to rupture, magnitude of the scenario earthquake, and the foundation conditions at the site,
2. scale the entire seed time history to match the peak ground acceleration (PGA) of the UHRS of interest, and
3. modify the frequency content of the scaled time history so that it loosely matches the target UHRS.

Two sets of horizontal and vertical acceleration time histories were developed for each of the two scenario earthquakes.

Following the development of the 100-year and 10,000-year return period earthquake scenarios and associated acceleration time histories, project team members from AMEC and IRG discussed the basis for the selection of ground motions that would be most appropriate for analyzing the seismic response and deformation of Qaraoun dam. The California Department of Water Resources, Division of Safety of Dams (DSOD) recommends that an 84th-percentile (median plus one standard deviation) deterministic ground motion be used for evaluating the seismic stability of dams that have "high consequences of failure". Following the DSOD guidelines, the team agreed that ground motions for the 2,475-year return period scenario earthquake, which are similar to the 84th percentile ground motions from the Yammouneh fault, would be appropriate for the deformation analysis of the dam, in lieu of the 10,000-year return period motions.

Deformation Analyses

The dynamic response and seismic deformation analysis of Qaraoun Dam was performed with the computer program FLAC2D. This approach involves two-dimensional, finite-difference analyses to evaluate the non-

linear dynamic response and permanent deformation of the maximum cross section of the embankment during the postulated seismic shaking at the dam site. Two different soil models for the rockfill were used to estimate the permanent deformation of the dam: a fully nonlinear "bounding surface hypo-plasticity" model, and a more traditional (and conservative) Mohr-Coulomb bi-linear constitutive model.

The dam was modeled as an unsaturated dumped rockfill embankment with an upstream concrete panel facing and concrete drainage gallery at the upstream toe. Properties of the rockfill material were selected based on a review of published literature on similar materials. Both horizontal (in the upstream/downstream direction) and vertical components of input earthquake motions were applied at the bedrock foundation underlying the dam. Analyses were performed using earthquake motions for the 100-year and 2,475-year scenario earthquakes. Preliminary analyses were performed to simulate the reservoir's hydrodynamic loads. The results of these analyses indicate that the effects of hydrodynamic loads acting on this sloping-face rockfill dam are not significant. This finding is consistent with results of similar studies described in the literature. Accordingly, analyses were performed without including the reservoir effects.

The results of the deformation analyses indicate that shaking from the 100-year earthquake scenario, having a peak horizontal bedrock acceleration of 0.15g, will cause an insignificant amount (i.e., less than 0.03 m) of permanent deformation at the crest and upstream and downstream toes of the dam. It is our judgment that these estimated deformations will not have a significant impact on the seismic performance of the dam.

Using the bounding surface hypo-plasticity model, shaking from the 2,475-year event, with peak bedrock acceleration of 0.8g, is expected to cause about 0.44 m of vertical and 0.45 m of horizontal permanent deformation at the crest of the dam, and **about 0.03 m of horizontal permanent displacement** at the upstream toe of the dam near the connection of the concrete facing to the drainage gallery. The estimated **maximum differential displacements** at the interface between the concrete face slab and the inspection galley is **less than 0.05 m**. Using the more conservative Mohr Coulomb constitutive model, the computed crest settlement was about 2.5 m, and the permanent horizontal deformation was about 2.9 m. Because of uncertainties in the analytical procedures, and based on the observed performance of similarly constructed dams shaken with large magnitude earthquakes, **it is the authors' judgment that the amount of deformation anticipated at the crest of the dam for this level of shaking will be in the range of about 1 m to 1.5 m**.

Since the crest of the dam is at Elev. 861.0 m, the top of the concrete parapet wall is at Elev. 863.0 m, and the normal maximum water level is at Elev. 858.0 m, the available freeboard to the top of the parapet wall is 5.0 m. The range of estimated earthquake-induced deformation and settlement of the embankment during the 2,475-year ground shaking (i.e., 1 to 1.5 m) is less than the available freeboard, and **overtopping of the dam is not expected**. The estimated deformations likely will cause:

- damage to the concrete parapet wall at the dam crest,
- sloughing of the rockfill on the dam's downstream face, and
- possible cracking of the concrete facing leading to increased leakage through the rockfill.

However, such effects are considered unlikely to impact the overall stability of the dam, or cause an uncontrolled release of reservoir water.

Comparisons with Case Histories

The predicted deformations of Qaraoun Dam for the 2,475-year scenario earthquake were compared to the documented performance of similar concrete-faced rockfill dams. Ishibuchi Dam in Japan, and Zipingpu Dam in China, were shaken by earthquakes of magnitudes of 6.9 and 7.9, respectively, with peak bedrock accelerations of 0.5g and 0.7g. Ishibuchi Dam settled 0.6 m and experienced cracking at the dam crest;

however, the concrete face slab on the upstream slope was reportedly undamaged. At Zipingpu Dam, the crest settled about 1 m, and the earthquake-induced deformations resulted in partial dislocation of several concrete slabs at the construction joints, with maximum outward bulging of 0.15 m. Portions of the parapet wall at the crest also collapsed, and open cracks (up to 3 cm wide) were observed between the downstream side of the crest road and the rock slope protection. Despite this damage, the dam remained stable and maintained its reservoir impounding capacity. The observed settlements at these two dams are of the same order of magnitude as those estimated for Qaraoun Dam, and help support the conclusion that the dam should perform adequately during the postulated 2,475-year scenario earthquake considered in this study.

Recommendations for Inspections Following a Seismic Event

While the analyses and evaluations described above indicate the dam should perform adequately, it is recommended that a detailed inspection of the dam be performed immediately following all earthquakes occurring within 50 km of the dam site and having a magnitude of 5.0 or greater. The inspection should include:

- draw down of the reservoir level,
- a survey of the settlement monuments on the crest and concrete facing,
- a careful review of the parapet wall and the concrete facing, including horizontal and vertical construction joints and water stops,
- confirming the integrity of the inspection gallery,
- monitoring the piezometers for evidence of an increasing phreatic surface within the dam, and
- frequent monitoring of the leakage weirs for increased flow and evidence of silt deposits.

Any damage to the dam resulting from earthquake shaking must be repaired prior to raising the reservoir to its normal operating level.

ملخص تنفيذي

بني سد القرعون في العام ١٩٦٠، وهو سد ركامي ذات واجهة خرسانية محاكية للمياه، يبلغ ارتفاع هذا السد ٦٠ مترًا بطول ١٠٩٠ متر ويقع في جنوب سهل البقاع في وسط لبنان الذي يقع بالقرب من الصفيحتين التكتونية الافريقية والعربية وبالتالي من نظام زلزالي (فوالق) نشط ومعقد تبداء من البحر الميت وتمر بلبنان إلى جنوب غرب آسيا، من اهم هذه الفيالق فالق اليمونة الحافل عبر التاريخ بنشاطٍ شكل هزات ارضية مرتفعة المستوى هزت واثرت في المنطقة بأكملها. إن هذه الهزات وبحسب الاحصاء تحصل ضمن فترات لا تتجاوز مئات السنين وهي ذات قدرة هائلة حيث من المحتمل ان تحدث كوارث وتدمير في البنى التحتية التي لم يلحظ الانسان اثناء بنائها تحمل مثل هذا المستوى من الهزات. لذلك، فإنه من الاهمية بمكان تقييم مقاومة هذه البنى للهزات الارضية مرتفعة المستوى وعلى وجه الخصوص تلك التي قد تحدث خسائر في الارواح والممتلكات. إن هذا الامر مهم جدًا بالرغم من الفترات المتباعدة لتردد حدوث مثل هذه الهزات (مئات السنين).

ولهذه الغاية سوف تشمل دراستنا هذه التالي:

١ - تقدير مستوى الهزات الزلزالية المحتملة في موقع سد القرعون وجواره وتطوير هزات ارضية افتراضية عالية المستوى ومماثلة لتلك التي حصلت بحسب الاحصاءات،

٢ - إجراء تحاليل لتقدير السلوك الزلزالي والتشوه المحتمل في جسم السد والناجم عن هذه الهزات المحتملة.

تحليل المخاطر الزلزالية المحتملة

إن عملية الهزات الارضية الافتراضية بمختلف المستويات تسمى "تحليل المخاطر الزلزالية المحتملة" او PSHA، وتهدف هذه العملية لتشكيل هزة ارضية افتراضية (موديل) على الحاسوب على جسم معين كالسد ومن ثم ملاحظة النتائج والوقوف عندها لمعرفة ما يمكن فعله على البنى الواقعية من تحسين في البناء وانشاء خطط للطوارىء في الحالات التي تفوق قدرة هذه البنى على التحمل، وهي تعتمد فيما تعتمد عليه من معطيات هامة واساسية للحصول على نتائج واقعية مثل المدى التسارعي الاقصى للهزات حيث يتم تسجيل الاستجابة لقّيم الطيف المرسل وتحديد مختلف التجاوزات للترددات السنوية للهزات او فترات العودة. إن فترات العودة، بالسنوات تعني عكس الترددات السنوية للتجاوزات. (إن هذه العبارات هي للمختصين اما ما يهم القارىء العادي بالاجمال فهو المعطيات الاحصائية عن الهزات التي حدثت على مدى السنين السابقة والتي تؤخذ بعين الاعتبار لمقارنة مستويات الهزات الاحتمالية المفترضة ومن مقارنة ذلك مع قدرة البنى التحتية على تحملها والمقصود طبعًا بهذه الدراسة سد القرعون).

إن تحليل المخاطر الزلزالية المحتملة (PSHA) بدأ بدراسة تفصيلية لضبط الصفائح التكتونية والتاريخ الزلزالي للمنطقة، حيث اعتمدت جميع الهزات الارضية المعروفة، اما مصادر تلك الهزات فتم تحديده على الشكل التالي:

أ) الفوالق النشطة والواضحة المعالم على القشرة السطحية للارض (اي بنية الفالق المحددة بوضوح والتي شكلت هزات ارضية خلال ٣٥٠٠٠ سنة سابقًا والتي تتجلى في الارض من تمزق السطح)، او

ب) المصدر المساحي للمناطق الزلزالية (أي المناطق التي لوحظ فيها تشويه الهزات الارضية والتي لا تلحظها خرائط الفوالق.

بعد ذلك، تم تحديد كل فالق بحسب موقعه، نوعه، طوله، سماكة التصدع القصوى، العمق، معدل الحركة السنوي والحد الاقصى لامكانية إطلاق الطاقة المعروفة بـــ (MMAX) وبنفس السياق تم تحديد كل منطقة زلزالية بحسب موقعها، نوع الفالق الموجود، طوله، سماكة التصدع القصوى، العمق، معدل الحركة السنوي والحد الاقصى لامكانية إطلاق الطاقة المعروفة بـــ (MMAX) وبمجرد تحديد خصائص جميع المصادر وعناوينها سيتم تطبيق العوامل الترجيحية لكل القيّم اعلاه بحسب خصائصها وميزاتها لتمثل احتمال حدوث اي تغيير بالقوة والنتيجة والتمايز فيما بينها بعد ان تدرس كل منها على حدى، وهذا الامر يمكن من تطوير نموذج موديل لسيناريوهات مختلفة لعدد من الهزات الارضية المحتملة وتحليلها بحسب موقعها وكما ذكرنا قوتها، كل ذلك اتى بسياق معين شمل تحديد ٦ فوالق واضحة المعالم على القشرة الارضية و٨ مناطق كمصادر زلزالية نشطة وملاصقة لسد القرعون، حيث تم اعتبار جميع المصادر الـــ١٤ المذكورة مصادرًا تشكل خطرًا على السد مع اختلاف بنسبة النشاط الزلزالي والطاقة القصوى الذي يمكن ان يطلقها كل مصدر.

إن **فالق اليمونة** الواقع على بعد ٢،٤ كلم إلى الغرب من سد القرعون يعتبر الاكثر خطورة زلزاليًا لقربه من السد ولاحتمال ارتفاع نسبة تحركه السنوي. بالرغم من ذلك، ومن اجل تطوير فهم الخطر الزلزالي بشكل عام، كان لا بد من تقييم كل المصادر (وليس فقط اليمونة القريب) لجهة القدرة المحتملة على اطلاق الطاقة والذي سيؤثر حكمًا على مستوى الهزات الارضية (تقاس بالتسارع) المؤثرة على موقع السد. لقد تم جمع كل المخاطر المحتملة من كافة المصادر الـــ ١٤ وتقييم تسارعها كاحتمالات سنوية وجعلها جمعاء بنفس مستوى التسارع الفرضي للموديل الذي سيتم تحليله.

تطوير مفهوم حركات الهزات الارضية

إن نطاق العمل لهذه الدراسة يتطلب تقدير مستوى الهزات الارضية لـــ ١٠٠ عام و١٠٠٠٠ عام (أي فترات العودة) " سيناريوهات الهزات الارضية ". ١٪ هو احتمال حصول هزات ارضية مشابهة لـــ ١٠٠ عام ماضية بالاعتماد على فترات العودة وذلك في سنة واحدة، و٤٠٪ للتجاوز خلال ٥٠ عامًا. ٠,٥٪ هي نسبة احتمال حدوث هزات ارضية مثل تلك التي حصلت منذ ١٠٠٠٠ عامًا من فترات العودة وذلك خلال ٥٠ عامًا بالعودة إلى ٢٤٧٥ عامًا من فترات العودة.

إن نتائج هذه الدراسة تفضي إلى ان المدى الاقصى للتسارع في موقع سد القرعون اذا ما احتسبنا ١٠٠ عام كفترات عودة تقدر بـــ ٠,١٥g (g– هي التسارع بالنسبة إلى الجاذبية) وهذا المستوى يمكن اعتباره مشابهًا إلى حد بعيد مع ذلك الذي حصل في المنطقة الملاصقة في العام ١٩٥٦ والتي بلغت قوته ٥,٨ درجات والمعروف بزلزال العام ١٩٥٦.

إن التسارع الارضي الاقصى لـــ ٢٤٧٥ سنة فترات عودة يقدر بـــ ٠,٧٨g . والمصدر الرئيسي لمثل هذا المستوى من الهزات الارضية والذي يبلغ ٧ إلى ٧,٥ درجات هو فالق اليمونة الواقع على بعد ٢,٤ كلم من سد القرعون. إن هذا المستوى من الهزات الارضية يعتبر مشابهًا لتلك الهزة التي يمكن ان تكون قد حدثت في المنطقة الملاصقة للسد في وادي البقاع في العام ١٧٥٩ والتي بلغت قوتها ٧,٤ درجات. **إن تقدير التسارع الارضي الاقصى لـــ ١٠٠٠٠ عام فترات عودة قد بلغ ١,٢g .**

قام الفريق بتطوير قراءة الاستجابة للاطياف بشكل موحد للمخاطر والمعروفة بـــ UHRS (التسارع الطيفي للاهتزازات البنيوية المختلفة) وذلك التطوير اعتمد على الـــ PSHA من اجل الوقوف على الاستجابة لمحتوى الترددات ومستوى الهزات لـــ ١٠٠عام، ٤٧٥ عام، ٩٧٥ عام، ٢٤٧٥ عام و ١٠٠٠٠عام من فترات عودة ولنتمكن بذلك من تصور سيناريوهات الهزات التي قد تحدث، استخدم الـــ UHRS لتطوير سيناريوهات التسارع وتواريخ احتمال حدوثها لـــ ١٠٠عام و١٠٠٠٠عام.

قد تم الاعتماد على مجموعتين من التسارع الذي حصل سابقاً افقي وعامودي من اجل تصور نوعين من الهزات الارضية.

متابعةً لهذا الامر واعتمادًا لـــ ١٠٠عام و ١٠٠٠٠عام من فترات العودة وما يرتبط بها من سيناريوهات تاريخ تسارع الوقت، قام اعضاء الفريق المشترك من AMEC وIRG بمناقشة قواعد تحديد حركات الارض والتي قد يكون لها الاهمية الكبرى في تحليل مدى تأثير الزلازل والتشوهات التي يمكن ان تحدثها في سد القرعون. ينصح قسم الموارد المائية في كاليفورنيا– وحدة آمان السدود الـــ (DSOD) باستخدام

٨٤٪ (انحراف معياري زائد واحد) لتحديد الحركات الارضية وكذلك لتقييم الاستقرار الزلزالي لسد القرعون الموجود في منطقة "خطر زلزالي عالية".

تماشيًا مع توجيهات الـــ DSOD، توافق الفريق ان الحركات الارضية لـــ ٢٤٧٥ عام من فترات العودة والتي تساوي إلى حد بعيد الـــ ٨٤٪ تحركات ارضية من فالق اليمونة، وقد تكون مناسبة اكثر لتحليل تأثير النشاط الزلزالي والتشوه الذي يمكن ان يلحقه بسد القرعون من الـــ ١٠٠٠٠عام فترات عودة للتحركات.

تحليل التشوهات

ان الاستجابة الديناميكية لتحليل تأثير الزلازل على سد القرعون قد تم تنفيذها على الحاسوب عبر برنامج FLAC2D. ينطوي هذا النهج ثنائي الابعاد على الفروقات المحدودة لتقييم التحليلات على ٣ خطوط للاستجابة الديناميكية والتشوه الدائم للمقطع الاقصى في هذا السد الركامي خلال الهزة الزلزالية المفترضة لموقع السد. لقد تم استخدام نموذجين تربة مختلفين للصخور الركامية لتقديرالتشوه المفترض في السد وهذين النموذجين هما: النموذج الاول يعتمد على الموجات المتعرجة "تغليف السطح لمنع اللدونة"، اما الاكثر تقليدًا (وتحفظًا) النموذج الثنائي للخط التأسيسي والمعروف بـــ Mohr-Coulomb bi-linear constitutive model. لقد تمت نمذجة السد كجسم ركامي غير مشبع مع واجهة خرسانية محاكية للمياه وقد تم وضع النفق الاسمنتي المخصص للمراقبة في مكان وجوده. كما وتم اختيار خصائص المواد الركامية كما نشرت في الابحاث المعدة لمثلها، مع اعتماد العاملين العامودي والافقي (في الاتجاه الاعلى للنهر والادنى منه) في مدى تأثير حركات الهزات الارضية على الصخور التي تفترش وتشكل قاعدة السد. بنيت التحاليل بواسطة اعتماد سيناريوهات تحرك الهزات الارضية لـــ ١٠٠عام و ٢٤٧٥عامًا. التحاليل الاولية شُكلت من اجل تقدير الحمل الهيدروديناميكي للخزان المائي لسد القرعون.

إن نتائج تحاليل التشوهات لـــ ١٠٠عام من سيناريوهات الهزات تشير إلى حد اقصى g٠,١٥ من التسارع الافقي المؤثر على صخور قاعدة السد، ما يمكن ان يسبب تشوهات بسيطة (لا تزيد عن ٠,٠٣ متر) في قمة السد والقاعدتين العليا والدنيا منه. **إن حكمنا على هذه النتائج هو ان اداء السد تجاه هذه القيم من الخطر الزلزالي سيكون جيدًا ولن يشكل اية آثار مدمرة.** ان استخدام النموذج الاول في التحاليل المذكور اعلاه (تحاليل الصخور الركامية) لحدوث الهزات في فترات العودة لـــ ٢٤٧٥عام **مع حد اقصى g٠,٨ تسارع على صخور الاساسات، يفترض ان يسبب تشوهات افقية تقدر بـــ ٠,٤٤ متر و٠,٤٥ من التشوهات العامودية في قمة السد، وتقريبًا ٠,٠٣ متر من التشققات في العقدة العلوية لقاعدة السد بالقرب من المسافة التي تربط الواجهة الخرسانية بنفق المراقبة، والحد الاقصى لهذه التغيرات في هذا المكان لن يتعدى الـــ ٠,٠٥ متر.** اما باستخدام النموذج الثاني اي الاكثر تحفظًا فقد قدرت التغيرات التي

يمكن ان تحصل بـــ ٢,٥متر من التسوية اوالانطباق و٢,٩ متر من التشوه الافقي. بسبب عدم اليقين من الاجراءات في هذا النموذج، وبناءً على التجارب في مراقبة السدود بنفس البنية بعد تعريضعها نظرياً لهزات ارضية قوية، وهذا حكم المؤلف للنموذج نفسه وللتقرير فإن التشوه المتوقع في قمة السد لمثل هذا المستوى من الهزات لن يزيد عن ١ إلى ١,٥ متر.

لما كانت قمة السد تقع على ارتفاع ٨٦١ متر عن سطح البحر والارتفاع الاقصى للجدار الاسمنتي الفاصل هو ٨٦٣ متر، ومستوى الارتفاع الاقصى للمياه هو ٨٥٨ متر، اي ان الفارق ما بين مستوى المياه الاقصى وارتفاع الجدار الفاصل الاقصى هو ٥ امتار. تبدو التقديرات للتشوهات والتسويات في جسم السد لاتزيد عن ١متر إلى ١,٥ متر اي اقل من الفارق ما بين اعلى مستوى للمياه والحد الاعلى للجدار الفاصل **ما يعني ان غرق السد او تدميره غير متوقع.** ان التشويهات المقدرة على الارجح سوف تسبب:

- تكسير في الجدار الفاصل الاسمنتي في قمة السد
- تساقط المواد الركامية التي تغطي الجهة الدنيا (الجنوبية) للسد، و
- احتمال تفسخات الواجهة الاسمنتية ما سوف يؤدي إلى زيادة في التسرب في جسم السد

ومع ذلك، من المرجح ان تؤثر هذه الامور على استقرار السد بشكل عام، وتؤدي الى اطلاق كميات من المياه يصعب السيطرة عليها.

مقارنة ما بين حالات مختلفة

تمت مقارنة السيناريوهات المحتملة للتشوهات باعتماد الـــ ٢٤٧٥عام والتي قمنا بدراستها في سد القرعون مع سدود ركامية ذات واجهة خرسانية، مثل سد ايشيبوشي في اليابان، سد زيبينغبو في الصين، والذين تعرضا إلى هزات بقوة ٦,٩ و ٧,٩ على التوالي وبتسارع اقصى بلغ g٠,٥ و٠,٧. استقر سد ايشيبوشي على فارق ٠,٦ متر وتعرض لبعض التفسخات في قمة السد. اما بالنسبة إلى سد زيبينغبو في الصين وبالرغم من قوة الهزة، فإن الواجهة الخرسانية المحاكية للمياه لم تتعرض للتلف، إن استقرار الفارق في قمة السد بعد التعرض للهزة بلغ متراً واحداً، اما التشوهات الناتجة عن هذه الهزة الارضية فقد ادت الى خلع جزئي لبعض الاجزاء من الواجهة الخرسانية وانتفاخات خارجية لم تبلغ اكثر من ٠,١٥ متر. كذلك كان هناك انطباق لجزء من الجدار الفاصل في قمة السد وتفسخ مفتوح (بعرض ٣ سنتم) تمت ملاحظته ما بين الجهة المعاكسة للمياه في الطريق على قمة السد والانحناء الصخري الحامي في نفس الجهة. بالرغم من هذه الآثار، فان السد حافظ على اسقراره وقدرته على تخزين المياه، وكنتيجة للمراقبة والمقارنة فان نفس التأثيرات متوقعة لسد القرعون في حال تعرض لنفس قوة الهزات في السدين المذكورين.

إن هذه المقارنة دعمت بشكل قاطع الاستنتاجات التي حصلنا عليها باعتمادنا على دراسة سيناريوهات الـــ ٢٤٧٥عام فترات عودة.

توصيات لمتابعة عمليات المراقبة بعد حدوث نشاط زلزالي

في حين ان التقييم والتحليلات المذكورة اعلاه تشير إلى ان اداء السد جيد وكاف، الا انه من المستحسن إجراء فحوصات تفصيلية للسد (مراقبة) مباشرةً بعد كل نشاط زلزالي يحدث على مسافة ٥٠ كلم من موقع السد وخصوصاً اذا ما بلغت قوة هذا النشاط او الهزات الـــ ٥ درجات، يجب ان تشمل هذه المراقبة التالي:

- انخفاض في مستوى المياه في خزان التجميع،
- دراسة استقصائية لقمة السد ولآثار استقرار التغيرات والواجهة الخرسانية،
- مراجعة دقيقة للجدار الفاصل والواجهة الامامية، والفواصل العامودية والافقية بما في ذلك عازل المياه او الـــ Water stop،
- التأكد من سلامة نفق المراقبة،
- مراقبة الآبار المحيطة بالسد وذلك من اجل الوقوف على اية ادلة لتسرب المياه اسفل جسم السد،
- الرصد المتكرر لنقاط التسرب من اجل الوقوف على اي ارتفاع في مستوى التسرب واذا ما كان هناك من وحول.

ان اي آثار تدميرية ناتجة عن هزات ارضية يجب ان تعطى اولوية في المعالجة قبل السماح باعادة مستوى المياه إلى المستوى الطبيعي للتشغيل.

1. INTRODUCTION

This report presents the results of a site-specific probabilistic seismic hazard assessment and seismic deformation analysis performed for Qaraoun Dam by AMEC Environment & Infrastructure, Inc. (AMEC) for International Resources Group (IRG) under the U.S. Agency for International Development/Litani River Basin Management Support Program (LRBMSP) for the Litani River Authority (LRA) of Lebanon. The work presented in this report was performed as part of IRG Contract No. EEP-I-00-04-00024-00, Task Order No. 7, dated May 23, 2011.

1.1. PURPOSE

The purpose of this study is to perform a probabilistic seismic hazard analysis (PSHA) for the project site, develop site-specific earthquake response spectra, develop earthquake time histories consistent with the target spectra, and use selected acceleration time histories to analyze the seismic deformation potential for Qaraoun Dam.

Our scope of services to accomplish the above-stated purposes is outlined in our proposal dated April 8, 2010. The primary tasks performed for this evaluation included:

- Performing data collection and review of available sources;
- Performing a Probabilistic Seismic Hazard Analysis (PSHA);
- Developing Uniform Hazard Response Spectra (UHRS) corresponding to return periods of 100 and 10,000 years (and later amended to include a 2,475 year return period) for representative bedrock outcrop conditions at the dam site;
- Identifying, selecting, and spectrally matching two sets of horizontal orthogonal-component and vertical-component time histories, based on the major contributors to the hazard and deaggregation results, for 100- and 10,000-year return period ground shaking levels(and later amended to develop time histories for the 2,475-year return period in lieu of the 10,000-year return period);
- Performing a two-dimensional finite-difference deformation analysis of the maximum section of the dam for two earthquake scenarios; and
- Preparation of this report.

1.2. REPORT ORGANIZATION

A brief project description is presented in Section 2.0. Section 3.0 details the probabilistic seismic hazard analysis and discusses the ground motion selection approach. The seismic deformation analyses are presented in Section 4.0. Section 5.0 summaries the general findings and conclusions of the PSHA and deformation analyses. The basis for our analyses and conclusions is presented in Section 6.0. References cited are compiled in Section 7.0.

This report includes three appendices. Appendix A presents rates of seismicity for the seismic source zones in the site region. Appendix B includes plots of the acceleration, velocity and displacement time histories and response spectra for the 100-year, 2,475-year, and 10,000-year return period ground motion levels, respectively. The electronic files of acceleration time histories are provided on a CD included in Appendix C.

1.3. PROJECT TEAM AND ACKNOWLEDGEMENTS

AMEC personnel that participated in this project and their primary responsibilities include:

- Dr. Faiz Makdisi, Principal Engineer, Principal-in-Charge
- Dr. Robert R. Youngs, Principal Engineer, Lead Seismologist
- Dr. Zhi-Liang Wang, Senior Engineer, Lead Analyst
- Mr. Justin Phalen, Senior Engineer, Project Manager
- Ms. Alexis Lavine, Senior Geologist, Peer Review
- Mr. Marc Ryan, Principal Engineer, Peer Review
- Ms. Courtney Johnson, Project Geologist, Seismic Source Characterization
- Ms. Debra Gilkerson, Staff Engineer, Ground Motion Analysis and Time History Development
- Dr. Jian Hu, Project Engineer, Seismic Deformation Analyst

The following personnel from the Litani River Authority (LRA) and IRG provided valuable support, review and direction during this study:

- Mr. Eric Viala, IRG, Chief of Party, Litani River Basin Management Support Program
- Mr. Wael Sabra, Civil Engineer, Litani River Authority
- Dr. John Smart, Independent Technical Reviewer for IRG
- Mr. Ali Abboud, General Director, Litani River Authority.

2. PROJECT AND FACILITY DESCRIPTION

Qaraoun Dam is located on the Litani River in the Bekaa Valley approximately 80 kilometers southeast of the Lebanese capital city of Beirut. The dam provides storage for the production of electricity and irrigation water for the Bekaa Valley. The dam structure is a concrete-faced rockfill embankment with a maximum height of 60 meters and a length of 1,100 meters.

The dam was constructed in the early to mid 1960s in two successive stages to allow for early filling of the reservoir (Halwani, et al., 1964). The first stage was completed in 1962 when the reservoir was allowed to store water up to an elevation of 838.0 meters. The second stage was completed in 1965 which brought the crest elevation to 861.0 meters and allowed the reservoir to store water up to an elevation of 858.0 meters. A 2-meter-high parapet wall was also installed along the crest to increase freeboard.

The abutment slopes are relatively gentle (about 8H:1V) along most of the longitudinal section of the dam until they abruptly drop into the valley formed by the Litani River. The main (maximum height) center section of the dam is located approximately halfway between the abutments as shown on Figure 2-1.

The main embankment is comprised of dumped rockfill placed in 10-meter thick lifts and then hydraulically washed with water. The upstream face of the embankment rockfill was constructed as a stratified zone where individual boulders were placed in a more dense state than the adjacent dumped rockfill. The thickness of this zone tapers from 5 meters at the toe to about 3 meters at the crest. The stratified rockfill slope is faced with a bituminous liner and covered with reinforced concrete slab panels. The concrete panels range from 0.5 meter thick near the toe, to 0.3 meter near the crest, with joints spaced about 14 meters horizontally, and typically 12 meters vertically. Horizontal joints are more frequent near the toe of the dam where higher differential displacements are expected. At the toe of the dam, the water stop joint installed between the concrete panels continues along the top of the inspection gallery until it meets the top of the bedrock on the upstream side of the gallery. The finished upstream face slopes at about 1.2H:1V near the toe, and gradually steepens to 0.9H:1V near the crest. The downstream face slopes at about 1.35H:1V and has a 6-meter wide access road berm at elevation 832.0 meters (Figure 2-2).

Infrequent measurements of survey monuments installed in the concrete slabs near the crest and the mid-height of the dam indicate that the crest had experienced post-construction settlement of up to 0.2 meters between its completion in 1965 and 1968. By the time of the next available documented survey, in 1990, the dam had experienced an additional 2.3 m of settlement. Subsequent surveys in 1993 and 2001 indicate very little (less than 0.1 m) settlement. As a result of these deformations, the concrete panel facing has experienced distress and cracking and has required patching events in 1979 and 2010. While there is no explicit information immediately available about the age of the existing parapet wall, it is understood to have originally been built sometime in 1967. However, the wall has recently been observed to be intact and in very good condition, indicating that it was built (or at the very least re-built or repaired) after the majority of the post-construction settlement had occurred.

The dam was outfitted with a reinforced-concrete drainage and inspection gallery at the upstream toe across most of the middle section of the dam as shown in Figures 2-1 and 2-2. The gallery is typically constructed in bedrock and has a 3.1-meter diameter circular opening; large enough for personnel access for inspection of

the drainage facilities. A grout curtain was installed below the inspection gallery (both vertical and inclined at an angle towards the reservoir) to control under seepage.

The reservoir is controlled either through a low-level intake on the right abutment that diverts water into a tunnel for hydropower generation downstream, or through a mid-level intake tower on the left abutment that passes water underneath the dam and directly into the Litani River downstream of the toe (Figure 2-1).

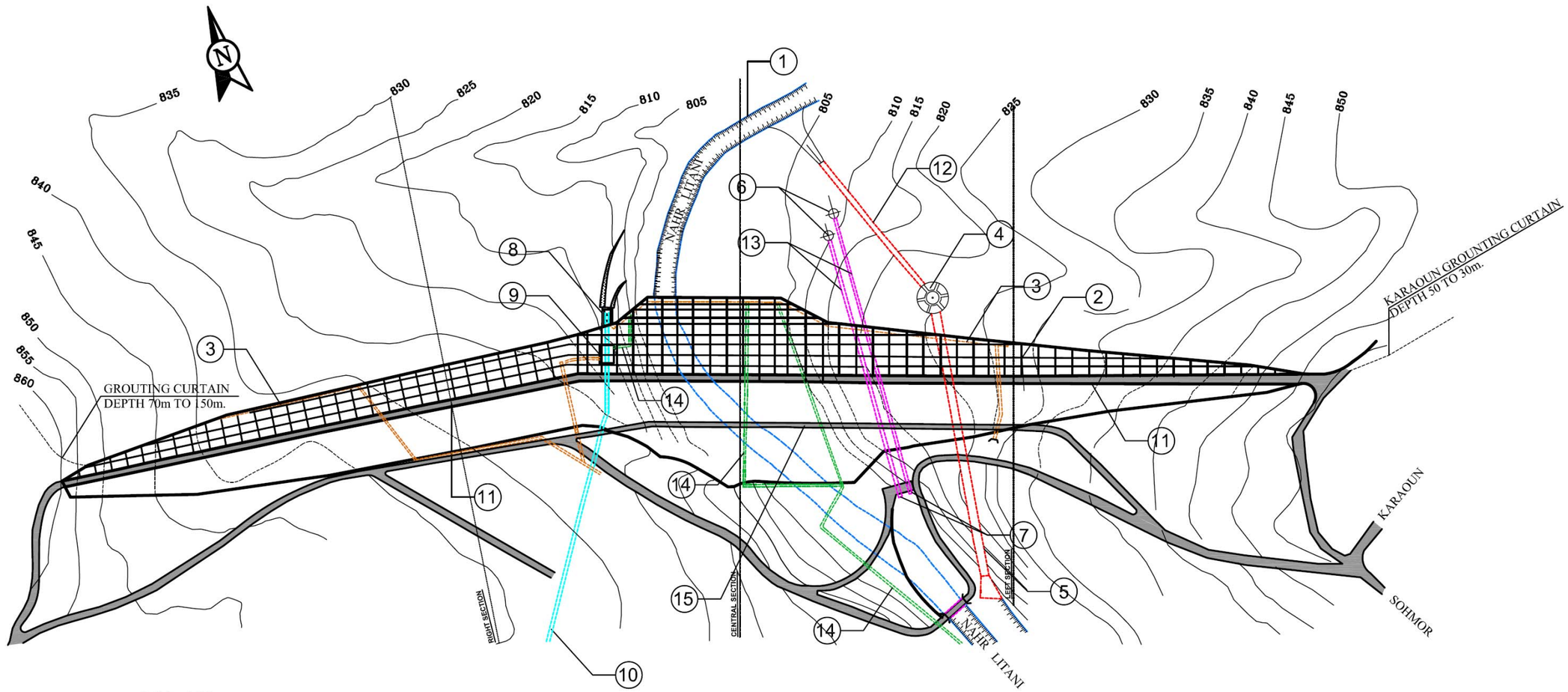

1. Litani River
2. Concrete - face plots
3. Inspection gallery
4. Spillway tower
5. Spillway tunnel
6. Washout towers
7. Washout valves
8. Hydropower intake
9. Intake valves chamber
10. Hydropower tunnel
11. Crest road : level 861.00
12. Diversion tunnel
13. Washout tunnels
14. Drainage gallery
15. Berm : Level 832

0m 50 100 200m

Qaraoun Dam Plan View

Seismic Deformation Analysis of Qaraoun Dam	OD11161570
AMEC Geomatrix	Figure **2-1**

DETAIL OF CONCRETE FACING

Scale : 1/50

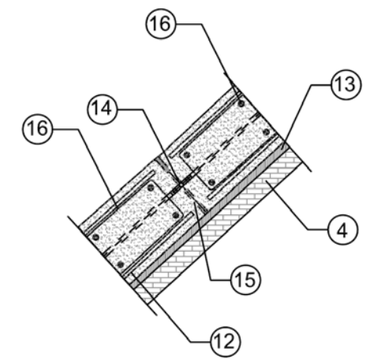

CENTRAL SECTION

Scale : 1/1000

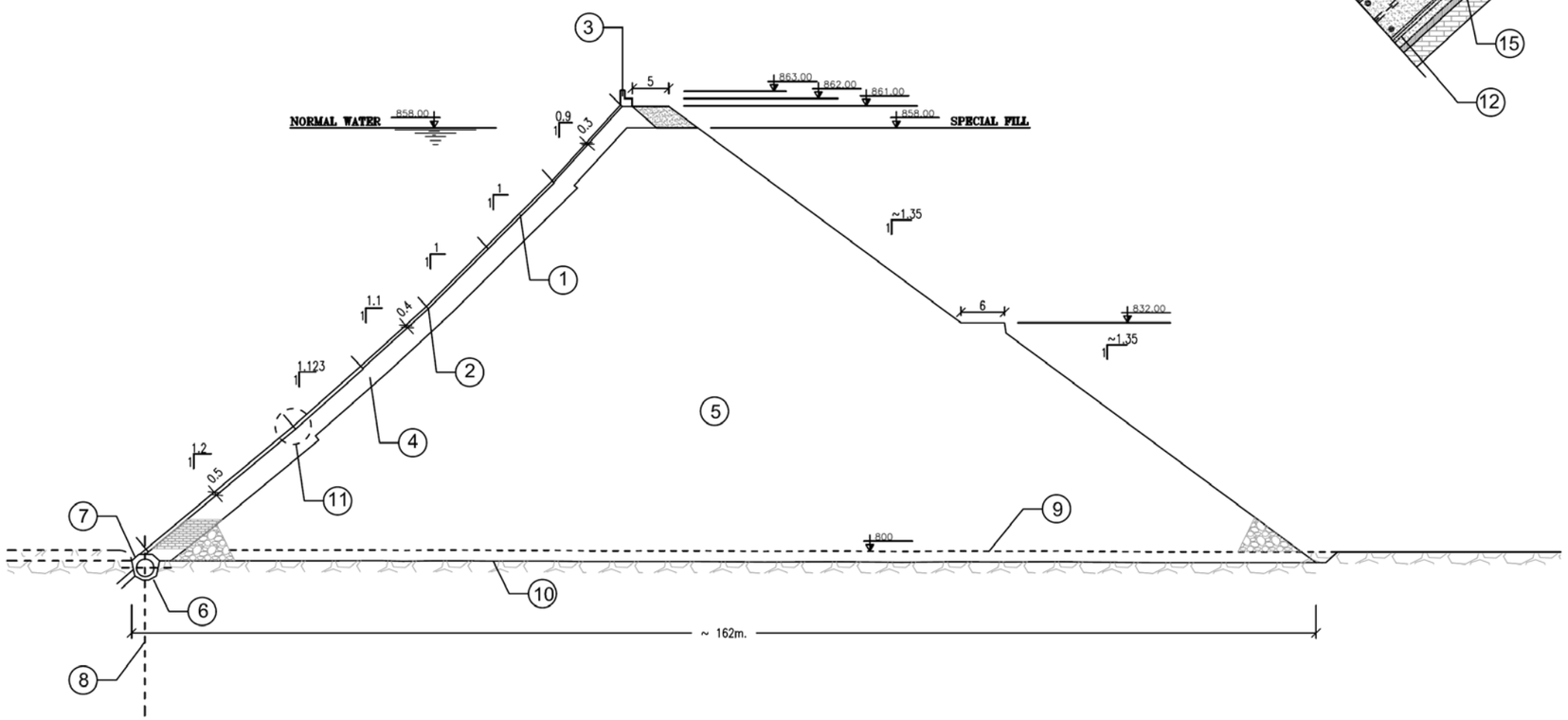

1. Concrete-face plots
2. Joints
3. Parapet
4. Stratified rockfill
5. Rockfill backfill
6. Inspection gallery
7. Foundations of plots
8. Cutoff
9. Natural ground
10. Rock foundation
11. Plot details
12. Asphaltic layer
13. Plain concrete layer
14. Water stop
15. Flexcell
16. Reinforcement

0m 20 40 50m

Qaraoun Dam Maximum (Center) Section	
Seismic Deformation Analysis of Qaraoun Dam	OD11161570
AMEC Geomatrix	Figure **2-2**

3. PROBABILISTIC SEISMIC HAZARD ANALYSIS

3.1. TECHTONIC SETTING AND SEISMICITY

An understanding of the regional tectonics, Quaternary geologic history, and seismicity of an area (i.e., the seismotectonic setting) facilitates the identification of geologic structures that should be modeled as seismic sources. It also provides context for developing tectonic models of crustal deformation that can be used in evaluating the tectonic role of individual geologic structures. Figure 3-1 shows the location of the Qaraoun Dam project site within the regional tectonic setting of the area. The following sections describe the regional tectonic setting and seismicity surrounding the site.

3.1.1. TECTONIC SETTING

The Qaraoun Dam site is located in a region of complex tectonic plate interaction along the Dead Sea fault system, which is a 1000-kilometer-long left-lateral transform fault system that forms the northwestern part of the boundary between the African plate on the west and the Arabian plate on the east (Figure 3-1). The Dead Sea fault system stretches between the Gulf of Aqaba, at the northern edge of the Red Sea, to the Taurus Mountains in southern Turkey. The southern and northern portions of the fault system are primarily expressed as prominent north-northeast-trending transform faults connected by a series of fault-bounded depressions (Garfunkel, 1981). The portion of the Dead Sea fault system located within Lebanon is often referred to as the Levant fault system. In the central portion of the Dead Sea fault system the Lebanese restraining bend, approximately 150 km long, is composed of left-lateral faults trending about N25E (Figure 3-2). Compression within the restraining bend is accommodated by northwest and southeast-dipping reverse faults that have formed the ranges that host Mount Lebanon, Mount Hermon, and the Anti-Lebanon hills (Carton et al., 2009). To the east of the restraining bend, the northeast-trending Palmyrides fold belt accommodates internal Arabian plate deformation (Carton et al., 2009). The Qaraoun Dam site is located in the southern part of the Lebanese restraining bend, to the east of the main left-lateral strike-slip fault of the Dead Sea fault system (Figure 3-2).

Several geologic studies indicate that activity on the Dead Sea fault system began during the mid-Miocene between about 14 and 6 million years ago (Bayer et al., 1988; Mimran et al. 1987; Garfunkel, 1981; Bartov et al., 1980).

Total displacement on the Dead Sea fault system has been determined to be 105 to 110 km based on detailed mapping south of the Sea of Galilee (Garfunkel, 1981; Quennell, 1984; Zaza et al., 1996). North of Lebanon, the total displacement on the transform, often termed the Ghab fault system, is about 30 km (Zaza et al., 1996). Detailed studies of offset geologic markers across the Dead Sea fault system indicate a long-term slip rate between 7 and 10 mm/yr during the past 4 to 5 million years (Garfunkel, 1981). A block model by ArRajehi et al. (2010) using GPS velocities across the Dead Sea fault region calculate a slip rate of approximately 4.3 to 4.9 mm/yr, with a minor extensional component, for the Dead Sea fault south of the restraining bend. Other block models utilizing GPS measurements in the region estimate slip rate values of about 3 to 6 mm/yr across the Dead Sea fault system south of the restraining bend (Reilinger et al., 2006; Vigny et al., 2006; Wdowinski et al., 2004). In Syria, north of the restraining bend, slip rates across the African-Arabian plate boundary are estimated at 4 to 5 mm/yr based on an elastic block model by Gomez et al. (2007).

3.1.2. SEISMICITY

The Dead Sea region of the eastern Mediterranean has been affected by numerous moderate to large magnitude earthquakes. These events are related primarily to activity along the tectonic plate boundary between the African and Arabian plates. The regional seismicity for the period between 2150 B.C. and A.D. 2011 is shown on Figure 3-3 (based on the U.S. National Geophysical Data Center (NGDC) 2011 Seismicity Catalog, described in detail in Section 3.3.1 of this report).

Numerous moderate to large magnitude earthquakes have caused damage to buildings in the region near the Qaraoun Dam site. A magnitude 7.4 earthquake occurred in the Bekaa Valley on November 25, 1759 with a shaking duration of about 50 seconds and a Modified Mercalli Intensity (MMI) of approximately XIII likely felt in the vicinity of Qaraoun Dam (Ambraseys and Barazangi, 1989). A magnitude 6.4 or larger earthquake on January 1, 1837 was felt in towns near the site, and aftershocks were felt for at least three months following the main shock (Ambraseys, 1997). At the location of the dam within Bekaa Valley, ground shaking intensity has been estimated to be a MMI of approximately VI to VII for the January 1837 event (Ben-Menahem, 1981).

The NGDC maintains a worldwide catalog of significant earthquakes that meet at least one of the following criteria: a) produced approximately $1 million (USD) in damage (or more); b) caused 10 or more deaths; c) had a magnitude of 7.5 or greater; had a MMI of X or greater; and/or e) generated a tsunami. The following list identifies significant earthquakes within 300 km (epicentral distance) of the site (NGDC, 2011) that caused regional damage between 2150 B.C. and A.D. 2011 with known magnitude or estimated magnitude based on MMI.

Significant Earthquakes within 300 Kilometers of the Qaraoun Dam Site

Year	Month	Day	Depth (km)	Magnitude	Closest Distance to Site (km)
-2150	0	0	---[1]	7.3	272
-1250	0	0	---	6.5	173
-31	9	2	---	7.0	173
115	12	13	---	7.5	286
362	5	24	---	6.4	249
746	1	18	---	7.0	173
1151	0	0	---	6.2	141
1160	0	0	---	6.1	173
1182	0	0	---	6.7	141
1202	5	20	---	7.6	29
1546	1	14	---	7.0	173
1759	10	30	---	6.4	63
1759	11	25	---	7.4	26
1834	5	23	---	6.3	249
1837	1	1	---	6.4	63
1872	4	3	---	7.3	298
1903	3	29	---	5.7	154
1927	7	11	33	6.3	173
1956	3	16	---	5.8	42
2004	2	11	27	5.3	208
2008	2	15	10	5.0	43

Note:

[1] "---" Indicates that the value is unknown.

3.2. SOURCE CHARACTERIZATION

The seismic hazard model for the study region includes the characterization of the sources of potential future earthquakes and the ground motions that they may produce. An important component of the seismic hazard model is the characterization of the uncertainties in identifying seismic sources and defining their parameters. A logic tree formulation is used to represent these uncertainties in the hazard model.

3.2.1. SOURCE CHARACTERIZATION

Two types of shallow crustal seismic sources are identified and characterized for the evaluation of earthquake hazard at the Qaraoun Dam site. The first type includes shallow crustal faults within about 100 km of the site

(Figure 3-4, Table 3-1). The second type includes areal seismic source zones (Figure 3-5). These seismic source zones characterize the distributed crustal seismicity in the site region that is not attributed to known or well characterized fault sources.

3.2.1.1. ACTIVE CRUSTAL FAULT SOURCES

Active crustal faults generally are defined as those that have been active during the Quaternary period (i.e., from 1.6 million years before present [Ma] to the present) and are likely to be active in the future. The six active crustal fault sources considered in this hazard analysis are recognized Quaternary faults that extend to within about 100 km of the site (Table 3-1, Figure 3-4). Faults included in the hazard analysis are judged to be active and capable of generating moderate magnitude (M 5 to 6) or larger earthquakes based on association with historical seismicity, and/or stratigraphic and/or geomorphic evidence of Quaternary activity (e.g., Gomez et al., 2003; Daëron et al., 2004; Carton et al., 2009). The key source characteristics used to develop input parameters for the PSHA are summarized in Table 3-1, along with uncertainties or probabilities identified for each fault parameter. The key source parameters include: style of faulting/sense of slip, geometry, fault length, depth of seismogenic rupture, segmentation, and slip rate.

Fault sources in this study are modeled as individual faults. Discontinuous faults or fault zones are generalized as a single continuous trace consisting of one or more straight line segments, so that the source-to-site distance and total length of the modeled fault are consistent with the mapped fault.

Long-term neotectonic and/or Quaternary slip rates for active faults considered in this analysis are reported in the available publications (e.g., Gomez et al., 2003; Daëron et al., 2004; Carton et al., 2009; ArRajehi et al., 2010). Information on displacement during the most recent event and recurrence time between earthquakes, when available, is used to supplement and constrain the values and probabilities of slip rates used to characterize each fault. Table 3-1 shows the slip rates and their uncertainties (expressed as relative probabilities in brackets) for crustal fault sources.

3.2.1.1.1. YAMMOUNEH FAULT

The Yammouneh fault is an approximately 297-km-long, vertical strike-slip fault located about 2.4 km west of the site. The southern end of the fault extends along the western side of the Sea of Galilee, where an extensional basin marks the boundary between the Yammouneh fault and Jordan Valley fault to the south. The Yammouneh fault makes up a majority of the Lebanese Restraining Bend in the Dead Sea fault system and accommodates a large portion of the transpressional motion in Lebanon as the African plate moves south with respect to the Arabian plate. Paleoseismicity studies of the Yammouneh fault, summarized by Klinger (2010), determined that the May 20, 1202 magnitude 7.6 earthquake occurred on the fault and that the fault has a recurrence period of approximately 800 years between large events. The slip rate on the Yammouneh fault is 5 $\pm$ 1 mm/yr (Gomez et al., 2007) or 3.8 to 6.4 mm/yr (Daëron et al., 2004).

3.2.1.1.2. ROUM FAULT

The Roum fault is an approximately 55-km-long normal fault located approximately 18 km southwest of the site. The fault displays primarily left-lateral strike-slip displacement, with little or no significant reverse displacement recognized (Carton et al., 2009; Gomez et al., 2006). The slip rate is estimated at approximately 1 mm/yr from a geomorphology and paleoseismicity study by Nemer and Meghroui (2006) and was estimated at 0.7 to 1.4 mm/yr by USAID (2007) for a seismic hazard study, based on an inferred rate of cumulative seismicity.

3.2.1.1.3. RACHAYA FAULT

The Rachaya fault is an approximately 51-km-long, southeast-dipping strike-slip fault that bounds the northwestern side of Mount Hermon, approximately 14 km southeast of the site. Slip rate on the Rachaya fault is estimated to be approximately 1 to 1.5 mm/yr based on a paleoseismic study by Gomez et al. (2003). The Rachaya and Serghaya faults have been considered potentially linked faults considered to rupture coseismically (Klinger, 2010; Nemer et al., 2008); however, the large distance between the two fault traces does not allow for these faults to be connected at the surface or at depth (see Figure 3-4 and Table 3-1). The

October 30, 1759 magnitude 6.4 earthquake was reportedly generated by either the Rachaya or Serghaya fault (Klinger, 2010).

3.2.1.1.4. SERGHAYA FAULT

The Serghaya fault is an approximately 122-km-long, left-lateral strike-slip fault that is located approximately 28 km east of the site. The slip rate is estimated at between 1 and 2 mm/yr of left-lateral strike-slip displacement based on studies by Gomez et al. (2003) and Gomez et al. (2001). Fault displacements during earthquake events are estimated at 1.8 to 2.6 meters and 60 to 90 km rupture lengths are estimated for the Serghaya fault (Gomez et al., 2001).

3.2.1.1.5. MOUNT LEBANON FAULT

The Mount Lebanon fault is an east-dipping reverse fault located approximately 32 km west of the site. The fault is mapped with an arcuate shape extending from the northern portion of the Roum fault for approximately 138 km offshore to the west of Beirut, and returning onshore near the city of Tripoli in northern Lebanon. The Mount Lebanon thrust accommodates a majority of the compressional motion that is caused by the stresses that have formed the Lebanese Restraining Bend. The fault has a dip of approximately 45 degrees within the seismogenic crust based on analyses of geophysics by Elias et al. (2007). The slip rate for the Mount Lebanon fault is estimated at between 1 and 4 mm/yr of reverse motion (Elias et al., 2007; Klinger, 2010).

3.2.1.1.6. JORDAN VALLEY FAULT

The Jordan Valley fault is the portion of the Dead Sea fault system that extends south of the Sea of Galilee. It is the major north-south trending, vertical structure that accommodates left-lateral strike-slip displacement between the African and Arabian tectonic plates. The Jordan Valley fault is estimated to accommodate a slip rate of approximately 2 to 6 mm/yr (ArRajehi et al., 2010; Klinger, 2010; Jaafar, 2008; Reilinger et al., 2006; Vigny et al., 2006).

3.2.1.2. AREAL SEISMIC SOURCE ZONES

The shallow (less than 35 km deep) earthquakes that cannot be spatially attributed to the mapped active fault zones shown on Figure 3-4 are modeled as separate areal source zones, shown as polygons on Figure 3-5. The size and extent of the areal source zones were delineated based on prominent geologic structures and consistent patterns of seismicity. In general, the boundaries between these morphostructural regions correspond to changes in the spatial pattern and magnitude distribution of earthquakes, such that zones are inferred to exhibit uniform seismicity.

The seismicity in the combined earthquake catalog (see Section 3.3.1 and Figure 3-3) is used to estimate the earthquake recurrence parameters for each of the areal source zones. Eight crustal areal seismic source zones that lie within about 300 km of the site (Figure 3-5) were modeled in the PSHA. The eight areal source zones are: Lebanese Restraining Bend, Jordan Valley Zone, Levantine Basin, Cyprus Zone, Cyprus Transform, Sinai Peninsula Zone, Syria Zone, and Arabian Shelf.

Earthquakes in the seismic source zones are modeled as occurring on planar fault sources distributed throughout the source area. Parameters used to characterize the areal source zones, and their weighted uncertainties, are listed in Table 3-2.

3.2.1.2.1. LEBANESE RESTRAINING BEND

The Lebanese Restraining Bend crustal areal source zone delineates an area of moderate seismicity in the crust along the plate boundary zone between the African and Arabian plates. The area encompasses the Lebanese restraining bend, a series of left-lateral faults trending about N25E that accommodate transform displacement resulting from the northwest-southeast-trending stresses of the region. Compression is accommodated by northwest- and southeast-dipping reverse faults throughout the zone. In the eastern part of the zone, the northeast-trending Palmyrides fold belt accommodates additional compression.

Major earthquakes within the restraining bend are primarily attributed to the major plate boundary faults, which are characterized as individual seismic fault sources (Section 3.2.1.1). The largest earthquake recorded in this zone not associated with a seismic fault source occurred in 1991 and had an approximate moment magnitude of M_W 4.9, as reported by available earthquake catalogs described in Section 3.3.1.

3.2.1.2.2. JORDAN VALLEY ZONE

The Jordan Valley crustal areal source zone delineates an area surrounding the extension of the Jordan Valley fault south of the step over and pull-apart basin at the Sea of Galilee. The zone is characterized by moderate magnitude (M 5-6) seismicity in the crust along the plate boundary zone between the African and Arabian plates that is oriented approximately north-south (Figure 3-5). The largest earthquake reported in this zone had an approximate magnitude of M_W 6.4 and occurred in the year A.D. 362, as reported by available earthquake catalogs described in Section 3.3.1. Because the zone has been built to incorporate the major plate boundary south of the Sea of Galilee, we believe it is likely that the maximum earthquake magnitude potential in the zone is similar to that of the Jordan Valley fault to the north (see Table 3-1 and Table 3-2).

3.2.1.2.3. LEVANTINE BASIN

The Levantine Basin source zone delineates an area of low to moderate seismicity in the oceanic crust underlying the Mediterranean Sea. The tectonic structure trend within the Levantine Basin is not well-constrained and is therefore assigned random orientation within the model. The largest earthquakes reported in this zone had an estimated magnitude of M_W 5.0 and occurred in 1970 and 1984, as reported by available earthquake catalogs described in Section 3.3.1.

3.2.1.2.4. CYPRUS ZONE

The Cyprus crustal areal source zone delineates an area of moderate to high seismicity to the northwest of the site (Figure 3-5). Tectonic stresses in the region are oriented northeast-southwest and have resulted in subduction of the African plate beneath the Eurasian plate to the southwest of the island of Cyprus. The same orientation of stresses to the east of Cyprus has resulted in primarily strike-slip displacements along the plate-bounding faults (Wdowinski et al., 2006). The tectonic structures within the Cyprus Zone have been assigned orientations trending primarily east-west and northeast-southwest, similar to the major faulting structures within the zone. The largest earthquake reported in this zone had an estimated magnitude of M_W 6.7 and occurred in 1996, as reported by available earthquake catalogs described in Section 3.3.1.

3.2.1.2.5. CYPRUS TRANSFORM ZONE

The Cyprus Transform crustal areal source zone delineates an area of moderate seismicity that includes the plate-bounding transform faults between the African and Eurasian plates to the north and northwest of the site (Figure 3-5). The general tectonic structure orientation assigned to the Cyprus Transform Zone is trending primarily northeast-southwest. The largest earthquake reported in this zone had an estimated magnitude of M_W 7.5 and occurred in the year A.D. 115, as reported by available earthquake catalogs described in Section 3.3.1.

3.2.1.2.6. SINAI PENINSULA ZONE

The Sinai Peninsula crustal areal source zone delineates an area of moderate to low seismicity in the crust of the African plate to the southwest of the site. The source zone is located immediately west of the plate-bounding faults between the African and Arabian plates (Figure 3-5) with assigned structural orientations trending approximately northeast-southwest and east-west. The largest earthquake reported in this zone, likely not associated with the plate boundary faults, was a magnitude M_W 5.7 event in 1903, as reported by available earthquake catalogs described in Section 3.3.1.

3.2.1.2.7. SYRIA ZONE

The Syria crustal areal source zone delineates an area of low seismicity in the stable continental crustal region of the Arabian Platform. The assigned structural trend is oriented approximately northeast-southwest. The largest earthquake reported in this zone was a magnitude M_W 5.2 event in 1996, as reported by available earthquake catalogs described in Section 3.3.1.

3.2.1.2.8. ARABIAN SHELF ZONE

The Arabian Shelf crustal areal source zone delineates an area of low seismicity in the stable continental crustal region of the Arabian Shield. The trend of tectonic structures within the Arabian Shelf zone is not well-constrained and is therefore assigned random orientations within the model. The largest earthquake reported in this zone was a magnitude M_W 6.7 event in 1182, as reported by available earthquake catalogs described in Section 3.3.1.

3.3. EARTHQUAKE GROUND MOTIONS

The probabilistic seismic hazard analysis (PSHA) was performed to characterize earthquake ground shaking that may occur at the project site during future seismic events in the region. The PSHA was conducted using seismic hazard codes (software programs) developed by AMEC Geomatrix[1]. The PSHA was conducted to estimate the probability of exceedance of peak ground acceleration (PGA) and response spectral accelerations (S_a at specified structural periods) at the site during selected exposure times. The seismic hazard and response spectra were developed for a rock outcrop foundation having a shear wave velocity in the upper 30 meters [V_{S30}] equal to 1,100 m/s. The site-specific seismic hazard analysis was performed to develop design response spectra that represent 100-year, 2,475-year, and 10,000-year return periods.

The PSHA is based on an assessment of the recurrence of earthquakes on and within potential seismic sources in the greater Lebanon region (as described in Section 3.2) and on ground motion attenuation relationships appropriate for the types of seismic sources in the region. The parameters needed for each seismic source include the rate of occurrence (frequency) of earthquakes for a range of magnitudes (earthquake recurrence relationships) and the maximum magnitude. The uncertainties in identifying seismic sources and identifying their model parameters are represented by a logic tree and used in this PSHA. The compilation of earthquake catalog, ground motion relationships, and parameters utilized in computing the ground motion hazard, are described below.

3.3.1. EARTHQUAKE CATALOG

The earthquake catalog used in this analysis was compiled from the Advanced National Seismic System composite earthquake catalog, ANSS (2011), NEIC (2011), NGDC/NEIC (2011), and IRIS (2011) catalogs. Historic events that occurred in the 20th Century in Lebanon and listed in a study by Khair (2001) were also included in the catalog. A combined catalog was developed by merging these catalogs and removing duplicate events. The catalog events were all converted to a common moment magnitude (M_W) scale based on relationships of records within the Global Centroid Moment Tensor (CMT) catalog (formally Harvard CMT). The conversion from surface wave magnitude (M_S) to M_W was developed using the Global CMT catalog in the region surrounding the site for events that have both M_S and M_W values reported. Similarly, events surrounding the site for which both body wave magnitude (M_b) and M_W values were available were used to develop conversions from M_b to M_W magnitudes. Linear regressions for both M_b and M_S to M_W were used as approximate conversion relationships for the catalog events.

The complete catalog, after duplicates were removed, consisted of 6,332 events. Aftershocks and foreshocks were then removed by first flagging potential aftershocks or foreshocks using the methods of Gardner and Knopoff (1974), Grünthal (1985, updated by pers. Comm., 2002), and Urhammer (1986). Any event flagged by two or more of the methods listed above was removed from the catalog. The resulting catalog consists of 3,603 independent events and covers the time period A.D. 115 to June 2011 (Figure 3-3).

---

[1] The primary computer codes used to perform the seismic hazard analysis were the Fortran executables xcd53 (12/09/09), haz51a (08/10), and tree50 (05/10/07). These or previous versions of the programs have been validated internally and through a PEER project. The PEER validation report is in draft form and has not yet been published (http://peer.berkeley.edu/lifelines/lifelines_pre_2006/summaries/607-wong.pdf).

3.3.2. MAXIMUM EARTHQUAKE MAGNITUDES

The maximum magnitude, M_{MAX}, for a seismic source represents the largest possible earthquake for that source, regardless of its frequency of occurrence. Thus M_{MAX} defines the upper limit of the earthquake recurrence relationship for the source. The approaches used to assess earthquake recurrence relationships and M_{MAX} are dependent on whether a fault or an areal source zone is being evaluated. The approaches used for each type of source are described below.

3.3.2.1. FAULT-SPECIFIC SOURCES

An evaluation of M_{MAX} for all fault sources, except the Yammouneh and Jordan Valley faults, was made using empirical relationships that relate fault rupture length and rupture area to maximum magnitude (Wells and Coppersmith, 1994). Equal weight was given to both the relationship using rupture length and that using rupture area. For large strike-slip faults, the relationships of Wells and Coppersmith (1994) underestimate results for events consistently larger than approximately M_w of 7.0 (Hanks and Bakun, 2008). Therefore, M_{MAX} for the Yammouneh and Jordan Valley faults was determined using the bi-modal method of Hanks and Bakun (2008) which relates rupture area to magnitude using different relationships for events above and below a specific rupture area. For each crustal fault, ranges of values for the rupture length, fault dip, and thickness of the seismogenic crust, including corresponding weights (relative probabilities) for different parameter values, were used to calculate the maximum earthquake magnitudes listed in Table 3-1. These calculations result in maximum magnitude distributions for each fault (i.e., all possible maximum magnitudes given the source parameters, their uncertainties, and the empirical relationships used to estimate them) that are used in the subsequent hazard calculations. Table 3-1 presents the weighted mean and range of these maximum magnitude distributions.

3.3.2.2. AREAL SOURCE ZONES

The maximum recorded earthquake and the range of maximum earthquake magnitudes and associated weights that were used to characterize the areal source zones are listed in Table 3-2. The M_{MAX} for each source zone was estimated with consideration given to the largest earthquake that is not associated with crustal faulting within the zone. The range of M_{MAX} values reflects the uncertainty in the seismogenic potential of other faults not consistently mapped or identified as active or potentially active faults within this region.

3.3.3. EARTHQUAKE RECURRENCE

3.3.3.1. FAULT-SPECIFIC SOURCES

The slip rate reflects the rate at which strain energy (seismic moment) accumulates along a fault. The geologically derived seismic moment rate is used to translate slip rate into earthquake recurrence rate by partitioning the moment rate into earthquakes of various magnitudes according to a recurrence model. The "characteristic earthquake" recurrence model (Youngs and Coppersmith, 1985) is judged to be more representative of the seismicity of an individual fault, than are exponential models that represent seismicity of regions. Therefore, the recurrence of earthquakes on fault sources is modeled using the "characteristic earthquake" recurrence model.

3.3.3.2. AREAL SOURCE ZONES

The earthquake recurrence relationships for areal source zones were determined from the historical seismicity of the region. Section 3.3.1 describes the development of the earthquake catalog for the Lebanon region. The earthquakes in the catalog are described in terms of the moment magnitude scale (Hanks and Kanamori, 1979). The catalog was analyzed to identify dependent events (earthquakes that were aftershocks or foreshocks of larger earthquakes) and to produce a set of earthquakes that can be considered to correspond to a Poisson process.

The earthquake recurrence in the areal source zones is represented with a truncated exponential model (Cornell and Van Marcke, 1969). The earthquake recurrence rates and Gutenberg-Richter b-values were

estimated using the observed seismicity (from the independent catalog) that occurred within each zone. The seismicity rates developed for each source zone are presented in Appendix A.

3.3.4. ATTENUATION RELATIONSHIPS

A ground motion attenuation model relates the amplitudes of peak acceleration and response spectral acceleration at the project site to earthquake magnitude, site conditions, source-to-site distance, and style of faulting. Past studies of strong-motion data indicate that the ground motions from various types of earthquake sources exhibit different characteristics in terms of the scaling of ground motion amplitudes with magnitude, source-to-site distance, and period of vibration. In addition, different attenuation models are required for different types of seismic sources such as crustal sources in seismically active regions (i.e., plate boundary regions), sources in stable-continental crust, and subduction-related (i.e., oceanic crust) sources. For this study we used empirically developed ground motion attenuation relationships. However, due to the lack of recorded strong motion data in and around Lebanon, no comparisons could be made between these relationships and actual recordings near the site.

Several attenuation models require the site stiffness input parameter V_{S30} (shear wave velocity within the upper 30 m). As there are no available direct measurements of V_{S30} in the foundation of the dam site, or in the vicinity of the dam, V_{S30} was estimated based on measurements of shear wave velocity in similar geologic materials from other studies. Qaraoun Dam is founded on sedimentary limestone formed during the late Cretaceous through the Neogene period (approximately 80 to 2.6 [Ma]) (Walley, 1997). Odum et al. (2007) reports measurements of V_{S30} in Aymamon limestone (Puerto Rico) on the order of 985 m/s with a maximum V_{SMAX} of 1220 m/s. Aymamon limestone was formed during the Miocene epoch (23 to 5.3 [Ma]), a subset of the Neogene period. Gartner Lee (2008) reports measurements of V_{S30} in limestone units of Amherstberg and Lucas formation (Southern Ontario, Canada) of about 1225 m/s with a maximum V_{SMAX} of 1800 m/s. Amherstberg and Lucas formations were formed during the Devonian period (416 to 359 [Ma]). Both of the sites in these examples are overlain by up to 10 m of soft soil/weathered rock, which can greatly reduce the V_{S30} from the V_{SMAX} measurement. Given the age (similar to the Aymamon limestone) and relatively intact condition of the bedrock at Qaraoun Dam, a V_{S30} of 1,100 m/s was selected as input to the attenuation relationships. This site condition is consistent with the National Earthquake Hazards Reduction Program (NEHRP) Site Class B designation for rock site conditions.

3.3.4.1. CRUSTAL ATTENUATION RELATIONSHIPS

Attenuation relationships appropriate for ground motions produced by crustal seismic sources in seismically active regions were selected and used in the seismic hazard analysis. The recently-developed Next Generation Attenuation (NGA) models along with two region-specific attenuation models were used to determine ground motion hazard at the Qaraoun Dam site for all of the modeled crustal faults and for all of the crustal areal source zones except for the Levantine Basin, Syria, and Arabian Shelf zones.

Based on the estimated shear wave velocity at the site, the five NGA relationships were considered appropriate to use for the randomly-oriented average horizontal component of ground motions: Abrahamson and Silva (2008), Boore and Atkinson (2008), Campbell and Bozorgnia (2008), Chiou and Youngs (2008), and Idriss (2008). The two regional models selected are: Ambraseys (2005), which was developed specifically for Europe and the Middle East, and Akkar and Bommer (2010), which was developed for Europe, the Mediterranean Region, and the Middle East.

The source-to-site distance terms used by each model are somewhat different from one another. The primary distance parameter, R_{rup}, is the closest distance of the site to the fault rupture plane. Other distance parameters include the closest horizontal distance to the surface projection of the rupture plane, R_{JB}, and the horizontal distance from the top edge of the rupture measured perpendicular to the fault strike, R_x. All distances are calculated in the PSHA and the appropriate values are used with each model.

The NGA models were developed using ground-motion data from California and other similar active tectonic regions of shallow crustal faulting. The developers did not find compelling evidence that the application of

their models should be restricted to any particular geographic region. Akkar and Bommer (2010) and Ambraseys (2005) relationships were developed using data from Europe, the Middle East, and the Mediterranean. Comparisons of predictions of these relationships with those of the NGA models have been performed for Italian data by Scasserra et al. (2009). Based on our review of available information and our understanding of the models, each of the six models was assigned equal weights for use in this PSHA study. The attenuation relationships by Akkar and Bommer (2010) and Ambraseys (2005) have not been developed for return periods beyond 3 seconds and 2.5 seconds, respectively; therefore, coefficients for use in these relationships were extrapolated beyond these limits using the available data.

3.3.4.2. STABLE CONTINENTAL REGION CRUSTAL ATTENUATION RELATIONSHIPS

Attenuation relationships for earthquakes occurring in regions considered to be stable continental crust have been developed primarily for application in central and eastern North America (CENA). Because of the limited strong motion data set for CENA, the models have been based primarily on numerical simulations of strong ground motions. For the most part, these models have been developed for rock sites with shear wave velocities in excess of 2,500 m/s. However, some more recent models have been developed for estimation of ground motions on sites with a VS30 as low as 760 m/sec. For this reason, we included the models of Atkinson and Boore (2006), a dynamic-corner frequency model, and Campbell (2003), a hybrid model. As described in Section 3.1, the interior Arabian Peninsula is considered a stable continental crust characterized by an extremely low occurrence of seismicity and few to no discernable faults or active structural features. The above models are applied to the Syria and Arabian Shelf zones that occupy the northwestern portion of the stable continental crust of the Arabian Shield and are weighted equally in the hazard estimation.

3.3.4.3. OCEANIC CRUSTAL ATTENUATION RELATIONSHIPS

Most past assessments of the ground motions produced by subduction zone earthquakes have concluded that there are differences between the motions produced by earthquakes that occur on the interface between the subducting oceanic plate and the overriding continental plate (interface earthquakes), and those produced by earthquakes occurring within the subducting oceanic plate (intraslab earthquakes). Because attenuation relationships developed for intraslab earthquakes are based on events that have occurred in the oceanic crust, attenuation models appropriate for calculating ground motions for intraslab earthquakes are used in the PSHA for the oceanic crust of the Levantine Basin.

Three models were selected for intraslab earthquakes that applied to the oceanic crust. These include: Zhao et al. (2006), Garcia et al. (2005), and Atkinson and Boore (2003) intraslab relationships for rock. The intraslab earthquake models were assigned equal weights for use in the PSHA.

3.4. GROUND MOTION HAZARD ANALYSIS

The following sections describe the ground motion hazard analysis performed for this study. The analysis methodology, results, and comparisons with previous studies are described in the following sections.

3.4.1. CALCULATIONS OF FREQUENCY OF EXCEEDANCE

The mathematical formulation used in most PSHAs assumes that the occurrence of damaging earthquakes can be represented as a Poisson process. Under this assumption, the probability that a ground motion parameter, Z, will exceed a specified value, z, in time period t is given by:

$$P(Z > z \mid t) = 1 - e^{-\nu(z)\cdot t} \leq \nu(z)\cdot t \qquad (3\text{-}1)$$

where $\nu(z)$ is the average frequency during time period t at which the level of ground motion parameter Z exceeds value z at the site from all earthquakes on all sources in the region. Equation (3-1) is valid provided that $\nu(z)$ is the appropriate average value for time period t. In this study, the hazard results are reported in terms of the frequency of exceedance $\nu(z)$.

The frequency of exceedance, $\nu(z)$, is a function of the frequency of earthquake occurrence, the randomness of size and location of future earthquakes, and the randomness in the level of ground motion they may produce at the site. It is computed by the expression:

$$\nu(z) = \sum_n \alpha_n(m^0) \int_{m^0}^{m^u} f(m) \left[\int_0^{\infty} f(r|m) \cdot P(Z > z|m,r) \cdot dr \right] \cdot dm \qquad (3\text{-}2)$$

where $\alpha_n(m^0)$ is the frequency of earthquakes on any given source n above a minimum magnitude of engineering significance, m^0; $f(m)$ is the probability density of earthquake size between m^0 and a maximum earthquake the source can produce, m^u; $f(r|m)$ is the probability density function for distance to an earthquake of magnitude m occurring on source n; and $P(Z>z|m,r)$ is the probability that, given an earthquake of magnitude m on source n, at distance r from the site, the peak ground motion will exceed level z. The frequency of earthquake occurrence, $\alpha_n(m^0)$, and the size distribution of earthquakes, $f(m)$, were determined by the earthquake recurrence relationships described in Section 3.3.3. The distribution for the distance between the earthquake rupture and the site was determined by the geometry of the seismic sources defined in Section 3.2. The conditional probability of exceedance, $P(Z>z|m,r)$, was determined using the ground-motion attenuation relationships defined in Section 3.3.4. The attenuation relationships define the level of ground motion in terms of a lognormal distribution.

In the hazard computations, the fault-specific sources were modeled by segmented planar surfaces. The source zones were modeled by closely spaced, planar pseudo-faults distributed throughout the zone. At each epicentral location, earthquake ruptures were placed with preferred orientations consistent with geologic structures in the source (see discussions of average fault trend in Section 3.2.1). Earthquakes were represented by rectangular rupture planes for the given magnitude earthquake using the rupture area relationships developed by Wells and Coppersmith (1994) and Hanks and Bakun (2008). The depth distribution for earthquakes was assumed to be concentrated at midcrustal depths.

The hazard was computed considering the contributions of earthquakes of magnitude M_W 5 and larger (m^0 = 5). At each ground motion level, the complete set of results forms a discrete distribution for frequency of exceedance, $\nu(z)$. The computed distributions were used to obtain the mean frequency of exceeding various levels of peak ground motion (mean hazard curves).

3.4.2. PROBABILITIES OF EXCEEDANCE

Detailed seismic hazard results are presented for the site showing contributions from individual sources to the total hazard. Figures 3-6, 3-7, and 3-8 show the total mean hazard at the site, and contributions from each individual source for peak ground acceleration (PGA), and spectral acceleration (S_a) at 0.2- and 1.0-second periods, respectively. The plots are presented in terms of the ground motion parameter (PGA or S_a) versus its mean annual frequency of exceedance. The annual frequency of exceedance is the inverse of the return period in years.

At all periods the hazard is dominated by the local Yammouneh fault. For PGA (Figure 3-6), the hazard is almost completely controlled by the Yammouneh fault. At longer periods (0.2 and 1.0 seconds) and at high frequencies of exceedance, while the Yammouneh fault still dominates the hazard, contributions from the Lebanese Restraining Bend zone and nearby crustal faults become more significant (Figures 3-7 and 3-8). The site lies within the Lebanese Restraining Bend zone and within 2.4 km of the Yammouneh fault; therefore, as may be reasonably expected, the hazard appears to be controlled by the closest seismic sources.

Figures 3-9a through Figure 3-9c present magnitude-distance contributions to the hazard (deaggregation) for PGA, and for S_a at 0.2- and 1.0-seconds, respectively, for ground motions at a return period of 100-years (annual frequency of 0.01). Figures 3-9d through Figure 3-9f show the results of the deaggregation for PGA,

and for S_a at 0.2- and 1.0-second at a 10,000-year return period. At these long return periods, the hazard at the site is dominated by the Yammouneh fault.

3.4.3. UNIFORM HAZARD RESPONSE SPECTRA

3.4.3.1. HORIZONTAL RESPONSE SPECTRA

PSHA results for the Qaraoun Dam site were calculated for peak ground acceleration and response spectral accelerations at ten spectral periods (0.075, 0.1, 0.2, 0.3, 0.4, 0.5, 1.0, 2.0, 3.0, and 4.0 seconds). The mean hazard curves for each spectral period were interpolated to obtain values of spectral acceleration associated with return periods of 100 and 10,000 years; these return periods correspond to probabilities of exceedance of approximately 39½ percent, and ½ percent in 50 years, respectively. These values were then connected by smooth curves to produce uniform hazard response spectra (UHRS) for five-percent damping. The UHRS for the 100- and 10,000-year return periods are plotted on Figure 3-10 and listed in Table 3-3. Also shown are the UHRS for 475-, 975-, and 2475-year return periods for reference.

3.4.3.2. VERTICAL RESPONSE SPECTRA

Vertical response spectra for the 100- and 10,000-year return periods were also developed for the Qaraoun Dam analysis. At this time, the ground motion models described in Section 3.3 do not include parameters to estimate vertical motions. Therefore, vertical response spectra were developed by estimating appropriate vertical/horizontal (V/H) ratios from previously developed attenuation relationships, and applying them to the horizontal UHRS. Previous attenuation relationships for crustal earthquakes developed by Abrahamson and Silva (1997), Campbell and Bozorgnia (2003), and Sadigh et al. (1993) provide coefficients for estimating vertical response spectra on rock sites.

The deaggregation of the hazard results at the 100- and 10,000-year return periods presented in Section 3.4.2 show that most of the contribution to the hazard is from a strike-slip event on the Yammouneh Fault in the range of M_w 6.8 to 8.2 at a distance of 2.4 km. AMEC, in partnership with Quest Structures, Inc., developed V/H ratios based on the previously mentioned attenuation relationships (AMEC and Quest, 2009). The ratios were developed for a combination of distances, magnitudes and faulting types. Final V/H ratios were computed using the geometric mean of the Abrahamson and Silva (1997), Campbell and Bozorgnia (2003), and Sadigh et al. (1993) attenuation relationships at a distance of 1 km and M_w = 7.5, as shown in Appendix 4 of AMEC and Quest (2009). A minimum V/H ratio of 0.50 was applied to periods where the geometric mean dropped below 0.5. Figure 3-11 shows the final (mean) V/H ratios selected to develop the vertical uniform hazard response spectra for Qaraoun Dam. The ratios were applied to both the 100- and 10,000-year return period horizontal spectra.

3.4.3.3. DETERMINISTIC SEISMIC HAZARD ANALYSIS

We developed deterministic response spectra for the median (50th), and 84th-percentile (median plus one standard deviation) ground motions based on scenario earthquakes on the Yammouneh, Roum, and Rachaya faults. These earthquakes are the largest contributors to the hazard at long periods as shown on Figure 3-6 through Figure 3-8.

The deterministic spectra were developed using the mean maximum magnitudes for these sources, the closest distance to the site, and the same set of weighted attenuation relationships as used for the probabilistic analysis. The deterministic earthquakes considered in the analysis are:

- M 7.2 strike-slip earthquake on the Yammouneh fault at a distance of 2.4 km from the site.
- M 6.8 strike-slip earthquake on the Rachaya fault at a distance of 14 km from the site.
- M 6.9 strike-slip earthquake on the Roum fault at a distance of 18 km from the site.

Results of the deterministic analysis are presented on Figure 3-12 and in Table 3-4. The deterministic 84th percentile response spectrum from the Yammouneh fault is compared with the uniform hazard spectra from

the probabilistic analyses in Figure 3-10. The deterministic 84th percentile spectrum from the Yammouneh fault corresponds to a UHRS at a return period of about 2,500 years.

3.4.4. NEAR FAULT DIRECTIVITY EFFECTS

The NGA relationships do not explicitly differentiate near-field effects; thus, it is necessary to modify the probabilistic results to account for near-field fault rupture effects. Near-field ground motion effects (termed Directivity Effects) at periods of vibration longer than 0.5 second are associated with large magnitude ($\geq M_W$ 6.5) earthquakes occurring on nearby faults. For fault ruptures propagating toward the site, the forward directivity effect produces a large-velocity pulse at the beginning of the strong shaking and results in enhancement of the long-period horizontal spectral accelerations particularly for the fault normal component of ground motion. For fault ruptures propagating away from the site, a de-amplification of long-period spectral acceleration is expected to occur. These near-field effects described by Somerville et al. (1997) are considered to be significant only for sites located within approximately 15 km of an active fault. A more recent study (Spudich and Chiou, 2008) evaluated near-field effects of fault directivity on expanded databases of earthquake ground motions and provided updated approaches to modify spectra for near-field effects.

Several faults are situated within 15 km of the site; however, the Yammouneh fault is the dominant contributor to the hazard and is therefore the fault likely to generate amplified long period motions as the result of forward directivity. The near-field effects of this source are accounted for probabilistically using fault characteristics and weighting from Table 3-1, and the methodology of Spudich and Chiou (2008) for the NGA attenuation relationships. Ruptures can occur anywhere along the Yammouneh fault, with no preferential initiation location. Directivity factors are computed for 20 rupture scenarios where the initiation point is stepped along the fault at 15 km spacing. The calculations are completed for all periods from 0.5 to 4 seconds. The strike of the Yammouneh fault is in a direction approximately normal to the longitudinal axis of Qaraoun Dam. The analyses proposed for the dam will be performed on a transverse cross-section of the dam that is normal to its longitudinal axis. The ground motions to be used as input to the analyses are in the transverse (upstream/downstream) direction. Accordingly ground motions representing the fault parallel component from an event on the Yammouneh fault should be used in the analyses. To account for fault orientation, the factors calculated from Spudich and Chiou (2008) were multiplied by Somerville et al. (1997) fault parallel factors for strike-slip faulting. The resulting period-dependent weighted average factors are close to 1.0. The resulting factors for each earthquake return period and the adjusted UHRS are presented in Table 3-3 and on Figure 3-13.

3.4.5. COMPARISON OF RESULTS WITH OTHER STUDIES

Previous studies on the seismic hazard of the region surrounding Qaraoun Dam by different agencies and independent researchers provide a comparison with the results of this study. Commonly, available reports and maps focus on peak ground acceleration (PGA) at return periods of 475 years and 2,475 years. Unless noted, the site conditions utilized by these previous reports are unknown. No previous studies were found to focus on return periods of 100 years or 10,000 years; therefore to help make a generic comparison, the PGA values calculated in this PSHA are 0.40g for a 475-year return period and 0.77g for a 2,475-year return period.

The Global Seismic Hazard Assessment Program (GSHAP) estimates a peak ground acceleration (PGA) value at Qaraoun Dam of approximately 0.25 g for a 475-year return period (Giardini et al., 1999). A study of earthquake hazard of Jordan and the surrounding areas by Jimenez et al. (2006) shows Qaraoun Dam located in a zone corresponding to PGA values of 0.30g to 0.35g for a 475-year return period, updating earlier studies that show the site in a zone with PGA values of about 0.15g to 0.25g for a 475-year return period (Fahmi et al., 1996; Jimenez et al., 2001). Al-Tarazi and Sandoval (2007) estimate a PGA value of between 0.15g and 0.20g for a 475-year return period in the region near the site. Seismic hazard maps produced for the U.S. Agency for International Development Assessment for Building Codes Project (Shapira and Hofstetter, 2007) show the site located in an area corresponding to PGA values of 0.2g to 0.3g for a 475-year return period.

A study of seismic hazard for Lebanon by Harajli et al. (1994) shows a PGA value of approximately 0.2g for a 475-year return period at the site. A more recent study of seismic hazard for Lebanon by Elnashari and El-

Khoury (2004) shows a PGA value of 0.20g to 0.21g for a 475-year return period, and 0.30g to 0.35g for a return period of 2,500 years. An analysis of seismic design for rockfill dams in Lebanon shows Qaraoun Dam located in a zone that corresponds to a PGA value of approximately 0.3g for a return period of 475 years (Geadah, 2006). However, it was not an independent study and was likely based on a study by Harajli et al. (2002).

Differences between previous ground motion estimates and values from this PSHA likely result from a combination of the use of different attenuation models, and how crustal faults are dealt with by each study. We note that a majority of the available previous studies do not account for the potential contribution of discrete fault sources to the seismic hazard, but use only historical seismicity to define the regional hazard. We also note that the available previous studies were completed prior to the recent investigations of slip rate for the Yammouneh fault (eg., Gomez et al., 2007; Daëron et al., 2004) and therefore do not incorporate the slip rates and maximum magnitude estimates that are greater than previously available.

3.5. DEVELOPMENT OF ACCELERATION TIME HISTORIES

This section describes the development of the 100-year and the 10,000-year return period spectrum-compatible time histories for use in the deformation and seismic stability analyses of Qaraoun Dam.

3.5.1. SELECTION OF SEED TIME HISTORIES

As discussed in the previous sections, the Yammouneh fault is the largest contributor to the total hazard. Therefore, time histories representative of crustal sources were selected for use in the dynamic analyses. The time histories consist of actual strong motion recordings from the Pacific Earthquake Engineering Research Center (PEER) NGA database that have been rotated into fault-normal and fault-parallel orientations.

Four seed time histories were selected for the analysis of Qaraoun Dam, two for each of the 100- and 10,000-year return period, respectively. The dominant earthquake that was identified from deaggregation of the PSHA (Figures 3-9a through 3-9f) and the magnitude-distance contribution to hazard is a M_W 7.2 strike-slip earthquake on the Yammouneh fault at a distance (R_{rup}) of 2.4 km.

The four seed time histories were selected from a larger list of potential matches of existing time histories, primarily based on the magnitude-distance and fault type combinations described above, similarity of the spectral shape to the target UHRS, and rock site conditions that are approximately similar to a V_{S30} of 1,100 m/s. The following range of parameters was used for the initial selection of candidate crustal time histories:

- Magnitude (M_W) between 6.5 and 8.0;
- Distance to fault rupture (R_{rup}) between 0 and 20 km;
- Strike-Slip, Normal, or Reverse Earthquakes; and
- V_{S30} between 400 and 1,400 m/s.

Additional criteria that were considered in selecting records for the final suite include the duration of strong shaking, a reasonable scaling factor, and overall quality of the natural record. We selected no more than one record from each earthquake in an effort to capture a range of earthquake characteristics in the ground motions. The four seed time histories selected for matching to the target spectra for each of the 100- and 10,000-year return periods, and the associated metadata for each record from the NGA database, are listed in Table 3-5.

3.5.2. DEVELOPMENT OF SPECTRUM-COMPATIBLE TIME HISTORIES

For Qaraoun Dam two sets of two-component spectrum-compatible acceleration time histories were developed to represent the 100-year return period design ground motions and two additional sets were developed to represent the 10,000-year return period design ground motions at the site. A total of 2 sets of

spectrum-compatible time histories were developed for each scenario earthquake. Each set of time histories consists of two components of motion; one horizontal and one vertical.

The time histories were modified using a time-domain approach such that their response spectra match the target spectra. The horizontal component of the seed time histories was matched to the uniform hazard response spectrum (UHRS) as modified by the near fault factors described in Section 3.4.4. The vertical component of the seed time histories was matched to the vertical target spectrum described in Section 3.4.3.2.

The spectral matching was performed using the time-domain procedure proposed by Lilhanand and Tseng (1988) and later modified by Abrahamson (1992). This approach makes small adjustments to the time histories, which are used to make non-stationary modifications to the original time history. This process preserves the non-stationary properties of the original time history. Thus, the time-domain approach can be used to develop a time history that matches a target spectrum yet still has a realistic displacement waveform.

The modifications of time histories were made using the program RSPMATCH (Abrahamson, 1993; current version released in 2006). The seed time histories were modified such that their spectra would be "loosely matched" to the target response spectra. In the matching process, the horizontal component of each time history was modified such that its response spectrum matched the target horizontal spectrum described in Section 3.4.3.1.

Figures 3-14a and 3-14b show the comparison between the spectra of the modified horizontal time history and the target spectra for the 100-year and the 10,000-year return periods, respectively. Comparison between spectra of the modified vertical time history and the vertical target spectra for the 100-year and the 10,000-year return period are shown on Figure 3-15a and Figure 3-15b, respectively.

Comparisons between the response spectra (5% damped) of the scaled, spectrum-compatible time histories, and the target response spectra are shown in Appendix B. The figures also show a comparison between the acceleration, velocity, and displacement time histories of the matched records and the scaled natural record for the 2 sets of time histories for 100- and 10,000-year return periods. The electronic files of the matched acceleration time histories are provided on a CD in Appendix C.

3.6. RECOMMENDED EARTHQUAKE SCENARIOS FOR DEFORMATION ANALYSES

Following the development of the 100-year and 10,000-year return period earthquake scenarios and associated acceleration time histories, project team members from AMEC and IRG discussed the basis for selection of ground motions that would be most appropriate for analyzing the seismic response and deformation of the dam. The California Department of Water Resources, Division of Safety of Dams (DSOD) recommends that an 84th-percentile deterministic ground motion be used for evaluating the seismic stability for dams that classify as "high consequences of failure" structures (Fraser and Howard, 2002). The DSOD (Fraser and Burns, 2004) performed deterministic and probabilistic seismic hazard studies for over 100 dam sites in California, to assess the level of conservatism in the selection of the 84th percentile level of ground shaking for evaluating the seismic stability of dams under their jurisdiction. Their study included regions of high slip-rate faults (slip rates in excess of 1 mm per year) such as the San Francisco Bay Area and the Los Angeles area. The results of their study indicated that for dams in the San Francisco area, the 84th percentile ground motions had return periods in the range of 1,000 to 4,000 years. Similarly for the Los Angeles area, deterministic 84th percentile ground motions had return periods between 500 and 10,000.

As stated in Section 3.4.3.3 above, deterministic estimates of ground motions for Qaraoun dam indicate that 84th percentile ground motions from a magnitude 7.2 earthquake on the Yammouneh fault (with a slip rate of about 6mm per year) correspond to a return period of about 2,500 years, which is within the range of estimates for high slip-rate fault regions in California, and adopted by the California DSOD. Ground motions for a return period of 2,475 years have a 2 percent chance of being exceeded in 50 years. Accordingly, the team agreed that a 2,475-year return period ground motion would be developed and used for the deformation

analysis in lieu of the initially specified 10,000-year return period. The development of the acceleration time histories for this level of shaking followed the same approach as described in Section 3.5 above. Figure 3-16a through Figure 3-16c show the results of the deaggregation for PGA, and for S_a at 0.2- and 1.0-second for the 2,475-year return period.

The seed time histories originally selected to match the 10,000-year return period target spectra, were spectrally matched to the 2,475-year return period response spectra. These records include the Tabas station recording from the magnitude 7.4 Tabas, Iran earthquake of 1978, and the Hector Mine station recording from the magnitude 7.1 Hector Mine, California earthquake of 1999. Figures 3-17a and 3-17b show the comparison between the target spectra for the 2,475-year return periods and the spectra of the modified horizontal and vertical time histories, respectively. The two sets of matched time histories are presented in Appendix B.

S:\OD11\161570\11_0909_sha-qd_fig_01.ai

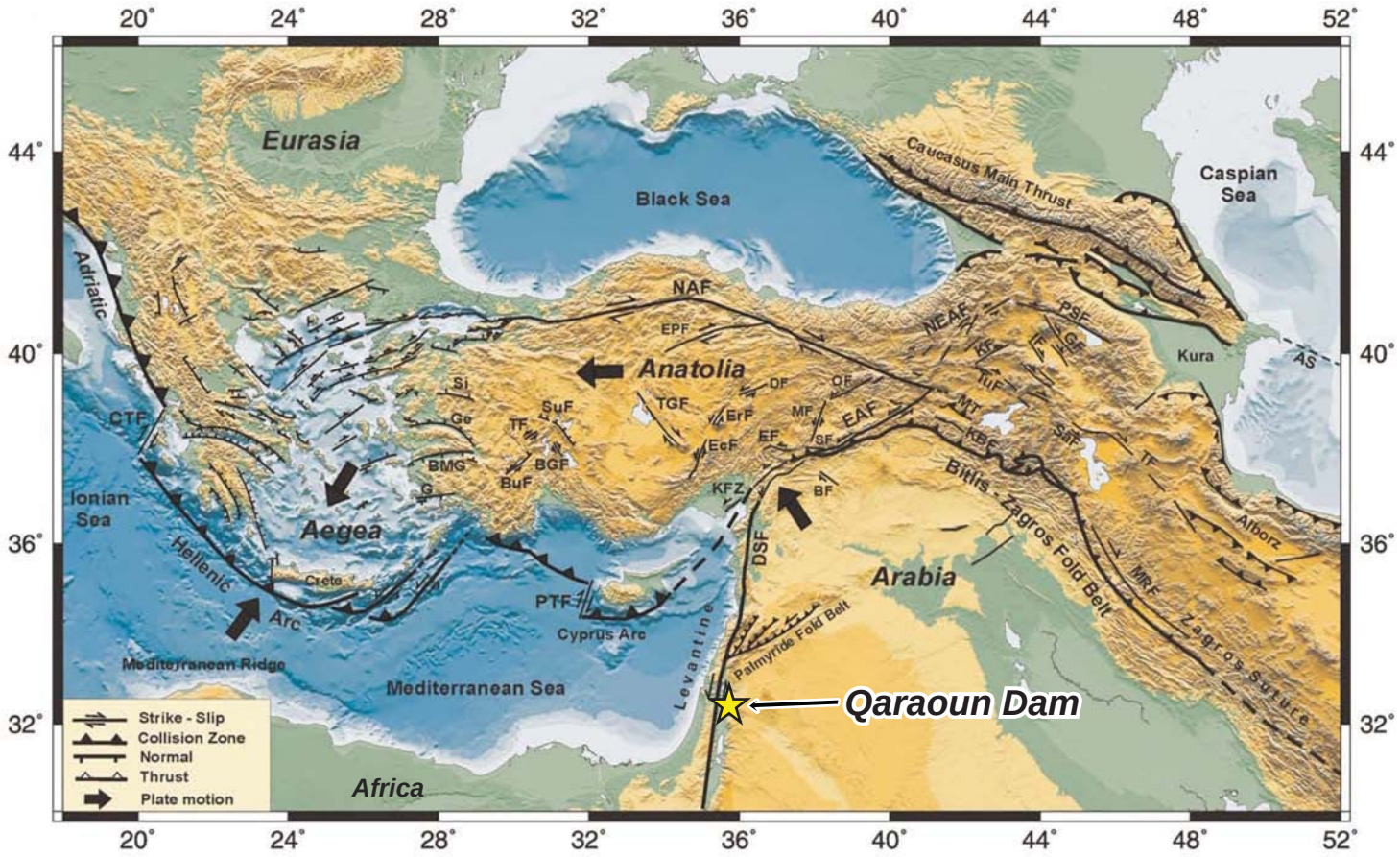

Map showing major tectonic features of the eastern Mediterranean region and complex collision of the African and Eurasian plates. Selected abbreviations: DSF, Dead Sea Fault; PTF, Paphos Transform Fault. Modified from Taymaz et al. (2007).

REGIONAL TECTONIC SETTING
Qaraoun Dam Hazard Study
Litani River Basin, Lebanon

By: CJ	Date: 09/09/2011	Project No.	OD11161570
amec		Figure	3-1

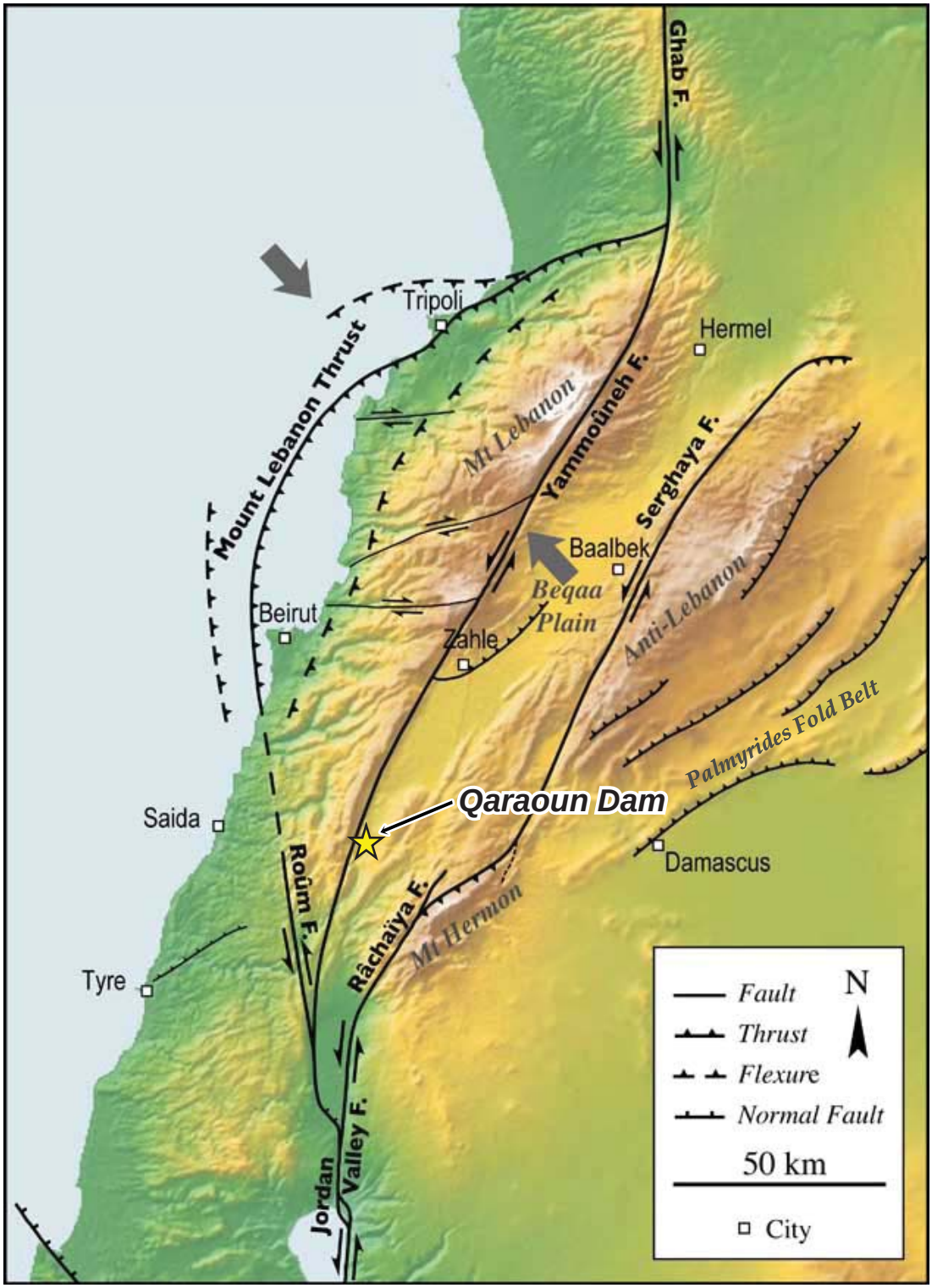

Map showing active faults in the Lebanese restraining bend. Thick gray arrows show the direction of shortening across the region. Modified from Daëron et al. (2004).

STRUCTURES OF THE
LEBANESE RESTRAINING BEND
Qaraoun Dam Hazard Study
Litani River Basin, Lebanon

By: CJ	Date: 09/09/2011	Project No.	OD11161570
amec		Figure	3-2

S:\OD11\161570\11_0909_sha-qd_fig_02.ai

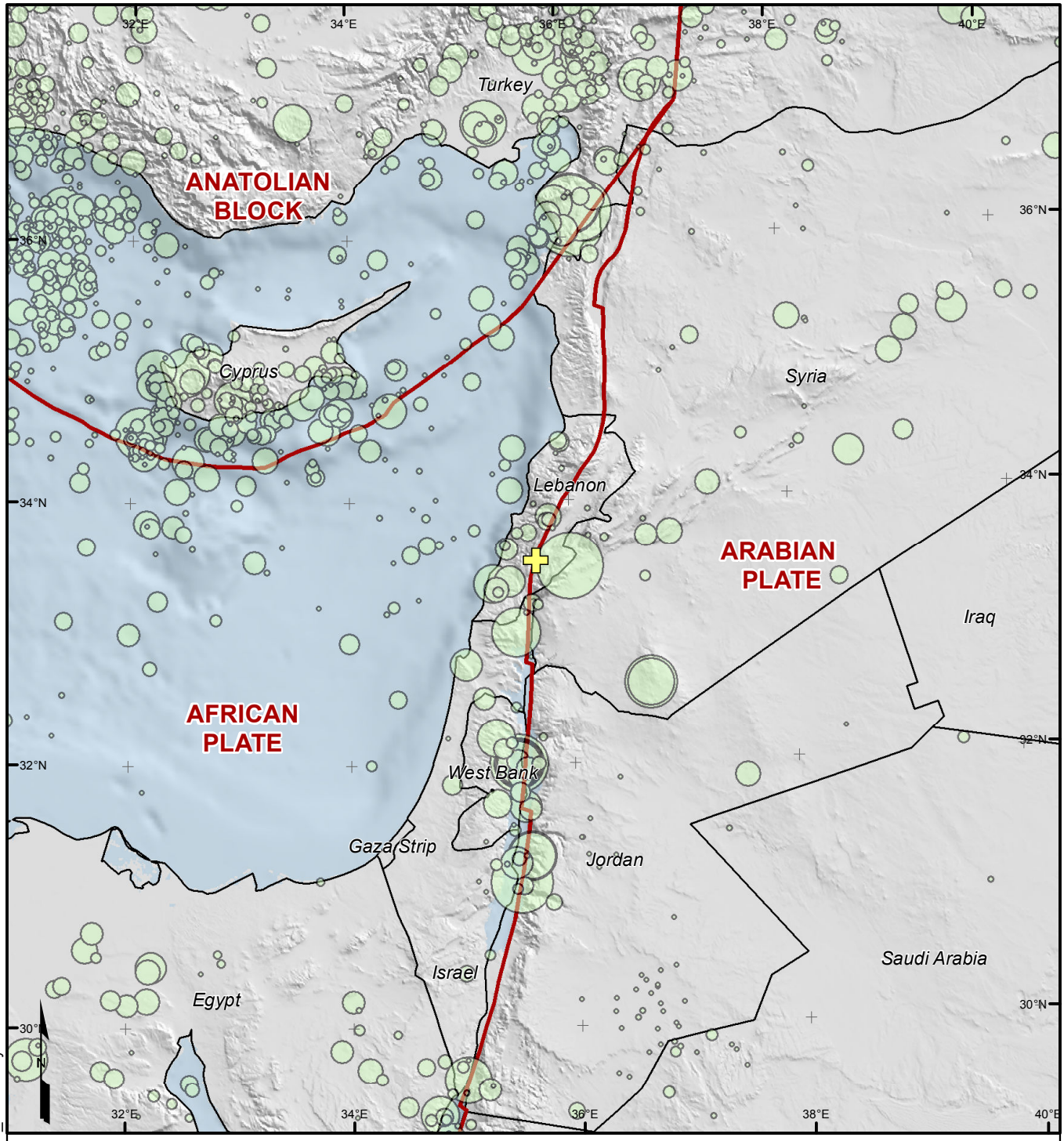

Explanation

Independent Seismicity (Magnitude > 3.5)

- 4.0
- 5.0
- 6.0
- 7.0

Plate boundary

0 50 100 200 Kilometers

INDEPENDENT SEISMICITY CATALOG
(2150 B.C. - A.D. 2011)
Qaraoun Dam Hazard Study
Litani River Basin, Lebanon

By: CJ	Date: 01/16/2012	Project No. OD11161570
amec		Figure 3-3

File path: S:\OD11\16157O\11_0816_mst23_fig_03_seismicity.mxd

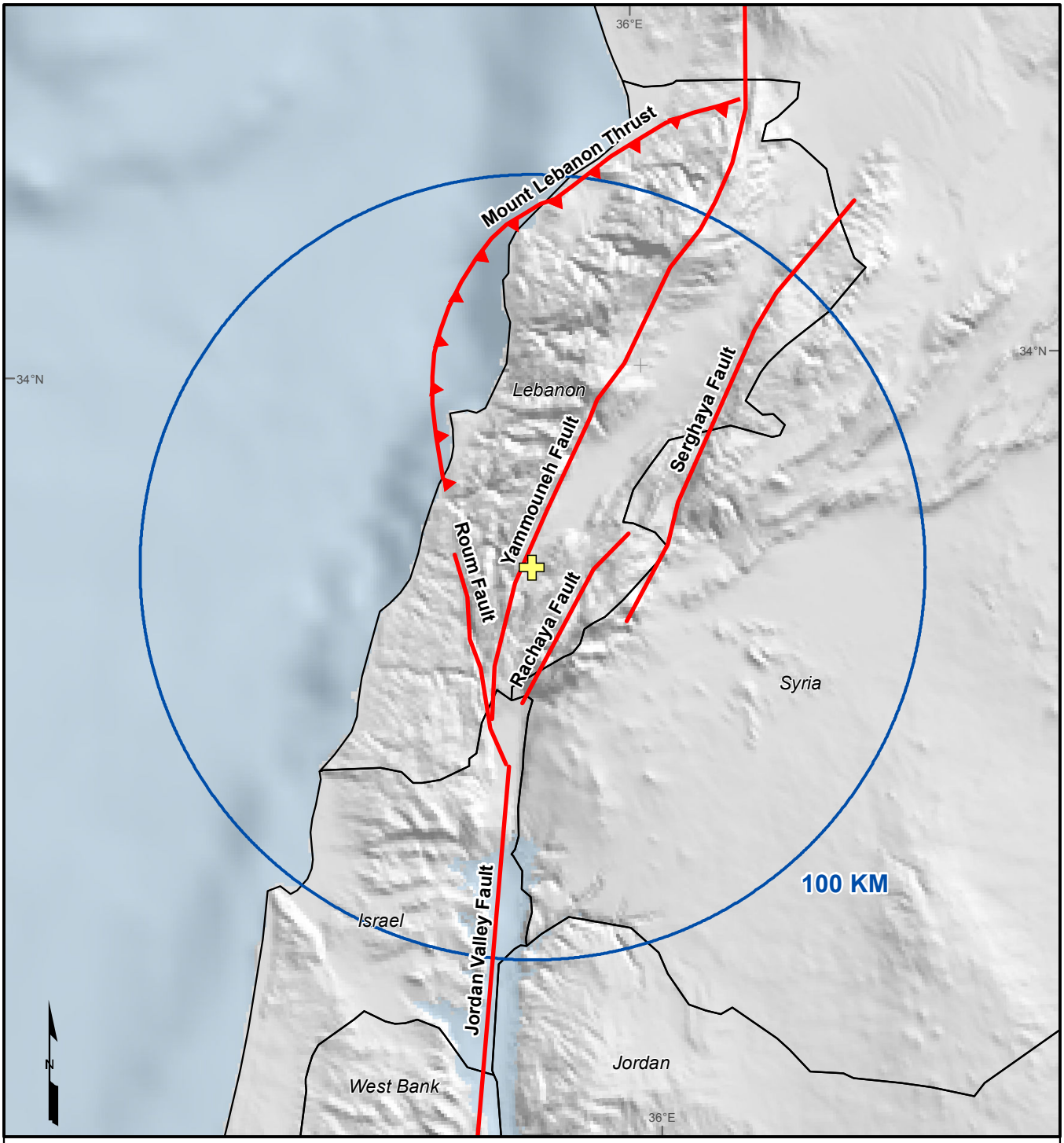

Explanation

Site Location

Strike-Slip Fault

Reverse Fault
(teeth on upthrown side)

0 25 50 100 Kilometers

SEISMIC SOURCE FAULTS WITHIN
100 KM OF THE SITE
Qaraoun Dam Hazard Study
Litani River Basin, Lebanon

By: CJ	Date: 01/16/2012	Project No. OD11161570
amec		Figure 3-4

File path: S:\OD11\16157O\11_0816_mst23_fig_04_faults.mxd

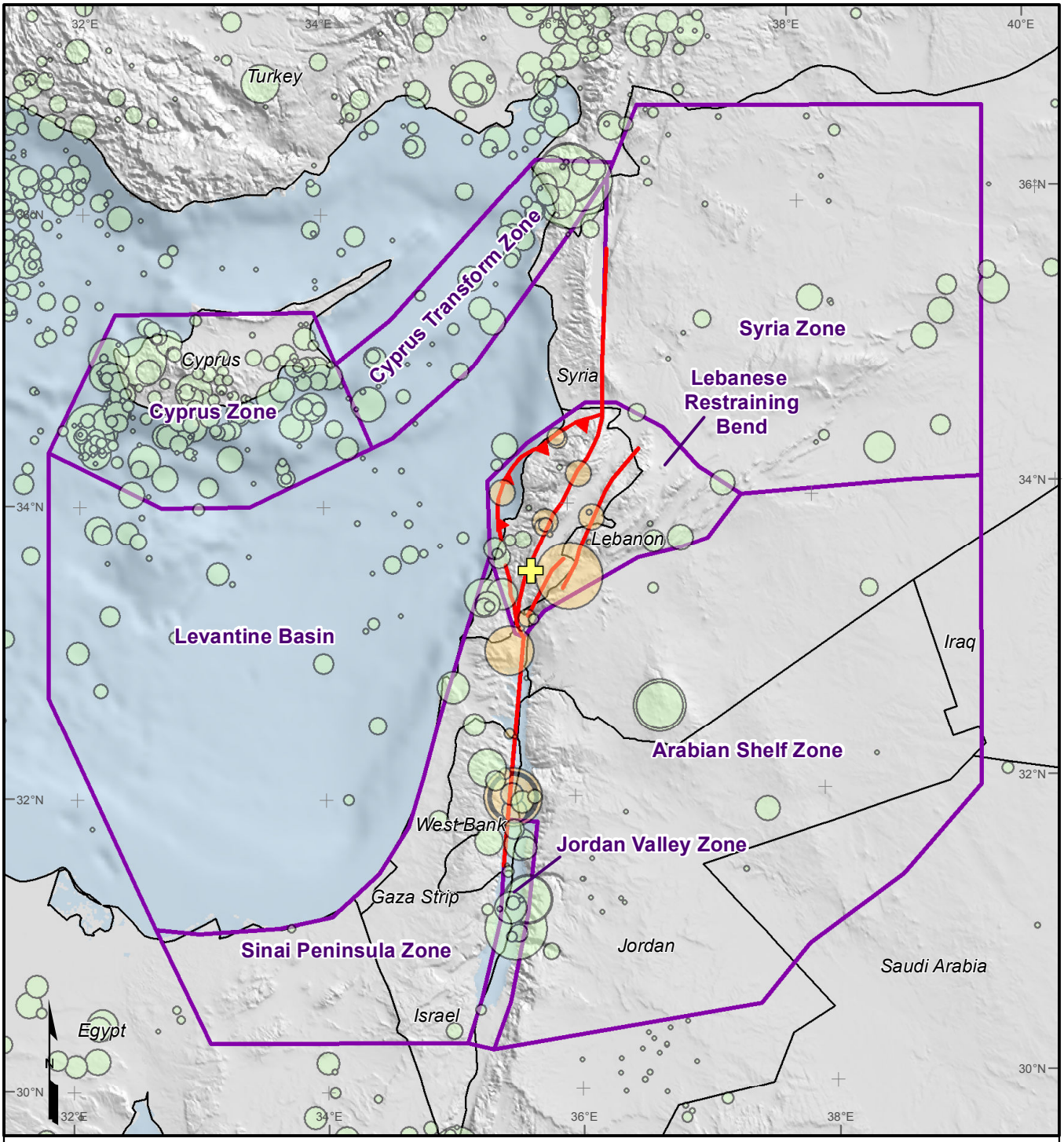

Explanation

- Site Location
- Earthquake on Fault
- Strike-Slip Fault
- Reverse Fault (teeth on upthrown side)

Independent Seismicity (Magnitude > 3.5)

- 4.0
- 5.0
- 6.0
- 7.0

0 50 100 200 Kilometers

CRUSTAL SEISMICITY (0-35 KM) AND AREAL SOURCE ZONES
Qaraoun Dam Hazard Study
Qaraoun Dam, Lebanon

By: CJ	Date: 01/16/2012	Project No. OD11161570
amec		Figure 3-5

File path: S:\OD11\16157O\11_0816_mst23_fig_05_zones.mxd

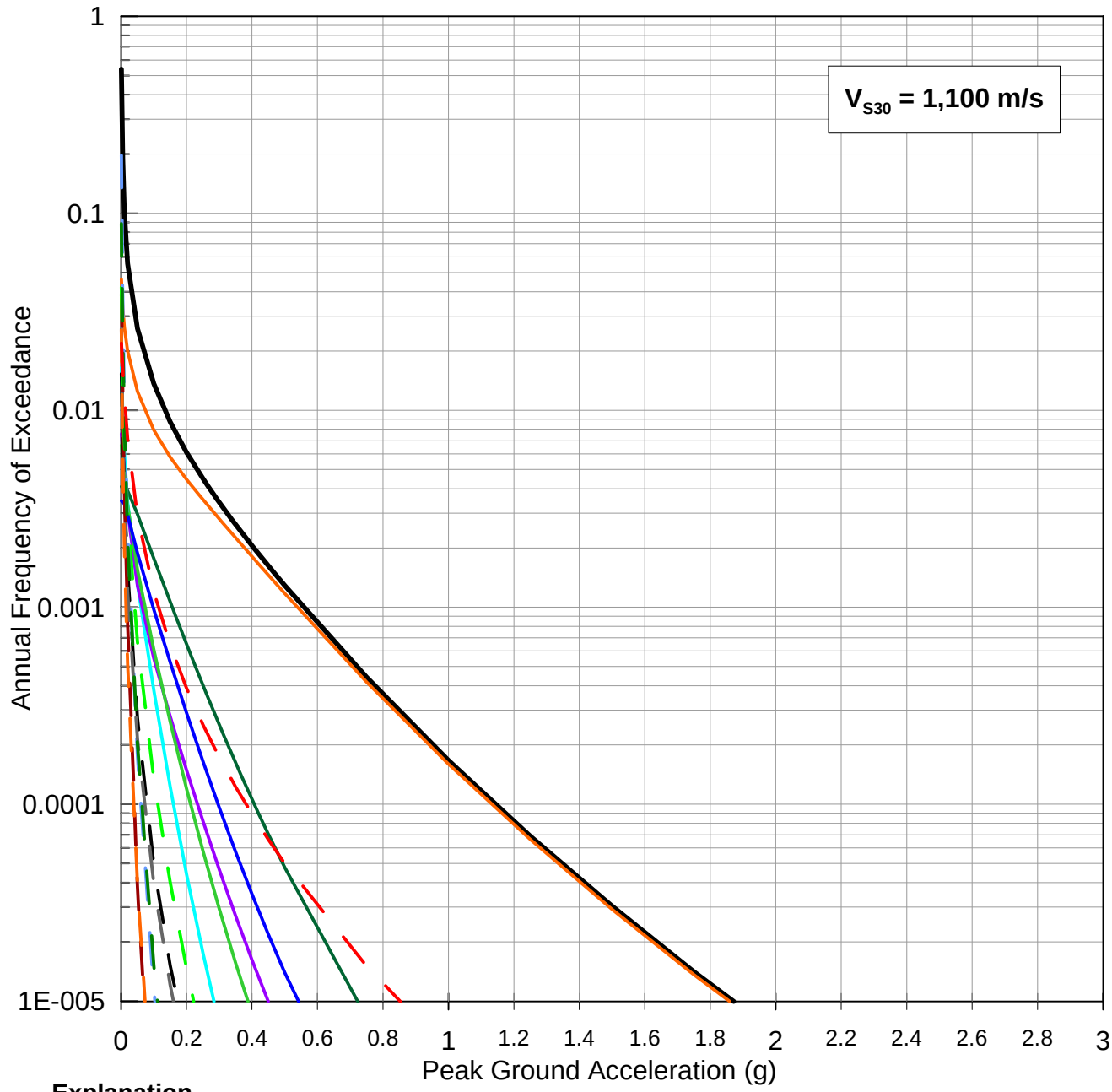

Explanation

Total

Crustal Faults
- Yammouneh
- Roum
- Rachaya
- Mount Lebanon Thrust
- Serghaya
- Jordan Valley

Areal Source Zones
- Levantine Basin
- Sinai Peninsula
- Syria
- Arabian Shelf

Areal Source Zones
- Lebanese Restraining Bend
- Jordan Valley
- Cyprus Transform
- Cyprus

PROBABILISTIC SEISMIC HAZARD ANALYSIS (PSHA) RESULTS AT PEAK GROUND ACCELERATION
Qaraoun Dam Hazard Study
Litani River Basin, Lebanon

By: DG	Date: 1/18/2012	Project No. OD11161570
AMEC Geomatrix		Figure 3-6

I:\Project\16000\OD11161570 - Qaraoun Dam\12000 CALCS EVALS ANALYSIS\Figures\rpt_figures

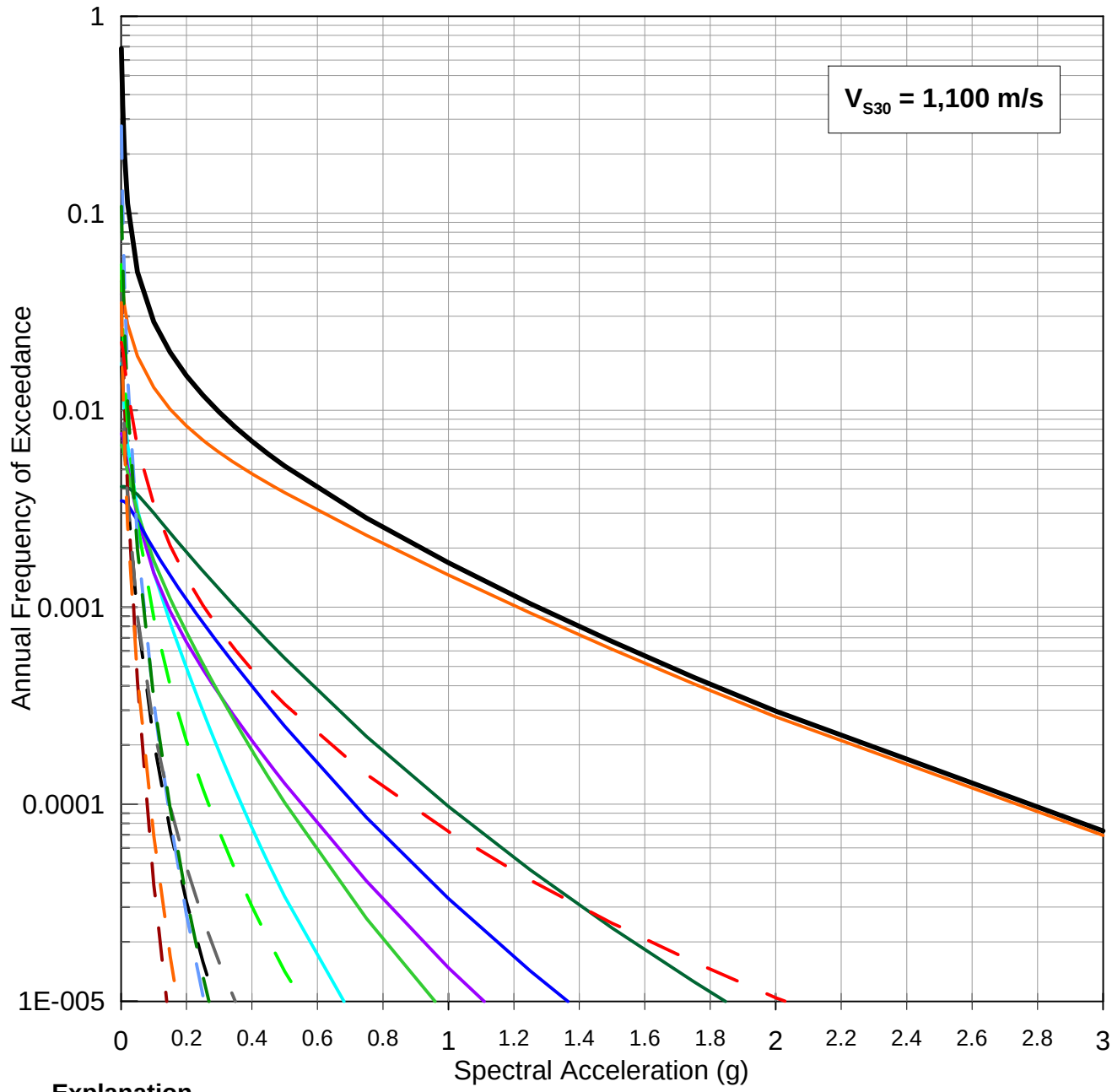

Explanation

Total

Crustal Faults
- Yammouneh
- Roum
- Rachaya
- Mount Lebanon Thrust
- Serghaya
- Jordan Valley

Areal Source Zones
- Levantine Basin
- Sinai Peninsula
- Syria
- Arabian Shelf

Areal Source Zones
- Lebanese Restraining Bend
- Jordan Valley
- Cyprus Transform
- Cyprus

PROBABILISTIC SEISMIC HAZARD ANALYSIS
(PSHA) RESULTS AT A PERIOD
OF 0.2 SECOND
Qaraoun Dam Hazard Study
Litani River Basin, Lebanon

By: DG	Date: 1/18/2012	Project No. OD11161570
AMEC Geomatrix		Figure **3-7**

I:\Project\16000\OD11161570 - Qaraoun Dam\12000 CALCS EVALS ANALYSIS\Figures\rpt_figures

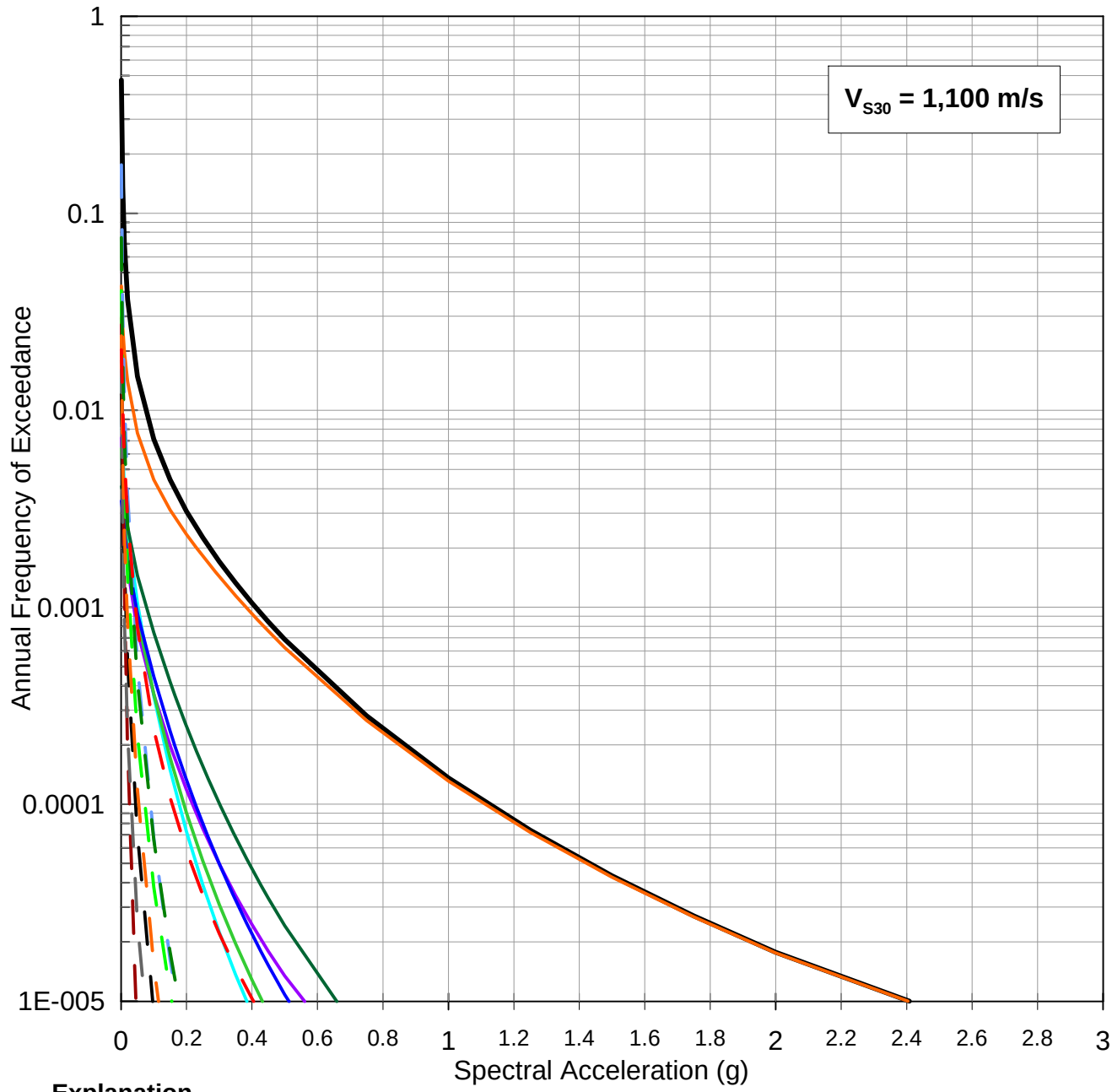

Explanation

Total

Crustal Faults
- Yammouneh
- Roum
- Rachaya
- Mount Lebanon Thrust
- Serghaya
- Jordan Valley

Areal Source Zones
- Levantine Basin
- Sinai Peninsula
- Syria
- Arabian Shelf

Areal Source Zones
- Lebanese Restraining Bend
- Jordan Valley
- Cyprus Transform
- Cyprus

PROBABILISTIC SEISMIC HAZARD ANALYSIS
(PSHA) RESULTS AT A PERIOD
OF 1.0 SECOND
Qaraoun Dam Hazard Study
Litani River Basin, Lebanon

By: DG	Date: 1/18/2012	Project No. OD11161570
AMEC Geomatrix		Figure **3-8**

I:\Project\16000\OD11161570 - Qaraoun Dam\12000 CALCS EVALS ANALYSIS\Figures\rpt_figures

V_{S30} = 1,100 m/s

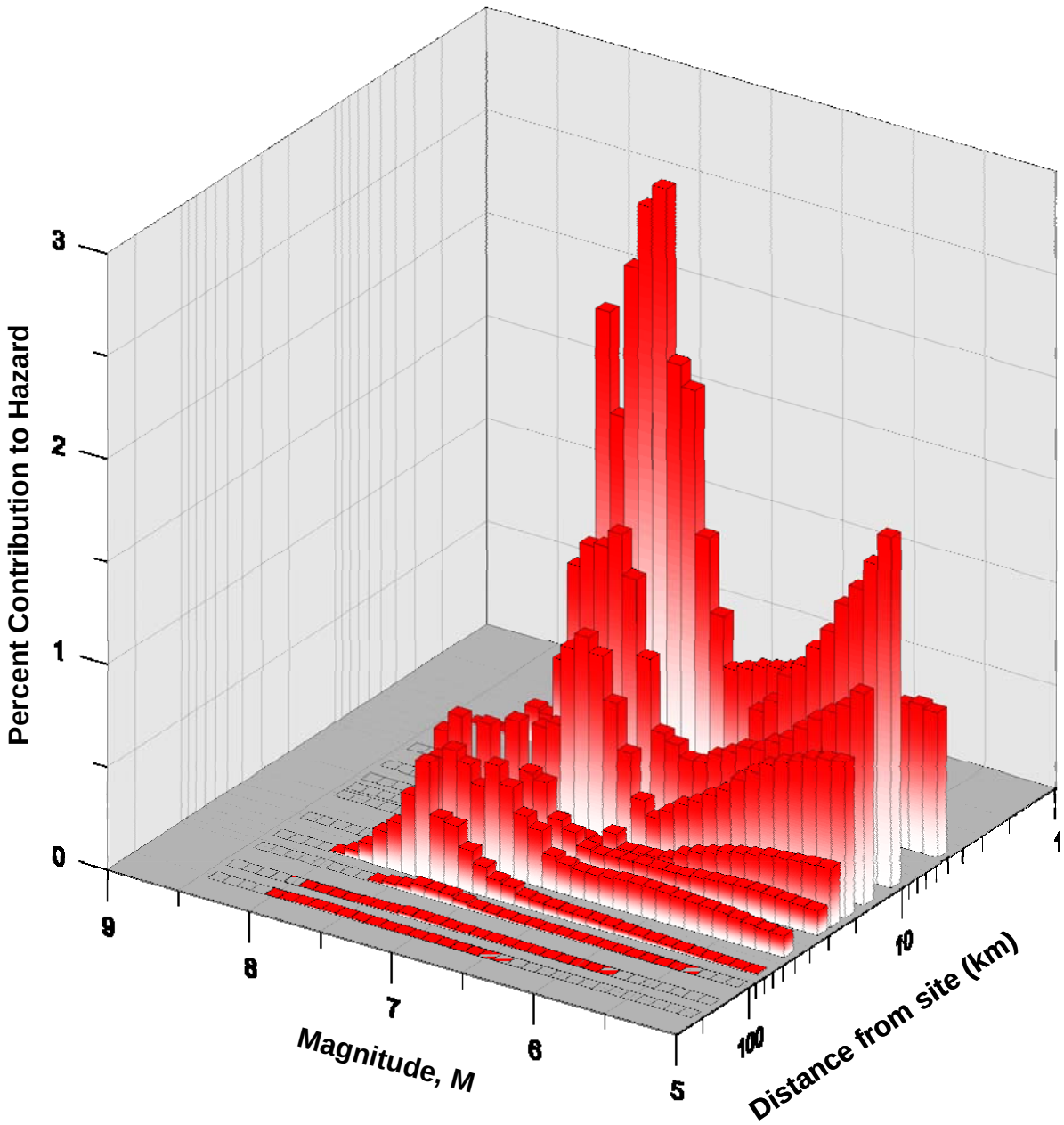

DEAGGREGATION OF PEAK GROUND ACCELERATION HAZARD FOR THE 100-YEAR RETURN PERIOD
Qaraoun Dam Hazard Study
Litani River Basin, Lebanon

By: DG	Date: 1/18/2012	Project No. OD11161570
AMEC Geomatrix		Figure 3-9a

I:\Project\16000\OD11161570 - Qaraoun Dam\12000 CALCS EVALS ANALYSIS\Figures\rpt_figures

V_{S30} = 1,100 m/s

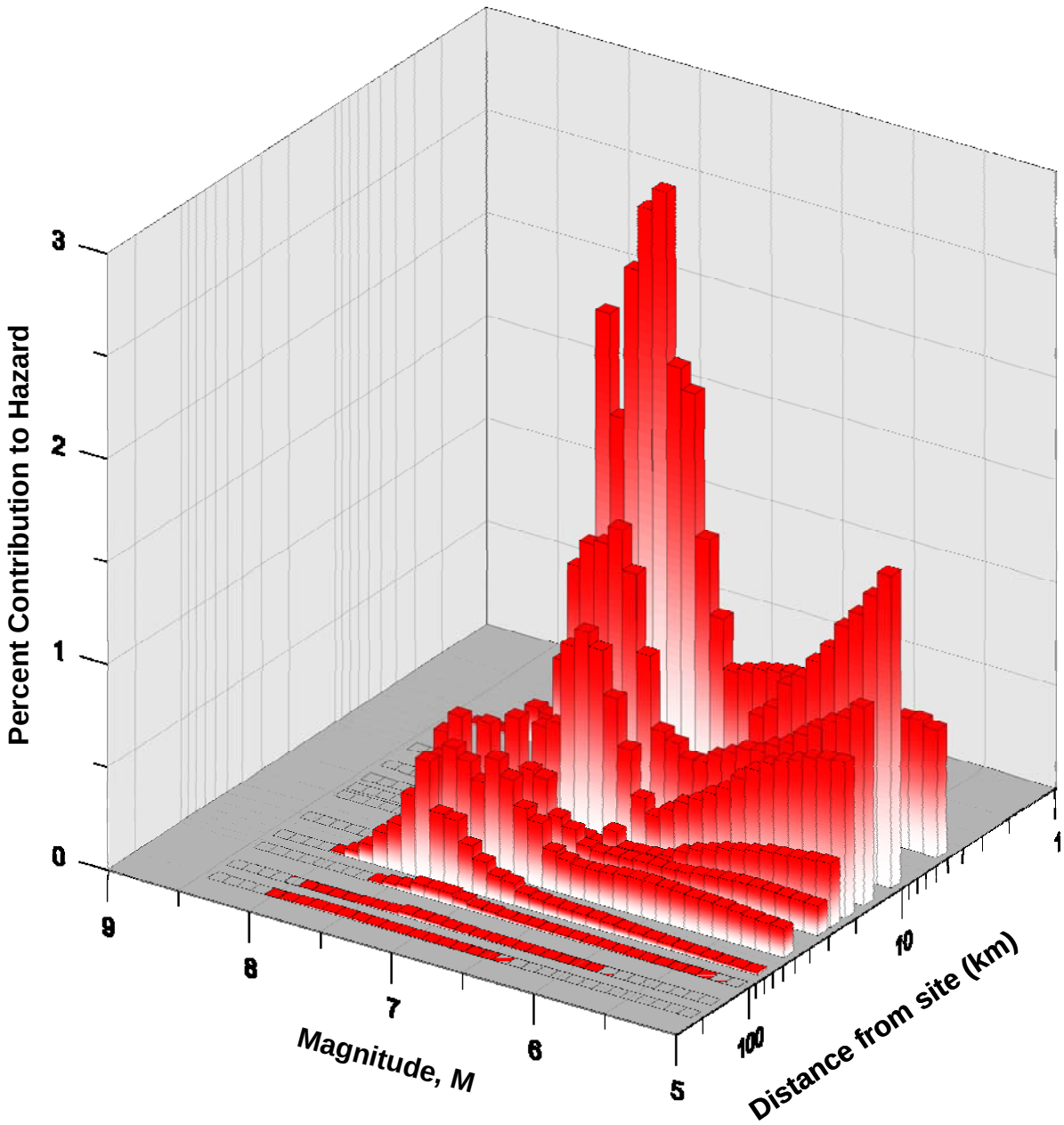

DEAGGREGATION OF 0.2 SECOND SPECTRAL ACCELERATION HAZARD FOR THE 100-YEAR RETURN PERIOD
Qaraoun Dam Hazard Study
Litani River Basin, Lebanon

By: DG	Date: 1/18/2012	Project No. OD11161570
AMEC Geomatrix		Figure 3-9b

I:\Project\16000\OD11161570 - Qaraoun Dam\12000 CALCS EVALS ANALYSIS\Figures\rpt_figures

V_{S30} = 1,100 m/s

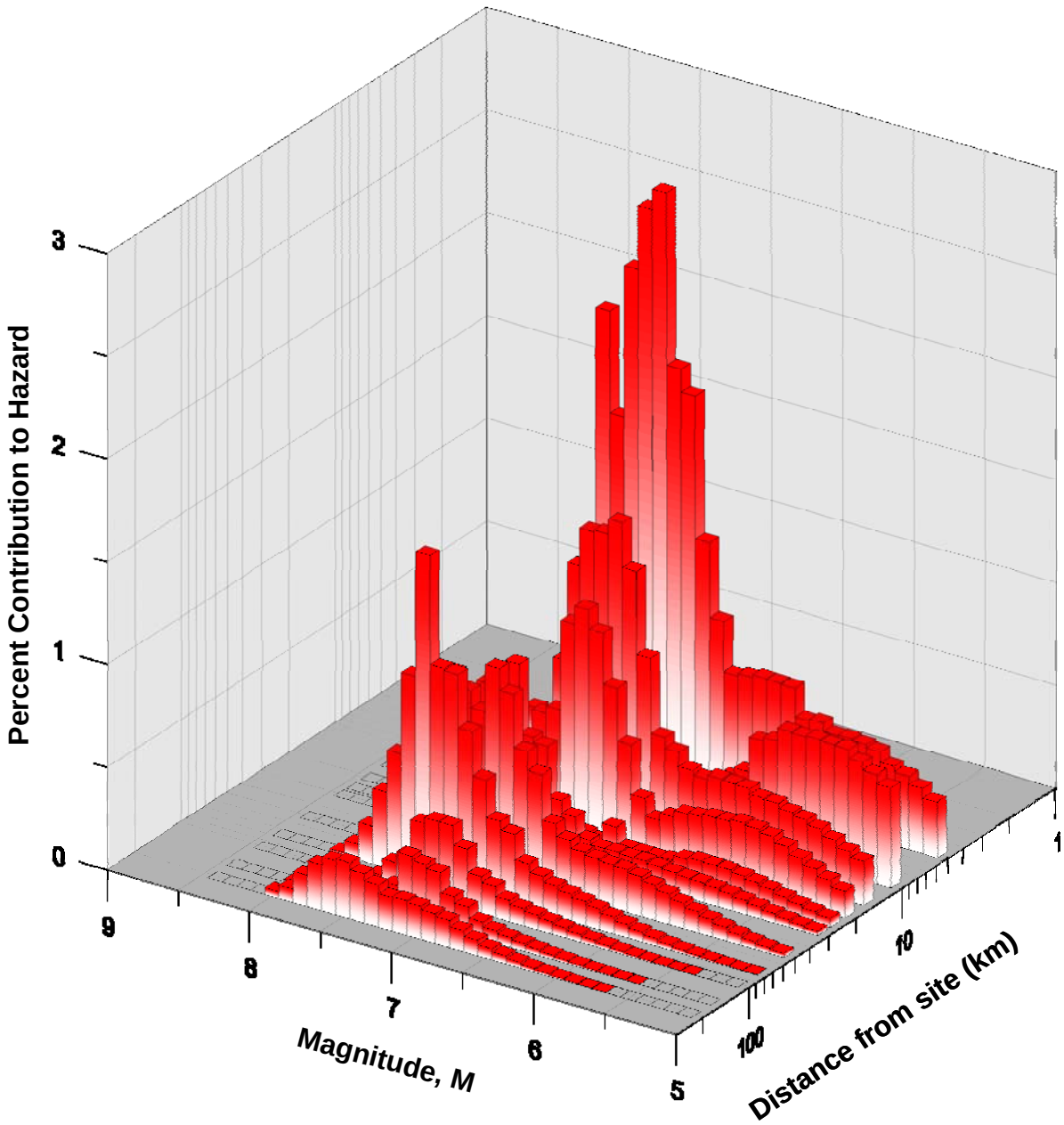

DEAGGREGATION OF 1.0 SECOND SPECTRAL ACCELERATION HAZARD FOR THE 100-YEAR RETURN PERIOD
Qaraoun Dam Hazard Study
Litani River Basin, Lebanon

By: DG	Date: 1/18/2012	Project No. OD11161570
AMEC Geomatrix		Figure 3-9c

I:\Project\16000\OD11161570 - Qaraoun Dam\12000 CALCS EVALS ANALYSIS\Figures\rpt_figures

V_{S30} = 1,100 m/s

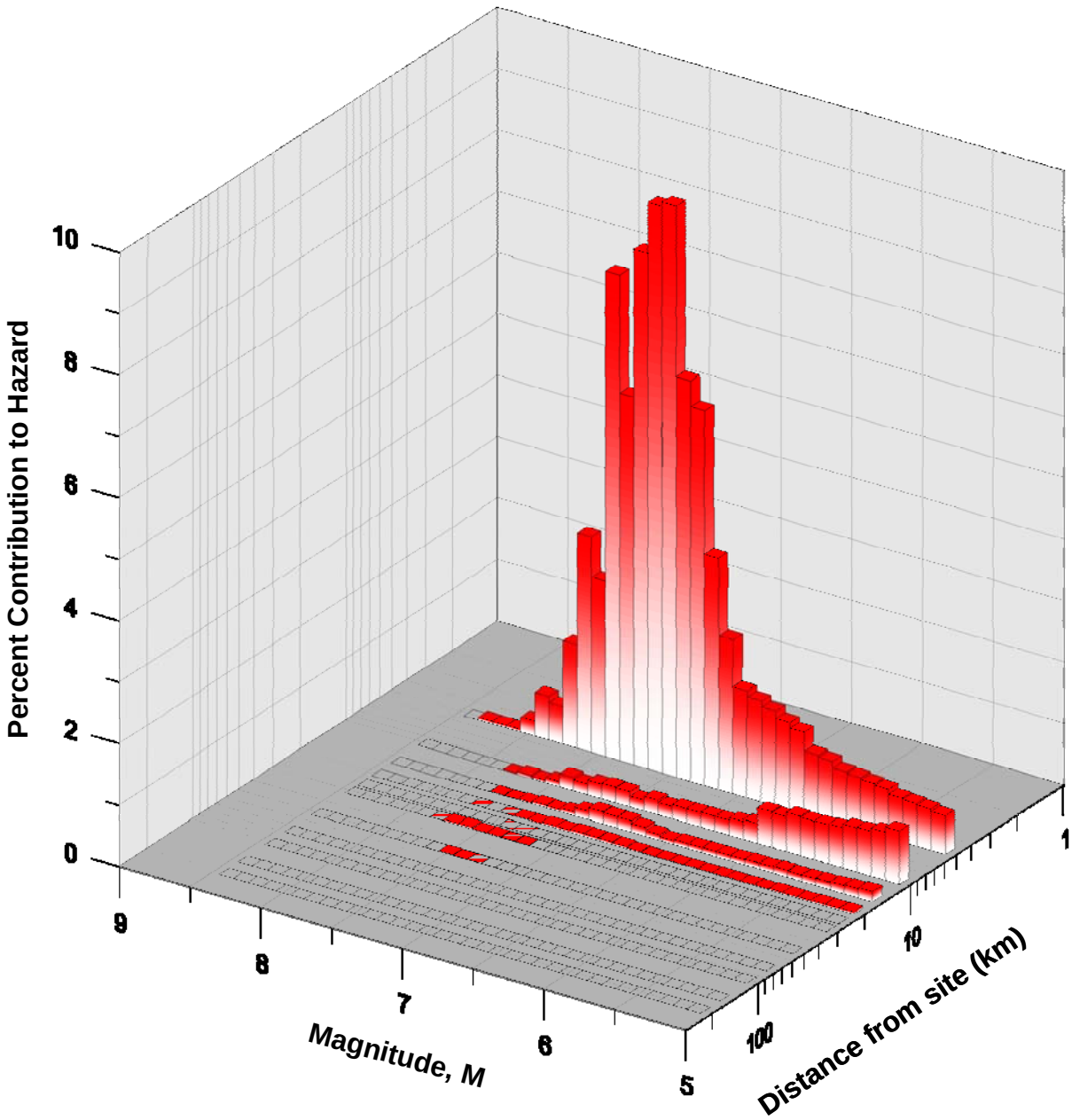

DEAGGREGATION OF PEAK GROUND ACCELERATION HAZARD FOR THE 10,000-YEAR RETURN PERIOD
Qaraoun Dam Hazard Study
Litani River Basin, Lebanon

By: DG	Date: 1/18/2012	Project No. OD11161570
AMEC Geomatrix		Figure 3-9d

I:\Project\16000\OD11161570 - Qaraoun Dam\12000 CALCS EVALS ANALYSIS\Figures\rpt_figures

V_{S30} = 1,100 m/s

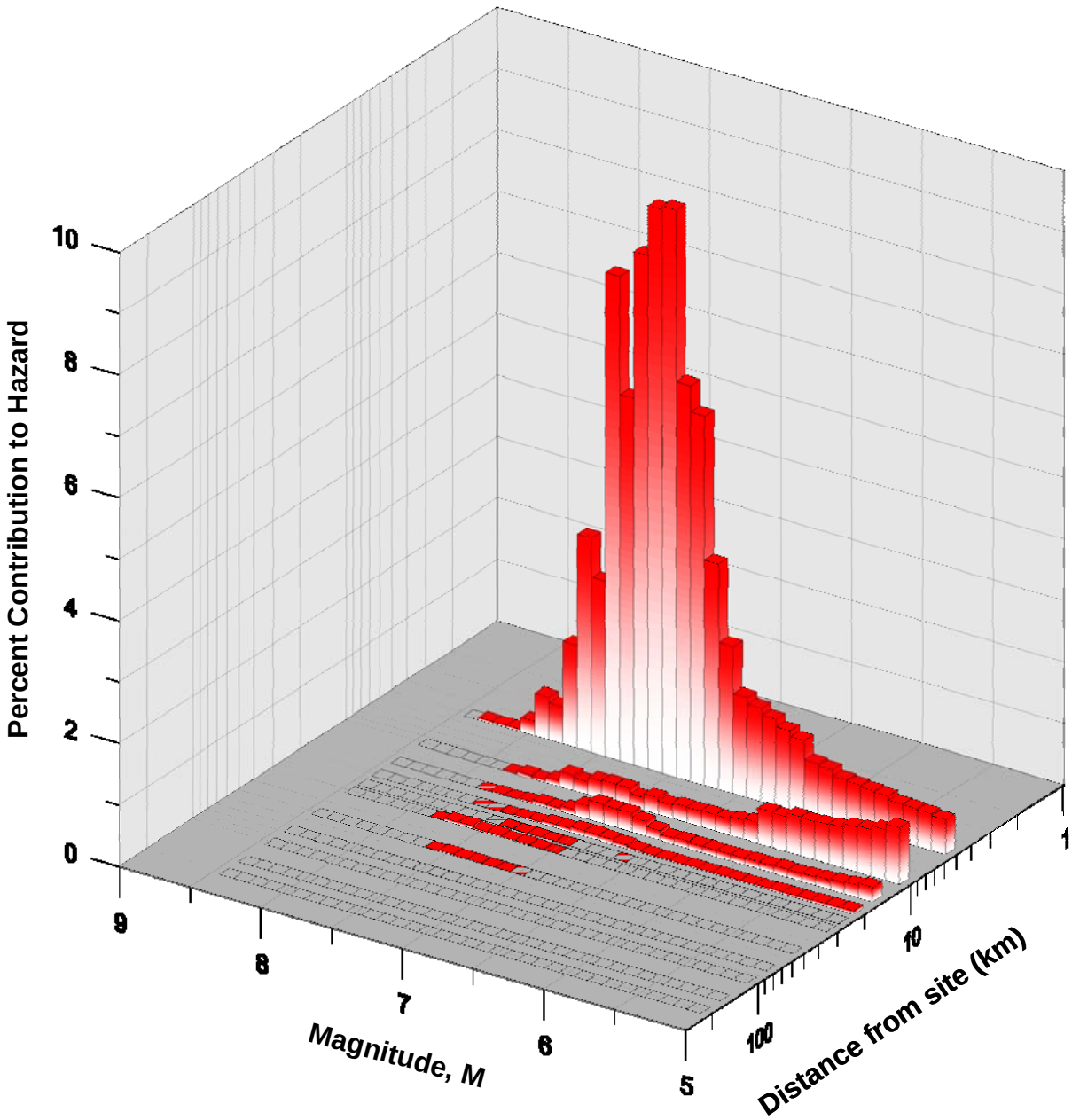

DEAGGREGATION OF 0.2 SECOND SPECTRAL ACCELERATION HAZARD FOR THE 10,000-YEAR RETURN PERIOD
Qaraoun Dam Hazard Study
Litani River Basin, Lebanon

By: DG	Date: 1/18/2012	Project No. OD11161570
AMEC Geomatrix		Figure 3-9e

I:\Project\16000\OD11161570 - Qaraoun Dam\12000 CALCS EVALS ANALYSIS\Figures\rpt_figures

V_{S30} = 1,100 m/s

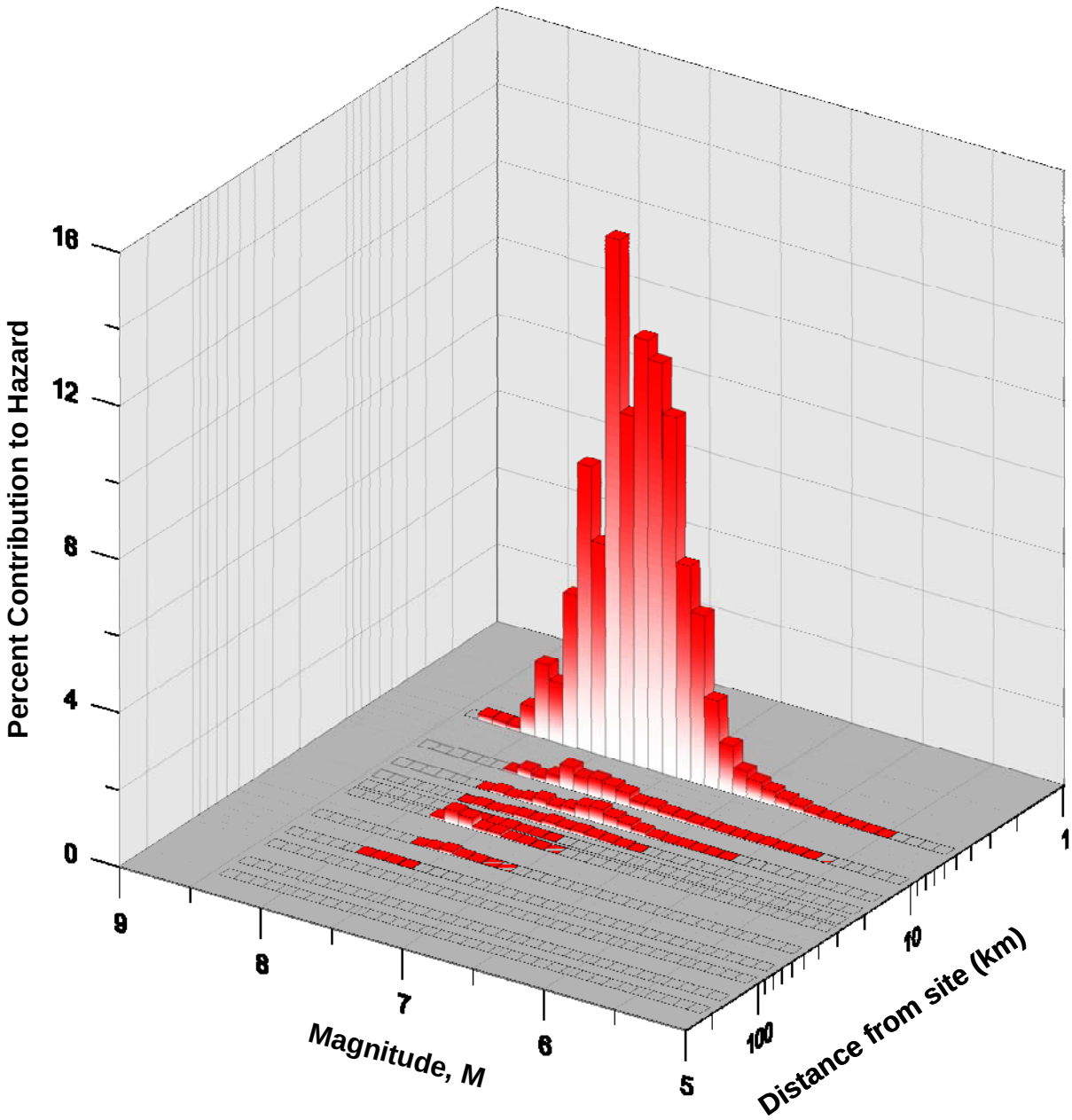

DEAGGREGATION OF 1.0 SECOND SPECTRAL ACCELERATION HAZARD FOR THE 10,000-YEAR RETURN PERIOD
Qaraoun Dam Hazard Study
Litani River Basin, Lebanon

By: DG	Date: 1/18/2012	Project No. OD11161570
AMEC Geomatrix		Figure 3-9f

I:\Project\16000\OD11161570 - Qaraoun Dam\12000 CALCS EVALS ANALYSIS\Figures\rpt_figures

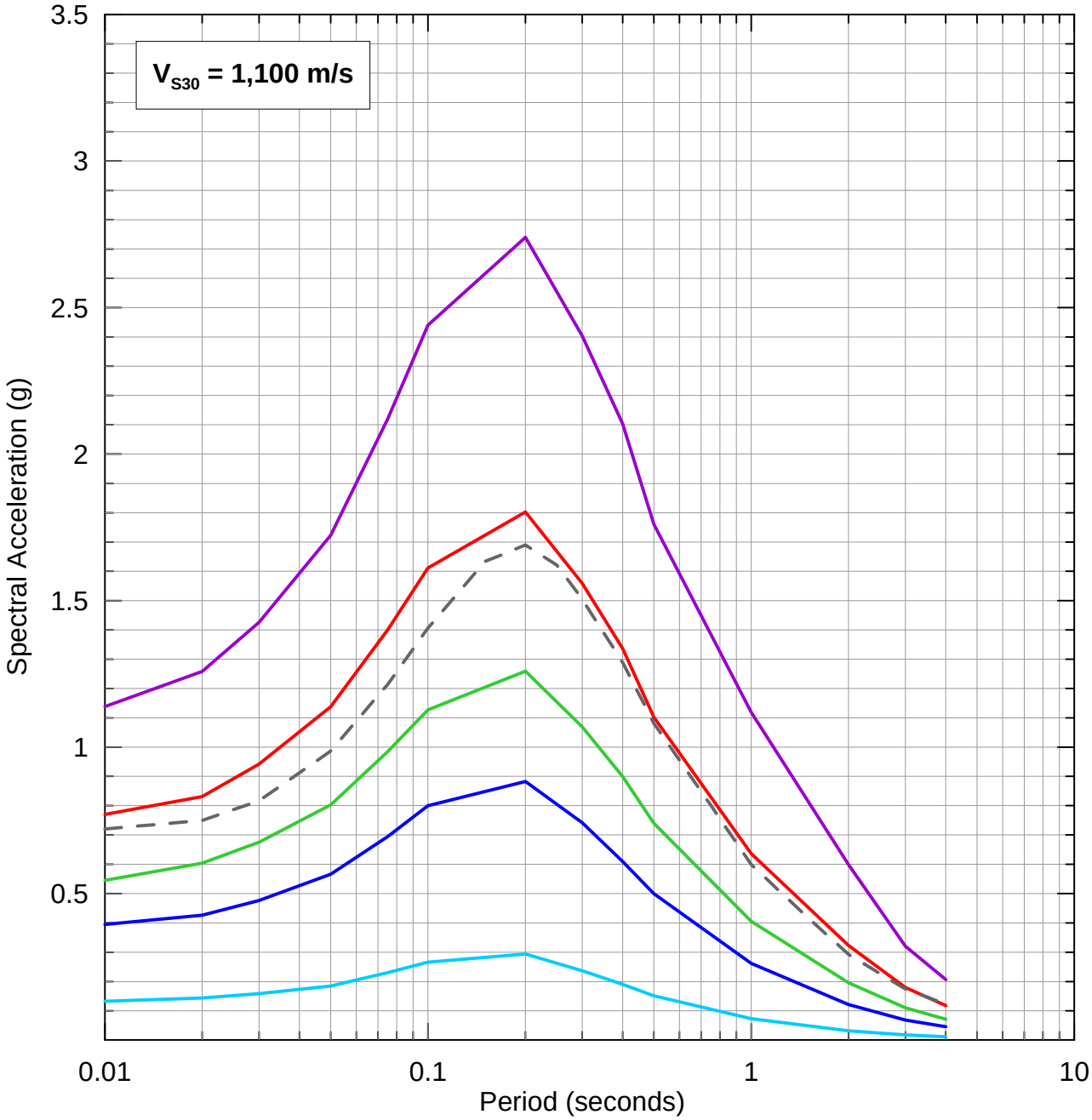

Note:
1. Spectra are five-percent damped.

Explanation

- 10,000 RP - 0.5% in 50 Years
- 2475 RP - 2% in 50 Years
- 975 RP - 5% in 50 Years
- 475 RP - 10% in 50 Years
- 100 RP - 39.5% in 50 Years
- Yammouneh Fault M 7.2 at 2.4 km 84th Percentile Deterministic

UNIFORM HAZARD SPECTRA
Qaraoun Dam Hazard Study
Litani River Basin, Lebanon

By: DG	Date: 1/18/2012	Project No. OD11161570
AMEC Geomatrix		Figure 3-10

I:\Project\16000\OD11161570 - Qaraoun Dam\12000 CALCS EVALS ANALYSIS\Figures\rpt_figures

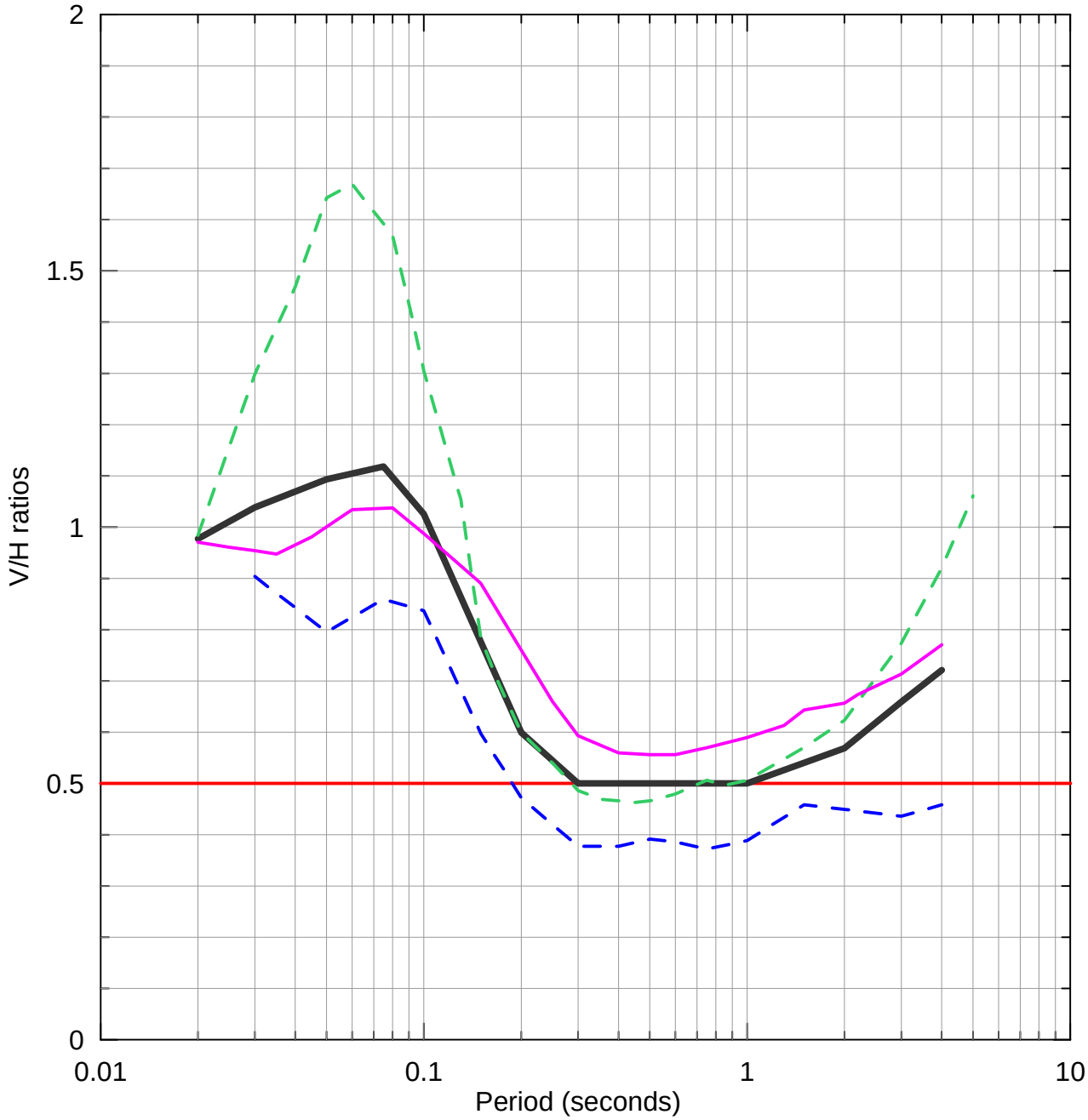

Explanation

- Final V/H (Mean of 3 relationships)
- Abrahamson & Silva (1997) Rock
- Campbell & Bozorgnia (2003) Firm Rock
- Sadigh et. al (1993) Rock
- 0.5

SPECTRAL ACCELERATION V/H RATIOS
Qaraoun Dam Hazard Study
Litani River Basin, Lebanon

By: DG	Date: 1/18/2012	Project No. OD11161570
AMEC Geomatrix		Figure **3-11**

I:\Project\16000\OD11161570 - Qaraoun Dam\12000 CALCS EVALS ANALYSIS\Figures\rpt_figures

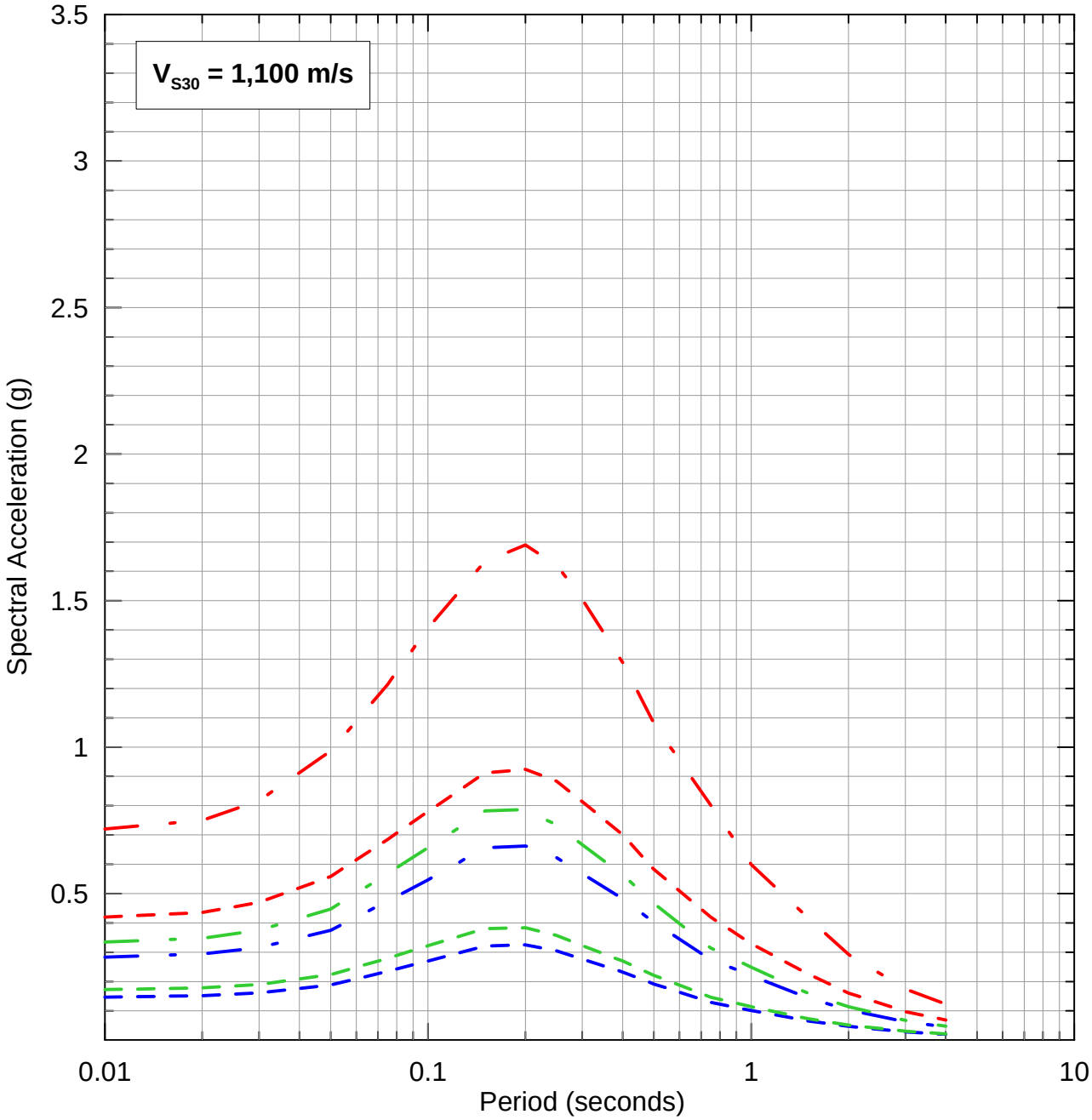

Explanation

- Yammouneh Fault M 7.2 at 2.4 km 50th Percentile
- Yammouneh Fault M 7.2 at 2.4 km 84th Percentile
- Rachaya Fault M 6.8 at 14 km 50th Percentile
- Rachaya Fault M 6.8 at 14 km 84th Percentile
- Roum Fault M 6.9 at 18 km 50th Percentile
- Roum Fault M 6.9 at 18 km 84th Percentile

Note:
1. Spectra are five-percent damped.

MEDIAN AND 84TH PERCENTILE HORIZONTAL DETERMINISTIC RESPONSE SPECTRA FOR CONTRIBUTING SOURCES
Qaraoun Dam Hazard Study
Litani River Basin, Lebanon

By: DG	Date: 6/3/2011	Project No. OD11161570
AMEC Geomatrix		Figure 3-12

I:\Project\16000\OD11161570 - Qaraoun Dam\12000 CALCS EVALS ANALYSIS\Figures\rpt_figures

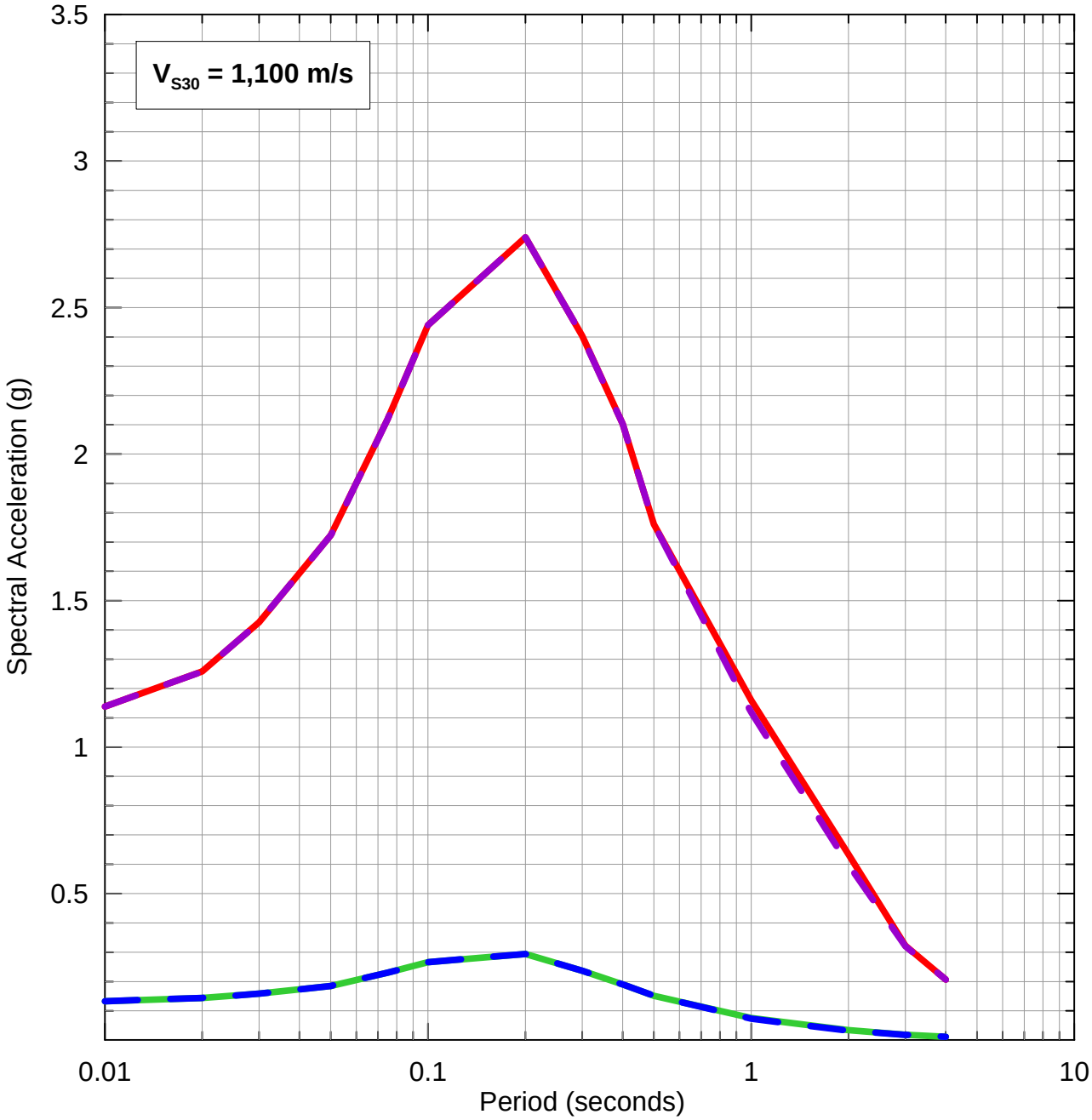

Note:
1. Spectra are five-percent damped.

Explanation

- 10,000 RP - 0.5% in 50 Years
- 10,000 RP - 0.5% in 50 Years Adjusted for Fault Parallel Near-Fault Directivity
- 100 RP - 39.5% in 50 Years Adjusted for Fault Parallel Near-Fault Directivity
- 100 RP - 39.5% in 50 Years

UNIFORM HAZARD SPECTRA ADJUSTED FOR FAULT PARALLEL NEAR-FAULT DIRECTIVITY FOR THE 100- AND 10,000-YEAR RETURN PERIODS
Qaraoun Dam Hazard Study
Litani River Basin, Lebanon

By: DG	Date: 1/18/2012	Project No. OD11161570
AMEC Geomatrix		Figure 3-13

I:\Project\16000\OD11161570 - Qaraoun Dam\12000 CALCS EVALS ANALYSIS\Figures\rpt_figures

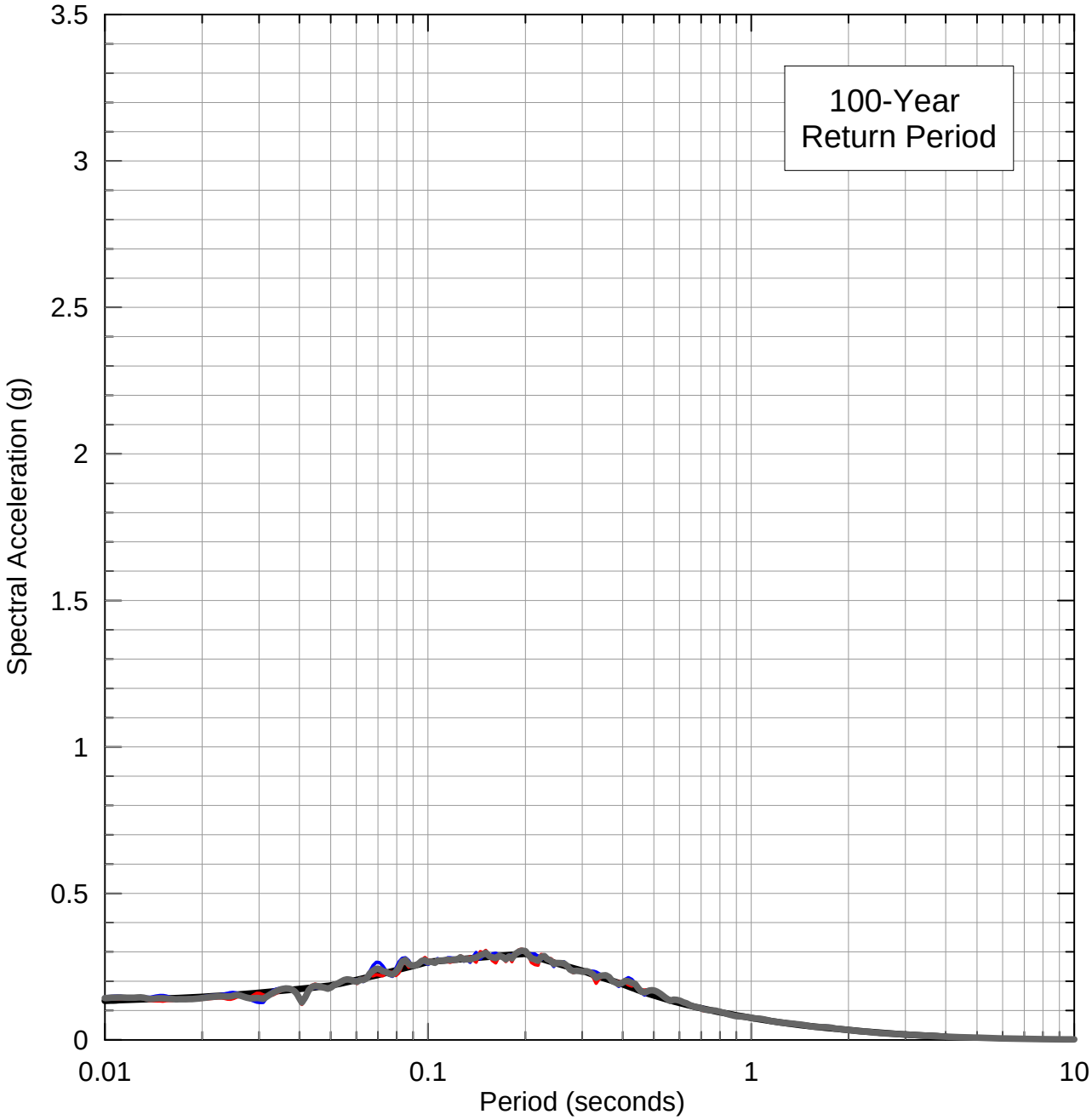

100-Year Horizontal Uniform Hazard Response Spectrum (UHRS) Adjusted for Near-Fault Directivity

Geometric Mean of Selected Records

Loma Prieta - SJ Santa Teresa Hills

Tabas - Dayhook

Notes:
1. Period range of interest for scaling is PGA (0.01) to 4.0 seconds.
2. Spectra are five-percent damped.

COMPARISON OF SPECTRA FOR HORIZONTAL MODIFIED TIME HISTORIES TO TARGET SPECTRUM FOR 100-YEAR RETURN PERIOD
Qaraoun Dam Hazard Study
Litani River Basin, Lebanon

DG	Date: 1/18/2012	Project No. OD11161570
AMEC Geomatrix		Figure 3-14a

I:\Project\16000\OD11161570 - Qaraoun Dam\12000 CALCS EVALS ANALYSIS\Figures\rpt_figures

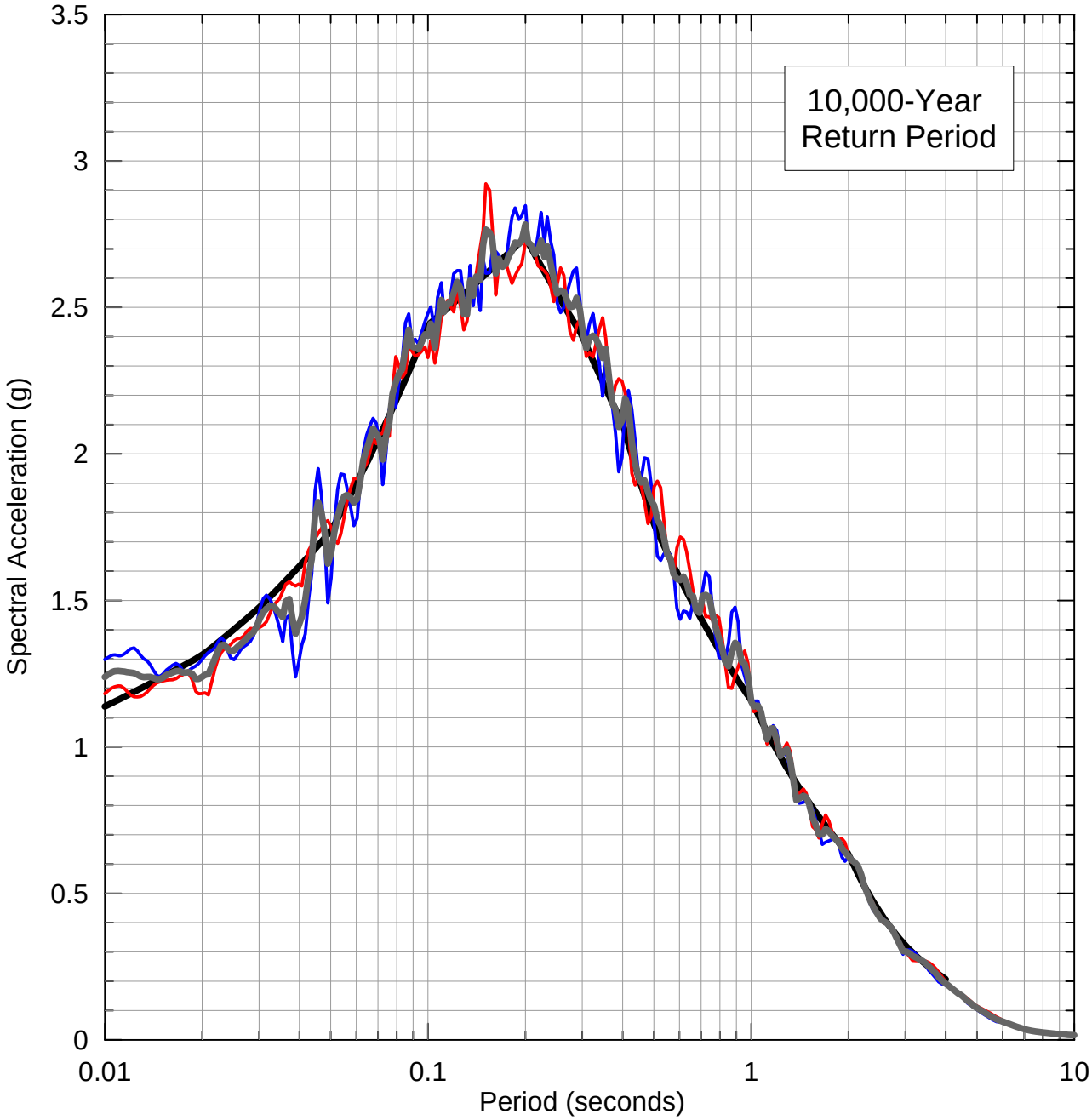

10,000-Year Horizontal Uniform Hazard Response Spectrum (UHRS) Adjusted for Near-Fault Directivity

Hector Mine - Hector

Tabas - Tabas

Geometric Mean of Selected Records

Notes:
1. Period range of interest for scaling is PGA (0.01) to 4.0 seconds.
2. Spectra are five-percent damped.

COMPARISON OF SPECTRA FOR HORIZONTAL MODIFIED TIME HISTORIES TO TARGET SPECTRUM FOR 10,000-YEAR RETURN PERIOD
Qaraoun Dam Hazard Study
Litani River Basin, Lebanon

By: DG	Date: 1/18/2012	Project No. OD11161570
AMEC Geomatrix		Figure 3-14b

I:\Project\16000\OD11161570 - Qaraoun Dam\12000 CALCS EVALS ANALYSIS\Figures\rpt_figures

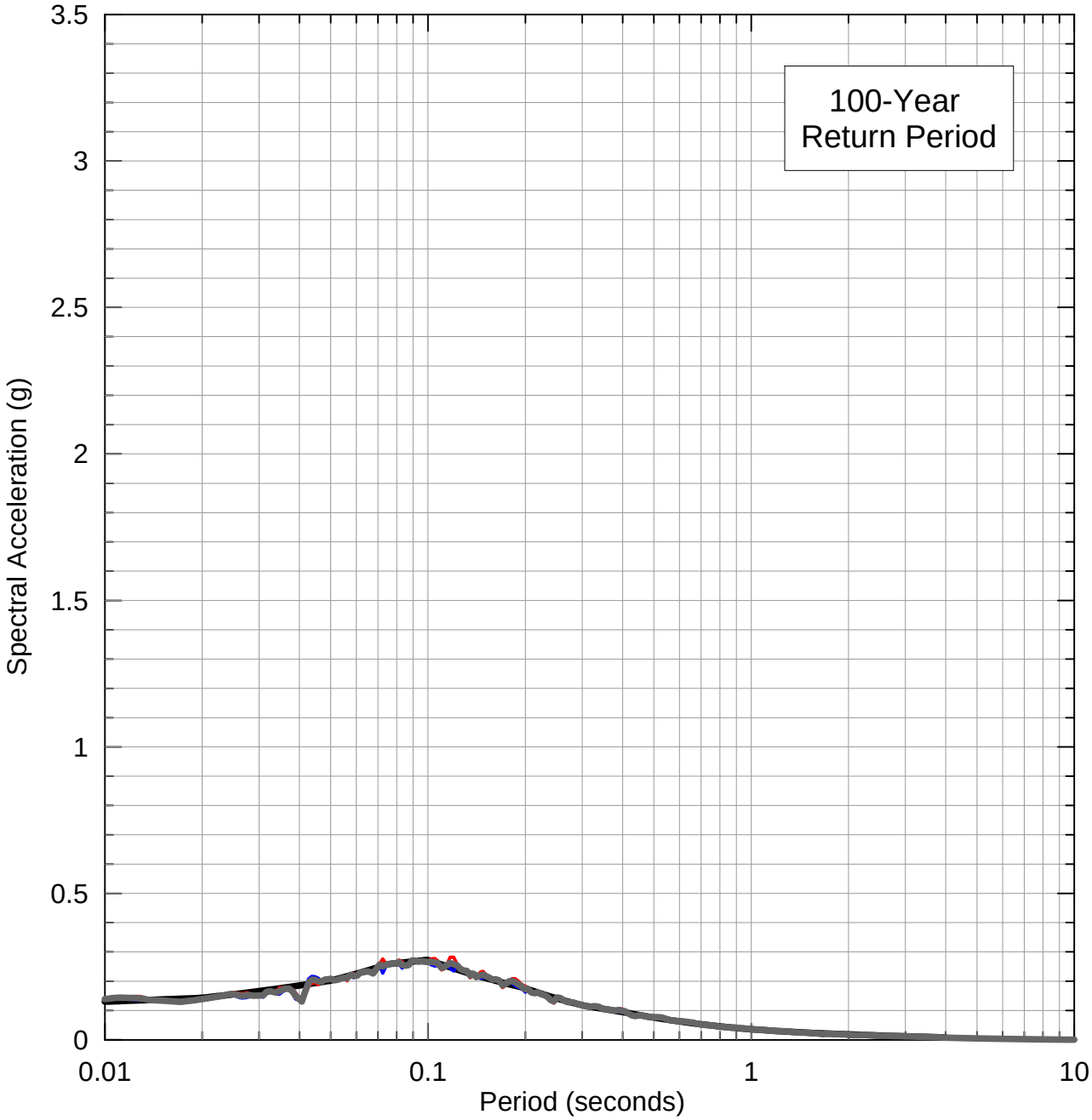

100-Year Vertical Uniform Hazard Response Spectrum (UHRS) Adjusted for Near-Fault Directivity

Geometric Mean of Selected Records

Loma Prieta - SJ Santa Teresa Hills

Tabas - Dayhook

Notes:
1. Period range of interest for scaling is PGA (0.01) to 4.0 seconds.
2. Spectra are five-percent damped.

COMPARISON OF SPECTRA FOR VERTICAL MODIFIED TIME HISTORIES TO TARGET SPECTRUM FOR 100-YEAR RETURN PERIOD
Qaraoun Dam Hazard Study
Litani River Basin, Lebanon

By: DG	Date: 1/18/2012	Project No. OD11161570
AMEC Geomatrix		Figure **3-15a**

I:\Project\16000\OD11161570 - Qaraoun Dam\12000 CALCS EVALS ANALYSIS\Figures\rpt_figures

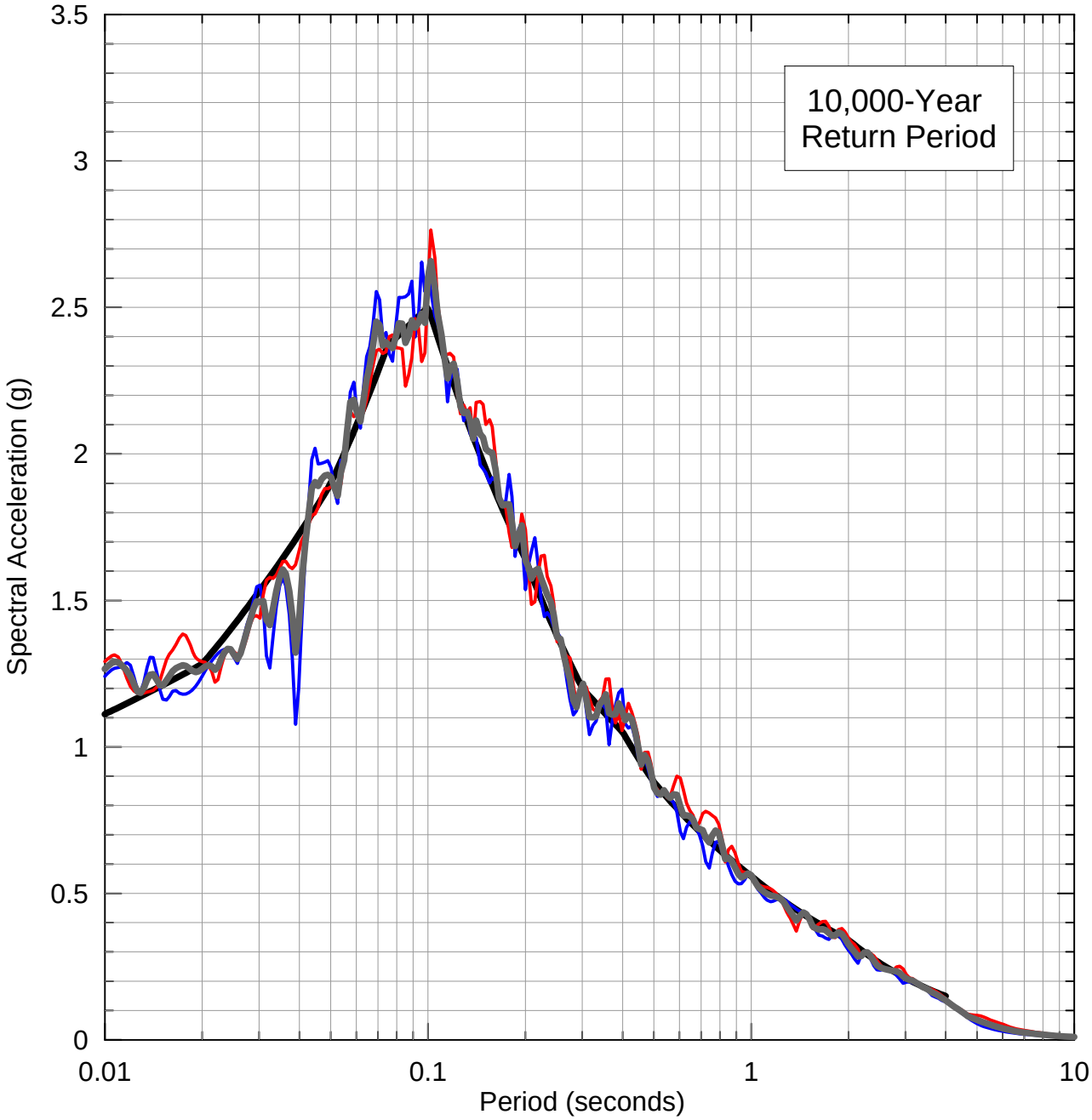

10,000-Year Vertical Uniform Hazard Response Spectrum (UHRS) Adjusted for Near-Fault Directivity

Hector Mine - Hector

Tabas - Tabas

Geometric Mean of Selected Records

Notes:
1. Period range of interest for scaling is PGA (0.01) to 4.0 seconds.
2. Spectra are five-percent damped.

COMPARISON OF SPECTRA FOR VERTICAL MODIFIED TIME HISTORIES TO TARGET SPECTRUM FOR 10,000-YEAR RETURN PERIOD
Qaraoun Dam Hazard Study
Litani River Basin, Lebanon

By: DG	Date: 1/18/2012	Project No. OD11161570
AMEC Geomatrix		Figure 3-15b

I:\Project\16000\OD11161570 - Qaraoun Dam\12000 CALCS EVALS ANALYSIS\Figures\rpt_figures

V_{S30} = 1,100 m/s

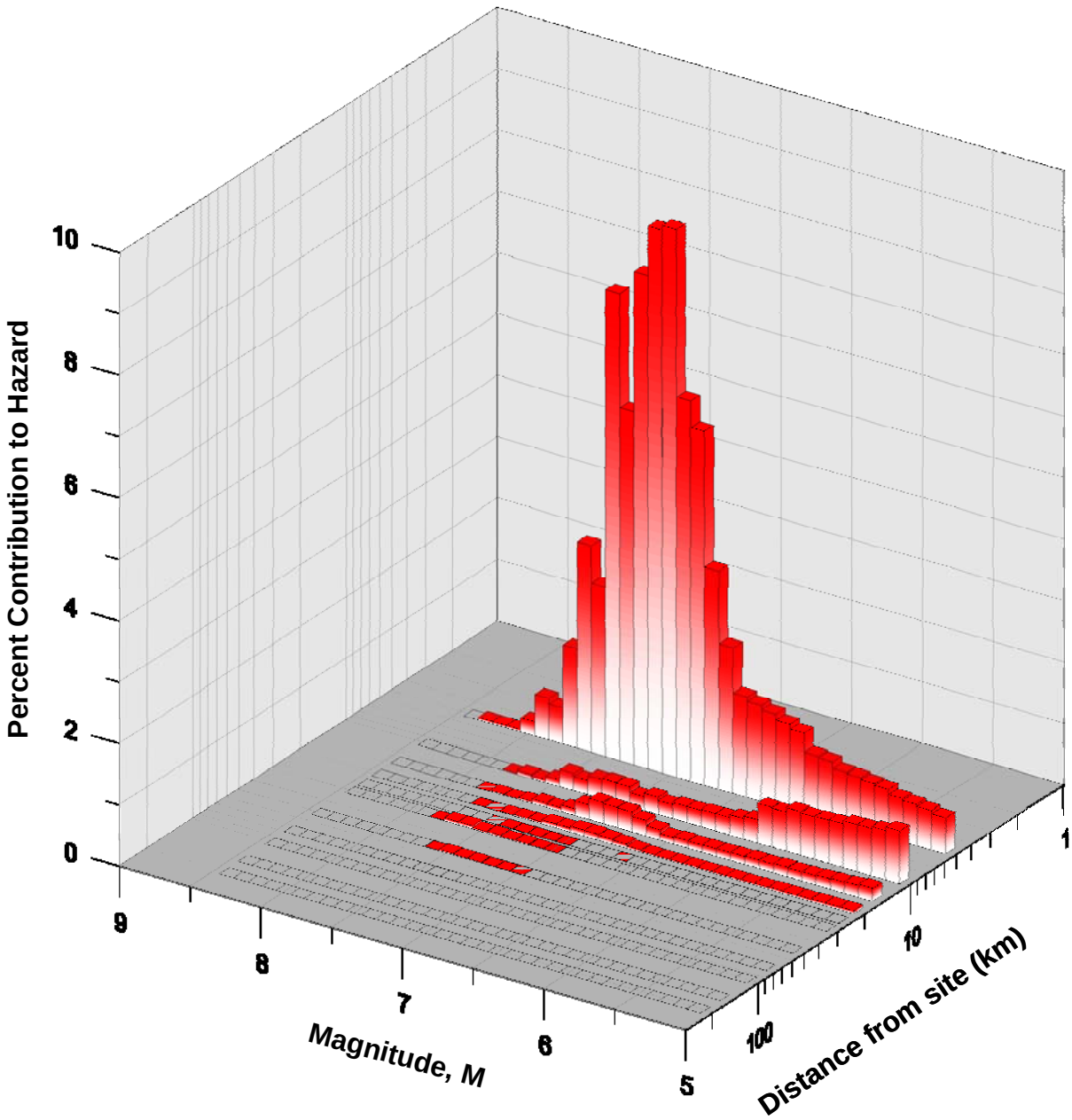

DEAGGREGATION OF PEAK GROUND ACCELERATION HAZARD FOR THE 2,475-YEAR RETURN PERIOD
Qaraoun Dam Hazard Study
Litani River Basin, Lebanon

By: DG	Date: 1/18/2012	Project No. OD11161570
AMEC Geomatrix		Figure 3-16a

I:\Project\16000\OD11161570 - Qaraoun Dam\12000 CALCS EVALS ANALYSIS\Figures\rpt_figures

V_{S30} = 1,100 m/s

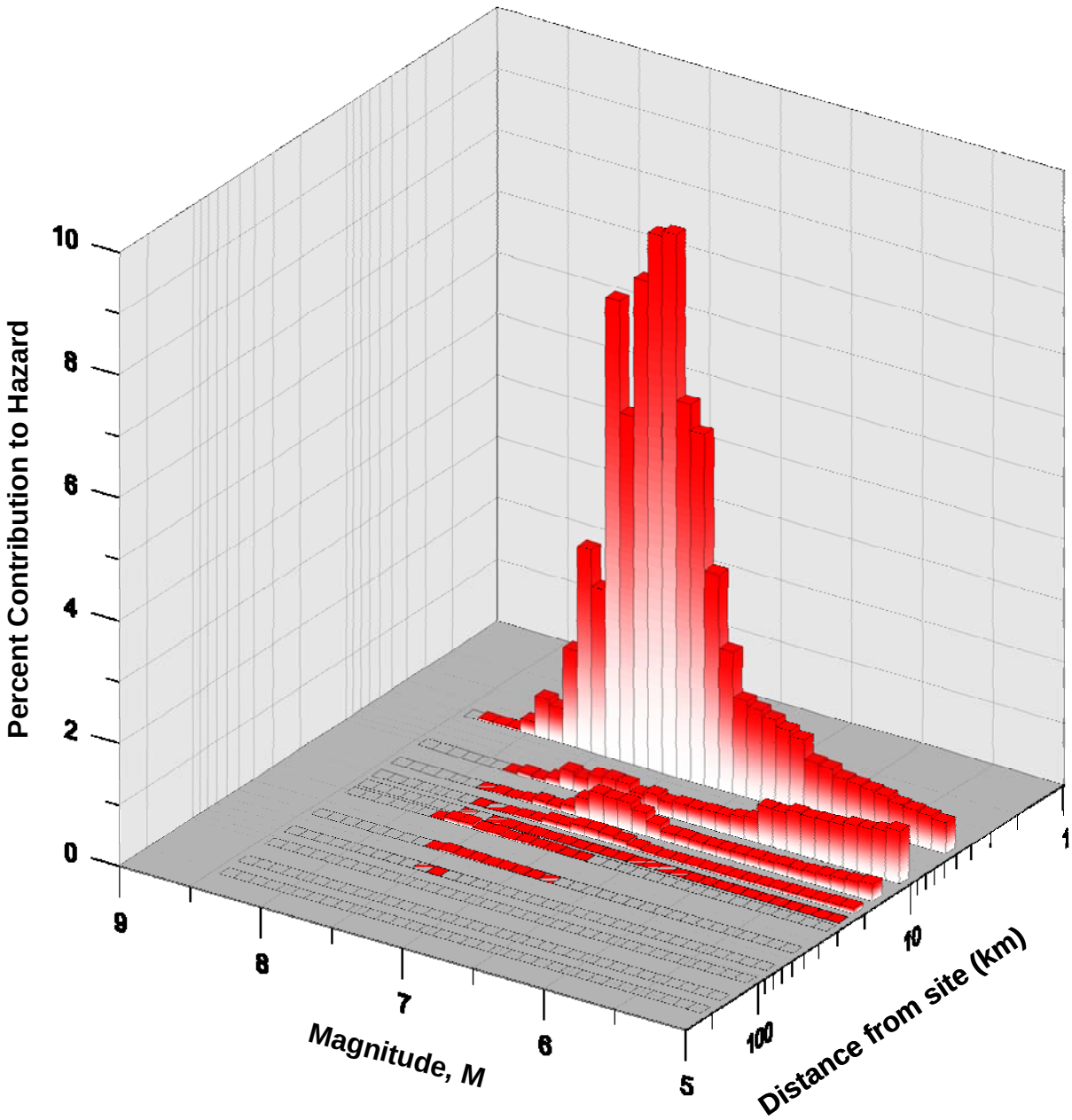

DEAGGREGATION OF 0.2 SECOND SPECTRAL ACCELERATION HAZARD FOR THE 2,475-YEAR RETURN PERIOD
Qaraoun Dam Hazard Study
Litani River Basin, Lebanon

By: DG	Date: 1/18/2012	Project No. OD11161570
AMEC Geomatrix		Figure 3-16b

I:\Project\16000\OD11161570 - Qaraoun Dam\12000 CALCS EVALS ANALYSIS\Figures\rpt_figures

V_{S30} = 1,100 m/s

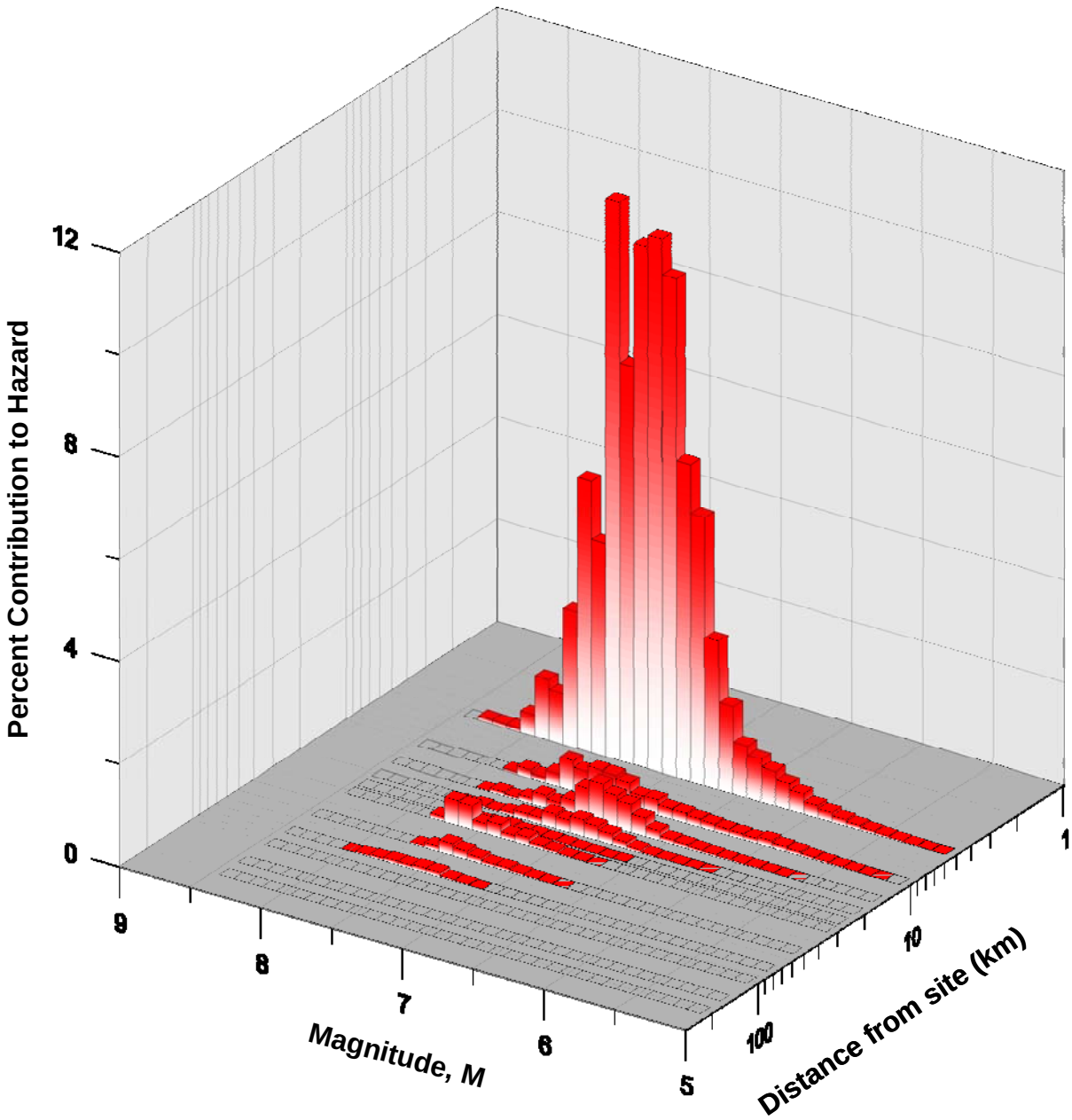

DEAGGREGATION OF 1.0 SECOND SPECTRAL ACCELERATION HAZARD FOR THE 2,475-YEAR RETURN PERIOD
Qaraoun Dam Hazard Study
Litani River Basin, Lebanon

By: DG	Date: 1/18/2012	Project No. OD11161570
AMEC Geomatrix		Figure 3-16c

I:\Project\16000\OD11161570 - Qaraoun Dam\12000 CALCS EVALS ANALYSIS\Figures\rpt_figures

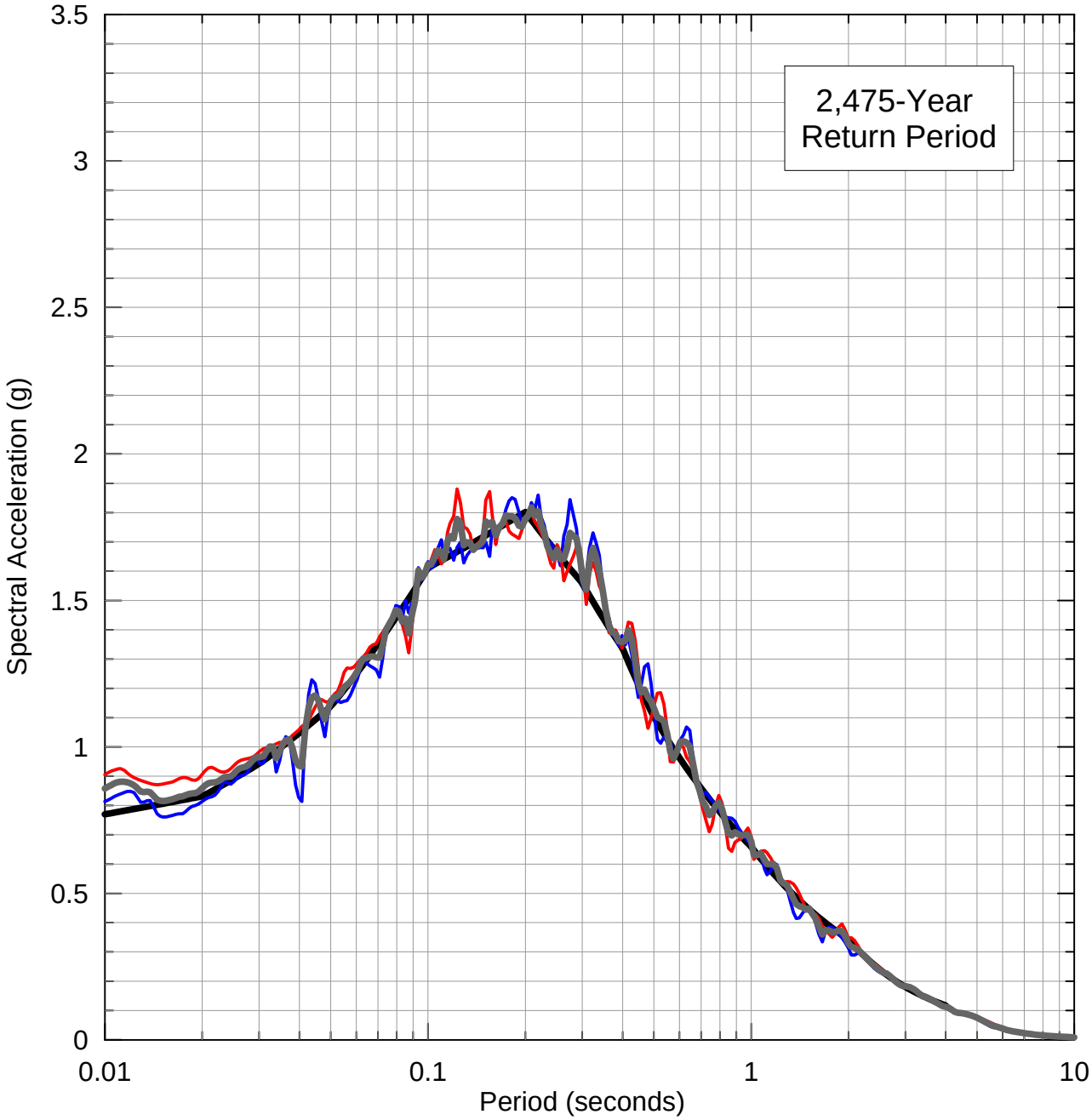

2,475-Year Horizontal Uniform Hazard Response Spectrum (UHRS) Adjusted for Near-Fault Directivity

Hector Mine - Hector

Tabas - Tabas

Geometric Mean of Selected Records

Notes:
1. Period range of interest for scaling is PGA (0.01) to 4.0 seconds.
2. Spectra are five-percent damped.

COMPARISON OF SPECTRA FOR HORIZONTAL MODIFIED TIME HISTORIES TO TARGET SPECTRUM FOR 2,475-YEAR RETURN PERIOD
Qaraoun Dam Hazard Study
Litani River Basin, Lebanon

By: DG	Date: 1/18/2012	Project No. OD11161570
AMEC Geomatrix		Figure 3-17a

I:\Project\16000\OD11161570 - Qaraoun Dam\12000 CALCS EVALS ANALYSIS\Figures\rpt_figures

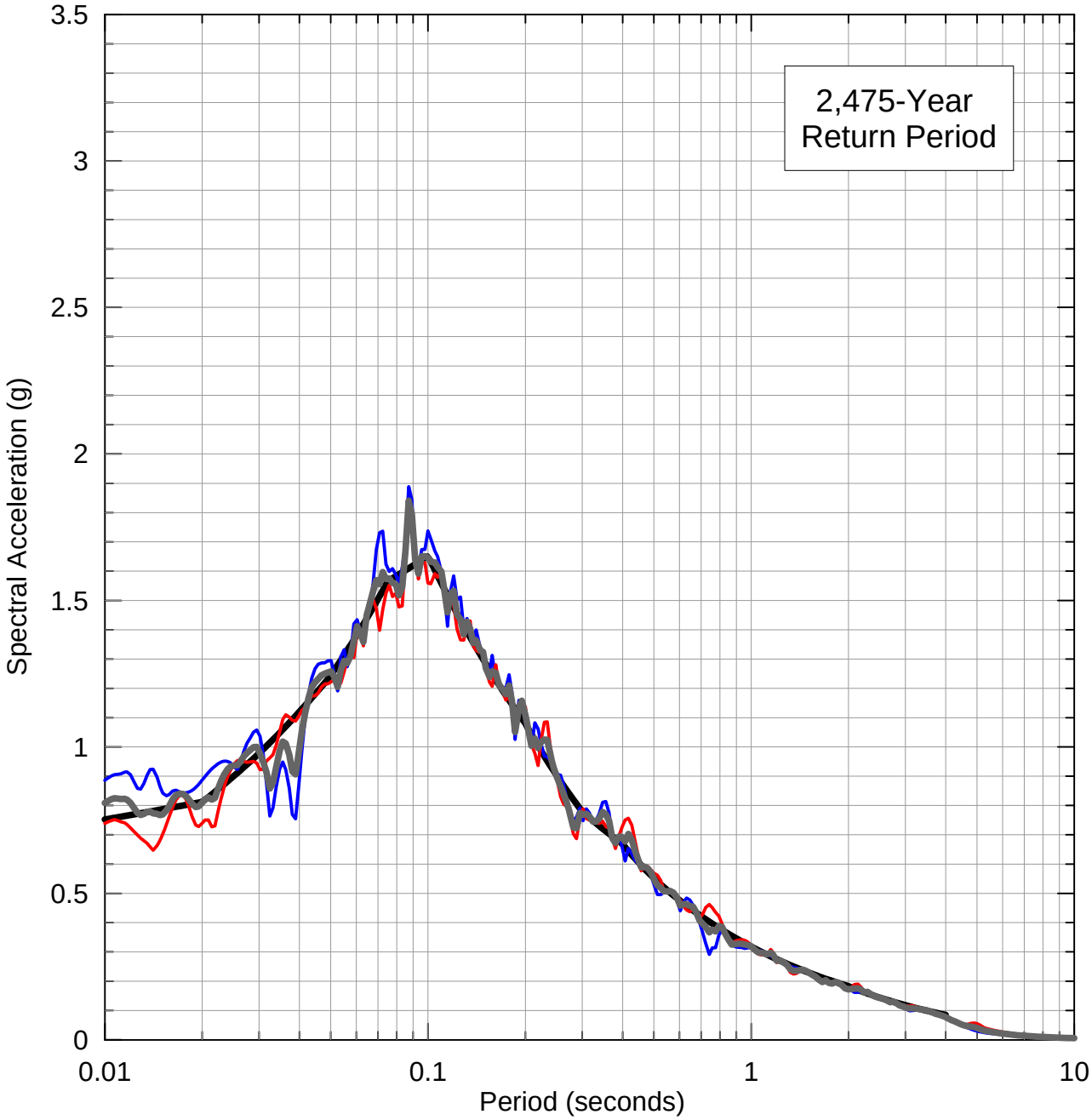

2,475-Year Vertical Uniform Hazard Response Spectrum (UHRS) Adjusted for Near-Fault Directivity

Hector Mine - Hector

Tabas - Tabas

Geometric Mean of Selected Records

Notes:
1. Period range of interest for scaling is PGA (0.01) to 4.0 seconds.
2. Spectra are five-percent damped.

COMPARISON OF SPECTRA FOR VERTICAL MODIFIED TIME HISTORIES TO TARGET SPECTRUM FOR 2,475-YEAR RETURN PERIOD
Qaraoun Dam Hazard Study
Litani River Basin, Lebanon

By: DG	Date: 1/18/2012	Project No. OD11161570
AMEC Geomatrix		Figure **3-17b**

I:\Project\16000\OD11161570 - Qaraoun Dam\12000 CALCS EVALS ANALYSIS\Figures\rpt_figures

4. NONLINEAR DEFORMATION ANALYSIS

4.1. APPROACH AND METHODOLOGY

The dynamic response and seismic deformations of Qaraoun Dam were estimated using the computer program FLAC (Fast Lagrangian Analysis of Continua) Version 6 (Itasca, 2005). This approach involves performing two-dimensional, finite-difference analyses to evaluate the dynamic response and permanent displacements of the central cross section of the dam (Figure 2-2) during the postulated seismic shaking at the dam site. The FLAC program was incorporated with a nonlinear bounding surface hypo-plasticity model for granular materials (Wang, 1990). The nonlinear bounding surface hypo-plasticity model is implemented in FLAC as a UDM (User-Defined-Model). The FLAC mesh developed for analysis was based on the maximum-height (central) cross section of the dam provided by IRG (Figure 2-2). The model was composed of four material types as illustrated in Figure 4-1: foundation bedrock, dumped rockfill, stratified rockfill, and concrete (for the drainage gallery and upstream embankment panel facing). The concrete drainage gallery and the adjacent bedrock are modeled with fine grid zones to more accurately calculate the response of the gallery. The concrete panels on the upstream face of the embankment are placed on the stratified rockfill layer and are modeled as structural elements (designated as "liner elements" in the FLAC program).

It was assumed that the concrete facing, drainage gallery, and the cut-off curtain provide an effective means of controlling seepage from the reservoir, and that the rockfill remains in an unsaturated condition. Under this assumption, the dam embankment rockfill was modeled as "moist." Static water pressure was applied to the concrete facing below the design reservoir level (elevation 858 m) and on the top of the bedrock upstream of the drainage gallery to model the reservoir water load.

In the dynamic analysis, a compliant boundary was specified along the base of the model to simulate the unbounded extent of the elastic foundation bedrock beneath the dam. The earthquake motions were input as a stress time history at this boundary. Free-field boundaries were used for the left- and right-side boundaries.

The effect of hydrodynamic pressure (additional pressure on the embankment from water sloshing up against the dam during an earthquake) on the concrete face of the dam was investigated by modeling the reservoir water on the upstream face of the dam with an additional grid of material representing the reservoir water. The results show that the impact of hydrodynamic pressure on permanent deformations is not significant (less than 15% increase to displacements at the dam crest compared to the analysis without hydrodynamic pressure). Studies by Bureau and others (1985) indicate that including the effects of reservoir hydrodynamic forces had no significant influence on the computed acceleration response of the dam. When including the hydrodynamic forces, their finite element analysis resulted in slightly lower accelerations, while the computed fundamental period was unchanged. The computed shear stresses within the rockfill were within 2 to 5 percent of the values computed when not including the hydrodynamic water loads.

It was also noted in this study that modeling hydrodynamic pressure by water zones increased the computation time and the potential for numerical instability. Hence, the hydrodynamic pressure was not included in the final FLAC runs presented in this report.

4.2. STATIC STRESSES AND STATIC PROPERTIES

To establish the state of stress in the dam before the earthquake, a static stress analysis was performed in FLAC. The resulting state of stress in the dam serves as the initial stress state for the dynamic analyses. The FLAC analyses were performed for a cross section representing the central section, as shown on Figure 2-2. The finite difference grid representing the cross section is shown on Figure 4-1. Table 4-1 summarizes the static material properties used in the analyses.

The construction sequence of the dam was not modeled. The dam mesh was set up in a single step and the loading was applied as a gravity turn-on. For the static stress analysis, the finite difference mesh was fixed at the bottom and was supported by vertical rollers at the left and right side boundaries to allow vertical, but not horizontal, displacement. The static stress analysis used the Mohr-Coulomb model and the stress state was first calculated (by gravity turn-on) using an assumed constant soil modulus. Then the stress-dependent moduli were obtained through iteration using the relationship developed by Duncan and Chang (1970) and modified by Duncan et al. (1980), and the parameters K, n, K_b and m listed in Table 4-1. The computed vertical stresses, horizontal stresses and shear stresses are presented on Figures 4-2 through 4-4, respectively.

The rockfill material is cohesionless, and its shear strength is governed by a friction angle (ϕ'), which varies with confining pressure. Leps (1970) and Duncan (2004) studied the effect of confining pressure on rockfill strength from a series of large-scale tests on a wide variety of rockfill types differing in parent material and particle size. Both studies recommend relationships between confining stress and drained friction angle that are largely dependent on the relative density, gradation, and strength of the individual particles as shown on Figure 4-5a. Barton and Kjærnsli (1981) also studied the effect of confining pressure on rockfill strength from a series of triaxial shear tests and concluded that three intrinsic characteristics of rock quality affect the overall strength: friction of the flat rock surface, roughness of the particle surface, and uniaxial compressive strength of the parent rock mass. If ϕ_b is the basic friction angle of flat, nondilatant surfaces of the rock material, R is the equivalent roughness (dimensionless) of the actual rock particles, and S is the equivalent strength (a measure of the compressive strength of the parent rock and particle size), the effective friction angle of the rockfill (ϕ')may be represented by:

$$\phi' = R \log(S/\sigma_n') + \phi_b \qquad (4\text{-}1)$$

where and σ_n' is the effective normal stress. Kulesza (1987) provides recommendations for these parameters for a variety of different rockfill placement conditions with parent material of good quality. For Qaraoun Dam, the rockfill strength can be estimated using ϕ_b = 30° and S = 2400 psi (16.5 MPa) with R values of 7.2 and 8.8 for the dumped rockfill and stratified rockfill, respectively. These values are summarized in Table 4-1. The effective friction angles were estimated for both zones as a function of confining pressure using equation 4-1 and plotted on Figure 4-5b. The trend for the dumped rockfill strength agrees quite well with the "average rockfill" relationship recommended by Leps (1970). The trend for the stratified rockfill strength is also within the range of values recommended by Leps (1970). The average strength curve from Duncan (2004) for the compacted rockfill at Diamond Valley Reservoir is also shown on the same figure. The strength envelope for the compacted rockfill is higher than the curve selected for the dumped rockfill for Qaraoun Dam. Effective friction angles estimated with this approach generate the contours of ϕ' shown on Figure 4-6 for the maximum section at Qaraoun Dam.

Table 4-1 Summary of Static Material Parameters

Parameters		Concrete	Bedrock
Density	(kg/m^3)	2400	2243
	(pcf)	150	140
Shear Modulus[1]	(Pa)	9.96E+09	1.87E+09
	(psf)	2.08E+08	3.91E+07
Bulk Modulus[1]	(Pa)	1.38E+10	3.12E+09
	(psf)	2.89E+08	6.52E+07

Parameters		Dumped Rockfill	Stratified Rockfill
Density	(kg/m^3)	1922	2082
	(pcf)	120	130
Friction Parameters[2]	R	7.2	8.8
	S	16548000 Pa	16548000 Pa
		2400 psi	2400 psi
	ϕ_b [deg]	30	30
	ϕ' [deg]	R $log(S/\sigma_n)+\phi_b$	R $log(S/\sigma_n)+\phi_b$
Cohesion	(Pa)	0	0
	(psf)	0	0
Parameters Used for Static Stress Analysis	k	450	450
	Kb	125	125
	m	0.2	0.2
	n	0.4	0.4
Young's Modulus	E	$k\ p_a(\sigma_m/p_a)^n$	$k\ p_a(\sigma_m/p_a)^n$
Bulk Modulus	B	$k_b\ p_a(\sigma_m/p_a)^m$	$k_b\ p_a(\sigma_m/p_a)^m$

[1] Bedrock modulus corresponding to Vs=3000 fps, ν=0.25, Concrete modulus corresponding to E=3,498,000 psi, ν=0.21

[2] Based on Kulesza (1987) and relationship proposed by Barton and Kjærnsli (1981)

4.3. NONLINEAR SOIL MODEL AND PARAMETERS

The nonlinear dynamic analysis was performed using the bounding surface hypo-plasticity model (Wang et al, 1990), the main features of which are illustrated in Figure 4-7. Some of the main features of the bounding surface hypo-plasticity model compared with equivalent linear and nonlinear hyperbolic models are:

1. a failure surface defined by friction angle is used to represent the shear strength of the coarse-grained soils;
2. within the framework of bounding surface plasticity, the soil modulus for each stress increment is defined as a function of stress loading level in terms of the "distance" to the failure surface and the maximum pre-stressed surface in the stress tensor space; thus, the stress-strain relationship is fully nonlinear during both loading and unloading conditions; and
3. the model is capable of modeling shear stress-induced volumetric change.

In undrained conditions, the tendency for volume change produces excess pore water pressure. This feature enables the prediction of liquefaction potential due to shear stress loading, and the potential for settlement after dissipation of the induced pore pressure. However, since the embankment was modeled as "moist" (non-saturated), the liquefaction potential feature was not activated, and thus the volumetric change component was not modeled in the current analysis.

Nine parameters are required in the dynamic response analyses based on the bounding surface hypo-plasticity model:

The effective friction angle (ϕ') can be estimated using the same relationship described for the static stress analysis in Section 4.2.

The parameter G_o is the modulus coefficient that defines the initial (maximum) elastic shear modulus, G_{max}, using the following equation:

$$G_{\max} = G_o p_a V(e)\sqrt{\frac{p}{p_a}} \qquad (4\text{-}2)$$

where:

$$V(e) = \frac{(2.973 - e)^2}{1 + e} \qquad (4\text{-}3)$$

and where p_a is the atmospheric pressure, e is the void ratio, and p is the mean effective confining pressure. The model parameter G_o can be related to the value K_{2max} in the relationship of Seed and Idriss (1970) shown below:

$$G_{max} = 1000\ K_{2max}\ (p)^{0.5} \qquad (4\text{-}4)$$

Thus, the corresponding parameter G_o in the bounding surface plasticity model can be converted from K_{2max} values through a factor that depends on void ratio:

$$G_o = 21.738 K_{2\max} / V(e) \qquad (4\text{-}5)$$

Data available on K_{2max} for rockfills, particularly for dumped rockfill such as used for the major part of Qaraoun Dam, is very limited. Back-analyses of K_{2max} were reported by Lai (1985) based on the behavior of two Mexican dams (El Infiernillo and La Villita) during several earthquakes that occurred between 1966 and 1979, and of Long Valley Dam in California, during the May 1980 Mammoth Lakes earthquake. Boulanger et

al. (1994) performed two- and three-dimensional dynamic response analyses of Cogswell Dam for ground motions recorded during the 1991 Sierra Madre and 1987 Whittier-Narrows earthquakes. They used the results of the response analyses and recorded ground motions to estimate the dynamic properties of the dam rockfill. Cogswell Dam is a 280-foot-high concrete-faced, dumped rockfill dam. Based on their studies, Boulanger et al. (1994) reported that the insitu dynamic properties of the rockfill comprising the body of Cogswell Dam appear to be reasonably represented by a K_{2max} value of 120 to 140, with the mid-range modulus degradation relationship proposed for gravels by Seed et al. (1986). Based on these studies, the values reported by Kulesza (1987) and reviewed and used by Geomatrix (1999) for the dumped rockfill at New Exchequer Dam, appear reasonable and were adopted for the present analyses. These values of K_{2max} and void ratio, e, for calculating G_o are listed in Table 4-2 (K_{2max} of 80 and 120, and void ratio of 0.5 and 0.4 were selected for the dumped rockfill and stratified rockfill zones respectively).

The parameter h_r characterizes the relationship between shear modulus and shear strain. Relationships of the normalized modulus reduction factor G/G_{max} and material damping ratio with shear strain (Darendeli, 2001) were used to generate target curves for each zone. The model parameter h_r for each zone was calibrated to provide modulus reduction and damping relationships with shear strain that match the target curves. Because the nature of the Darendeli relationships is stress-dependent, the parameter h_r is also stress-dependent and varies throughout the dam (Figure 4-8). Figures 4-9 and 4-10 show the modulus reduction and damping ratio relationships (both target curves and calibrated/matched curves) for 4 locations (confining pressures) underneath the crest.

Two additional parameters (k_r and d) are used in the effective stress analyses to simulate pore water pressure changes. In the case of Qaraoun Dam, the rockfill is not saturated; thus, the two parameters are inactive (by assigning values of 100 and 150 to them, respectively).

The parameter b does not have a clear physical meaning; it is used to vary the shape of the effective-stress path in the model simulation. A default value of 2 often is used, and was used here.

The parameter ν is the well-known elastic parameter Poisson's ratio. An estimated value of 0.33 was used for all of the rockfill material zones. The foundation bedrock has a value of 0.25, and concrete has a value of 0.20.

The parameter R_p represents the so-called phase transformation line. For this study, $R_p = R_f$ was used.

All of the calibrated model parameters assigned to the materials in the cross section analyzed for this study are presented in Table 4-2 below.

Table 4-2: Summary of Nonlinear Soil Model Parameters for Dynamic Analyses

Material	ϕ' (degrees)	K_{2max}	G_o[1]	h_r	k_r	d	Poisson's Ratio	b	R_p/R_f	Void Ratio e
Dumped Rockfill	From static analysis	80	427	Calibrated based on Darendeli (2001)	100	150	0.33	2	1.0	0.5
Stratified Rockfill	From static analysis	120	552	Calibrated based on Darendeli (2001)	100	150	0.33	2	1.0	0.4

[1] $G_o=21.738*(1+e)*K_{2max}/(2.973-e)^2$

It should be noted that the two constitutive models used in this study do not model the effect of seismically-induced volumetric straining of the rockfill. Large shear stresses propagating through the embankment have the potential to consolidate portions of the rockfill that may have been placed in a loose manner. While the bounding surface hypo-plasticity model has the ability to account for volumetric strains, the parameters that

are needed to model this behavior cannot be estimated without extensive field and laboratory tests on representative samples of the rockfill, which are not available. Furthermore, it is not common to incorporate volumetric straining potential in these types of analyses, and there are no published examples in practice to use as guides for developing these parameters. Section 4.8 provides a discussion for qualitatively addressing the volumetric straining effects in the overall estimates of deformation of the dam.

4.4. STRUCTURAL AND INTERFACE ELEMENTS

The concrete panels on the upstream face of the embankment were modeled as "liner elements" in the FLAC numerical model. Based on the cross section detail of the center section (Figure 4-1) the concrete panels were modeled as three sections with different thicknesses corresponding to the stratified fill thickness behind them. The thickness, density, and elastic modulus of the concrete liner elements are listed in Table 4-3.

Table 4-3: Input Parameters for Liner Elements

Elevation	Thickness		Unit Weight		Young's Modulus		Poisson's Ratio
(m)	(m)	(ft)	(kg/m^3)	(pcf)	(Pa)	(psi)	
800-820	0.5	1.63	2400	150	2.64E+10	3,830,000	0.2
820-854	0.4	1.30	2400	150	2.64E+10	3,830,000	0.2
854-861	0.3	0.98	2400	150	2.64E+10	3,830,000	0.2

The concrete panels are in contact with the stratified rockfill layer on the upstream face of the embankment. The shear resistance at the contact surface (i.e., the interface between concrete panels and rockfill) is normally modeled as a Mohr-Coulomb (frictional) type of behavior. In the FLAC model, this behavior was simulated using a built-in interface element. Interface elements were assigned at the contact surface between the concrete panels (liner elements) and the stratified rockfill, based on our experience working on similar projects. The shear resistance (in terms of cohesion and friction angle), shear stiffness Ks, normal stiffness Kn, and tension limit selected for the interface elements are shown in Table 4-4.

Table 4-4: Input Parameters for Interface Elements

Cohesion		Friction Angle	K_s		K_n		Tension Limit
(Pa)	(psf)	(degree)	(kg/m^3)	(pcf)	(kg/m^3)	(pcf)	(psf)
4790	100	45	6.08E+05	3.80E+04	1.92E+07	1.20E+06	100

4.5. ANALYSIS RESULTS USING POSTULATED GROUND MOTIONS

The nonlinear dynamic analysis was performed using as input the four spectrally-matched time histories (both horizontal and vertical components) for the 100-year and 2,475-year return periods developed from the PSHA in Section 3.0 and shown on Figures 4-11 and 4-12 (100-year) and Figure 4-20 and 4-21 (2,475-year). For the analyses, a full reservoir elevation was assumed at about Elev. 858 meters. A summary of the key results of these analyses are shown in Table 4-5. The results of the analyses show that the permanent crest settlement is calculated to be about 0.03 meter for the 100-year events and between about 0.35 and 0.44 meter for the 2,475-year events. The peak horizontal accelerations at the dam crest are calculated to be between about 0.32g and 0.40g for the 100-year events, and between about 1.47g and 1.84g for the 2,475-year events.

Table 4-5: Summary of FLAC Nonlinear Analysis Key Results

Earthquake		Direction	Input Motion Peak Acceleration (g)	Peak Acceleration at Dam Crest (g)	Displacement at Dam Crest at the end of Earthquake (m)
100-year Event	Dayhook Record	Horizontal	0.147	0.32	0.013
		Vertical	0.135	0.16	-0.028
	San Jose STH Record	Horizontal	0.138	0.40	0.019
		Vertical	0.143	0.20	-0.031
2,475-year Event	Tabas Record	Horizontal	0.813	1.47	0.45
		Vertical	0.885	1.26	-0.44
	Hector Mine Record	Horizontal	0.905	1.84	0.29
		Vertical	0.738	1.14	-0.35

4.5.1. 100-YEAR EVENT (DAYHOOK RECORD)

The input earthquake ground motion time histories for the 100-year event are shown on Figure 4-11 (for the horizontal upstream/downstream component) and Figure 4-12 (for the vertical component) for the Dayhook Station record of the Tabas earthquake. Figures 4-13 and 4-14 show contours of the computed horizontal and vertical displacements, respectively, at the end of the earthquake. The deformed shape of the embankment (with displacements shown at a magnification factor of 50) is shown on Figure 4-15. The deformed mesh on Figure 4-15 shows that the crest will have a tendency to settle and the embankment will have a tendency to deform in the downstream direction during the postulated ground shaking. A contour plot of the maximum shear strain at the end of the earthquake is shown on Figure 4-16. The plot shows that the maximum shear strain near the crest is less than 0.2 percent. The computed horizontal and vertical displacement time histories at the dam crest and at the upstream toe (near the connection of the concrete face slab to the drainage gallery), for this event, are shown on Figure 4-17. The permanent horizontal deformation was estimated to be about 0.01 m at the crest of the dam. The permanent crest settlement was estimated to be about 0.03 m. The peak displacement at the upstream toe is about 0.02m, and the permanent displacement at the end of shaking is negligible (less than 0.005m).

Acceleration time histories at various locations on the dam slopes and crest are shown on Figures 4-18 (for the horizontal direction), and Figure 4-19 (for the vertical direction). The computed peak horizontal acceleration at the crest is about 0.32g, and the peak vertical acceleration is 0.16g.

4.5.2. 2,475-YEAR EVENT (TABAS RECORD)

The input earthquake ground motion time histories for the 2475-year event are shown on Figure 4-20 (for the horizontal upstream/downstream component) and Figure 4-21 (for the vertical component) for the Tabas Station record of the Tabas earthquake. Figures 4-22 and 4-23 are the contours of the computed horizontal and vertical displacements, respectively at the end of the earthquake. The deformed shape of the embankment (with displacements shown at a magnification factor of 5) is shown on Figure 4-24. The deformed mesh shown on Figure 4-24 indicates that the crest will have a tendency to settle and the embankment will have a tendency to deform in the downstream direction during the postulated ground shaking. A contour plot of the maximum shear strain at the end of the earthquake is shown on Figure 4-25. The computed maximum shear strains are in the vicinity of the crest of the dam, and are in the range of 1 to 2 percent. The computed horizontal and vertical displacement time histories at the dam crest and at the upstream toe (near the connection of the concrete face slab to the drainage gallery), for this event, are shown

on Figure 4-26. The permanent horizontal deformation at the end of shaking was estimated to be about 0.45 m at the crest of the dam. The permanent crest settlement was estimated to be about 0.44 m. The computed peak displacement at the upstream toe during shaking is about 0.15m. However, the permanent displacement at the end of shaking is about 0.05 m.

Acceleration time histories at various locations on the dam slopes and crest are shown on Figure 4-27 (for the horizontal direction) and Figure 4-28 (for the vertical direction). The computed peak horizontal acceleration at the crest is about 1.5g, and the computed vertical acceleration is about 1.3g.

To estimate the response and displacement near the interface between the concrete face slab and the inspection gallery, the time history of relative displacement between two adjacent points (one at the face slab just above the its connection with the gallery, and the second on top of the gallery just upstream of the face slab), were computed and are presented on Figure 4-29. As shown on Figure 29, for the 100-year event, the computed relative displacements at the end of earthquake shaking were negligible (0.002 m and 0.004 m for the horizontal and vertical displacements, respectively). The computed relative displacements for the 2,475-year event were 0.02 m and 0.04 m, for the horizontal and vertical displacements, respectively. Such displacements are not considered excessive, and can be tolerated by the joints and water stops at the interface between the face slab and the gallery.

4.5.3. RESULTS USING ADDITIONAL DEVELOPED ACCELERATION TIME HISTORIES

Analyses were also performed using an additional set of time histories for each of the two scenario earthquakes (the 100-year and the 2,475-year events). These time histories are the San Jose, Santa Teresa Hills station record of the Loma Prieta earthquake, and the Hector Mine station record of the Hector Mine Earthquake. Results of the two additional analyses (100-year event [San Jose STH record] and 2,475-year event [Hector Mine record]) are similar to those described above, but are not presented here in detail. The key analysis results are included in Table 4-5. Figures 4-30 and 4-31 show the computed horizontal and vertical displacement time histories at the crest and at the upstream toe from these two events. The permanent horizontal deformation and settlement at the crest of the dam were calculated to be about 0.02 m and 0.03 m, respectively, for the 100-year event (San Jose STH record). The permanent horizontal deformation and settlement at the crest of the dam were calculated to be about 0.29 m and 0.35 m, respectively, for the 2,475-year event (Hector Mine record).

4.6. SENSITIVITY ANALYSIS USING MOHR-COULOMB MODEL

The FLAC analysis described above was also performed using a simpler, yet widely-used elasto-plastic constitutive model for the rockfill for comparison with the non linear hypo-plasticity model. The Mohr-Coulomb model is an elastic, perfectly plastic model that behaves in a linear elastic fashion when the stresses are within the yield (failure) surface, but produces unrestrained non-recoverable shear strains (plastic flow) once shear stresses reach the user-defined yield surface.

It was found that for the small earthquake event (100-year event, Dayhook record), the responses of the dam from the bounding surface hypo-plasticity model and Mohr-Coulomb model are similar. For this event, the permanent crest deformations calculated using the Mohr-Coulomb model were about 0.02 m (horizontal) and 0.003 m (vertical) versus about 0.02 m and 0.03 m using the bounding surface model. The computed horizontal and vertical displacement time histories at the dam crest and at the upstream toe (near the connection of the concrete face slab to the drainage gallery), for this event, are shown on Figure 4-32.

For the large earthquake event (2,475-year event, Tabas record) however, the deformations of the dam from the Mohr-Coulomb model were significantly greater than those calculated from the bounding surface hypo-plasticity model. The crest deformations calculated using Mohr-Coulomb model were about 2.9 m (horizontal) and 2.5 m (vertical) versus about 0.45 m and 0.44 m using the bounding surface model. The computed horizontal and vertical displacement time histories at the dam crest and at the upstream toe (near the connection of the concrete face slab to the drainage gallery), for this event, are shown on Figure 4-33.

The difference between the results of the two models is due to the large stresses that are developed from the 2,475-year event that are sustained in the plastic range of the Mohr-Coulomb model. The computed maximum shear strain increments in the vicinity of the dam crest were in the range of 10 to 20 percent, indicating significant unrestrained yielding that resulted in excessive deformation. Hence, the results from the Mohr-Coulomb analyses were judged to be conservative, and the bounding surface hypo-plasticity model was deemed more reasonable to model the rockfill behavior given the high level of shaking. However, it should be noted that there are uncertainties associated with most constitutive models and thus the results obtained from these analyses are compared with the observed performance of similar embankments in past earthquakes, and are used to guide engineering judgment in assessing the dam's seismic performance. A discussion of the performance of embankments during past earthquakes is presented in Section 4.7 below.

4.7. PERFORMANCE OF EMBANKMENTS DURING PAST EARTHQUAKES

The results of the deformation analyses are compared with the observed performance of similar concrete-faced rockfill embankments during past earthquakes. Ishibuchi Dam, a 53-meter-high concrete-faced rockfill dam built in 1953, was shaken by the 2008 magnitude 6.9 Miyage earthquake in Japan (Matsumoto et al., 2011). Similar to Qaraoun Dam, Ishibuchi Dam was constructed of dumped rockfill, with a zone of placed rockfill underlying the concrete face slab. The dam was located about 11 km from the epicenter of the earthquake. The estimated peak ground acceleration at the base of the dam was about 0.6 to 0.7g. The recorded acceleration at the crest of the dam was 1.5g in the transverse (upstream/downstream) direction, 0.95g in the longitudinal (cross-canyon) direction, and about 2.0g in the vertical direction. The dam crest settled 0.6 meters at the maximum section, which is about one percent of the height of the dam. The earthquake-induced settlement caused an uneven surface and cracking of the pavement at the crest, however, the concrete face on the upstream slope was reportedly undamaged. The observed settlement of Ishibuchi Dam is of the same order of magnitude of the computed deformations for Qaraoun Dam in this study using the bounding surface plasticity model and for similar levels of ground motions.

Cogoti Dam, an 85-meter-high concrete-faced rockfill dam in Combarbalá, Chile, was shaken by a magnitude 7.9 earthquake (which occurred about 88 km from the site) with estimated peak bedrock horizontal acceleration at the site of 0.2g. The dam settled about 0.4 meters, approximately equal to the settlement experienced by the dam prior the earthquake, about 4.5 years after its completion (Arrau et al., 1985). Although the dam was constructed of high-lift dumped rockfill without compaction or water sluicing, the earthquake caused no damage to the concrete face slabs.

Cogswell Dam is an 85-meter-high concrete-faced, dumped rockfill dam founded on bedrock in a narrow V-shaped canyon in Southern California. The dam was shaken by several earthquakes (Boulanger et al, 1994). The 1971 San Fernando M_w 6.6 earthquake (with an epicenter about 43 km west of the dam) was estimated to have produced a peak horizontal ground acceleration of 0.15g at the dam site. No damage was reported, and less than 8 millimeters of crest settlement was attributed to this event. This level of acceleration is similar to the 100-year ground motions used for Qaraoun Dam. However, the contributing magnitude of the earthquake for Qaraoun Dam is M_w 7.2. The computed settlement for Qaraoun Dam for this level of shaking was 28 millimeters.

Bureau et al. (1985), and Bureau (2009) used the observed performance of rockfill dams to develop an empirical relationship between relative crest settlement and an "Earthquake Severity Index" (ESI). The relative crest settlement is defined as ($\Delta H/H$), where ΔH is the crest settlement in millimeters, and H is the height of the dam in meters. ESI is a quantifier of the local intensity of seismic shaking, and accounts for both its maximum amplitude and duration. It is expressed as:

$$ESI = PGA \cdot (M - 4.5)^3 \qquad (4\text{-}6)$$

where PGA is the peak bedrock ground acceleration (in terms of g), and M is earthquake magnitude. The earthquake magnitude is intended to account for the effect of duration. Using about 62 case histories they developed the relationships shown on Figure 4-34.

Bureau (2009) described the behavior of Zipingpu Dam in China that was severely shaken by the May 2008 M_w 7.9 Wenchuan Earthquake. The dam, a 156-meter-high concrete-faced rockfill dam, located about 17 km from the epicenter (and closer to the fault rupture) experienced crest settlements of about 0.7 to 1.0 meter. The duration of ground shaking of this large magnitude earthquake was reported to last about 120 seconds. The peak acceleration recorded at the base of the dam was 0.5g; the crest acceleration was reported at 2.0g. The earthquake-induced ground shaking and deformation resulted in partial dislocation of several concrete slabs at the construction joints, with maximum outward bulging of 15 centimeters. Portions of the parapet wall at the crest collapsed. Open cracks up to 3 centimeters wide were observed between the downstream side of the crest road and the rock slope protection. The dam, however, remained stable and maintained its reservoir impounding capacity. Using the observed performance data of Zipingpu Dam, in terms of the relative crest settlement and the ESI, the performance of this dam plots along the median (50th percentile) relationship shown on Figure 4-34. It is noted that Zipingpu Dam was reported to be designed and built in 2005 to modern design and construction standards. On the other hand, the performance of Ishibuchi dam plots above the 84th percentile of the data, reflecting the loose nature of the dumped rockfill material in the 1953 dam.

The published relationships presented in Figure 4-34 were used to compare the predicted performance of Qaraoun Dam for the postulated ground motions with the observed performance of other concrete-faced rockfill dams. For ground motions associated with the 100-year return period, the PGA is 0.15g and the earthquake magnitude is M_w of 7.2, thus the ESI is about 2.95. The computed crest settlement using the nonlinear hypo-plasticity model is 28 to 31 millimeters; for the Qaraoun Dam height of 61 meters, $\Delta H/H$ is about 0.5. Similarly, for the 2,475-year ground motions, the PGA is 0.8 to 0.9g resulting in an ESI of about 17. The computed settlements were about 350 millimeters to 440 millimeters resulting in $\Delta H/H$ of 6 to 7. These values are plotted on Figure 4-34, and indicate computed deformations that are in reasonable agreement with the observed performance of similar concrete-faced rockfill embankments (shown in red square symbols on Figure 4-34) during past earthquakes. The results of the deformation analysis using the Mohr-Coulomb model are also plotted on Figure 4-34 showing the range of potential deformation estimates using the two approaches. As can be seen from the plot, the computed deformations using the Mohr Coulomb model for the 2,475-year ground motions appear to be conservative.

4.8. OVERALL ESTIMATE OF DEFORMATION POTENTIAL

It is important to consider all of the information presented in this report to arrive at a reasonable estimate of the deformation potential of Qaraoun Dam. Our preferred bounding surface hypo-plasticity model estimates about 0.44 m of settlement at the crest for the 2,475-year return period event, compared to a more traditional, and arguably more conservative, Mohr-Coulomb constitutive model that estimates about 2.5 m of settlement for the same level of shaking. It is our judgment that the Mohr-Coulomb model represents a conservative estimate of deformation that was not observed in documented case-histories for similar dams experiencing similar levels of shaking. The bounding surface hypo-plasticity model, while more consistent with observed performance of other rockfill dams, did not include the effect of volumetric change. Therefore, the expected range of possible deformation may be somewhere between the two estimates.

The dam is composed of dumped rockfill, which is inherently loose and has the potential to consolidate. This is evidenced by the large amount of static settlement measured in the years following construction (refer to Section 2). Since the preferred model in this study did not incorporate seismically-induced volumetric straining, it may be appropriate to increase the calculated deformations to account for this effect.

When considering the range of computed deformations from the two analytical models used in this study, the nature of the dumped rockfill comprising the embankment, and the observed performance of similar dams subjected to similar levels of shaking, our estimate for earthquake-induced permanent settlement at Qaraoun

Dam is in the range of about 1 to 1.5 m for the 2,475-year return period event. Horizontal deformations in the vicinity of the crest may be considered to be similar.

It should be noted that, while deformations predicted by the bounding surface model at the crest of the dam may be increased for the effect of volumetric straining, deformations predicted at the upstream toe of the dam are not subject to these adjustments (i.e., the rockfill cannot consolidate to a denser state at the toe). Therefore, it is our judgment that the toe displacements estimated by the bounding surface model (Section 4.5) are appropriate.

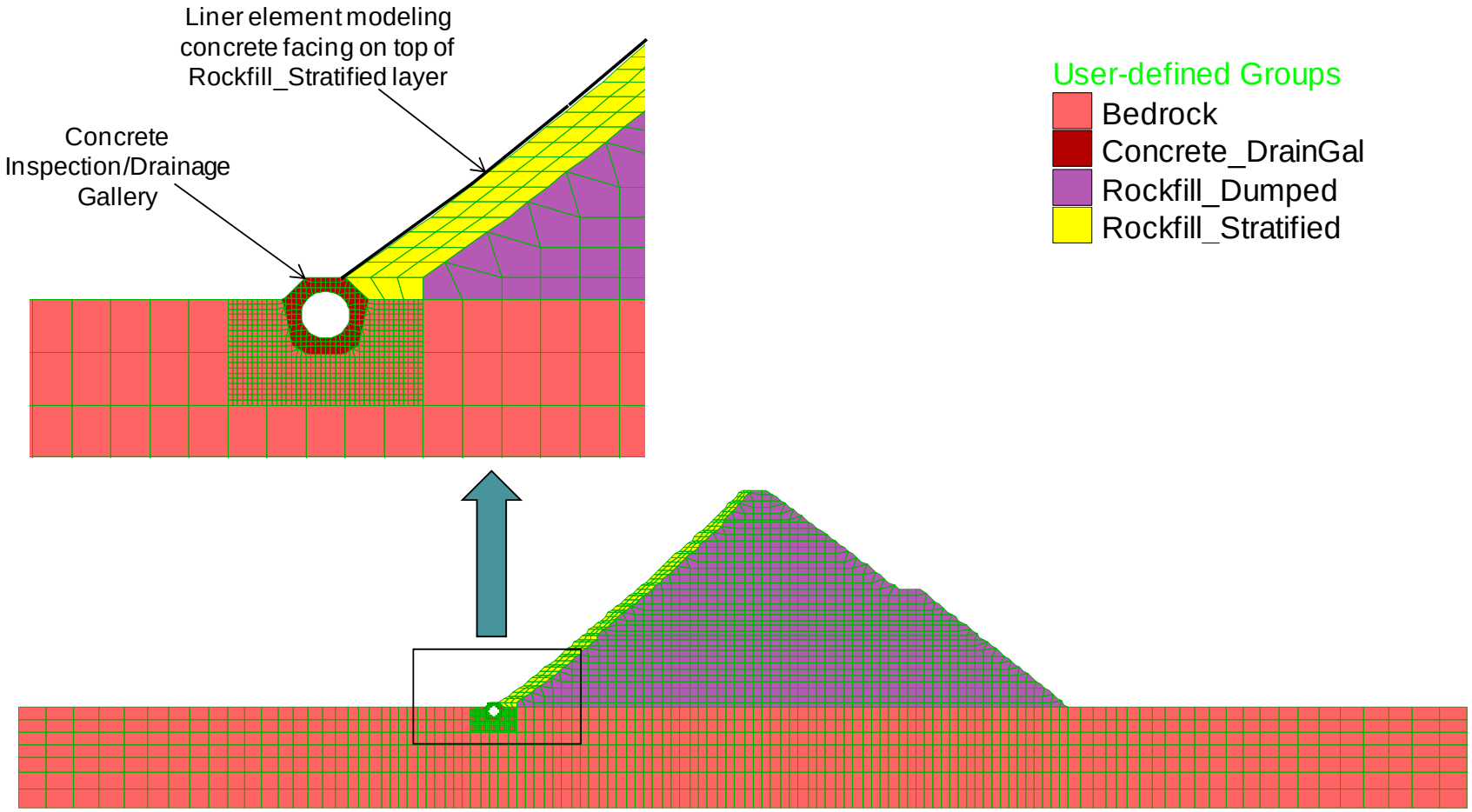

FLAC Grid and Material Zones
Qaraoun Dam Maximum (Center) Section

Seismic Deformation Analysis of Qaraoun Dam	OD11161570
AMEC Geomatrix	Figure **4-1**

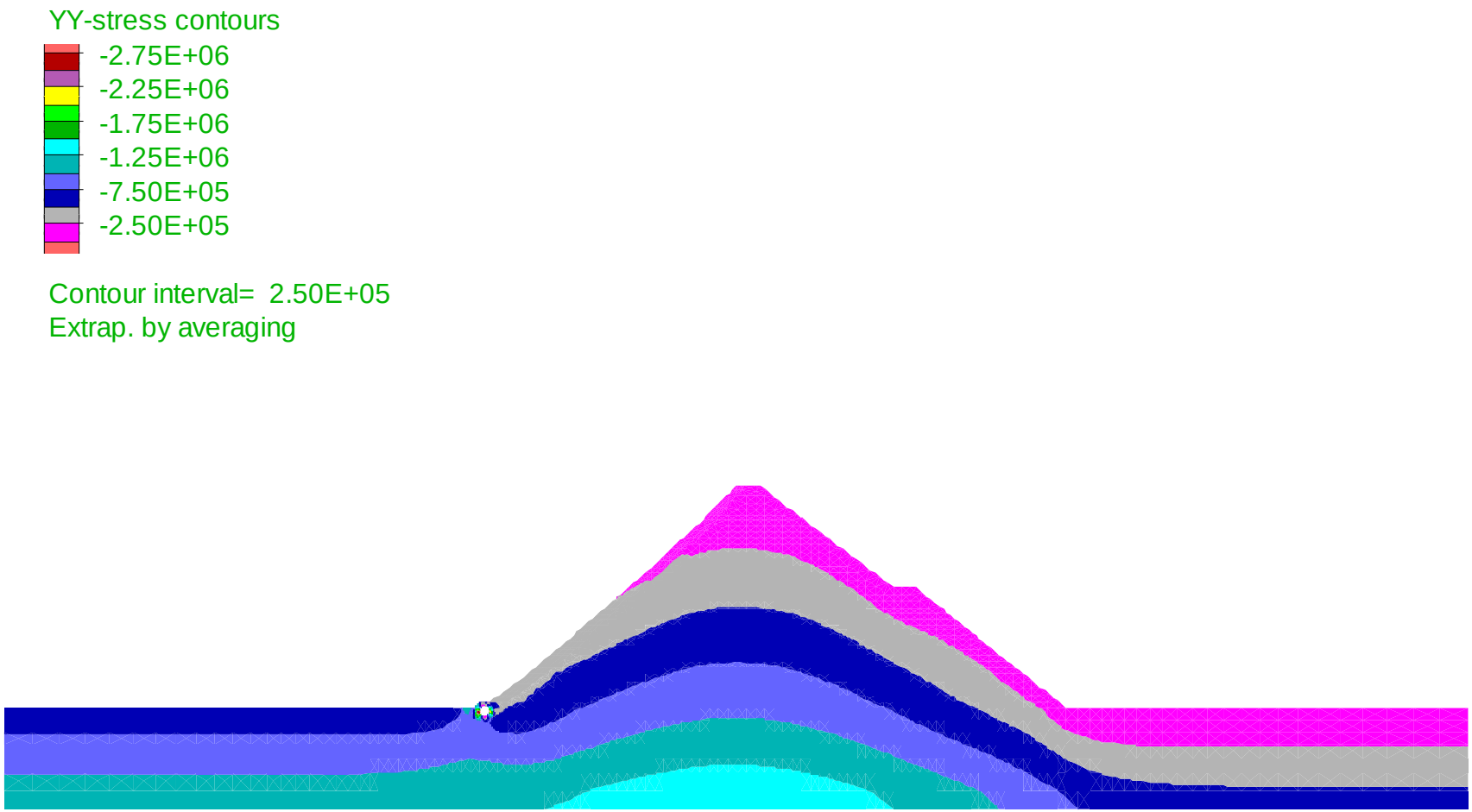

Contours of Static Vertical Stress (Pa)	
Seismic Deformation Analysis of Qaraoun Dam	OD11161570
AMEC Geomatrix	Figure **4-2**

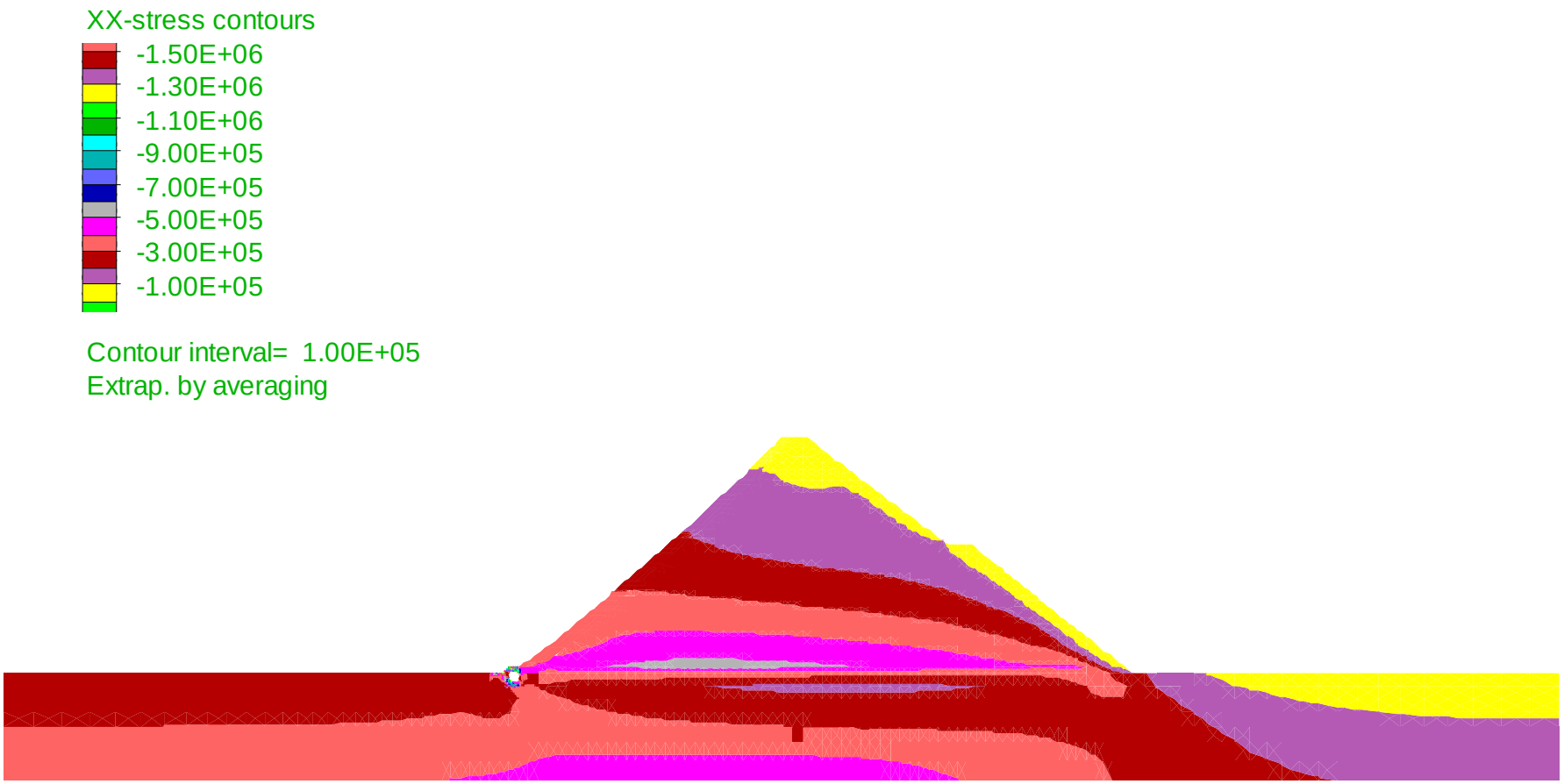

Contours of Static Horizontal Stress (Pa)

Seismic Deformation Analysis of Qaraoun Dam	OD11161570
AMEC Geomatrix	Figure **4-3**

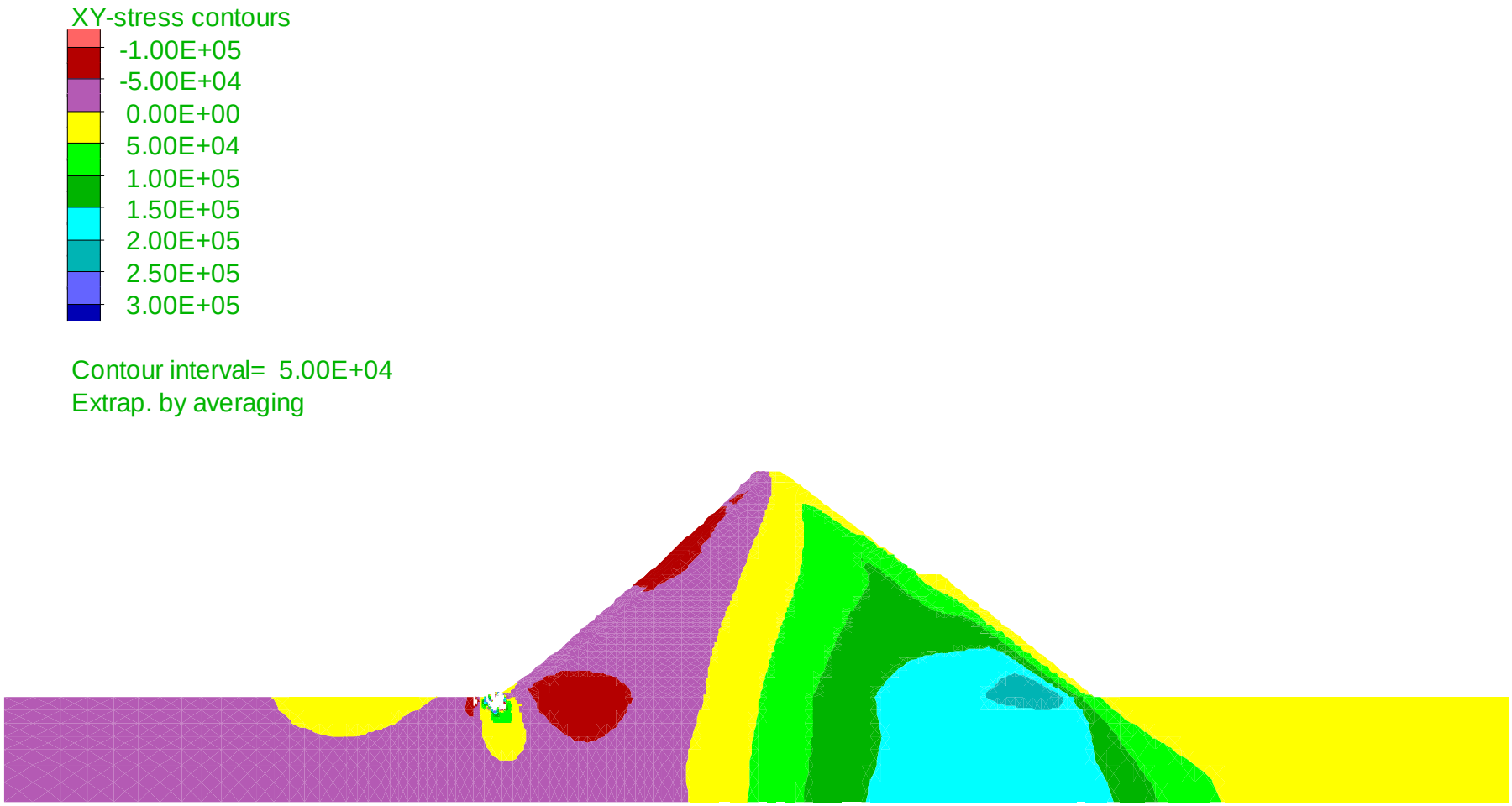

Contours of Static Shear Stress (Pa)	
Seismic Deformation Analysis of Qaraoun Dam	OD11161570
AMEC Geomatrix	Figure **4-4**

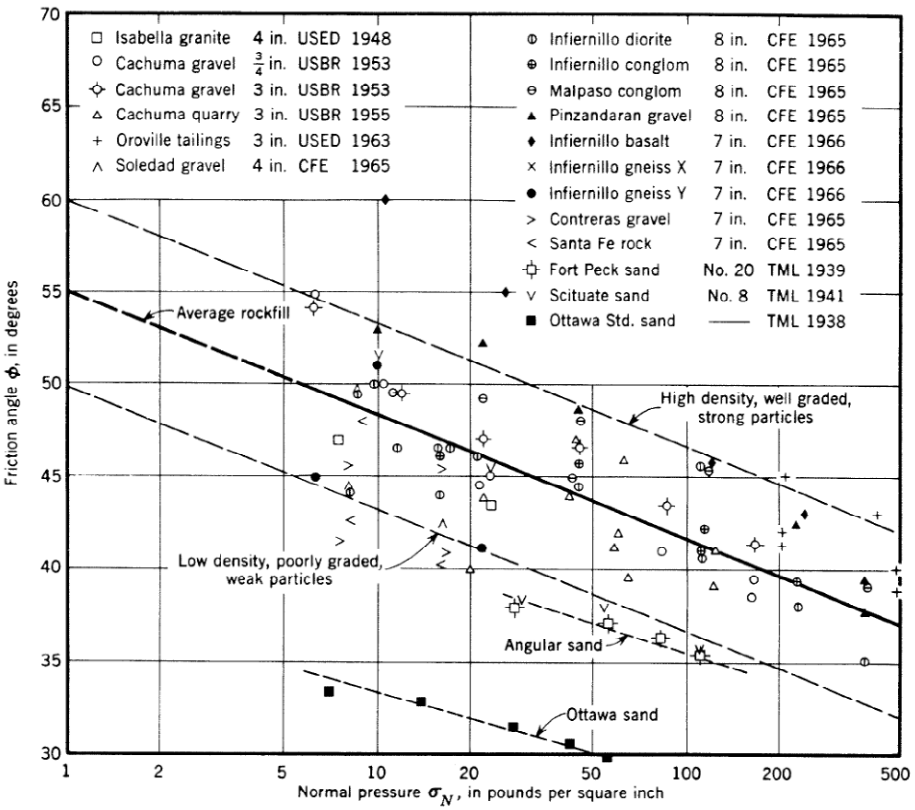

Leps (1970)

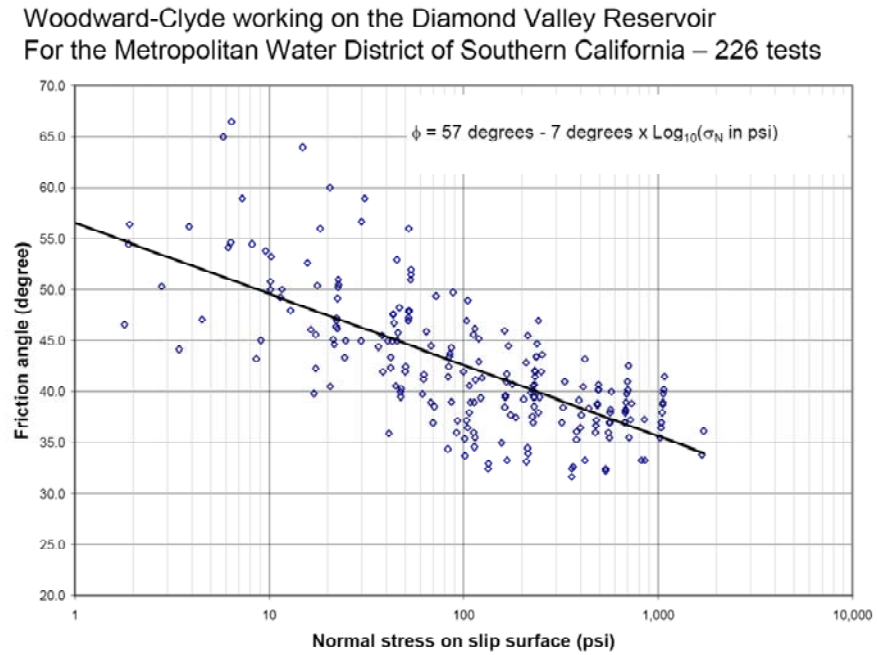

Duncan (2004)

Stress-Dependent Shear Strength of Rockfill after Leps (1970) and Duncan (2004)	
Seismic Deformation Analysis of Qaraoun Dam	OD11161570
AMEC Geomatrix	Figure **4-5a**

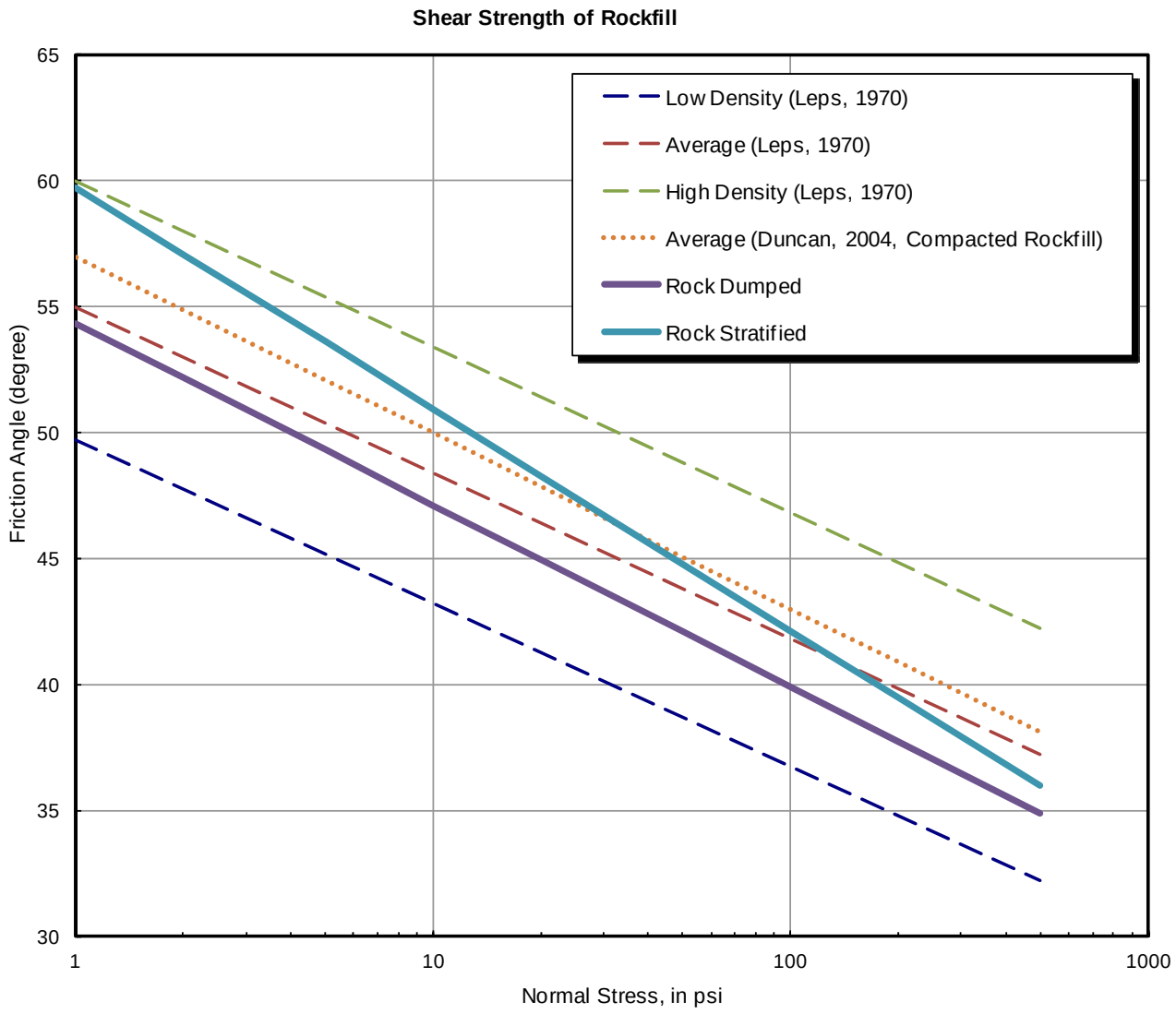

Stress-Dependent Shear Strength of Rockfill Used In This Analysis

Seismic Deformation Analysis of Qaraoun Dam	OD11161570
AMEC Geomatrix	Figure **4-5b**

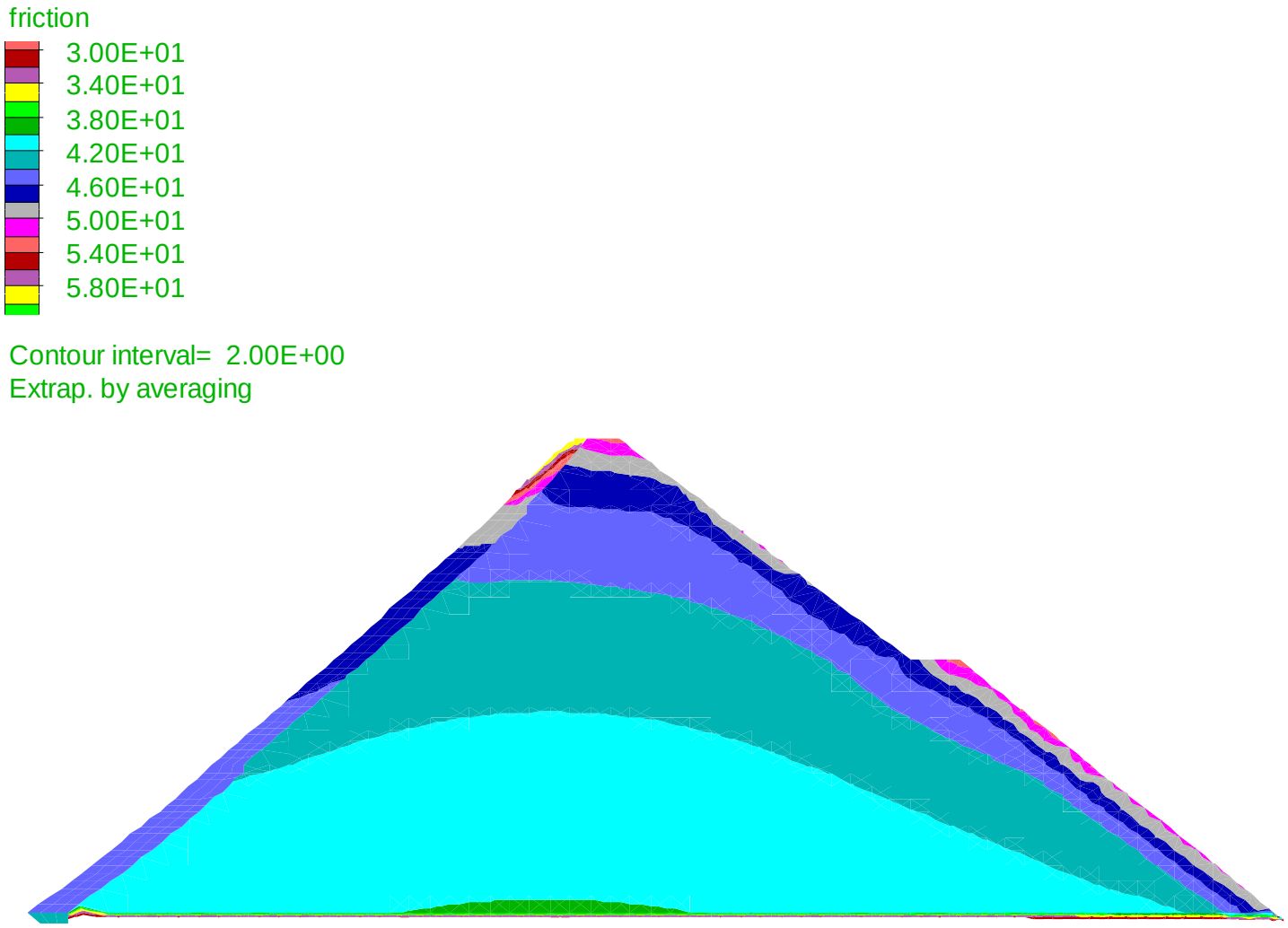

Contours of Friction Angle (Degrees)

Seismic Deformation Analysis of Qaraoun Dam	OD11161570
AMEC Geomatrix	Figure **4-6**

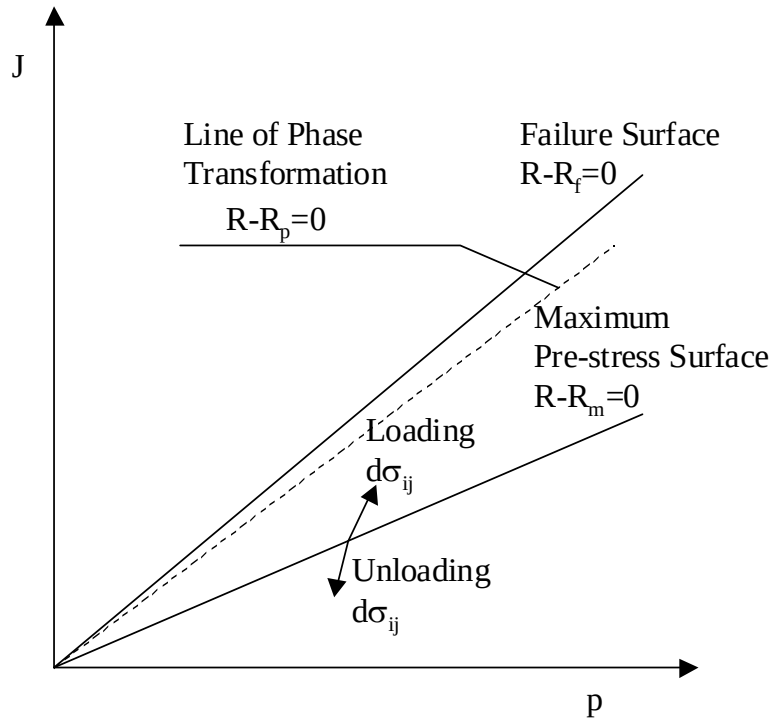

(a) Surfaces and stress variables in J-p plane

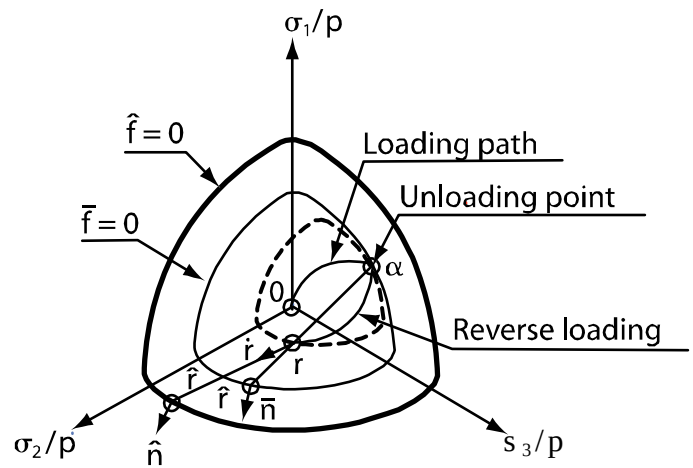

(b) Surfaces and stress variables in p = constant plane

Bounding Surface Hypoplasticity Model (Wang et al., 1990)	
Seismic Deformation Analysis of Qaraoun Dam	OD11161570
AMEC Geomatrix	Figure **4-7**

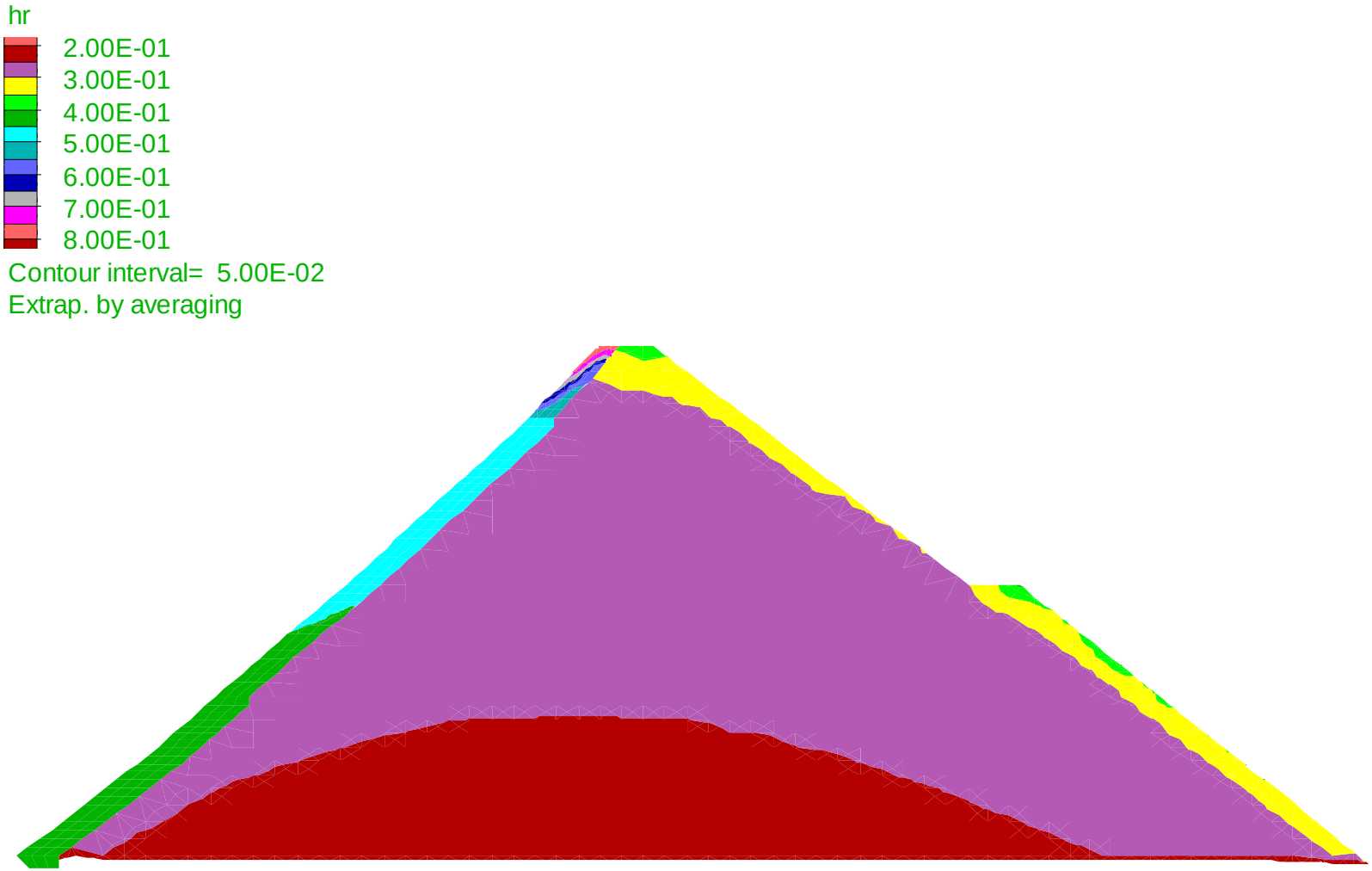

Contours of Modulus Reduction Parameter *hr*

Seismic Deformation Analysis of Qaraoun Dam	OD11161570
AMEC Geomatrix	Figure **4-8**

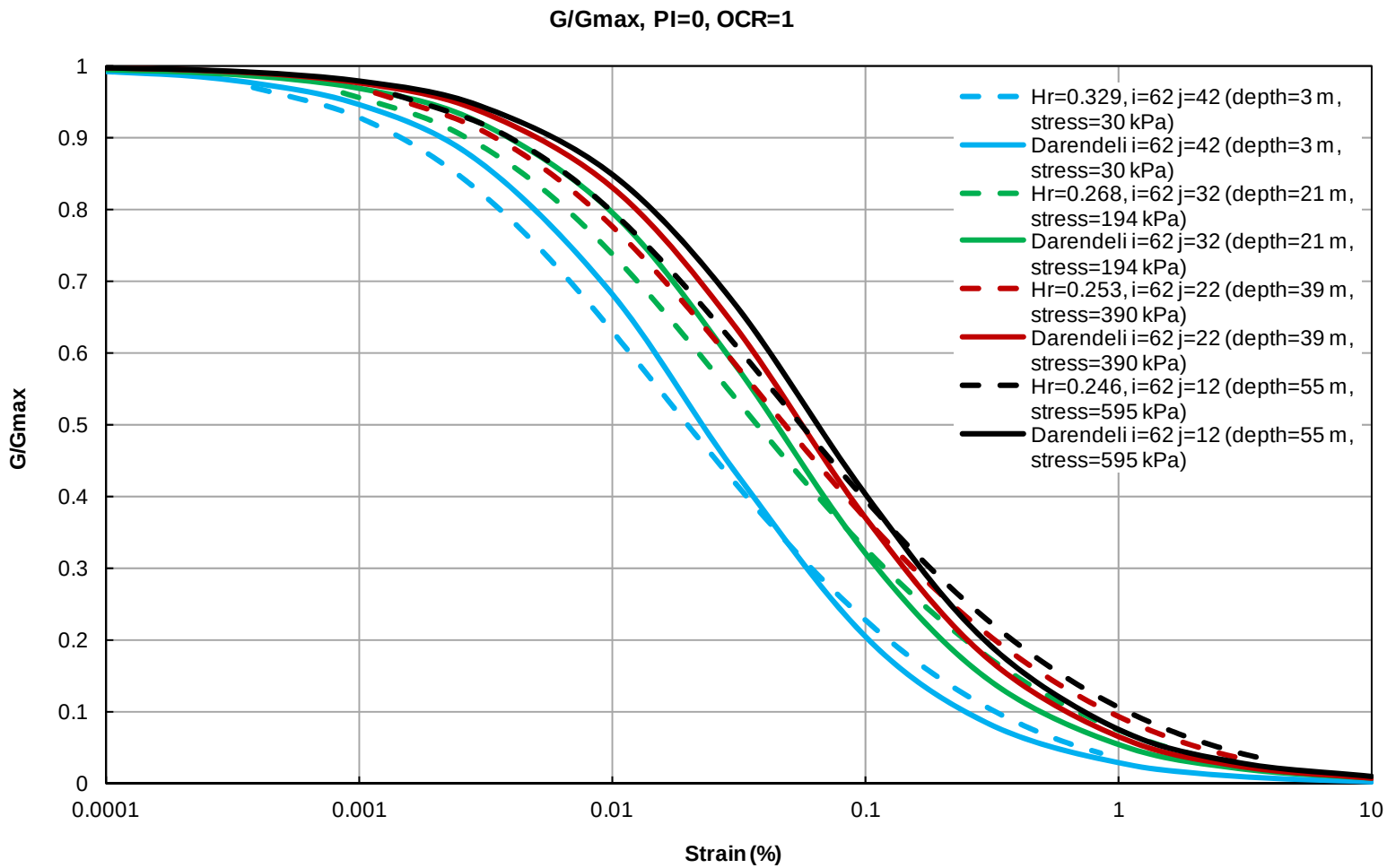

Zone id	Confining Stress σ_m	
i=62	(kPa)	(psf)
j=42	30	625
j=32	194	4058
j=22	390	8139
j=12	595	12420

Modulus Reduction Relationships (after Darendeli 2001)

Seismic Deformation Analysis of Qaraoun Dam	OD11161570
AMEC Geomatrix	Figure **4-9**

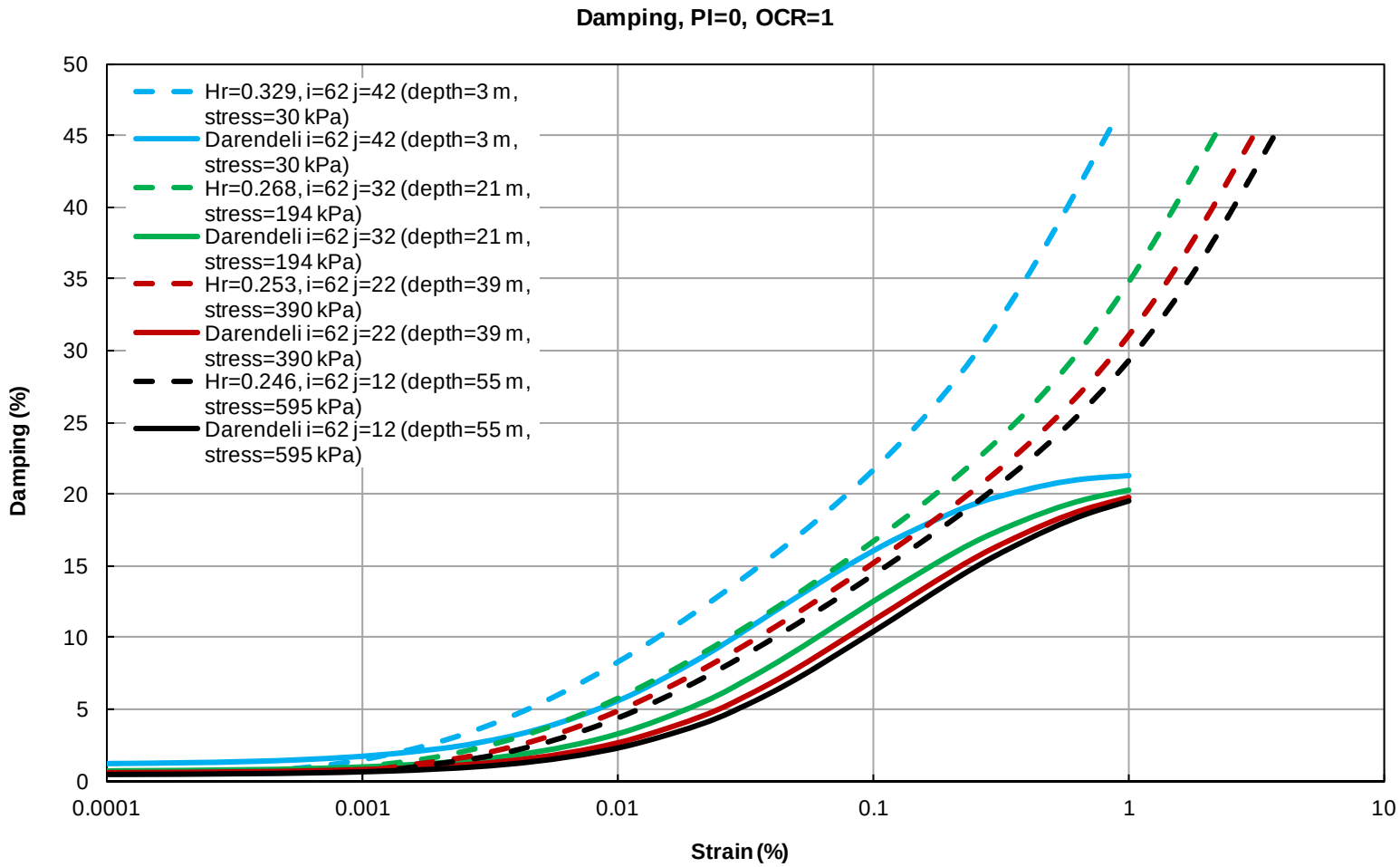

Zone id	Confining Stress σ_m	
i=62	(kPa)	(psf)
j=42	30	625
j=32	194	4058
j=22	390	8139
j=12	595	12420

Damping Ratio Relationship (after Darendeli 2001)

Seismic Deformation Analysis of Qaraoun Dam	OD11161570
AMEC Geomatrix	Figure **4-10**

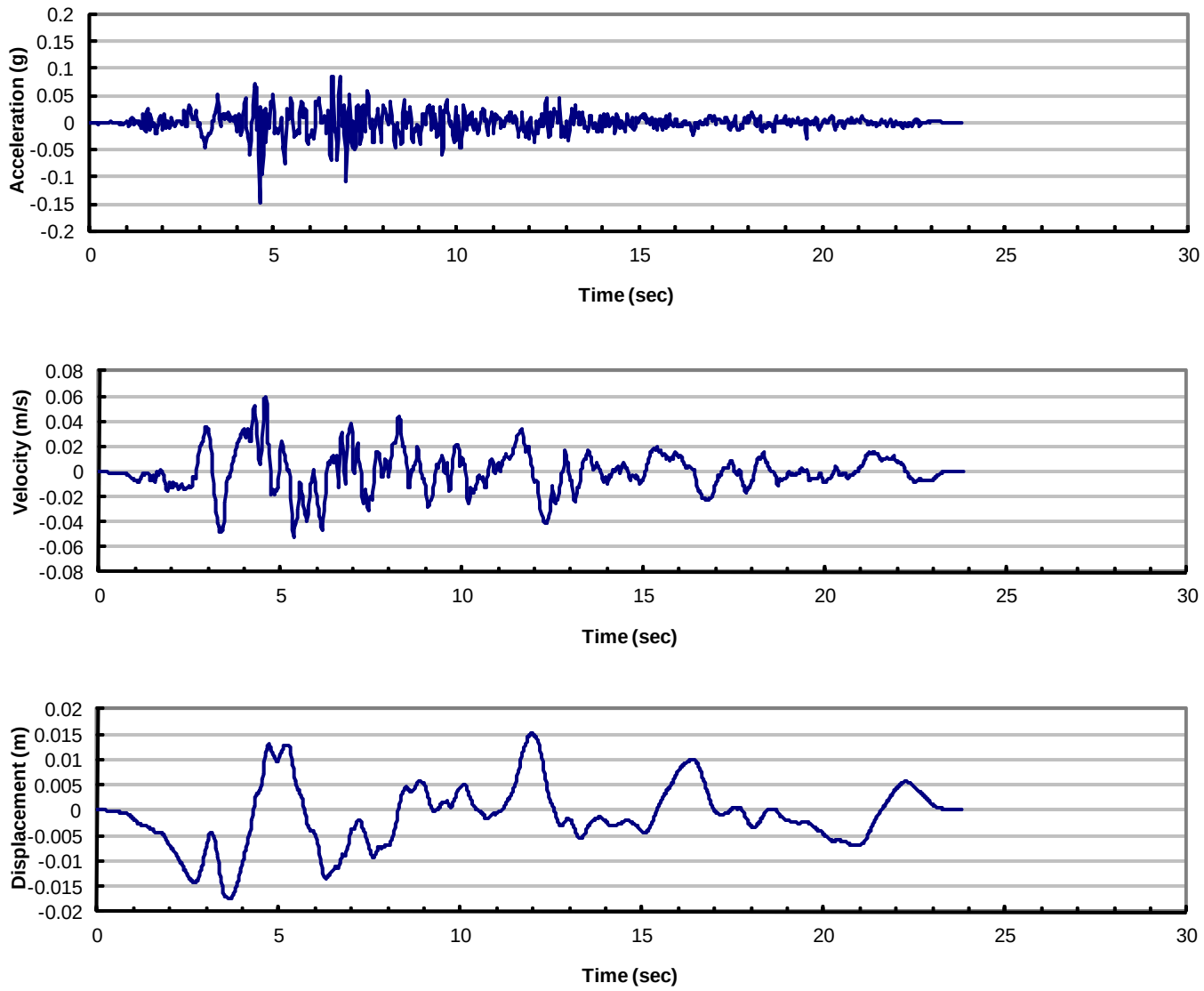

Input Earthquake Ground Motion (Horizontal)
100-yr Event (Dayhook Record)

Seismic Deformation Analysis of Qaraoun Dam	OD11161570
AMEC Geomatrix	Figure **4-11**

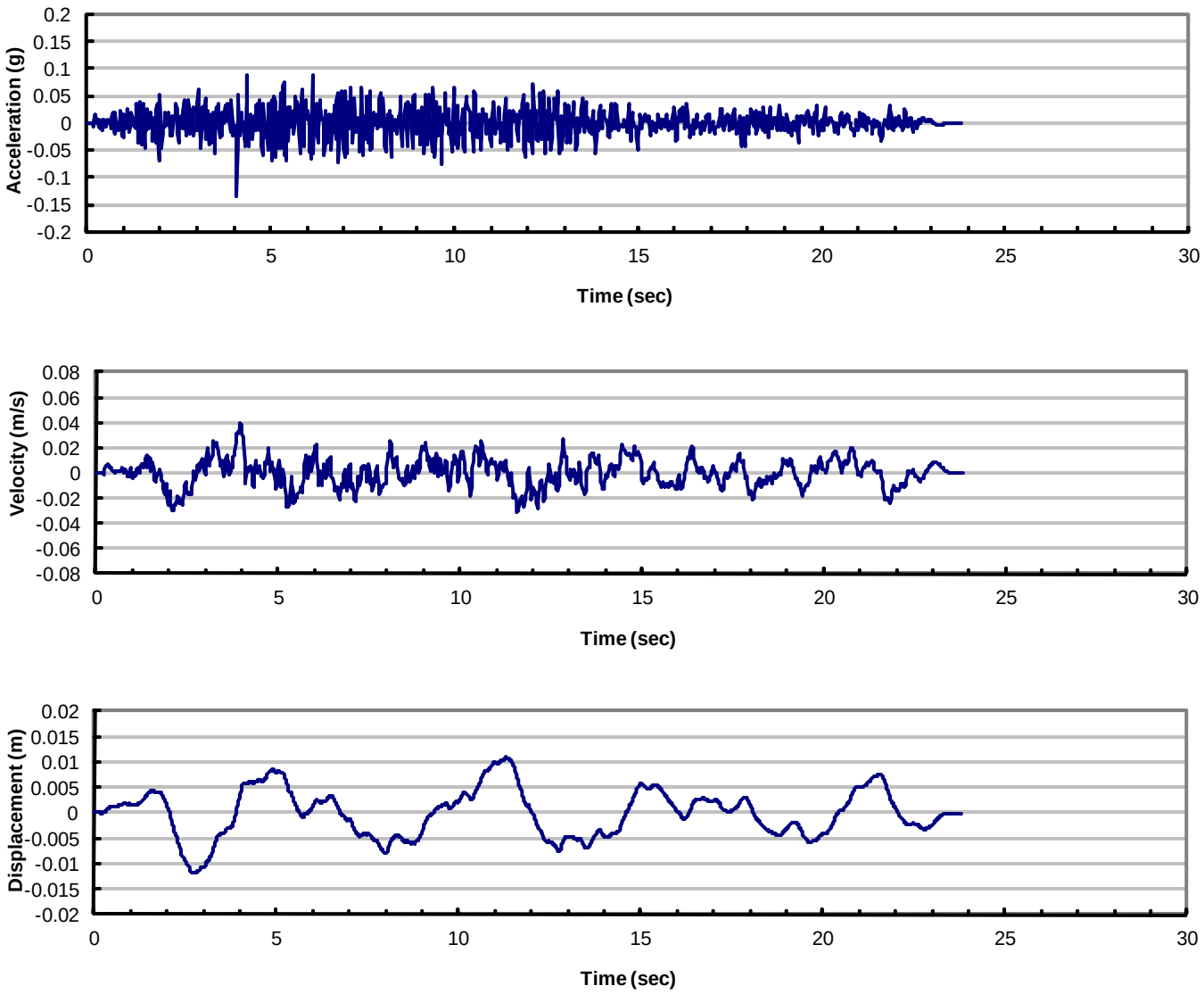

Input Earthquake Ground Motion (Vertical)
100-yr Event (Dayhook Record)

Seismic Deformation Analysis of Qaraoun Dam	OD11161570
AMEC Geomatrix	Figure **4-12**

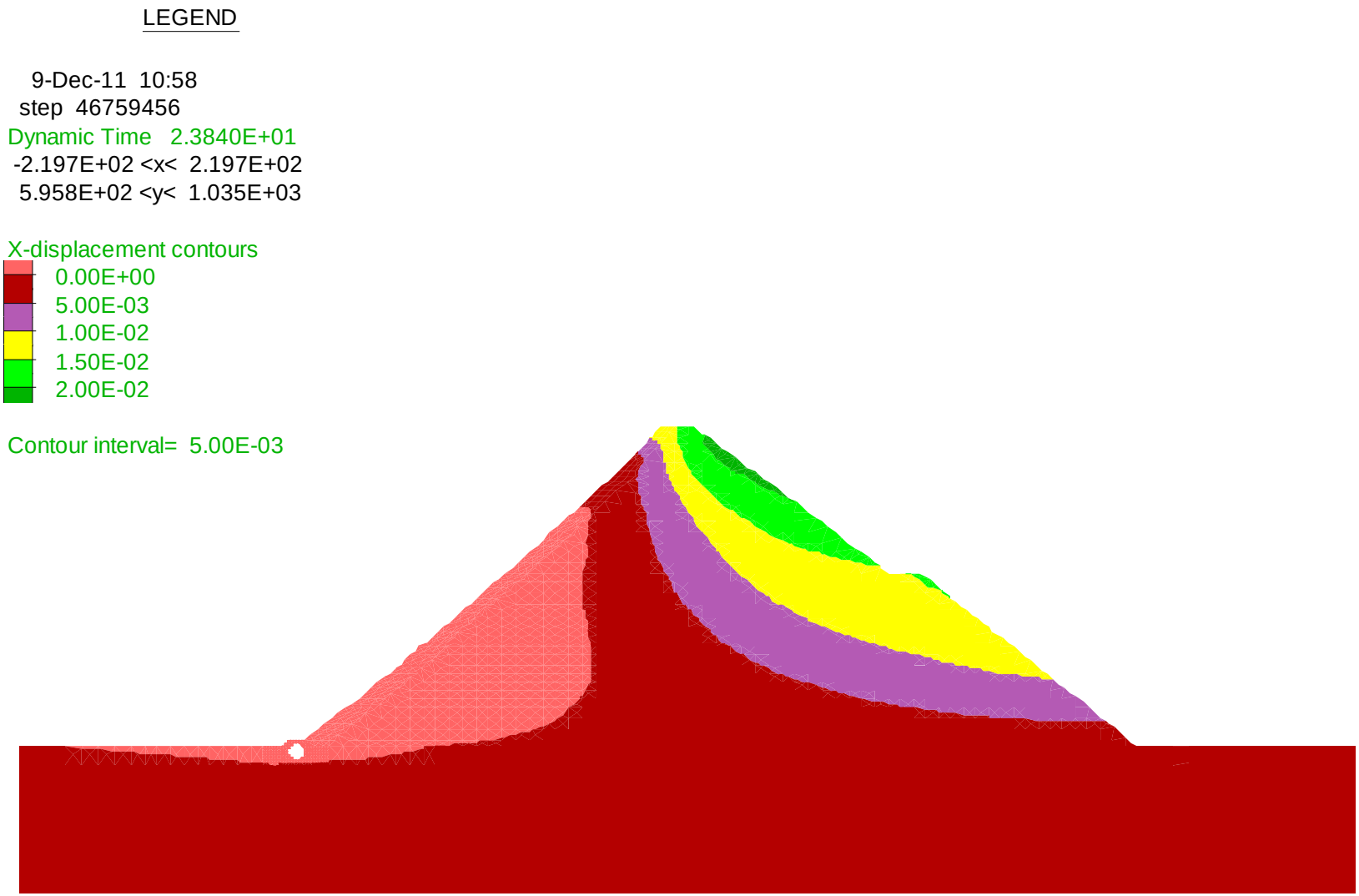

Positive horizontal (X) displacement denotes displacement in downstream direction

Contours of Horizontal Displacement (m) at End of Earthquake, 100-yr Event (Dayhook Record)	
Seismic Deformation Analysis of Qaraoun Dam	OD11161570
AMEC Geomatrix	Figure **4-13**

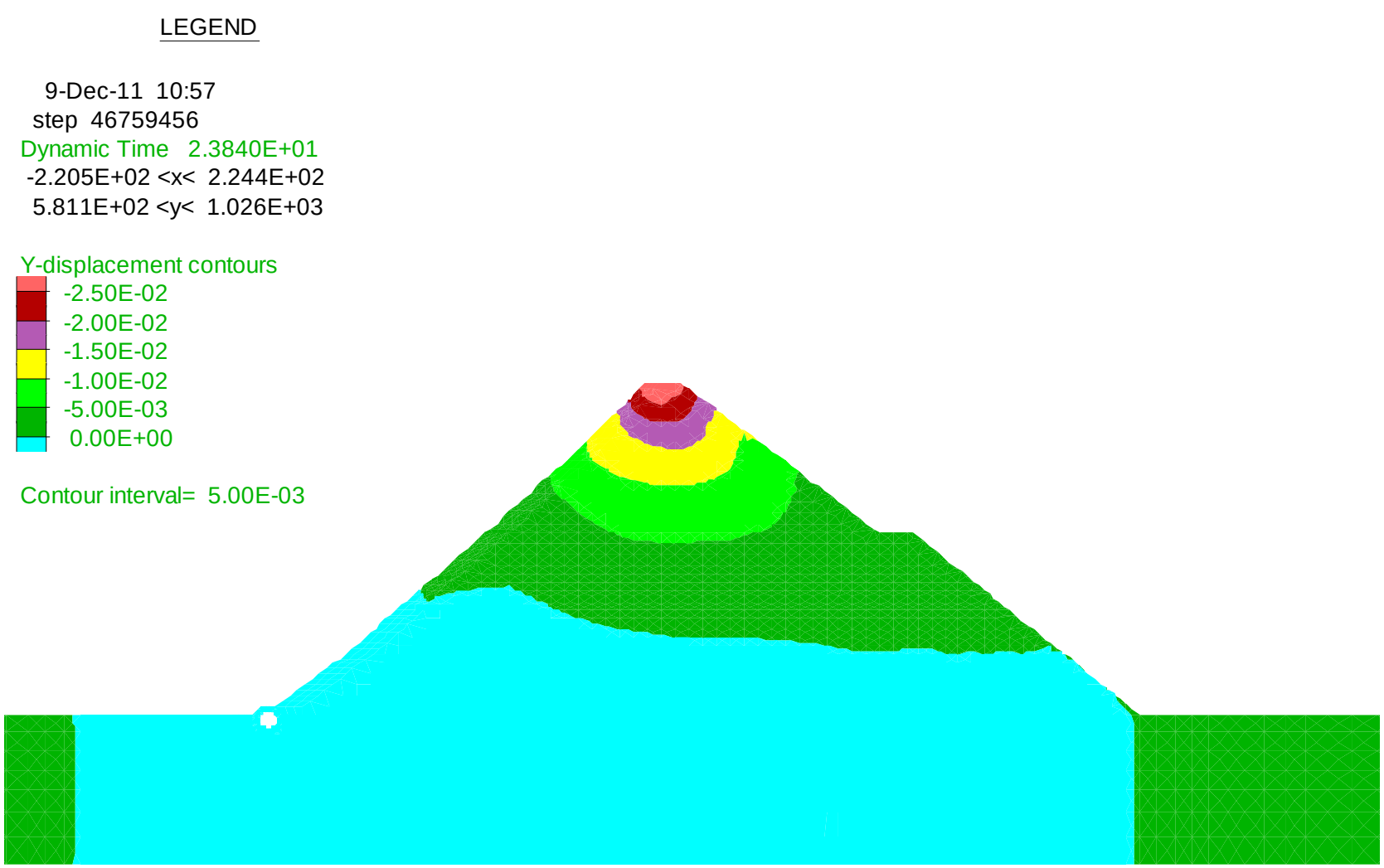

Negative Vertical (Y) displacement denotes displacement downward (settlement)

Contours of Vertical Displacement (m) at End of Earthquake, 100-yr Event (Dayhook Record)	
Seismic Deformation Analysis of Qaraoun Dam	OD11161570
AMEC Geomatrix	Figure **4-14**

LEGEND

9-Dec-11 10:40
step 46759456
Dynamic Time 2.3840E+01
-2.332E+02 <x< 2.333E+02
5.822E+02 <y< 1.049E+03

Exaggerated Grid Distortion
Magnification = 5.000E+01
Max Disp = 3.301E-02

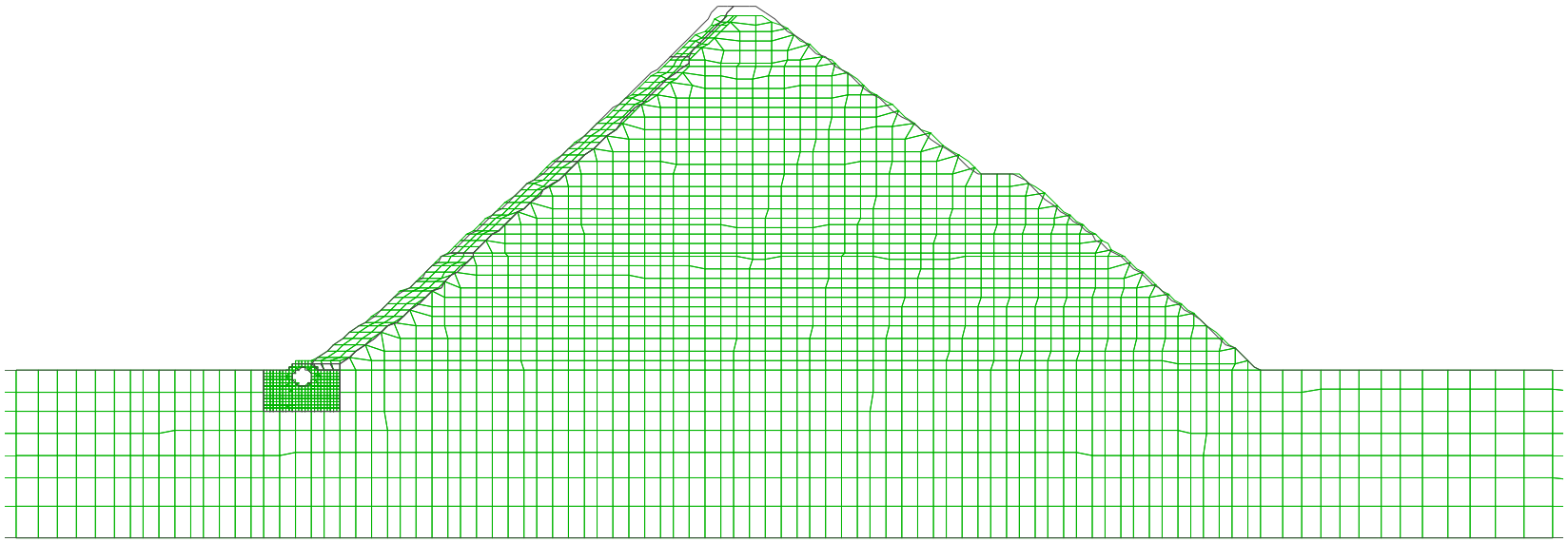

Computed Deformed Mesh at End of Earthquake, 100-yr Event (Dayhook Record)

Seismic Deformation Analysis of Qaraoun Dam	OD11161570
AMEC Geomatrix	Figure **4-15**

LEGEND

9-Dec-11 10:56
step 46759456
Dynamic Time 2.3840E+01
-2.197E+02 <x< 2.197E+02
5.958E+02 <y< 1.035E+03

Max. shear strain increment
0.00E+00
2.50E-04
5.00E-04
7.50E-04
1.00E-03
1.25E-03
1.50E-03

Contour interval= 2.50E-04
Extrap. by averaging

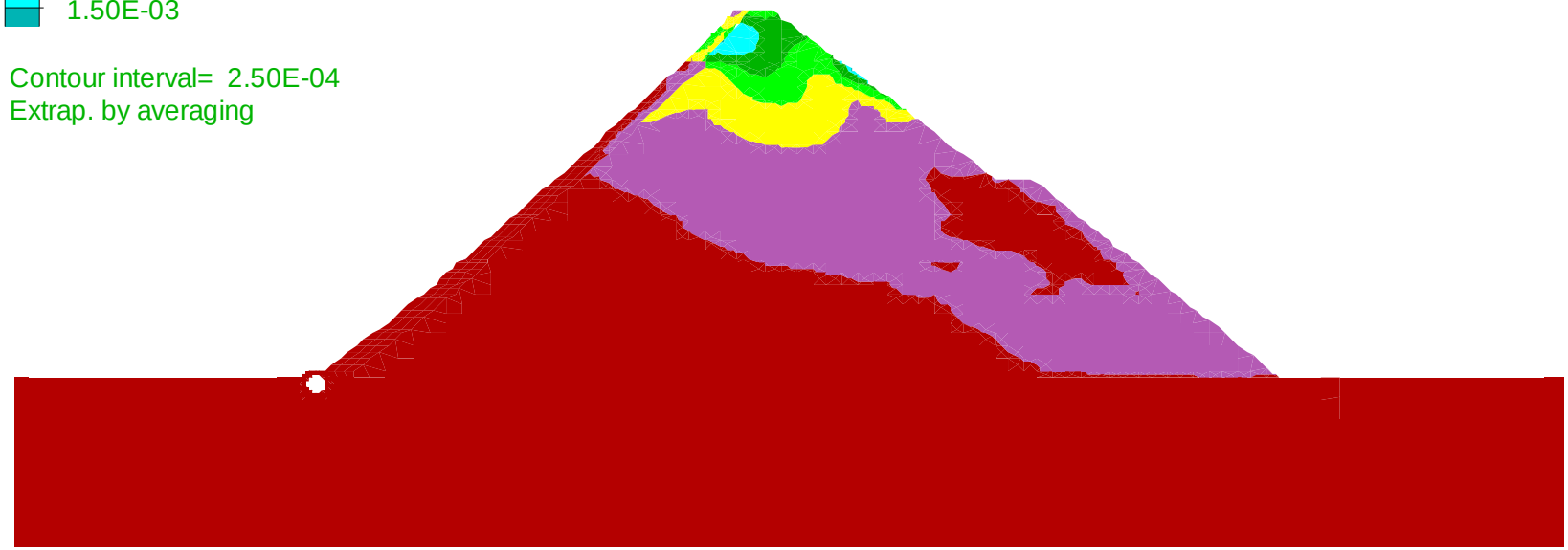

Contours of Maximum Shear Strain Increment (SSI) at End Earthquake, 100-yr Event (Dayhook Record)

Seismic Deformation Analysis of Qaraoun Dam	OD11161570
AMEC Geomatrix	Figure **4-16**

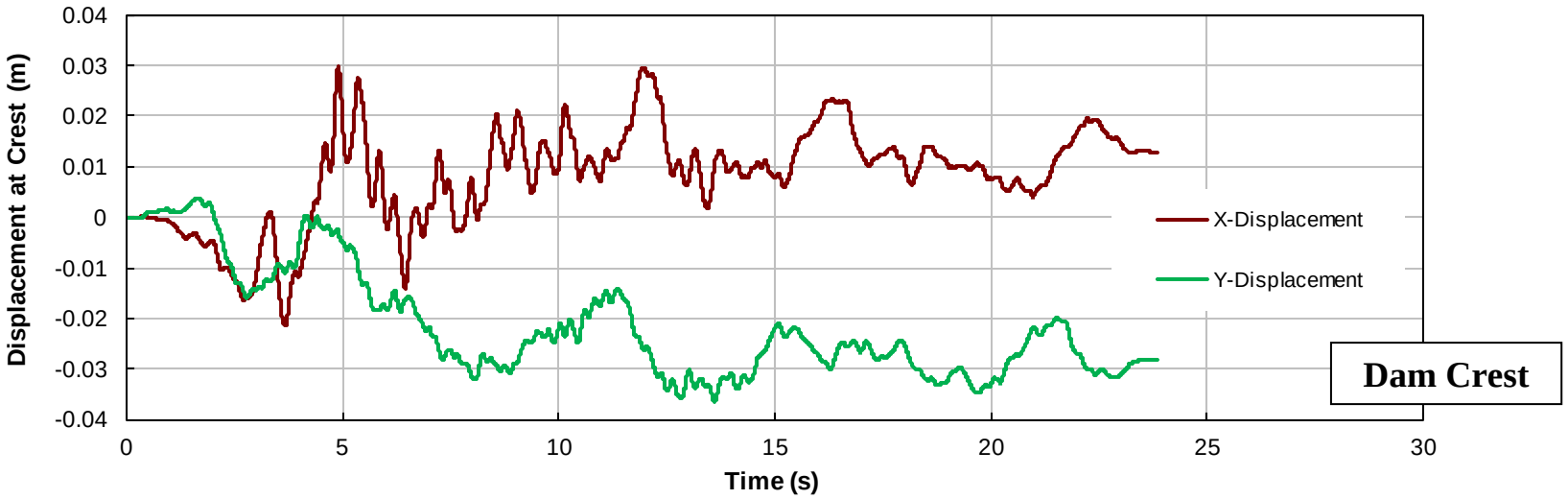

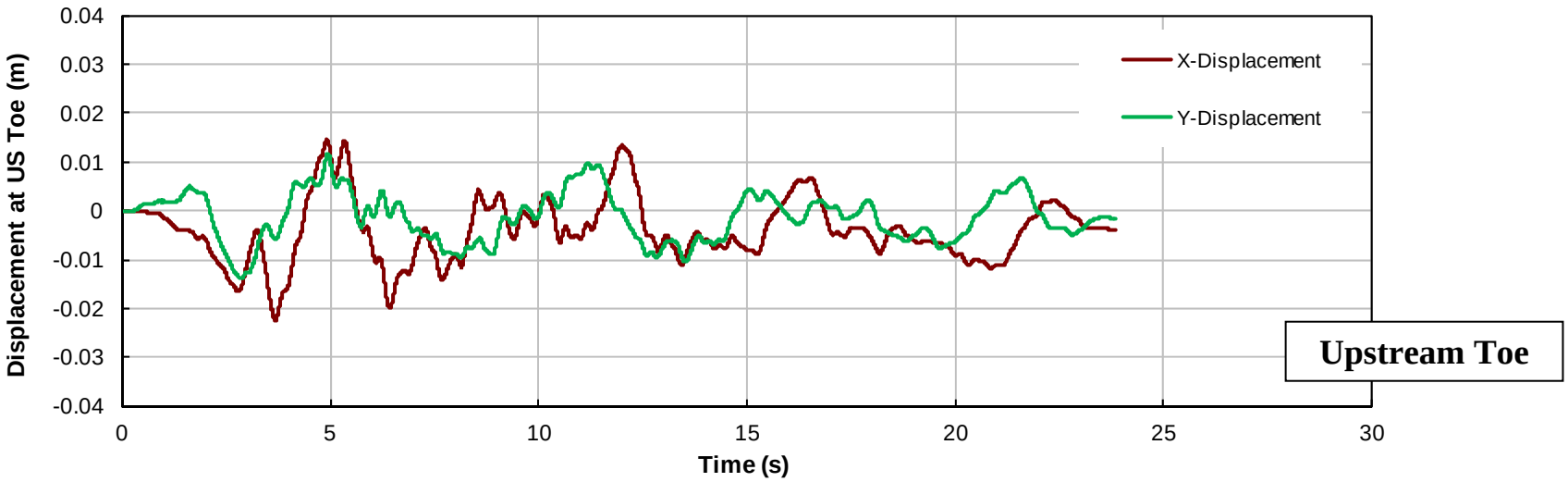

Positive horizontal (X) displacement denotes displacement downstream direction
Negative Vertical (Y) displacement denotes displacement downward (settlement)

Computed Horizontal (X) and Vertical Displacement (Y) Time Histories at the Crest and at the US Toe, 100-yr Event (Dayhook Record)	
Seismic Deformation Analysis of Qaraoun Dam	OD11161570
AMEC Geomatrix	Figure 4-17

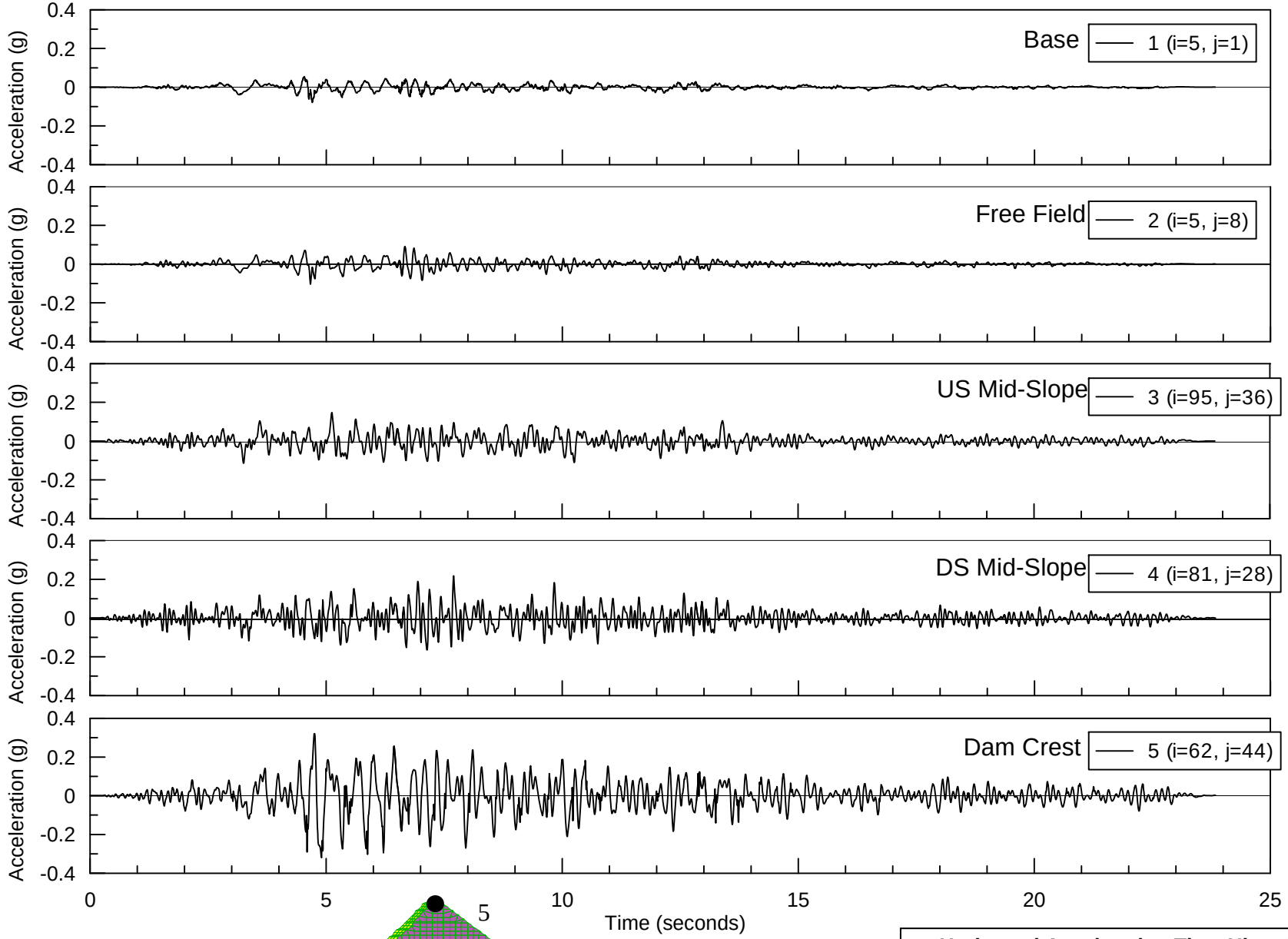

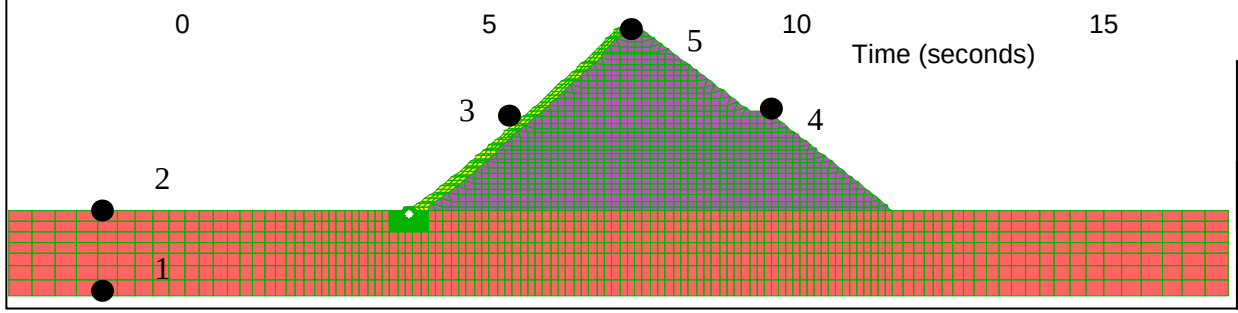

Horizontal Acceleration Time Histories at Various Locations, 100-yr Event (Dayhook Record)

Seismic Deformation Analysis of Qaraoun Dam	OD11161570
AMEC Geomatrix	Figure **4-18**

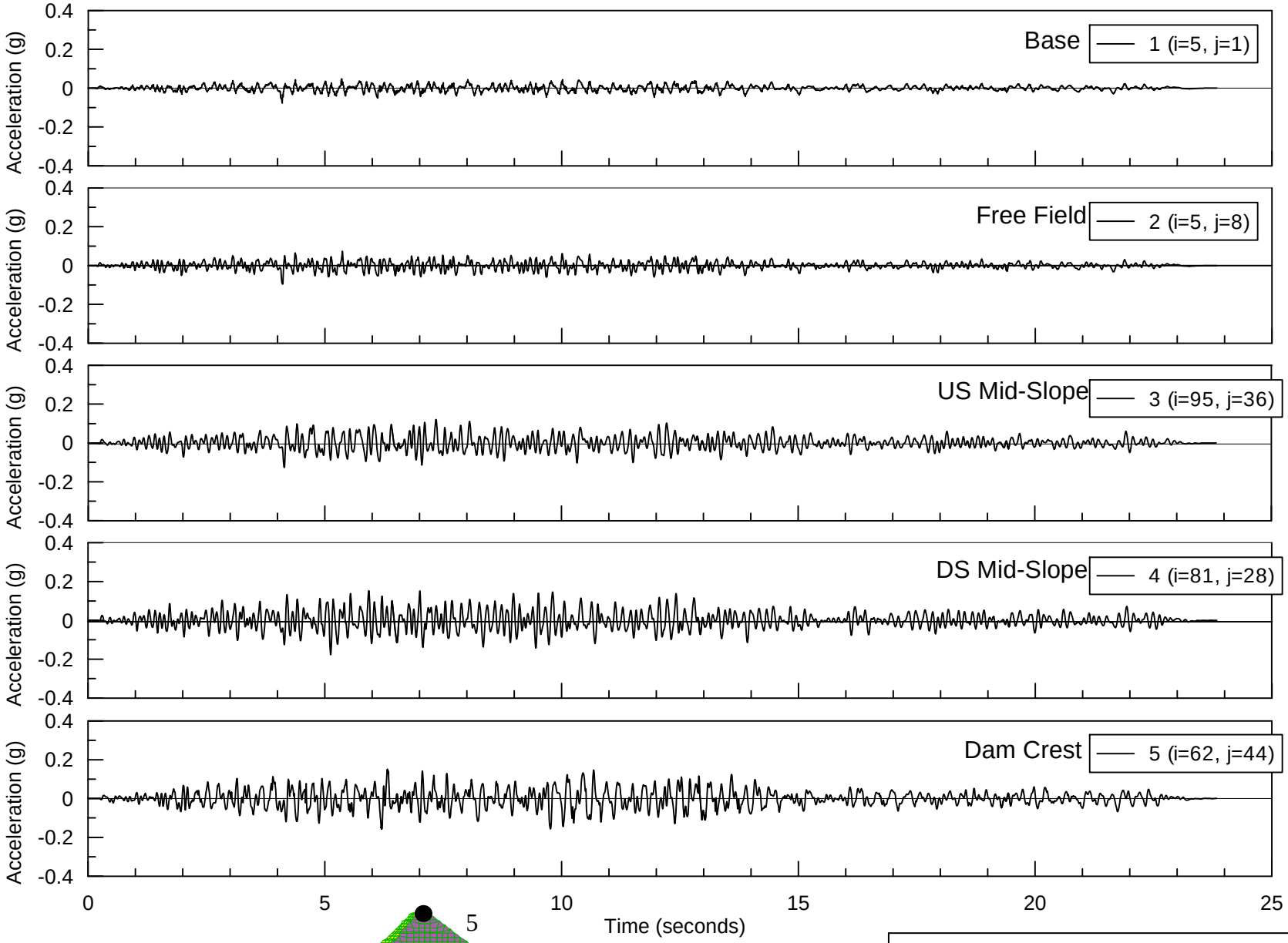

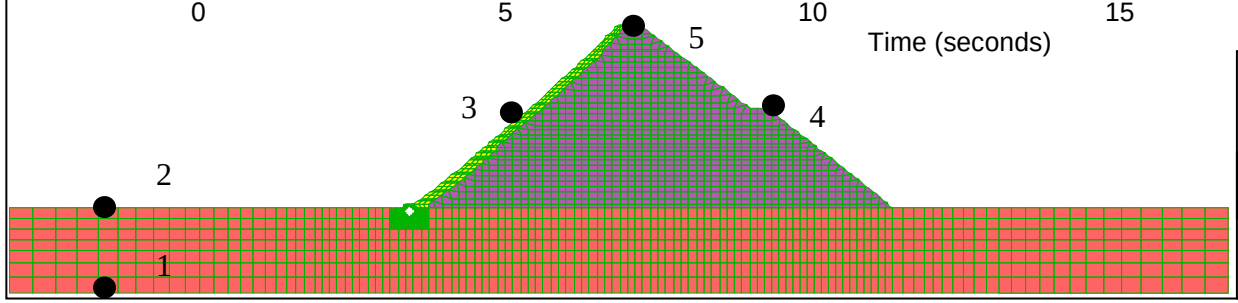

Vertical Acceleration Time Histories at Various Locations, 100-yr Event (Dayhook Record)

Seismic Deformation Analysis of Qaraoun Dam	OD11161570
AMEC Geomatrix	Figure **4-19**

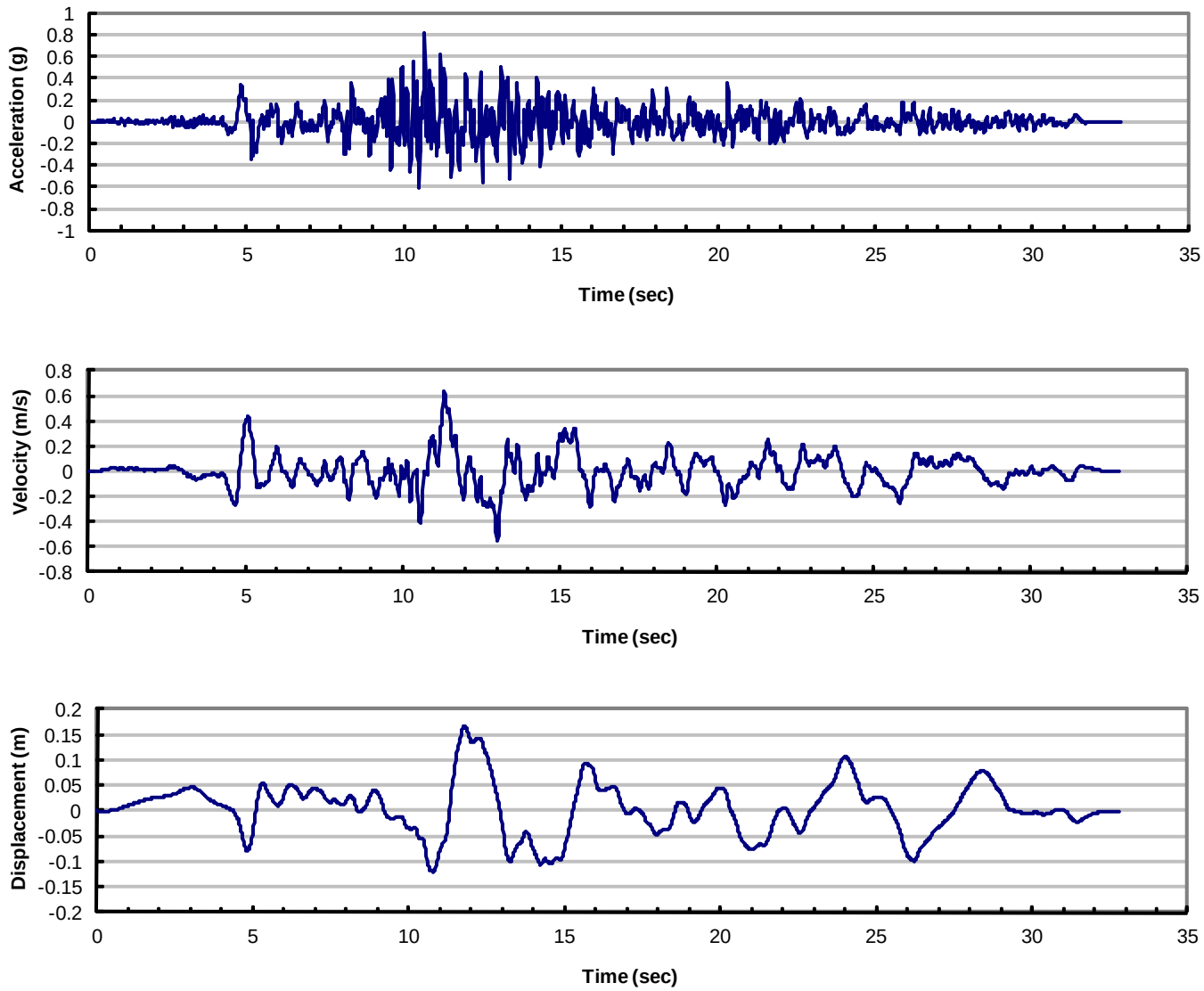

Input Earthquake Ground Motion (Horizontal)
2,475-yr Event (Tabas Record)

Seismic Deformation Analysis of Qaraoun Dam	OD11161570
AMEC Geomatrix	Figure **4-20**

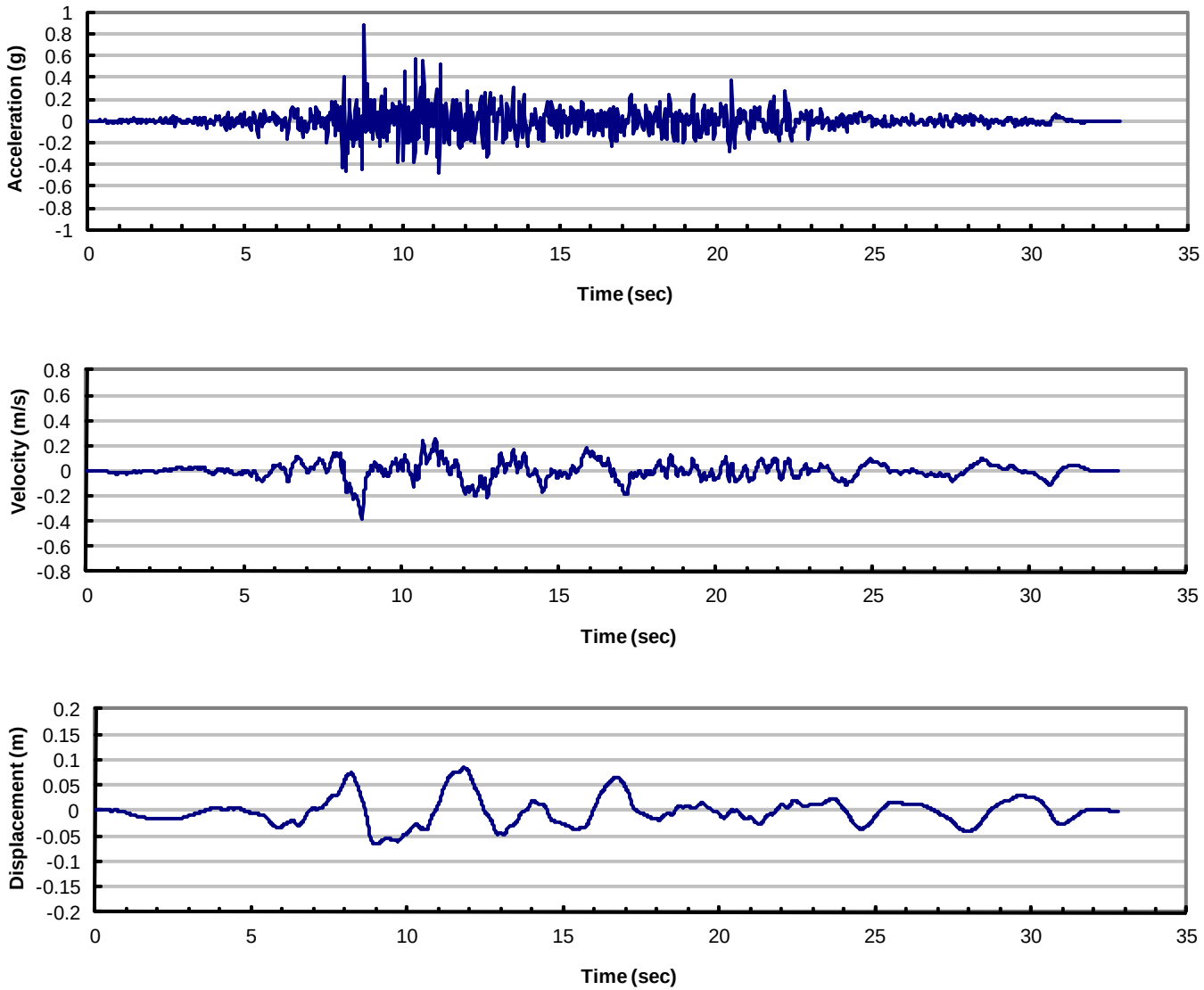

Input Earthquake Ground Motion (Vertical)
2,475-yr Event (Tabas Record)

Seismic Deformation Analysis of Qaraoun Dam	OD11161570
AMEC Geomatrix	Figure **4-21**

LEGEND

9-Dec-11 10:53
step 64405202
Dynamic Time 3.2840E+01
-2.197E+02 <x< 2.197E+02
5.955E+02 <y< 1.035E+03

X-displacement contours
0.00E+00
1.00E-01
2.00E-01
3.00E-01
4.00E-01
5.00E-01

Contour interval= 1.00E-01

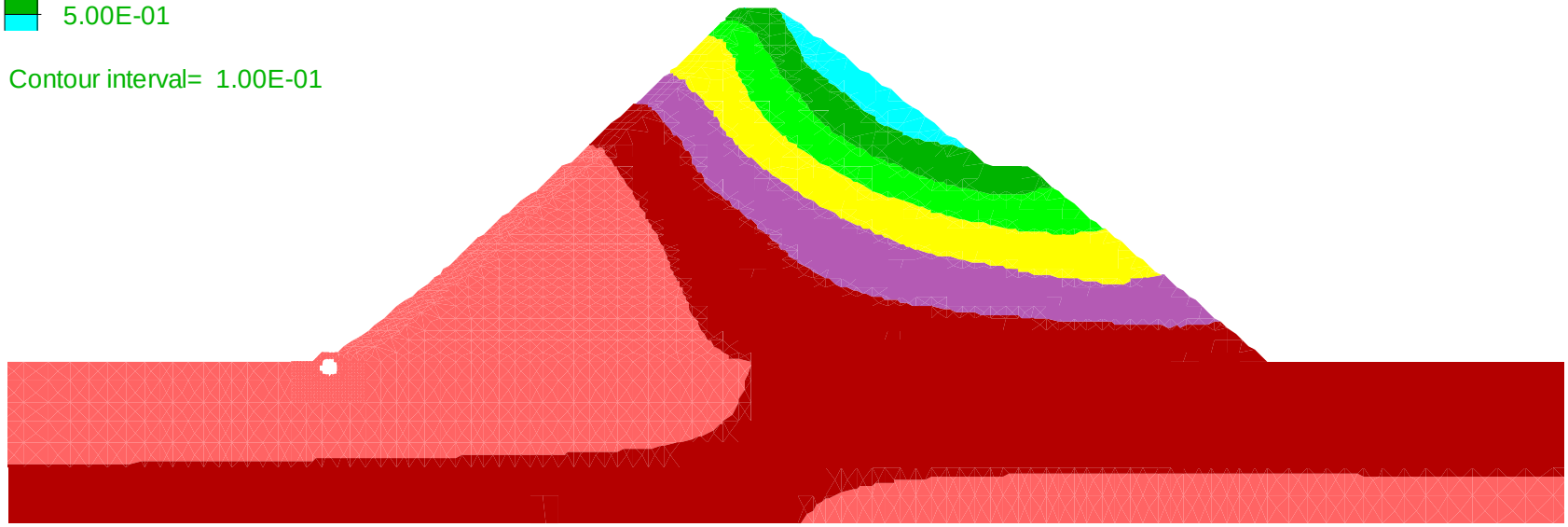

Positive horizontal (X) displacement denotes displacement downstream direction

Contours of Horizontal Displacement (m) at End of Earthquake, 2,475-yr Event (Tabas Record)

Seismic Deformation Analysis of Qaraoun Dam	OD11161570
AMEC Geomatrix	Figure **4-22**

LEGEND

9-Dec-11 10:51
step 64405202
Dynamic Time 3.2840E+01
-2.205E+02 <x< 2.244E+02
5.811E+02 <y< 1.026E+03

Y-displacement contours
-4.00E-01
-3.00E-01
-2.00E-01
-1.00E-01
0.00E+00

Contour interval= 1.00E-01

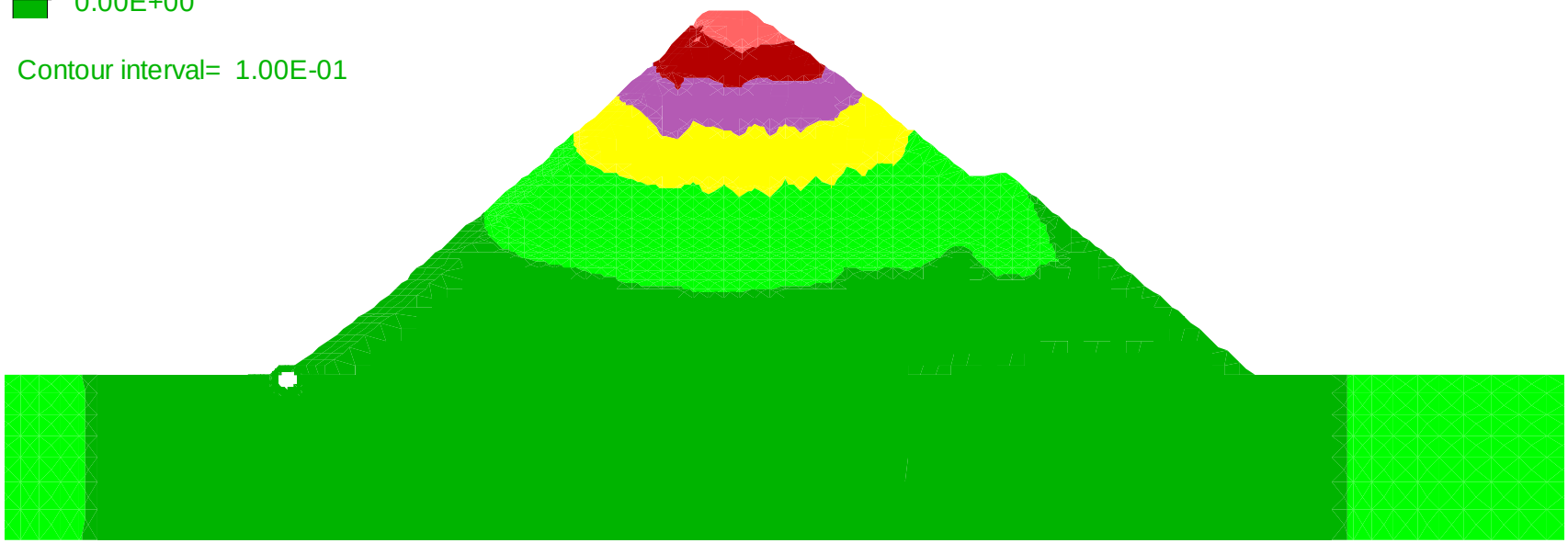

Negative Vertical (Y) displacement denotes displacement downward (settlement)

Contours of Vertical Displacement (m) at End of Earthquake, 2,475-yr Event (Tabas Record)

Seismic Deformation Analysis of Qaraoun Dam	OD11161570
AMEC Geomatrix	Figure **4-23**

LEGEND

9-Dec-11 10:45
step 64405202
Dynamic Time 3.2840E+01
-2.342E+02 <x< 2.343E+02
5.811E+02 <y< 1.050E+03

Exaggerated Grid Distortion
Magnification = 5.000E+00
Max Disp = 6.664E-01

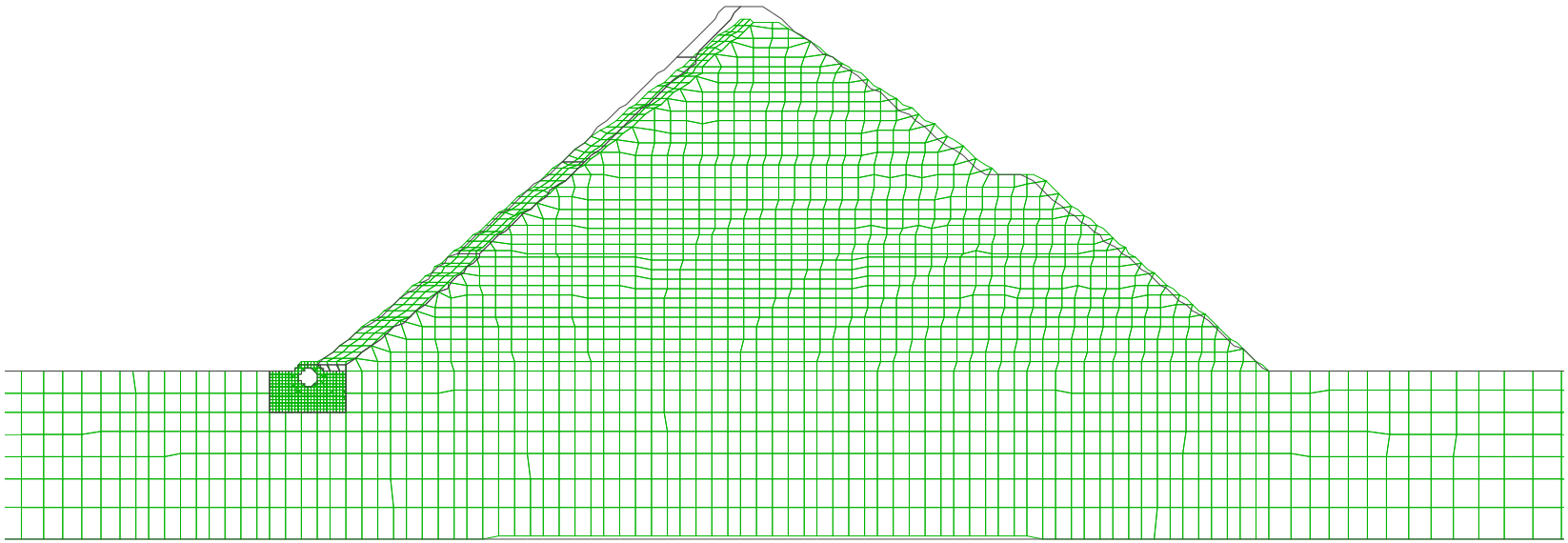

Computed Deformed Mesh at End of Earthquake, 2,475-yr Event (Tabas Record)

Seismic Deformation Analysis of Qaraoun Dam	OD11161570
AMEC Geomatrix	Figure **4-24**

LEGEND

9-Dec-11 10:48
step 64405202
Dynamic Time 3.2840E+01
-2.197E+02 <x< 2.197E+02
5.955E+02 <y< 1.035E+03

Max. shear strain increment
0.00E+00
2.50E-03
5.00E-03
7.50E-03
1.00E-02
1.25E-02
1.50E-02
1.75E-02
2.00E-02
2.25E-02

Contour interval= 2.50E-03
Extrap. by averaging

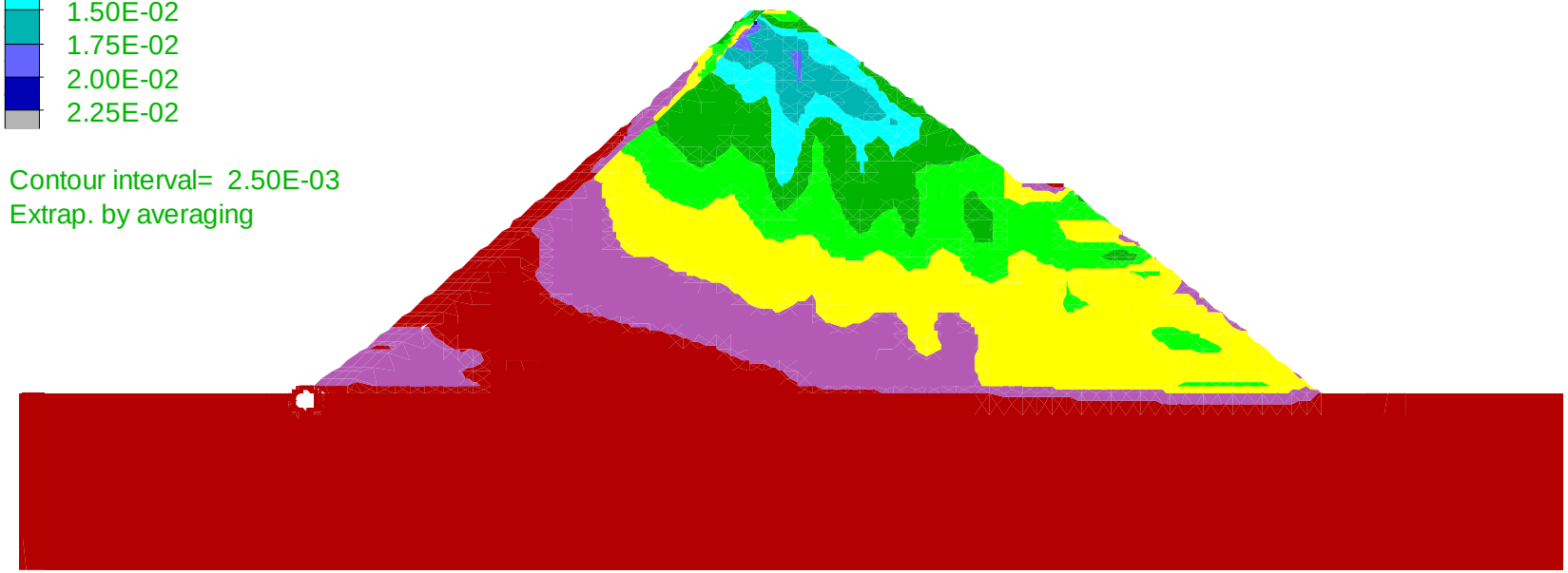

Contours of Maximum Shear Strain Increment (SSI) at End of Earthquake, 2,475-yr Event (Tabas Record)	
Seismic Deformation Analysis of Qaraoun Dam	OD11161570
AMEC Geomatrix	Figure **4-25**

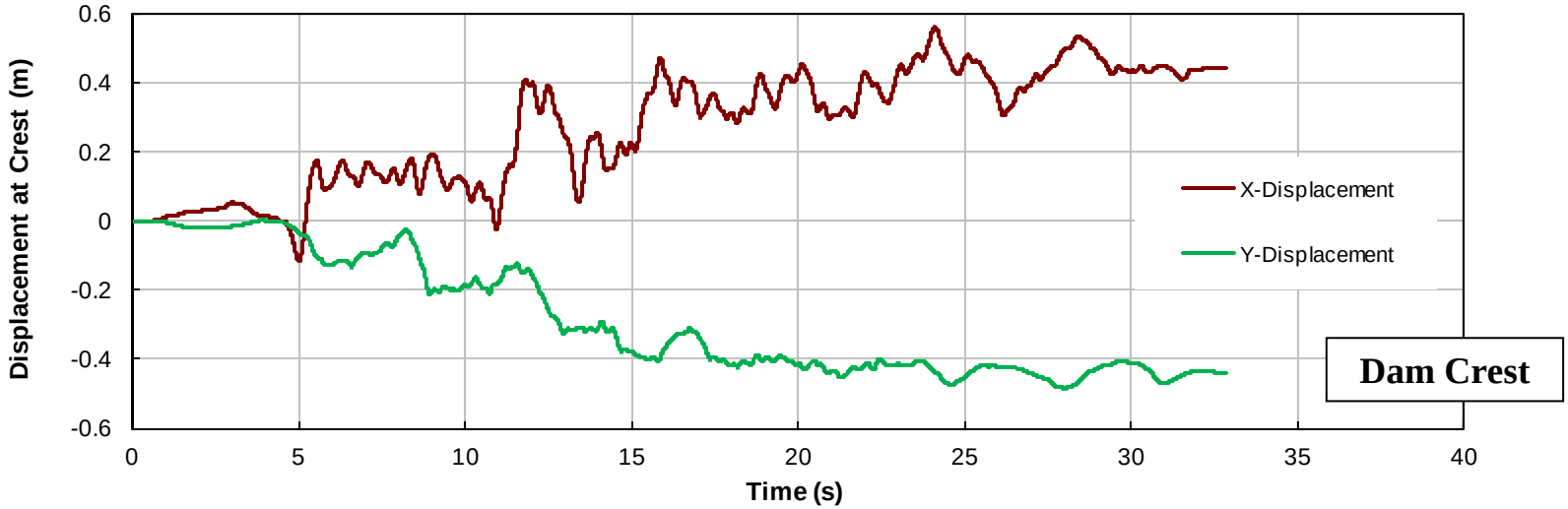

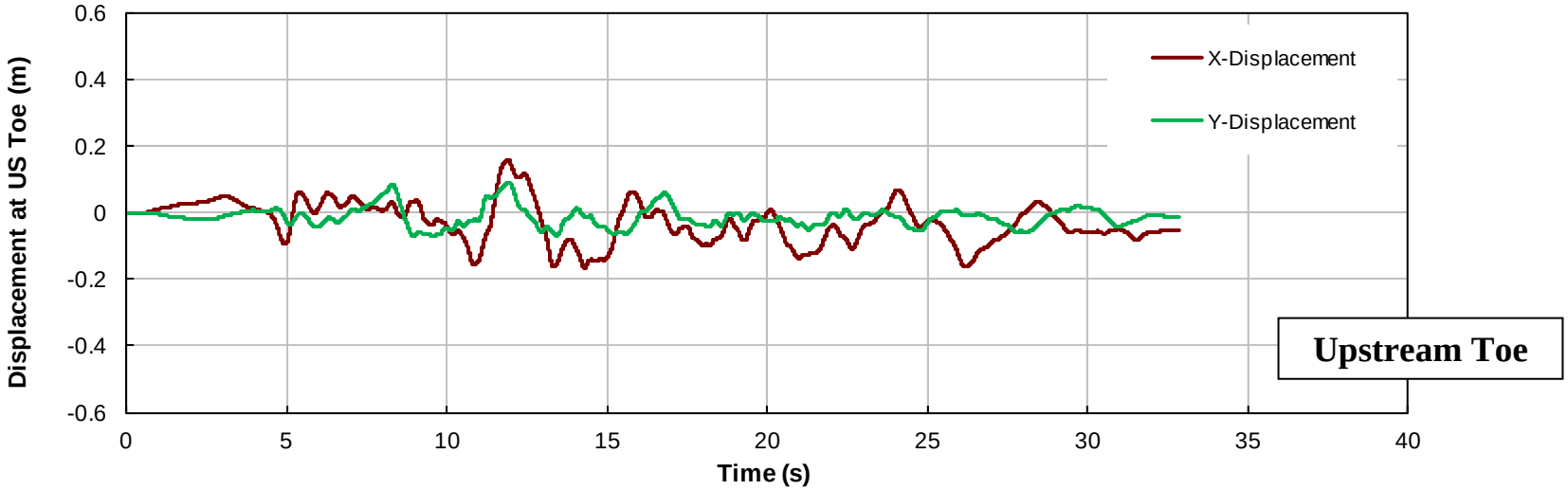

Positive horizontal (X) displacement denotes displacement downstream direction
Negative Vertical (Y) displacement denotes displacement downward (settlement)

Computed Horizontal (X) and Vertical (Y) Displacement Time Histories at the Crest and at the US Toe, 2,475-yr Event (Tabas Record)	
Seismic Deformation Analysis of Qaraoun Dam	OD11161570
AMEC Geomatrix	Figure 4-26

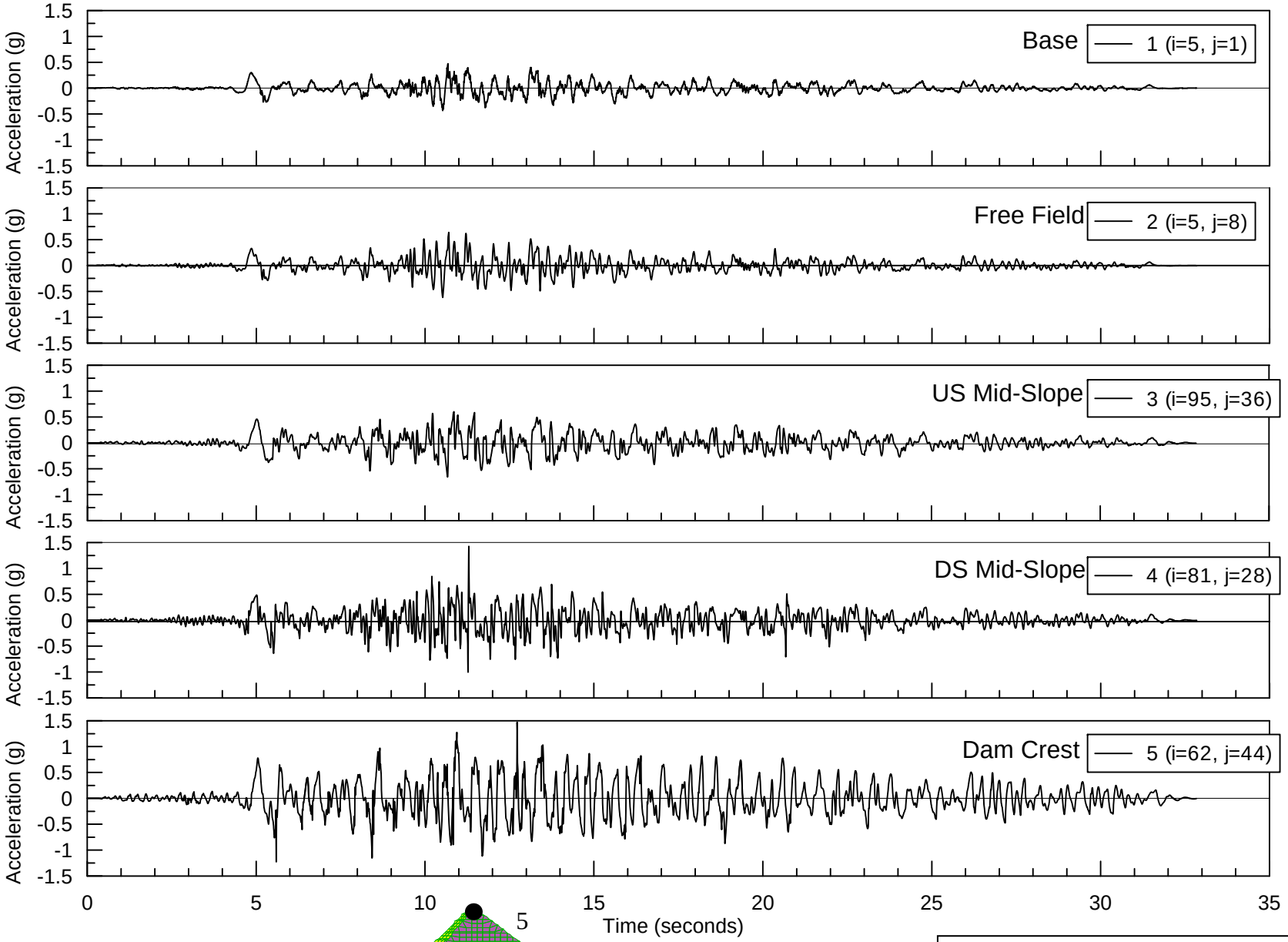

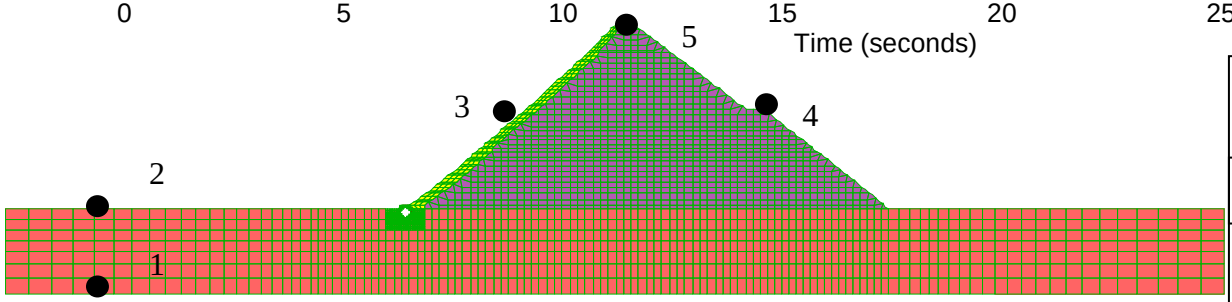

Horizontal Acceleration Time Histories at Various Locations, 2,475-yr Event (Tabas Record)

Seismic Deformation Analysis of Qaraoun Dam	OD11161570
AMEC Geomatrix	Figure **4-27**

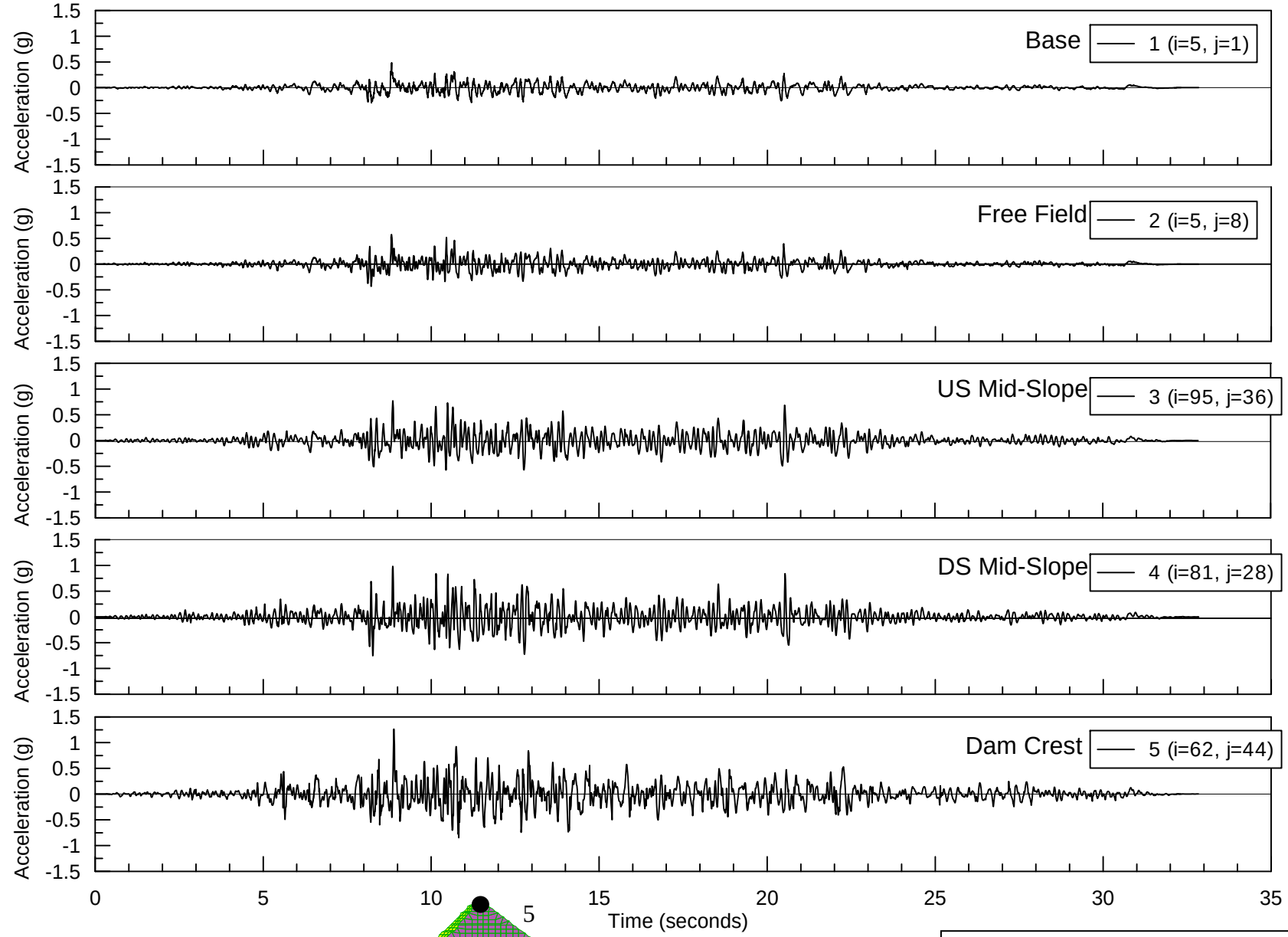

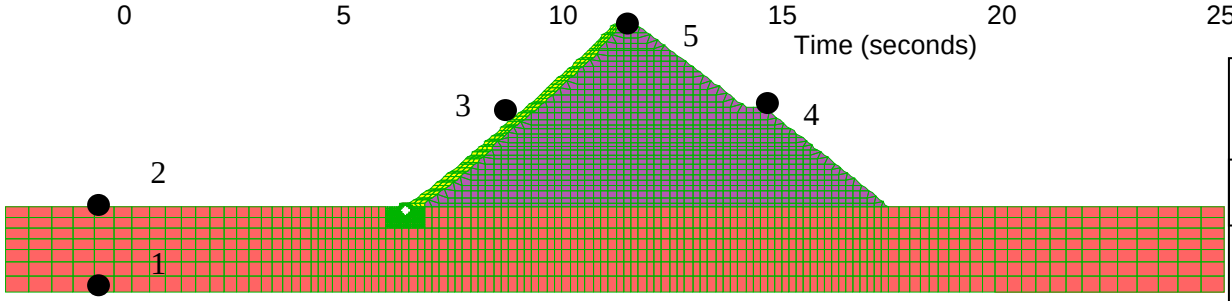

Vertical Acceleration Time Histories at Various Locations, 2,475-yr Event (Tabas Record)

Seismic Deformation Analysis of Qaraoun Dam	OD11161570
AMEC Geomatrix	Figure **4-28**

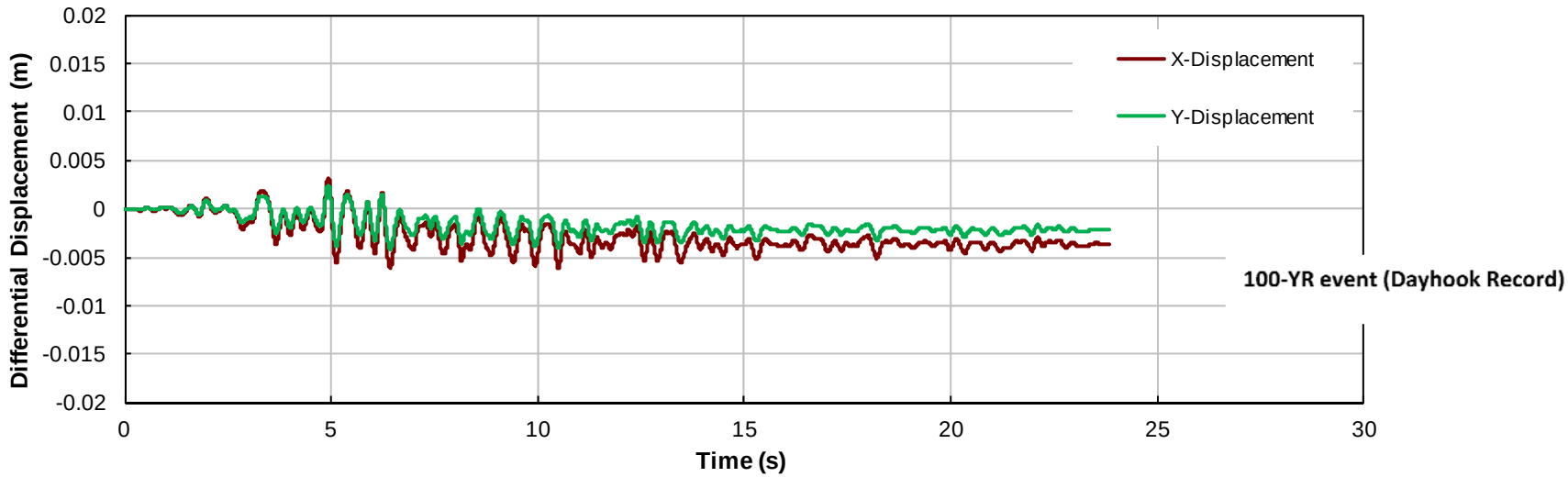

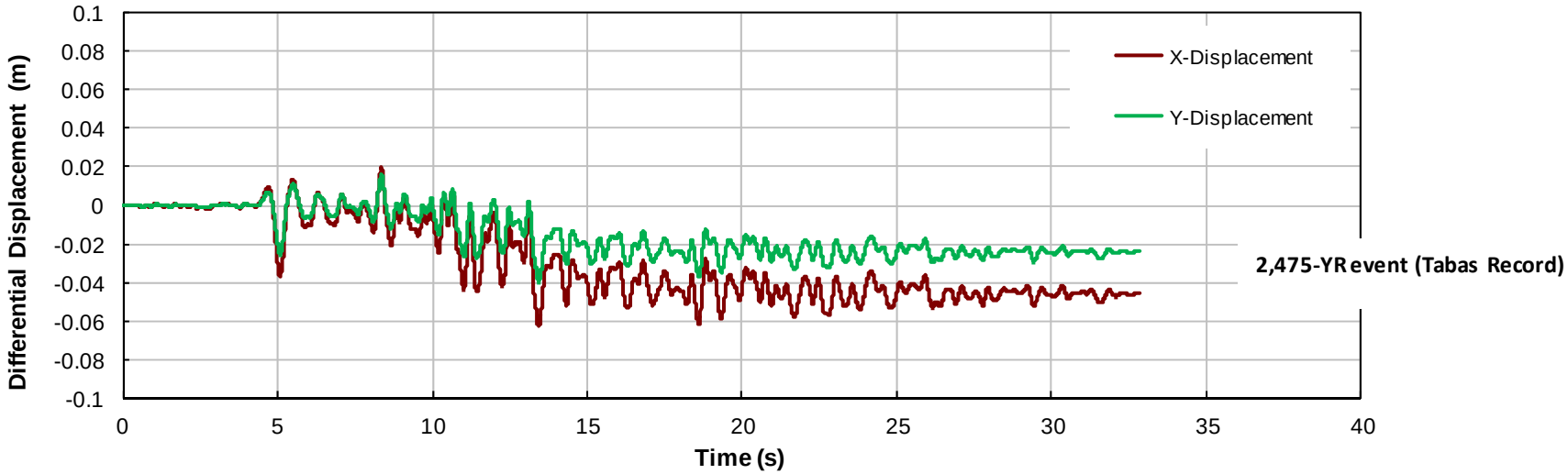

Differential Displacement between Bottom of Face Slab and Gallery, Horizontal (X) and Vertical (Y)

Seismic Deformation Analysis of Qaraoun Dam	OD11161570
AMEC Geomatrix	Figure **4-29**

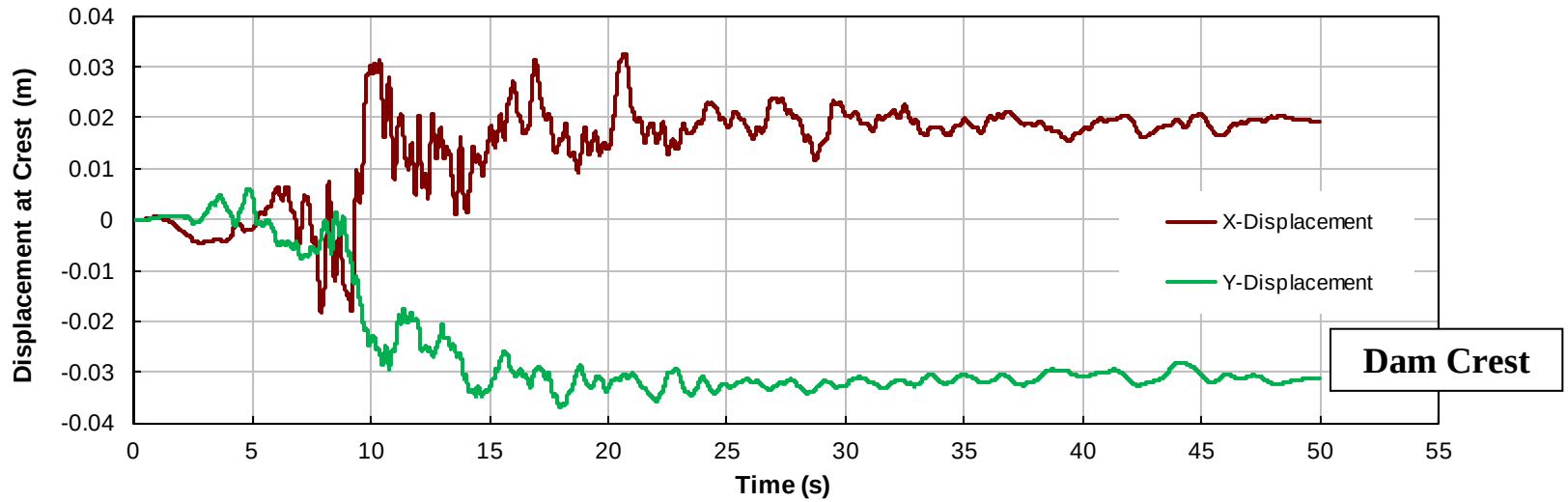

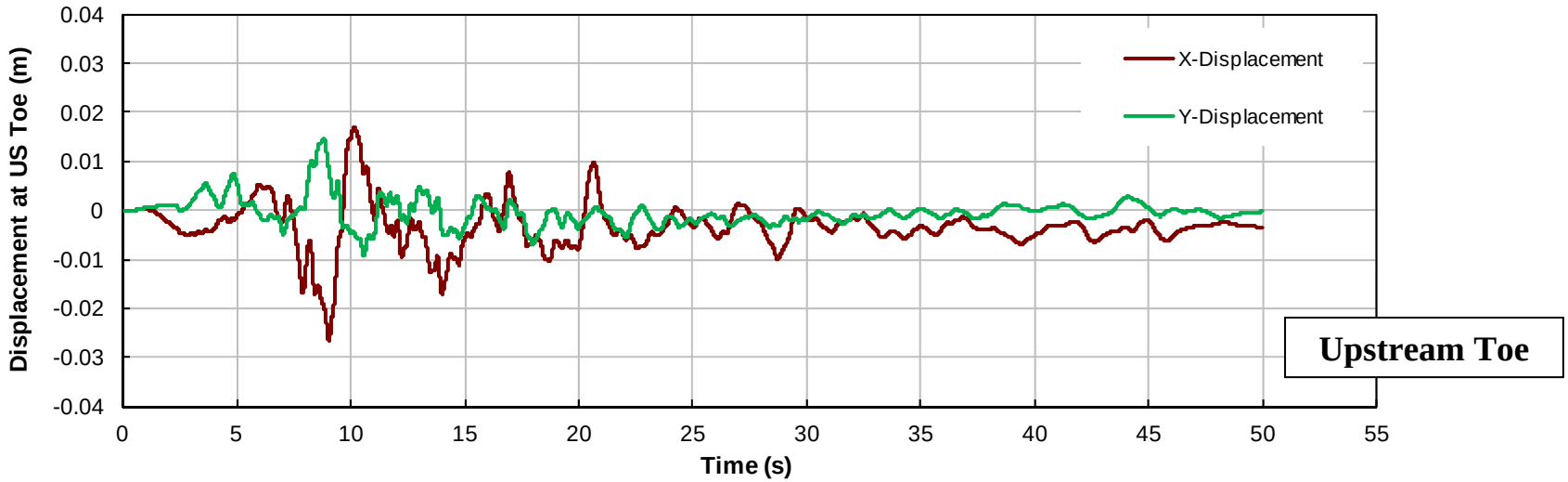

Positive horizontal (X) displacement denotes displacement downstream direction
Negative Vertical (Y) displacement denotes displacement downward (settlement)

Computed Horizontal (X) and Vertical (Y) Displacement Time Histories at the Crest and at the US Toe, 100-yr Event (San Jose-STH Record)	
Seismic Deformation Analysis of Qaraoun Dam	OD11161570
AMEC Geomatrix	Figure 4-30

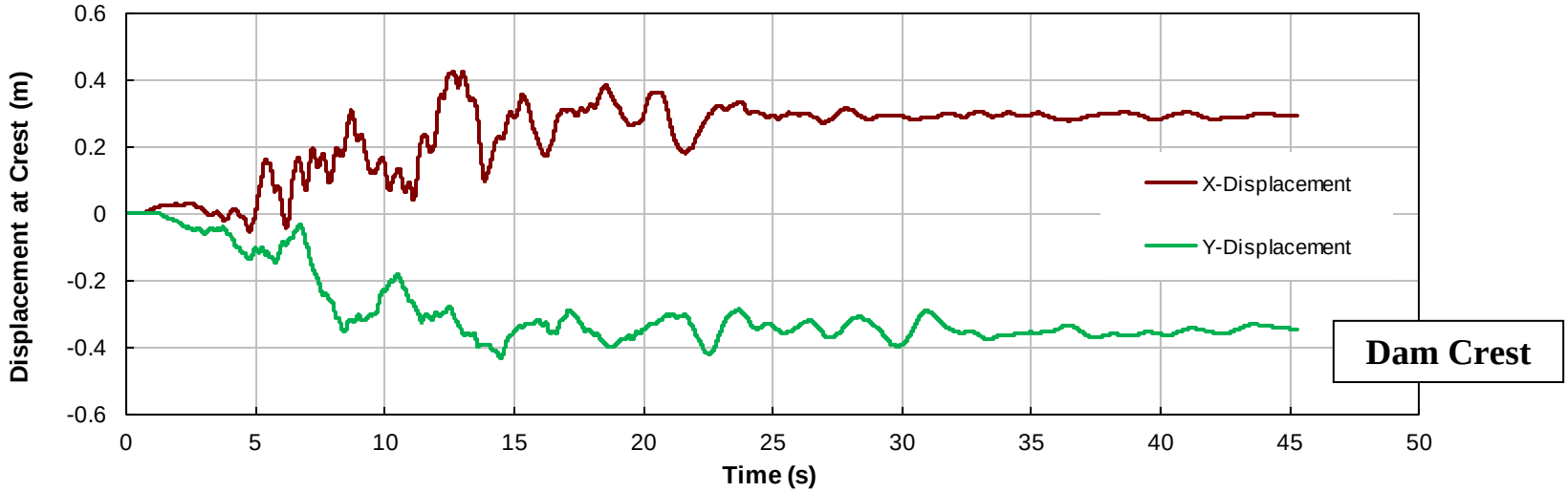

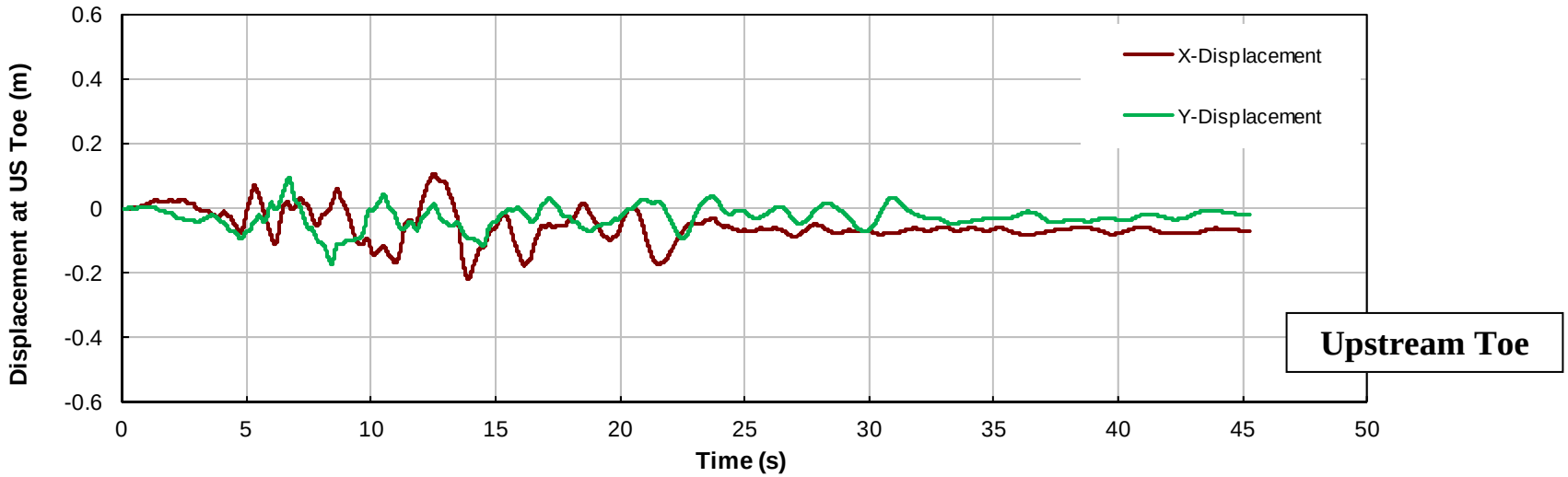

Positive horizontal (X) displacement denotes displacement downstream direction
Negative Vertical (Y) displacement denotes displacement downward (settlement)

Computed Horizontal (X) and Vertical (Y) Displacement Time Histories at the Crest and at the US Toe, 2,475-yr Event (Hector Mine Record)	
Seismic Deformation Analysis of Qaraoun Dam	OD11161570
AMEC Geomatrix	Figure 4-31

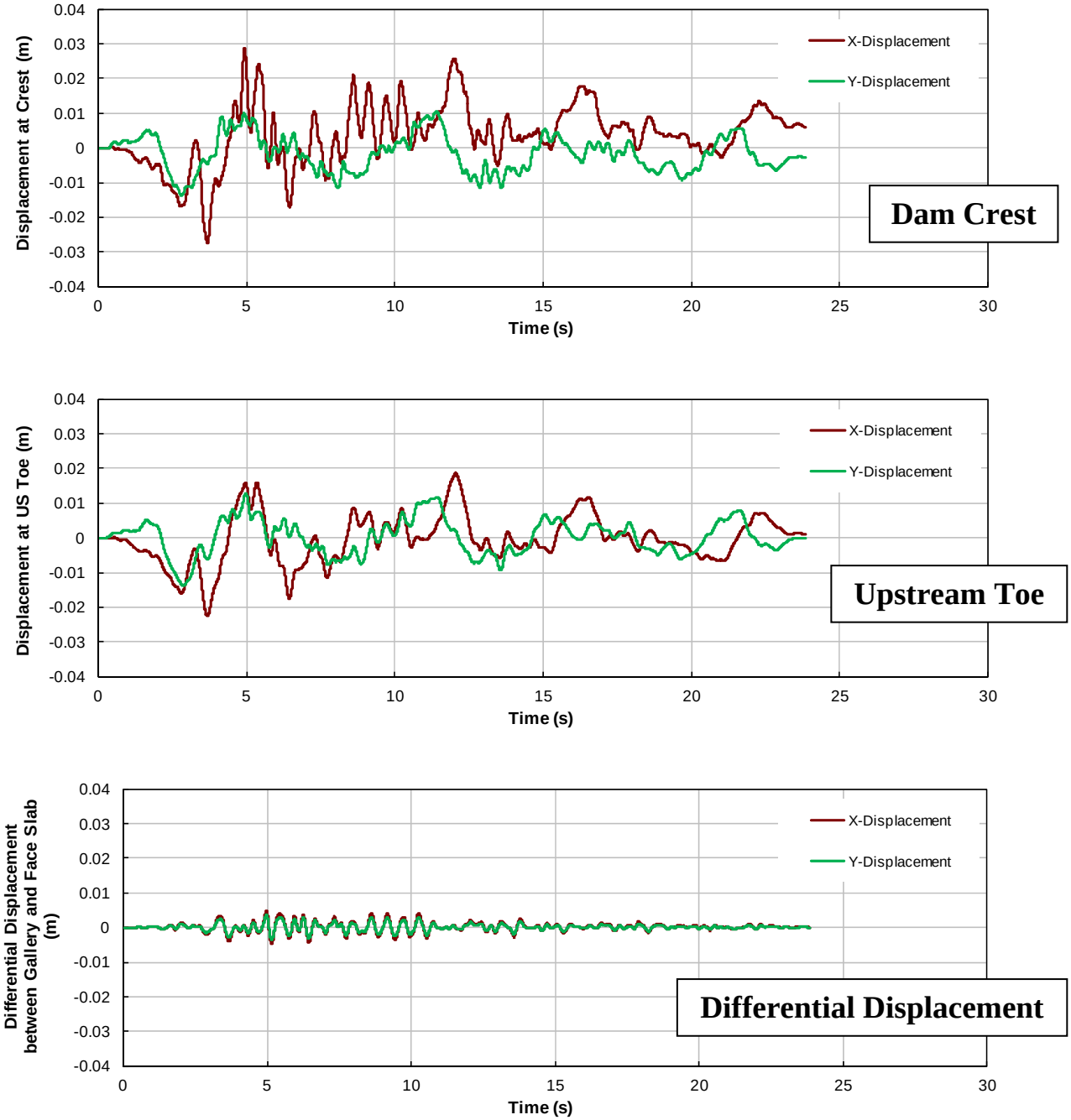

Computed Horizontal (X) and Vertical (Y) Displacement Time Histories at the Crest and at the US Toe, and Differential Displacement at US Toe, using the Mohr-Coulomb Model, 100-yr Event (Dayhook Record)

Seismic Deformation Analysis of Qaraoun Dam	OD11161570
AMEC Geomatrix	Figure **4-32**

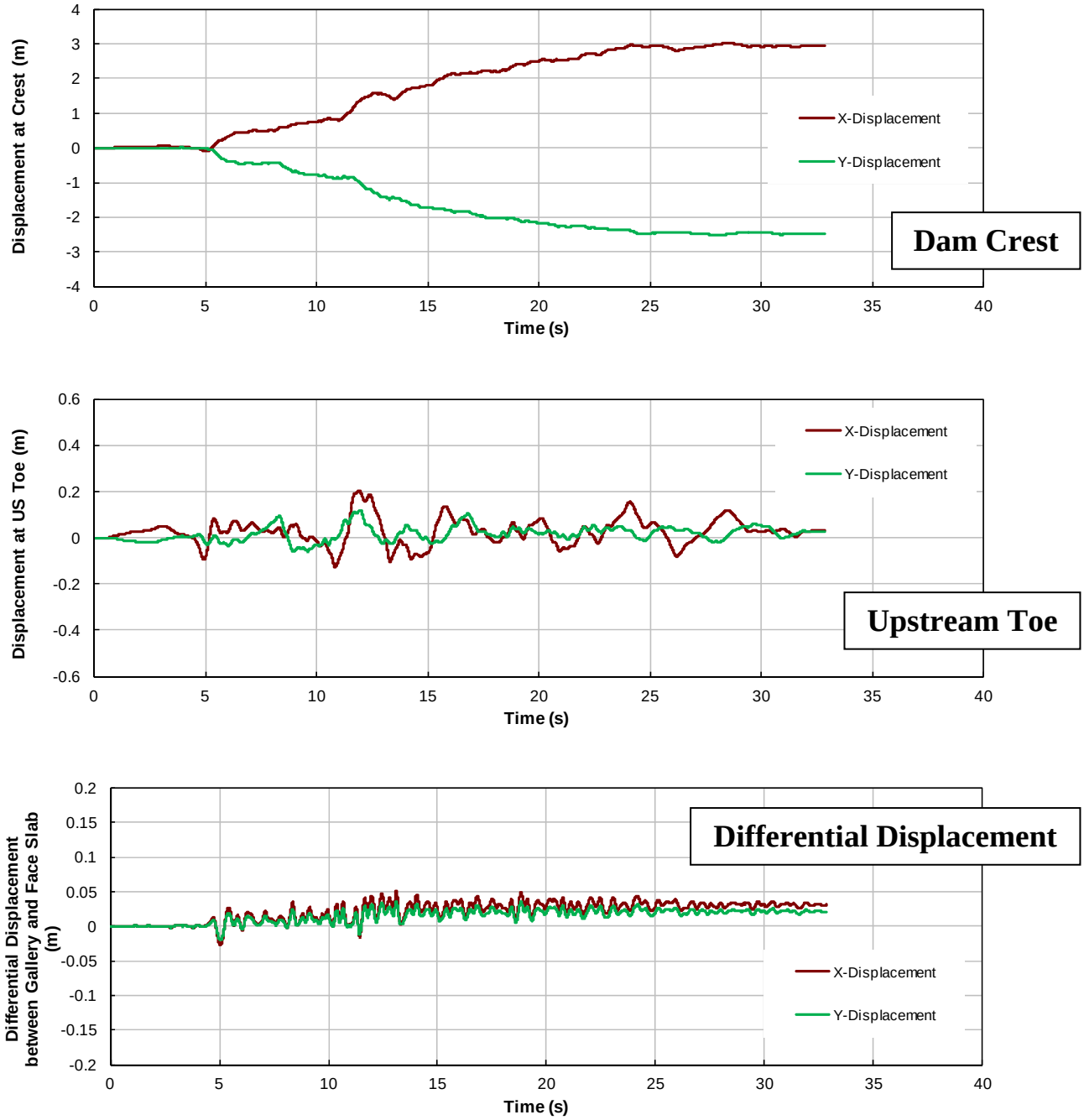

Computed Horizontal (X) and Vertical (Y) Displacement Time Histories at the Crest and at the US Toe, and Differential Displacement at US Toe, using the Mohr-Coulomb Model, 2,475-yr Event (Tabas Record)

Seismic Deformation Analysis of Qaraoun Dam	OD11161570
AMEC Geomatrix	Figure **4-33**

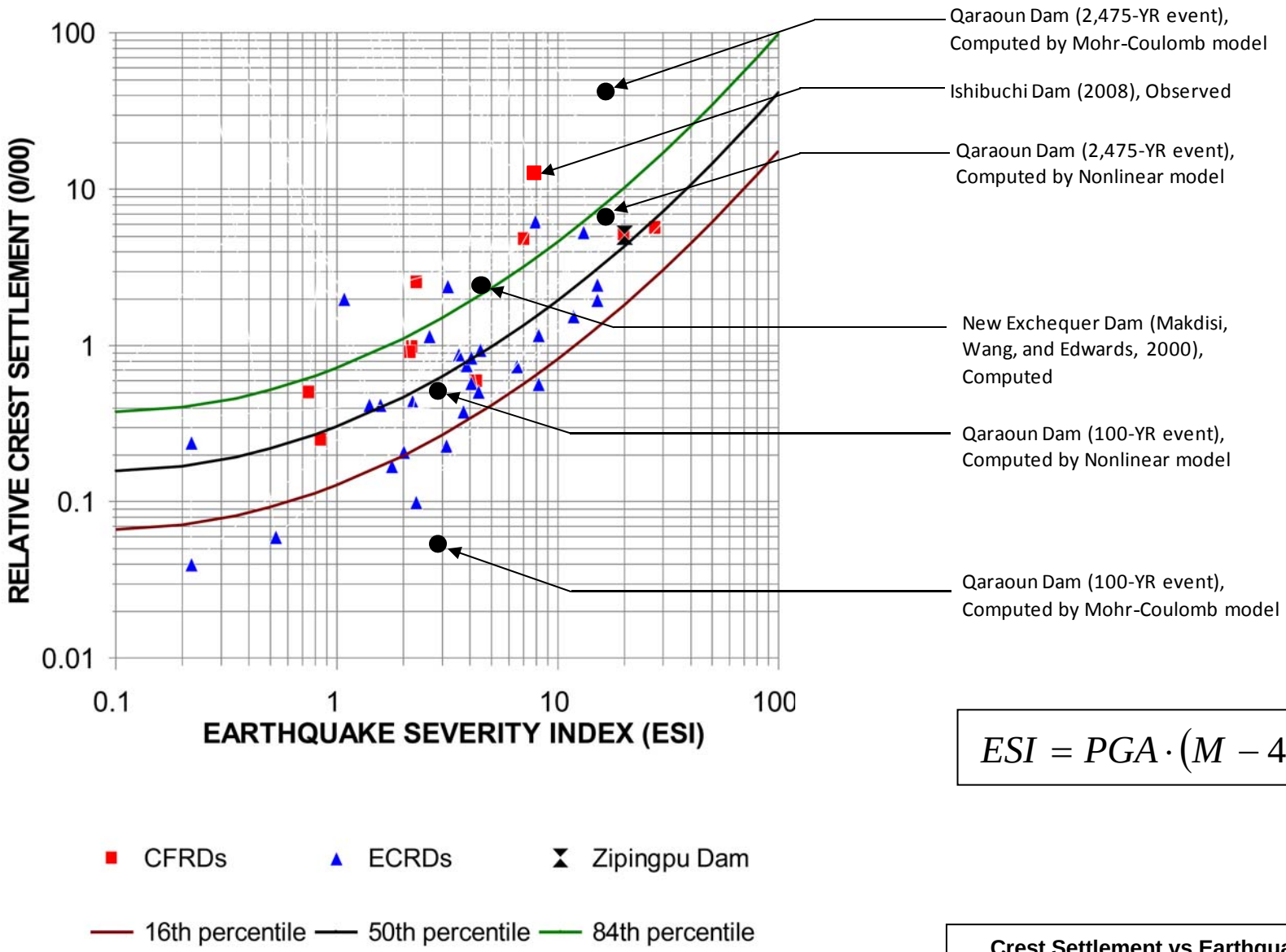

$$ESI = PGA \cdot (M - 4.5)^3$$

Crest Settlement vs Earthquake Severity Index (ESI) – (From Bureau, 2009)

Seismic Deformation Analysis of Qaraoun Dam	OD11161570
AMEC Geomatrix	Figure **4-34**

5. SUMMARY AND CONCLUSIONS

A probabilistic seismic hazard analysis (PSHA) was performed to estimate the level of shaking at the site of the 60-meter-high concrete-faced Qaraoun Dam from potential seismic sources in the vicinity, and to select earthquake ground motions for use in analysis of the dynamic response and deformation of the dam embankment. The dam response and earthquake-induced deformation were estimated using dynamic finite-difference (FLAC) analyses for postulated ground motions from two scenario earthquakes.

A detailed study was performed of the tectonic setting and historical seismicity of the region where all known earthquakes have occurred. Sources of those earthquakes were identified as either active crustal faults (i.e., well-defined fault structures that have generated earthquakes within the past 35,000 years and that are manifested at the ground by surface rupture) or areal seismic source zones (i.e., regions where earthquakes have been observed to originate that are not attributed to a specific mapped fault). Each of the fault sources was characterized by its proximity to the site, type of faulting, maximum length of faulting, maximum thickness of rupture, dip, annual slip rate, and maximum potential for energy release (M_{MAX}). Each of the areal seismic zones was characterized by its proximity to the site, type of faulting, maximum thickness of rupture, dip, and M_{MAX}. Once all sources were identified and characterized, subjective weighting factors were applied to each characteristic value to represent the probability of occurrence for that particular value. A probabilistic model was then developed to represent a finite number of individual earthquake scenarios in the vicinity of the dam site. For Qaraoun Dam, six active crustal faults and eight areal seismic source zones were identified as potential seismic sources.

All 14 seismic sources were considered to contribute to the seismic hazard at the dam with varying levels of activity and maximum energy release. The Yammouneh Fault, located approximately 2.4 km west of Qaraoun Dam, was estimated to contribute the most to the seismic hazard due to its close proximity to the dam and its relatively high annual slip rate. However, for the development of the overall seismic hazard, each source was evaluated for its potential to release an amount of energy that would lead to a specific level of shaking (measured as acceleration) at the dam site. The overall annual probability of the dam to experience (or exceed) a particular level of acceleration is the sum of the annual probabilities from all seismic sources to that level of acceleration.

The results of the analysis are presented in terms of peak ground acceleration and response spectral values for various specified annual frequencies of exceedance, or return periods. The return period, in years, is defined as the inverse of the annual frequency of exceedance. The scope of work for this study required the development of ground shaking levels for 100-year, and 10,000-year return periods. A ground shaking level for the 100-year return period has a one percent chance of being exceeded in one year, or about 40 percent chance of being exceeded in 50 years. The 10,000-year return period ground motion has approximately 0.5 percent chance of being exceeded in 50 years. Ground motions were also developed for a two percent chance of being exceeded in 50 years to be consistent with the results of deterministic estimates of ground motions from the nearby active Yammouneh fault. The two percent chance of being exceeded in 50 years corresponds to a 2,475-year return period.

The results of seismic hazard indicate that the peak ground acceleration at the dam site for the 100-year return period is about 0.15g. This level of computed acceleration may be considered similar to what might have been experienced in the vicinity of the epicentral region of the magnitude 5.8 earthquake that occurred

in the area in 1956. The estimated peak ground acceleration for the 2,475-year return period is about 0.78g. The dominant source for this level of shaking is a magnitude 7.0-7.5 earthquake on the Yammouneh fault about 2.4 km from the dam site. This level of ground shaking may be considered similar to what might have been experienced in the epicentral region of the magnitude 7.4 earthquake that occurred in the Bekaa Valley in 1759. The estimated peak ground acceleration for the 10,000-year return period is about 1.2g.

Uniform hazard response spectra, UHRS, (spectral accelerations at various structural periods of vibration) were developed from the PSHA to represent the frequency content and level of shaking for the 100-year, 475-year, 975-year, 2475-year, and 10,000-year return period earthquake scenarios. The UHRS were then used to develop scenario acceleration time histories for the 100-year and 10,000-year events in the following manner:

1. select a recorded (seed) acceleration time history from the historical record that closely represents the distance to rupture, magnitude of the scenario earthquake, and the foundation conditions at the site,
2. scale the entire seed time history to match the peak ground acceleration (PGA) of the UHRS of interest, and
3. modify the frequency content of the scaled time history so that it loosely matches the target UHRS.

Two sets of horizontal and vertical acceleration time histories were developed for each of the two scenario earthquakes.

Following the development of the 100-year and 10,000-year return period earthquake scenarios and associated acceleration time histories, project team members from AMEC and IRG discussed the basis for selection of ground motions that would be most appropriate for analyzing the seismic response and deformation of Qaraoun dam. The California Department of Water Resources, Division of Safety of Dams (DSOD) recommends that an 84th percentile deterministic ground motion be used for evaluating the seismic stability of dams that have "high consequences of failure." Following the DSOD guidelines, the team agreed that a 2,475-year return period ground motion that provides ground shaking levels similar to the 84th percentile ground motions from a magnitude 7.2 earthquake on the Yammouneh fault, would be appropriate for the deformation analysis of the dam, in lieu of the 10,000-year return period motions.

The dynamic response and seismic deformation analysis of Qaraoun Dam was performed with the computer program FLAC2D. This approach involves performing two-dimensional, finite-difference analyses to evaluate the non-linear dynamic response and permanent deformation of the maximum cross section of the embankment during the postulated seismic shaking at the dam site. Two different soil constitutive models for the rockfill were used to estimate the permanent deformation of the dam: a fully nonlinear "bounding surface hypo-plasticity" model, and a more traditional (and conservative) bi-linear Mohr-Coulomb constitutive model.

The dam was modeled as an unsaturated dumped rockfill embankment with an upstream concrete panel facing and concrete drainage gallery at the upstream toe. Properties of the rockfill material were selected based on a review of published literature on similar materials. Both horizontal (in the upstream/downstream direction) and vertical components of input motions were applied at the bedrock foundation underlying the dam. Analyses were performed using time histories for the 100-year and 2,475-year ground motions. Preliminary analyses were performed to simulate the reservoir's hydrodynamic loads. The results of these analyses indicate that the effects of including the hydrodynamic loads for this sloping-face rockfill dam were not significant. This finding is consistent with results of similar studies in the literature. Accordingly, the analyses were performed without including the reservoir effects.

The results of the deformation analyses indicate that shaking from the 100-year earthquake scenario, having a peak horizontal bedrock acceleration of 0.15g, will cause an insignificant amount (i.e., less than 0.03 m) of

permanent deformation at the crest and upstream and downstream toes of the dam. It is our judgment that these estimated deformations will not have a significant impact on the seismic performance of the dam.

Using the bounding surface hypo-plasticity model, shaking from the 2,475-year event, with peak bedrock acceleration of 0.8g, is expected to cause about 0.44 m of vertical and 0.45 m of horizontal permanent deformation at the crest of the dam, and about 0.03 meter of horizontal permanent displacement at the upstream toe of the dam near the connection of the concrete facing to the drainage gallery. The estimated differential displacements at the interface between the concrete face slab and the inspection galley was less than 0.05 m. Using the more conservative Mohr Coulomb constitutive model, the computed crest settlement was about 2.5 m, and the permanent horizontal deformation was about 2.9 m. Because of uncertainties in the analytical procedures, and based on the observed performance of similarly constructed dams shaken with large magnitude earthquakes, it is the authors' judgment that the amount of deformation anticipated at the crest of the dam for this level of shaking likely will be in the range of about 1 m to 1.5 m.

Since the crest of the dam is at Elev. 861.0 m, the top of the concrete parapet wall is at Elev. 863.0 m, and the normal maximum water level is at Elev. 858.0 m, the available freeboard to the top of the parapet wall is 5.0 m. The range of estimated earthquake-induced deformation and settlement of the embankment during the 2,475-year ground shaking (i.e., 1 to 1.5 m) are less than the available freeboard, and overtopping of the dam is not expected. The predicted deformations likely will cause

- damage to the concrete parapet wall at the dam crest,
- sloughing of the rockfill on the dam's downstream face, and
- possible cracking of the concrete facing leading to increased leakage through the rockfill.

However, such effects are considered unlikely to impact the overall stability of the dam, or cause an uncontrolled release of reservoir water.

The predicted deformations of Qaraoun Dam for the 2,475-year scenario earthquake, were compared to the documented performance of similar concrete-faced rockfill dams. Ishibuchi Dam in Japan, and Zipingpu Dam in China, were shaken by earthquakes of magnitudes of 6.9 and 7.9, respectively, with peak bedrock accelerations of 0.5g and 0.7g. Ishibuchi Dam settled 0.6m and experienced cracking at the dam crest; however, the concrete face slab on the upstream slope was reportedly undamaged. At Zipingpu Dam, the crest settled about 1m, and the earthquake-induced deformations resulted in partial dislocation of several concrete slabs at the construction joints, with maximum outward bulging of 0.15 m. Portions of the parapet wall at the crest also collapsed, and open cracks (up to 3 cm wide) were observed between the downstream side of the crest road and the rock slope protection. Despite this damage, the dam remained stable and maintained its reservoir impounding capacity. The observed settlements at these two dams are of the same order of magnitude as those estimated for Qaraoun Dam, and help support the conclusion that the dam should perform adequately during the postulated 2,475-year scenario earthquake considered in this study.

While the analyses and evaluations described above indicate the dam should perform adequately, it is recommended that a detailed inspection of the dam be performed immediately following all earthquakes occurring within 50 km of the dam site and having a magnitude of 5.0 or greater. The inspection should include:

- draw down of the reservoir level,
- a survey of the settlement monuments on the crest and concrete facing,
- a careful review of the parapet wall and the concrete facing, including horizontal and vertical construction joints and water stops,
- confirming the integrity of the inspection gallery,

- monitoring the piezometers for evidence of an increasing phreatic surface within the dam, and
- frequent monitoring of the leakage weirs for increased flow and evidence of silt deposits.

Any damage to the dam resulting from earthquake shaking must be repaired prior to raising the reservoir to its normal operating level.

6. BASIS FOR ANALYSES AND CONCLUSIONS

This report was prepared for the exclusive use of the Litani River Basin Management Support Program. The conclusions and other considerations presented in this report are intended for the evaluation of Qaraoun Dam in the Litani River Basin, Lebanon. The conclusions were developed using information available for the site and our understanding of the current geologic conditions. No new or additional field investigations were performed by AMEC during the present study.

In the performance of our professional services, AMEC, its employees, and its agents comply with the standards of care and skill ordinarily exercised by members of our profession practicing in the same or similar localities. No warranty, either express or implied, is made or intended in connection with the work performed by us, or by the proposal for consulting or other services, or by the furnishing of oral or written reports or findings. We are responsible for the analyses and conclusions contained in this report, which are based on data related only to the specific project and location discussed herein. In the event conclusions based on these data are made by others, such conclusions are not our responsibility unless we have been given an opportunity to review and concur with such conclusions in writing.

7. REFERENCES

Arrau, L., Ibarra, I. and Noguera, G., 1985, Performance of Cogoti Dam under seismic loading, Proceedings of the Symposium on Concrete Face Rockfill Dams Design, Construction and Performance, sponsored by the ASCE Geotechnical Engineering Division in conjunction with the ASCE Convention in Detroit, Michigan, (J. Barry Cook and James L. Sherard, editors), October 21, 1985.

Barton, N., and Kjærnsli, B., 1981, Shear strength of rockfill: Journal of the Geotechnical Engineering Division, ASCE, v. 107, no. GT7, p. 873-891.

Boulanger, R.W., Merry, S.M., Bray, J.D., and Mejia, L.H., 1994, Three-dimensional dynamic response analyses of Cogswell Dam during the 1991 Sierra Madre and 1987 Whittier Narrows earthquakes: Center for Geotechnical Modeling, University of California at Davis, Report No. UCD/CGM-94/02, November.

Bureau, G., 2009, Seismic performance of rockfill dams, United States Society of Dams Newsletter, March, 2009.

Bureau, G, Volpe, R.L., Roth, W.H., and Udaka. T., 1985, Seismic analysis of concrete face rockfill dams, Proceedings of the Symposium on Concrete Face Rockfill Dams Design, Construction and Performance, sponsored by the ASCE Geotechnical Engineering Division in conjunction with the ASCE Convention in Detroit, Michigan, (J. Barry Cook and James L. Sherard, editors), October 21, 1985.

Darendeli, B.M., 2001, Development of a New Family of Normalized Modulus Reduction and Material Damping: Ph.D. dissertation, University of Texas at Austin.

Duncan, J.M., 2004, Friction Angles for Sand, Gravel, and Rockfill, notes on a lecture presented at the Kenneth L. Lee Memorial Seminar, Long Beach, California, April 28.

Duncan, J.M., and Chang, C.-Y., 1970, Nonlinear analysis of stress and strain in soils: Journal of the Soil Mechanics and Foundation Division, ASCE, v. 96, no. SM5, p. 1629-1653, September.

Duncan, J.M., Byrne, P., Wong, K.S., and Mabry, P., 1980, Strength, stress-strain and bulk modulus parameters for finite-element analyses of stresses and movements in soil masses: University of California, Berkeley, Report No. UCB/GT/80-01.EERI 2002

Fraser , W.A. and Howard, J.K., 2002, Guidelines for Use of the Consequence-Hazard Matrix for selection of ground motion parameters, California Department of Water Resources, Division of Safety of Dams, October 4, 2002.

Fraser, W.A. and Burns, R.G., 2004, Evaluating the conservatism of deterministic ground motions using probabilistic seismic hazard analysis. Presentation at the Association of Engineering Geologists 2004 Annual Meeting, Dearborn, Michigan.

Halwani, S., Lajeat, J.-P., Chardonnet, E., Pernon, J.-P., Gerard, P., 1964, Le Barrage de Karaoun sur le Litani (Liban), Numèro entierement consacré au 8, Congrés International des Grands Barrages, Avril.

Geomatrix Consultants, 1999, Seismic stability of New Exchequer Dam, Report prepared for Merced Irrigation District, Snelling, California, November.

Itasca, 2005, FLAC, Fast Lagrangian Analysis of Continua, Version 6.0, User's Guide: Itasca Consulting Group, Inc., Thrasher Square East, 708 South Third Street, Suite 310, Minneapolis, Minnesota.

Kulesza, R.L., 1987, New Exchequer Dam report on stability analyses, supplement to April 1987 Fourth Part 12 Dam Safety Report, Prepared for Merced Irrigation District, August.

Lai, S.S., 1985, Analysis of seismic response of prototype earth and rockfill dams: Ph.D. dissertation, University of California, Berkeley.

Leps, T.M., 1970, Review of Shearing Strength of Rockfill, Journal of Soil Mechanics and Foundation Division, ASCE, Vol. 96, No. SM4, pp.1159-1170.

Leps, T.L., 1992, Review of Safety of New Exchequer Dam (fifth five-year report): F.E.R.C. Project No. 2179-CA: Prepared for Merced Irrigation District, April.

Makdisi, F.I., Wang, Z.-L., and Edwards, W.D., 2000, "Seismic Stability of New Exchequer Dam and Gated Spillway Structure," Twentieth Annual USCOLD Lecture Series, Seattle, Washington, July 10-14.

Matsumoto, N., Yoshida, H., and Kasai, T., 2011, Performance of the Ishibuchi Dam during the Miyage Earthquake, Hydropower and Dams, Issue One, pp. 2-5.

Seed, H.B., Idriss, I.M., 1970. Soil moduli and damping factors for dynamic response analyses, Earthquake Engineering Research Center, Report No. EERC 70-10, University of California, Berkeley, California.

Seed, H.B, Wong, R.T., Idriss, I.M., and Tokimatsu, K., 1986, Moduli and damping factors for dynamic analyses of cohesionless soils: Journal of Geotechnical Engineering, v. 112, no. 11, November.

Wang, Z.L., 1990, Bounding Surface Hypoplasticity Model for Granular Soils and its Applications, Ph.D. Dissertation. University of California, Davis, U.M.I. Dissertation Information Service, Order No. 9110679, Ann Arbor, MI 48106.

Wang, Z.L., Dafalias, Y.F., Shen, C.K., 1990, Bounding Surface Hypoplasticity Model for Sand, ASCE Journal of Engineering Mechanics, v.116, n.5., p. 983-1001.

APPENDIX A

Seismicity Rates for Source Zones

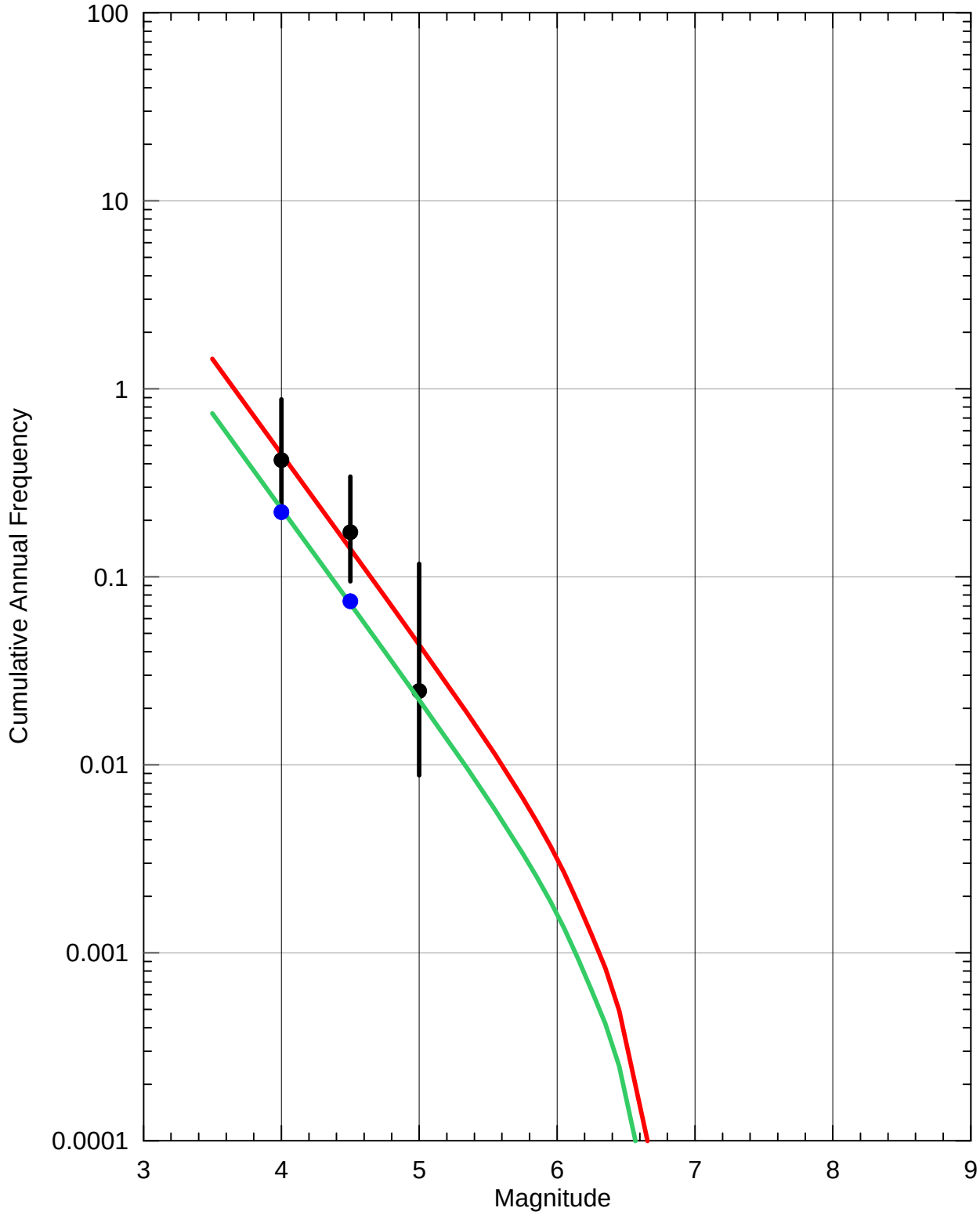

- Observed-all seismicity
- Predicted Mean-all seismicity
- Observed-fault seismicity removed
- Predicted Mean-fault seismicity removed

SEISMICITY RATE FOR SOURCE ZONE
LEBANESE RESTRAINING BEND
Qaraoun Dam Hazard Study
Litani River Basin, Lebanon

By: DG	Date: 9/9/2011	Project No. OD11161570
AMEC Geomatrix		Figure **A-1**

I:\Project\16000\OD11161570 - Qaraoun Dam\12000 CALCS EVALS ANALYSIS\Figures\memo_figures\seismicity_rates

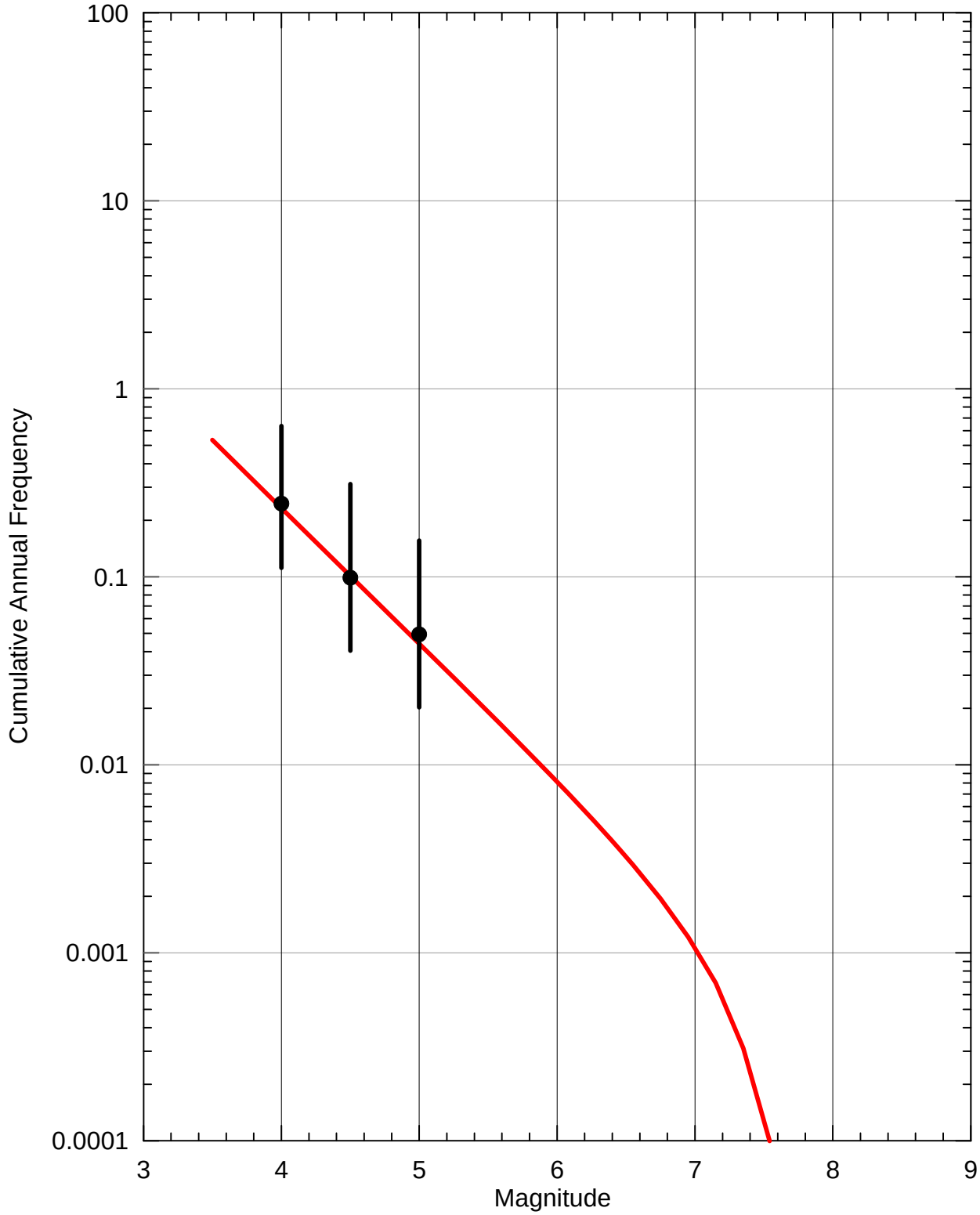

Observed
Predicted Mean

SEISMICITY RATE FOR SOURCE ZONE
JORDAN VALLEY ZONE
Qaraoun Dam Hazard Study
Litani River Basin, Lebanon

By: DG	Date: 9/9/2011	Project No. OD11161570
AMEC Geomatrix		Figure **A-2**

I:\Project\16000\OD11161570 - Qaraoun Dam\12000 CALCS EVALS ANALYSIS\Figures\memo_figures\seismicity_rates

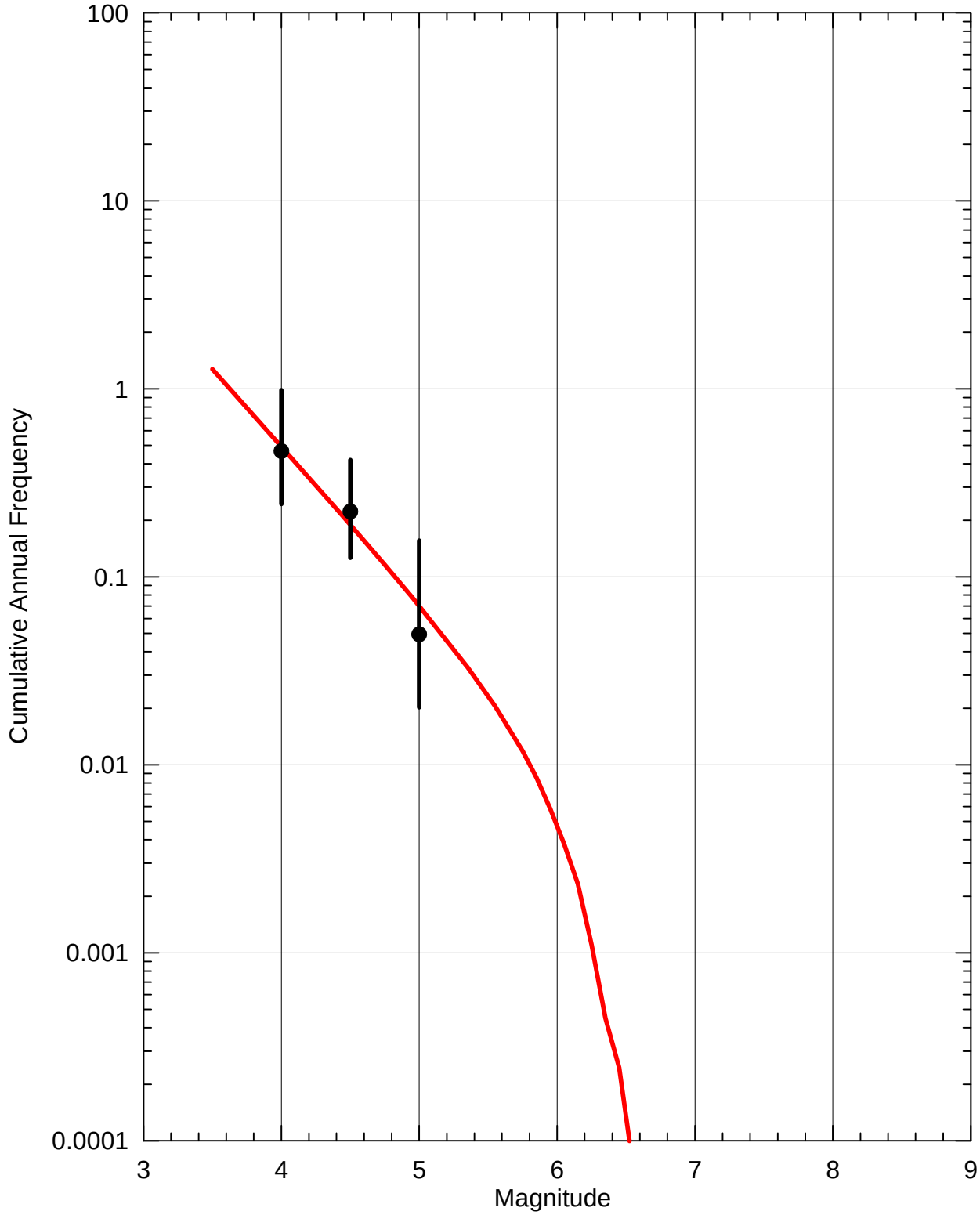

Observed
Predicted Mean

SEISMICITY RATE FOR SOURCE ZONE
LEVANTINE BASIN
Qaraoun Dam Hazard Study
Litani River Basin, Lebanon

By: DG	Date: 9/9/2011	Project No. OD11161570
AMEC Geomatrix		Figure **A-3**

I:\Project\16000\OD11161570 - Qaraoun Dam\12000 CALCS EVALS ANALYSIS\Figures\memo_figures\seismicity_rates

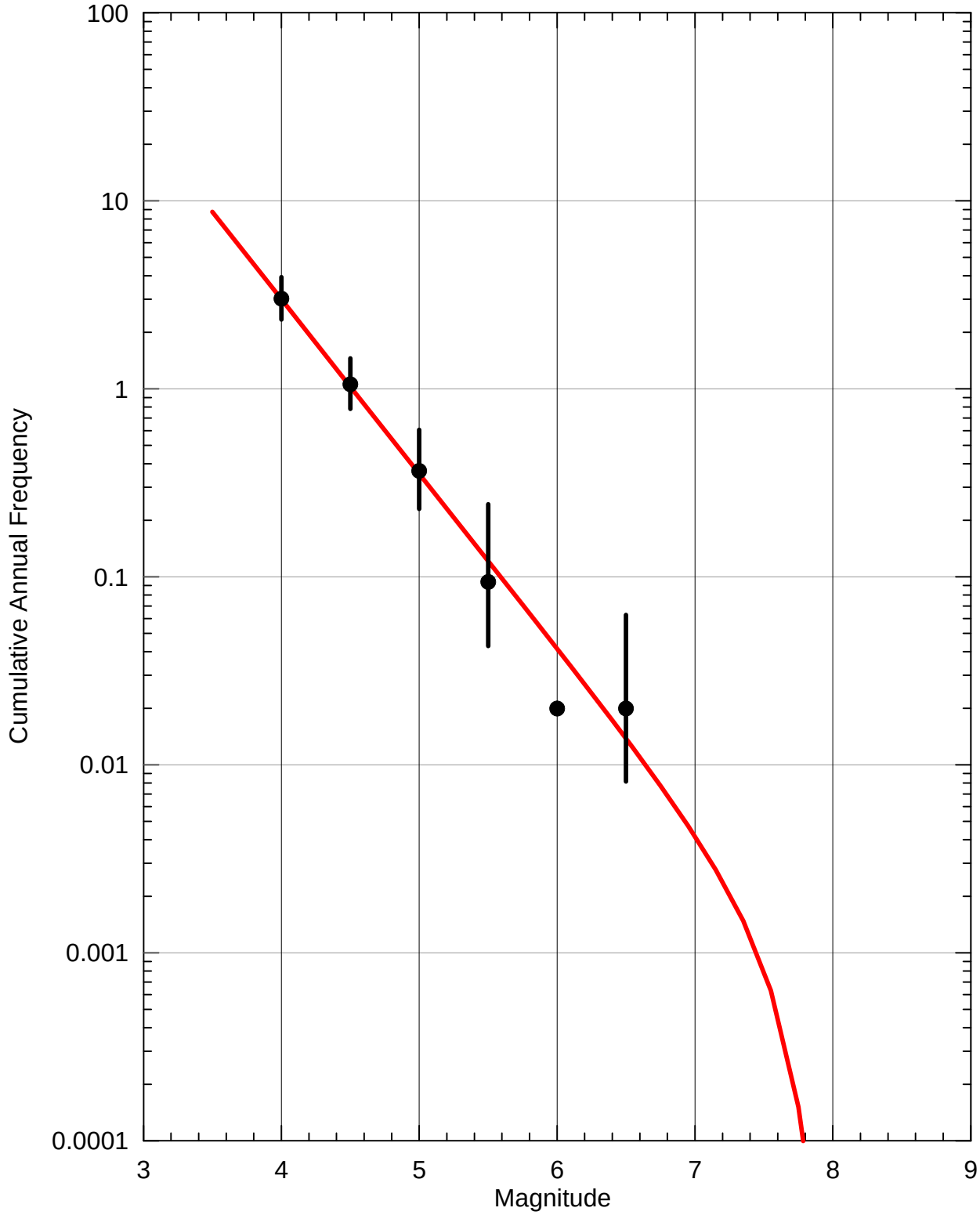

Observed
Predicted Mean

SEISMICITY RATE FOR SOURCE ZONE
CYPRUS ZONE
Qaraoun Dam Hazard Study
Litani River Basin, Lebanon

By: DG	Date: 9/9/2011	Project No. OD11161570
AMEC Geomatrix		Figure **A-4**

I:\Project\16000\OD11161570 - Qaraoun Dam\12000 CALCS EVALS ANALYSIS\Figures\memo_figures\seismicity_rates

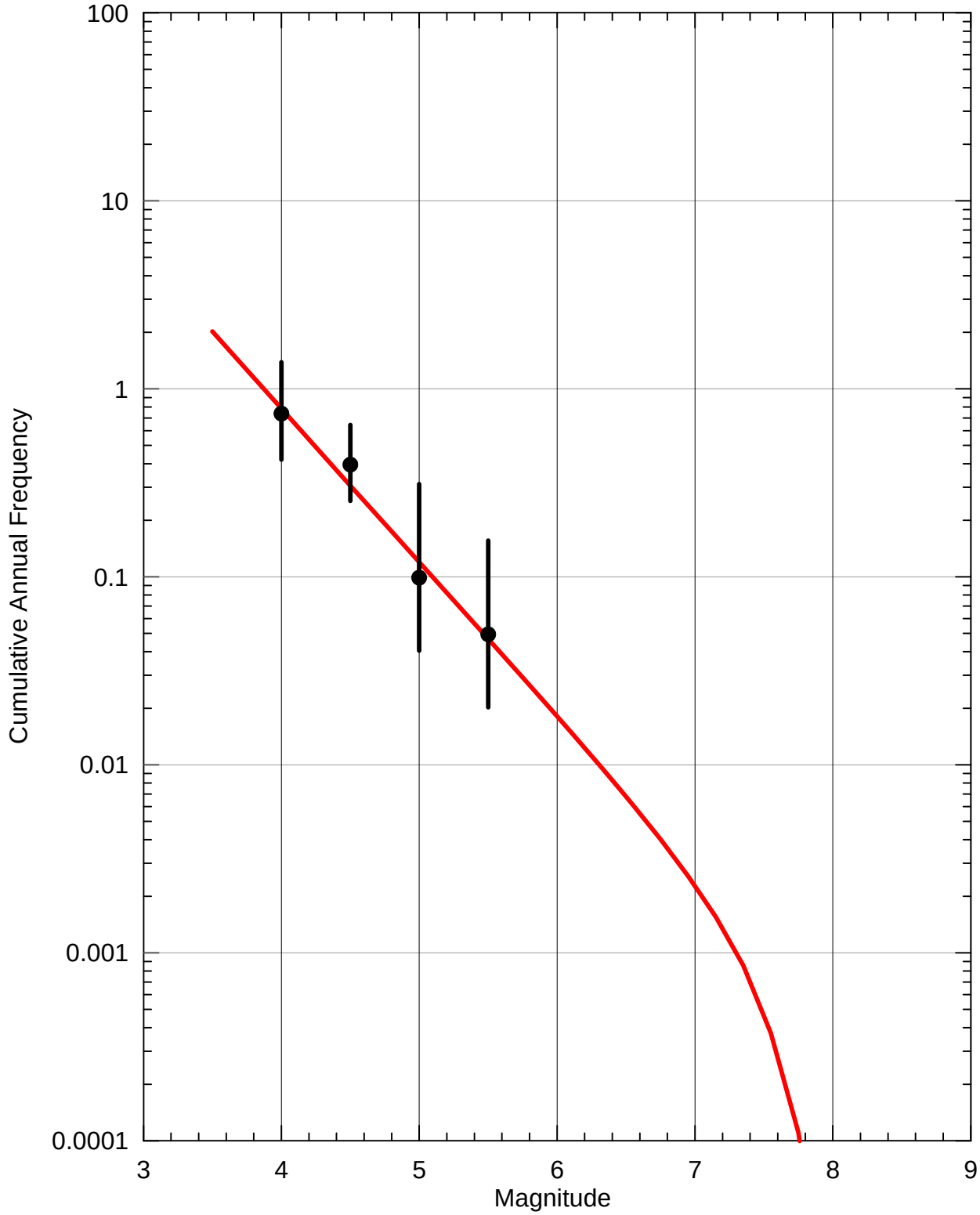

Observed
Predicted Mean

SEISMICITY RATE FOR SOURCE ZONE
CYPRUS TRANSFORM
Qaraoun Dam Hazard Study
Litani River Basin, Lebanon

By: DG	Date: 9/9/2011	Project No. OD11161570
AMEC Geomatrix		Figure **A-5**

I:\Project\16000\OD11161570 - Qaraoun Dam\12000 CALCS EVALS ANALYSIS\Figures\memo_figures\seismicity_rates

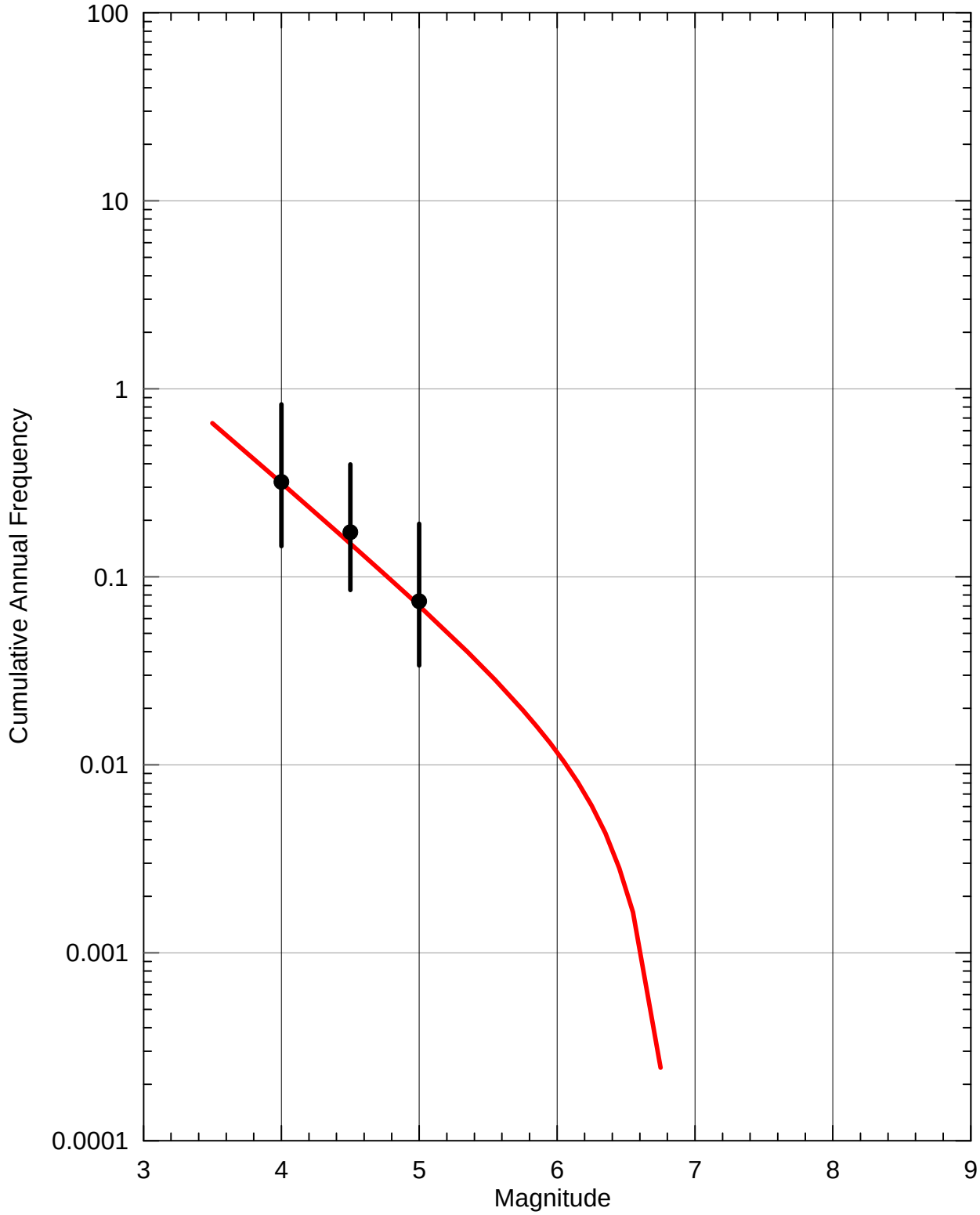

Observed
Predicted Mean

SEISMICITY RATE FOR SOURCE ZONE
SINAI PENINSULA ZONE
Qaraoun Dam Hazard Study
Litani River Basin, Lebanon

By: DG	Date: 9/9/2011	Project No. OD11161570
AMEC Geomatrix		Figure **A-6**

I:\Project\16000\OD11161570 - Qaraoun Dam\12000 CALCS EVALS ANALYSIS\Figures\memo_figures\seismicity_rates

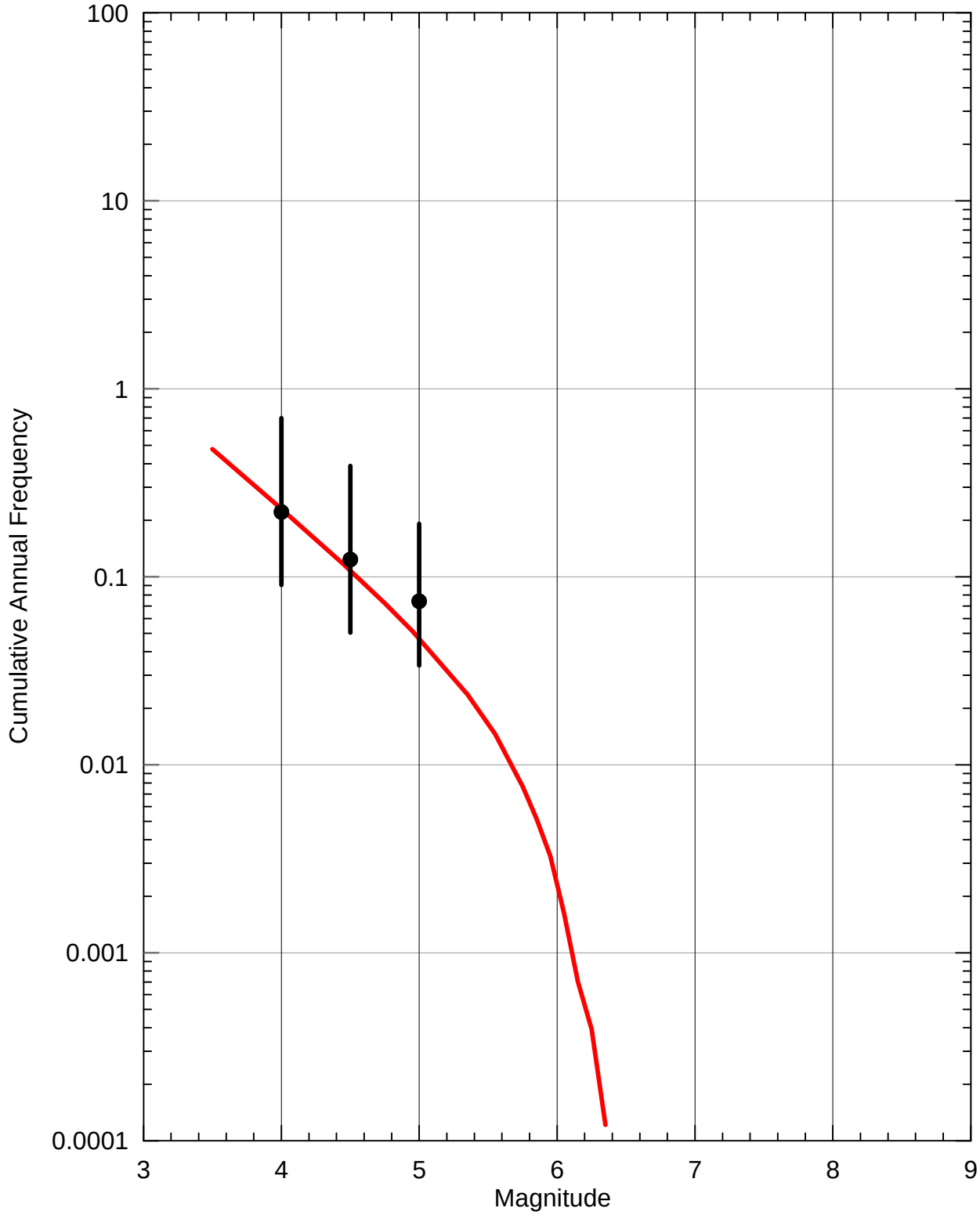

Observed
Predicted Mean

SEISMICITY RATE FOR SOURCE ZONE
SYRIA ZONE
Qaraoun Dam Hazard Study
Litani River Basin, Lebanon

By: DG	Date: 9/9/2011	Project No. OD11161570
AMEC Geomatrix		Figure **A-7**

I:\Project\16000\OD11161570 - Qaraoun Dam\12000 CALCS EVALS ANALYSIS\Figures\memo_figures\seismicity_rates

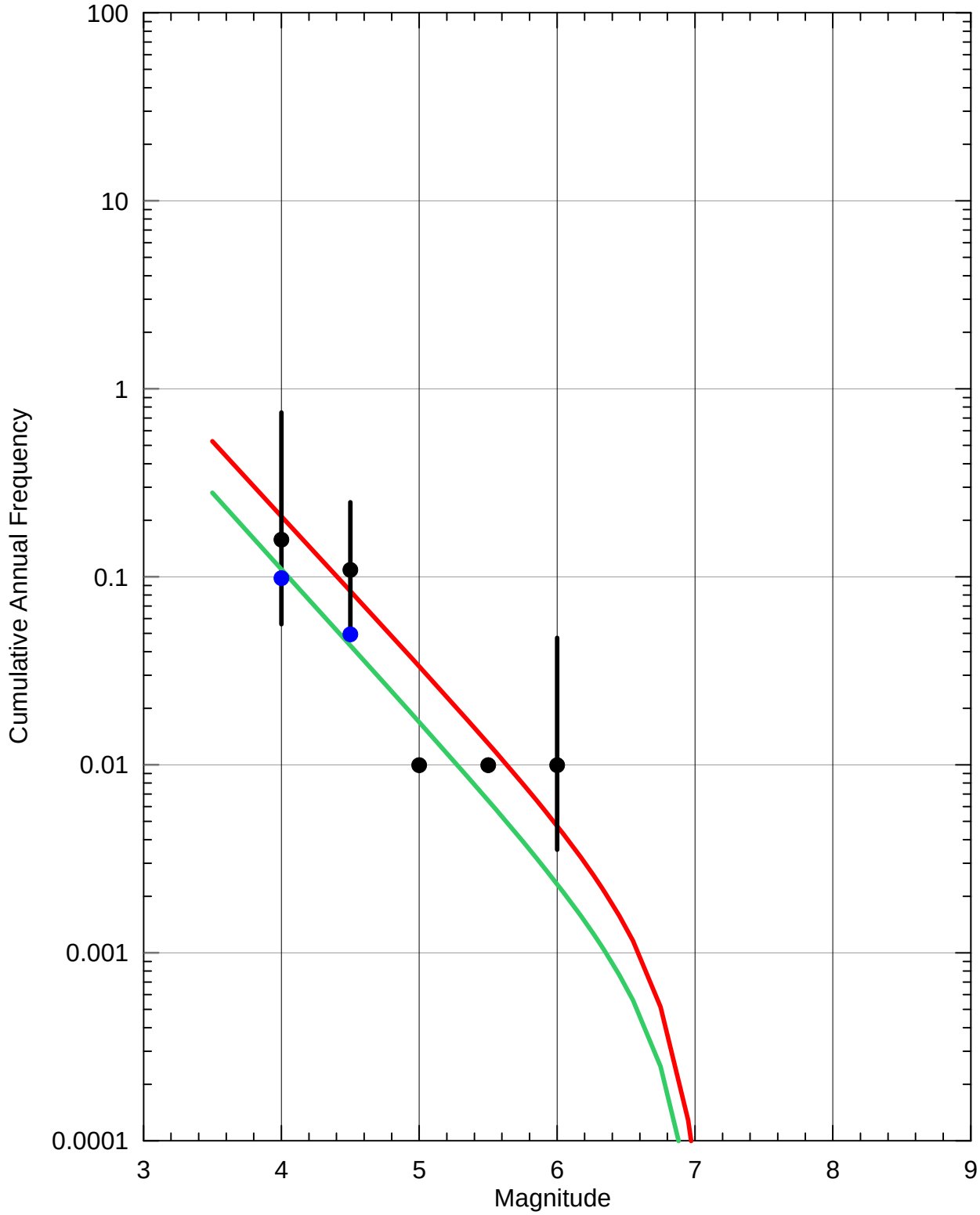

- Observed-all seismicity
- Predicted Mean-all seismicity
- Observed-fault seismicity removed
- Predicted Mean-fault seismicity removed

SEISMICITY RATE FOR SOURCE ZONE
ARABIAN ZONE
Qaraoun Dam Hazard Study
Litani River Basin, Lebanon

By: DG	Date: 9/9/2011	Project No. OD11161570
AMEC Geomatrix		Figure **A-8**

I:\Project\16000\OD11161570 - Qaraoun Dam\12000 CALCS EVALS ANALYSIS\Figures\memo_figures\seismicity_rates

APPENDIX B

Acceleration, Velocity, and Displacement Time History Plots and Response Spectra Matched to the 100-, 2,475-, and 10,000-Year Return Periods

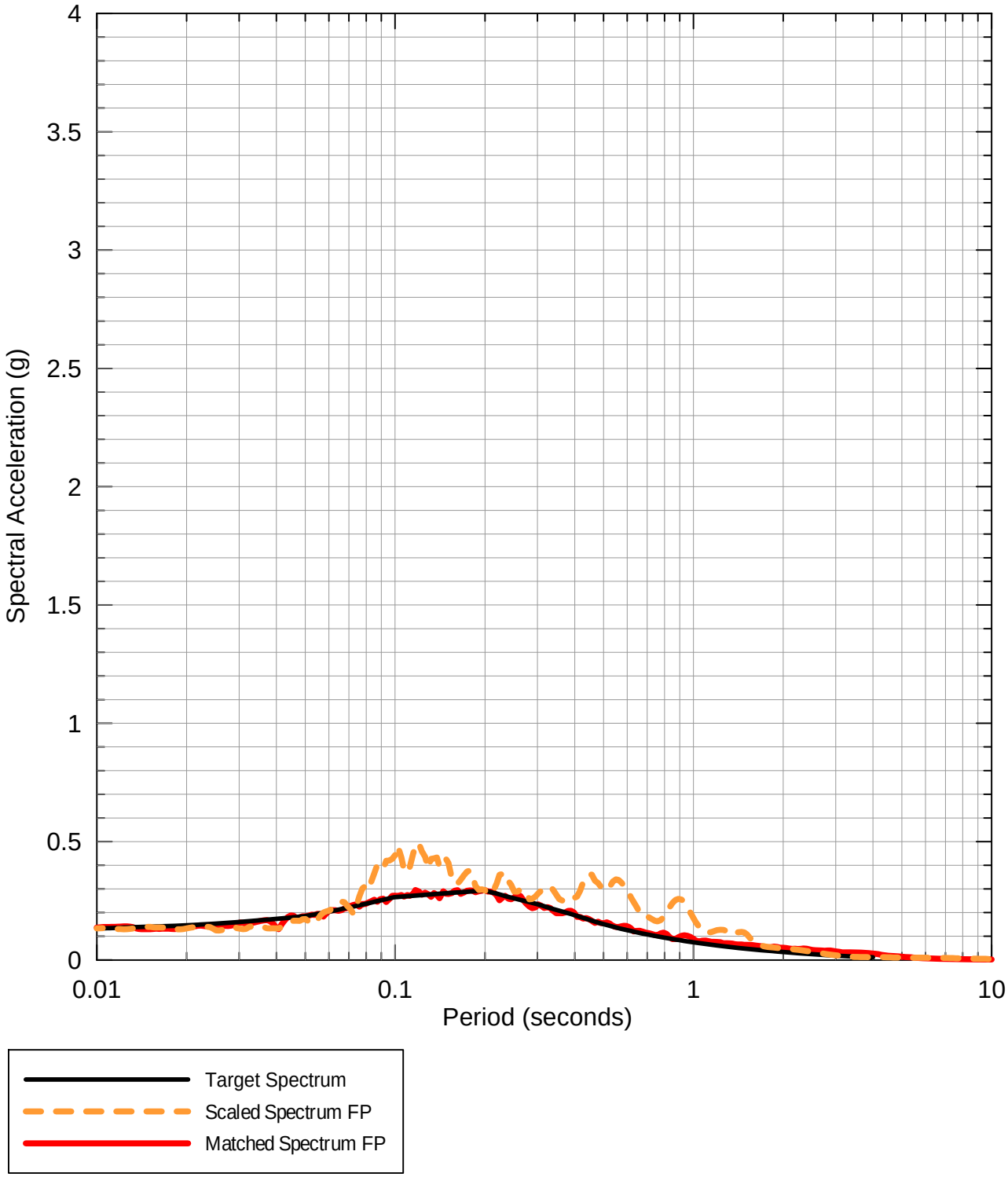

Horizontal Response Spectra
1989, Loma Prieta, SJ Santa Teresa Hills
Matched to 100-Year RP Target Spectrum
Qaraoun Dam Hazard Study
Litani River Basin, Lebanon

By: DG	Date: 9/9/2011	Project No. OD11161570
AMEC Geomatrix		Figure **B-1a**

I:\Project\16000\OD11161570 - Qaraoun Dam\12000 CALCS EVALS ANALYSIS\Figures\memo_figures\TH plots

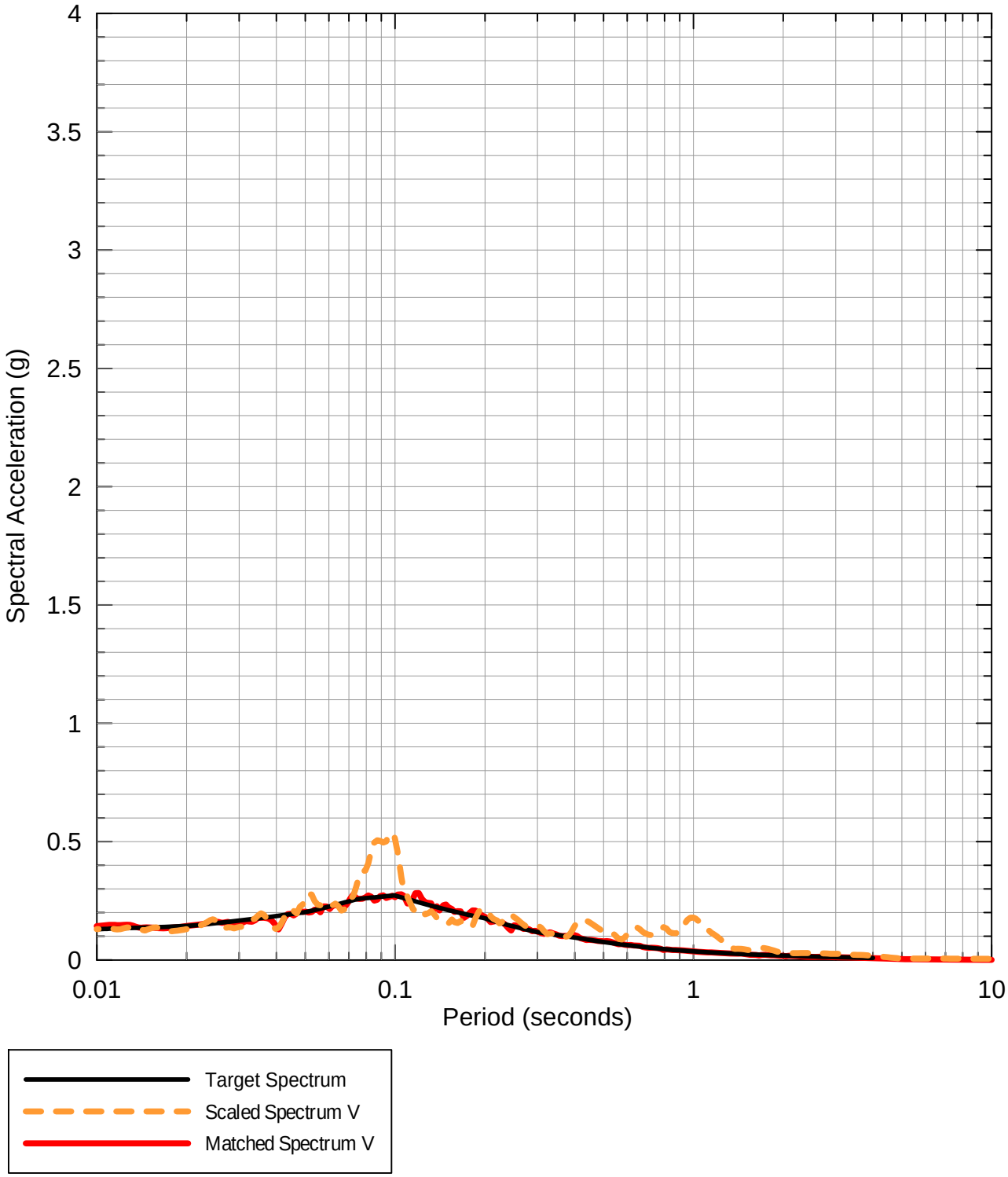

Vertical Response Spectra
1989, Loma Prieta, SJ Santa Teresa Hills
Matched to 100-Year RP Target Spectrum
Qaraoun Dam Hazard Study
Litani River Basin, Lebanon

By: DG	Date: 9/9/2011	Project No. OD11161570
AMEC Geomatrix		Figure **B-1b**

I:\Project\16000\OD11161570 - Qaraoun Dam\12000 CALCS EVALS ANALYSIS\Figures\memo_figures\TH plots

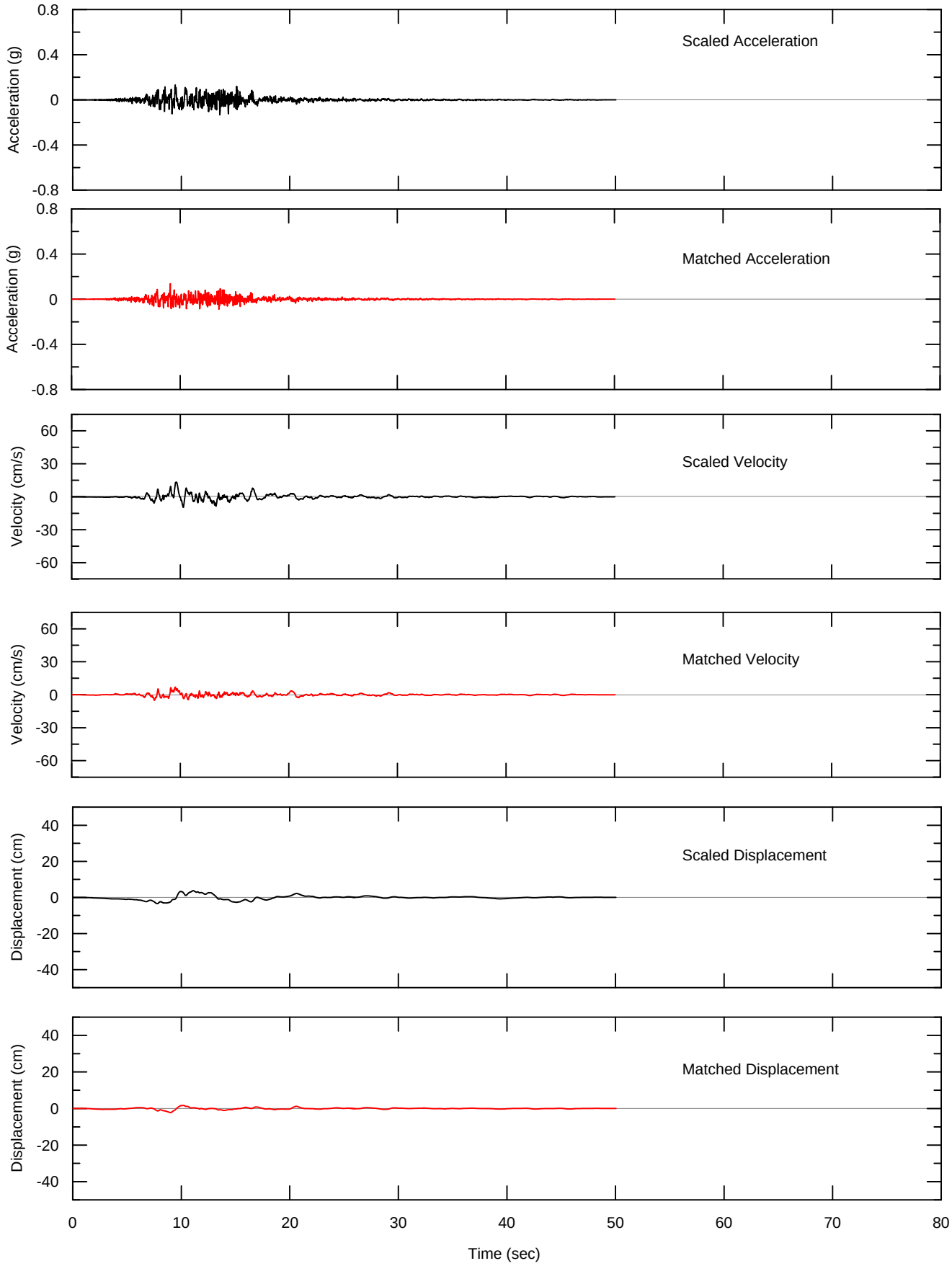

1989, Loma Prieta, SJ Santa Teresa Hills, FP
Matched to 100-Year RP Target Spectrum
Qaraoun Dam Hazard Study, Lebanon

By: DG | Date: 9/9/2011 | Project No. OD11161570

AMEC Geomatrix

Figure **B-1c**

I:\Project\16000\OD11161570 - Qaraoun Dam\12000 CALCS EVALS ANALYSIS\Figures\memo_figures\TH plots

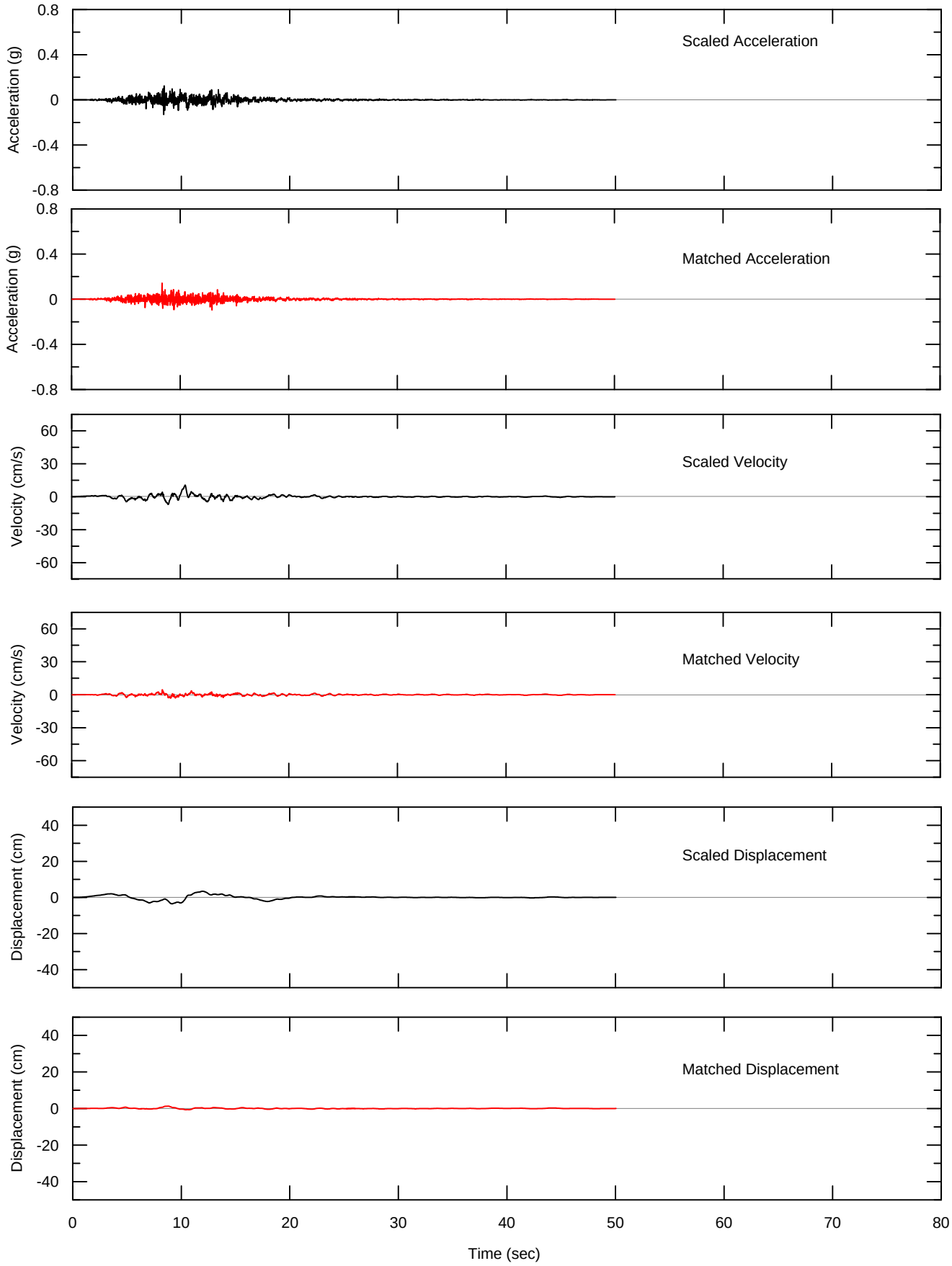

1989, Loma Prieta, SJ Santa Teresa Hills, V Matched to 100-Year RP Target Spectrum Qaraoun Dam Hazard Study, Lebanon	By: DG	Date: 9/9/2011	Project No. OD11161570
	AMEC Geomatrix		Figure **B-1d**

I:\Project\16000\OD11161570 - Qaraoun Dam\12000 CALCS EVALS ANALYSIS\Figures\memo_figures\TH plots

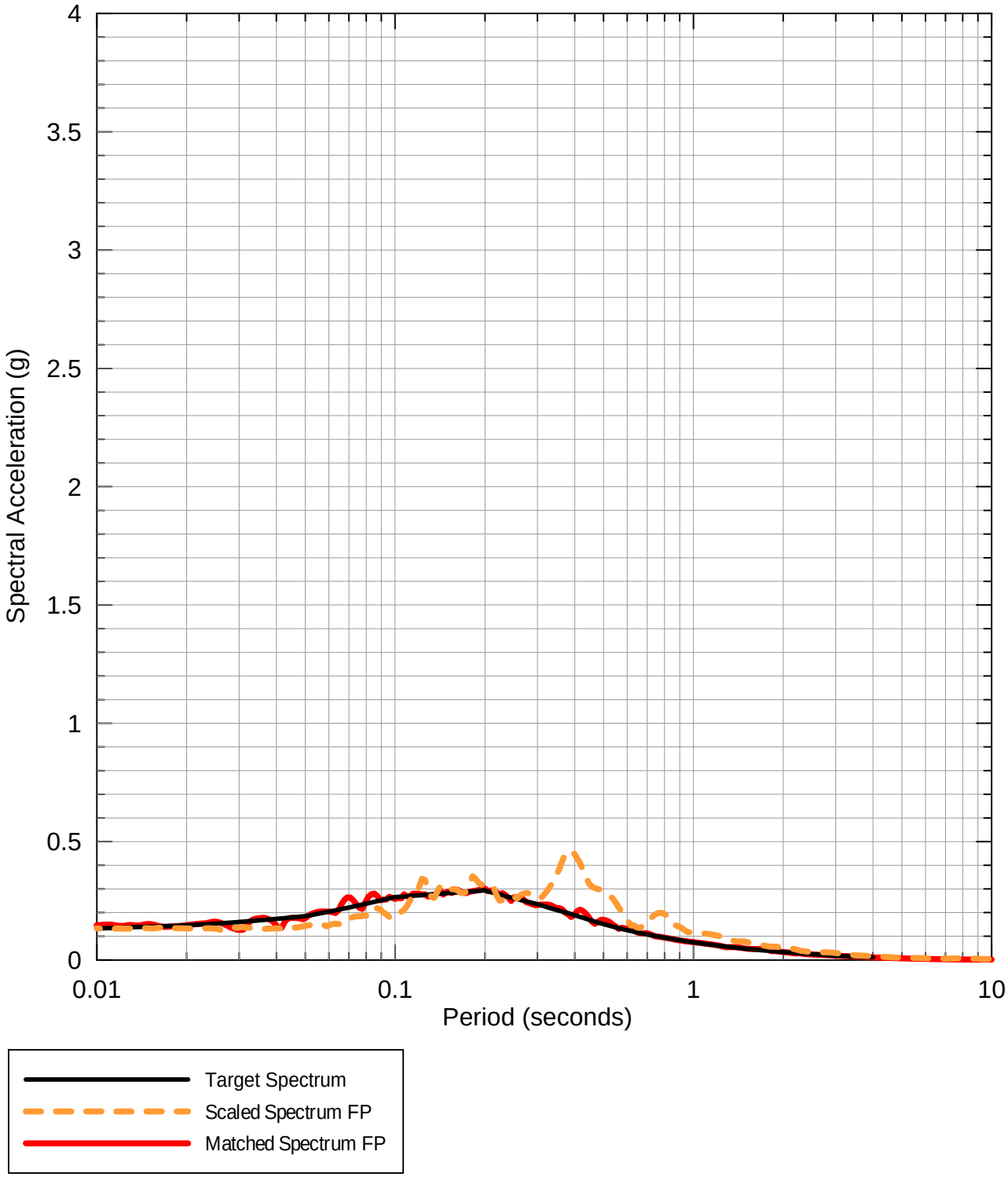

Horizontal Response Spectra
1978, Tabas - Iran, Dayhook
Matched to 100-Year RP Target Spectrum
Qaraoun Dam Hazard Study
Litani River Basin, Lebanon

By: DG	Date: 9/9/2011	Project No. OD11161570
AMEC Geomatrix		Figure **B-2a**

I:\Project\16000\OD11161570 - Qaraoun Dam\12000 CALCS EVALS ANALYSIS\Figures\memo_figures\TH plots

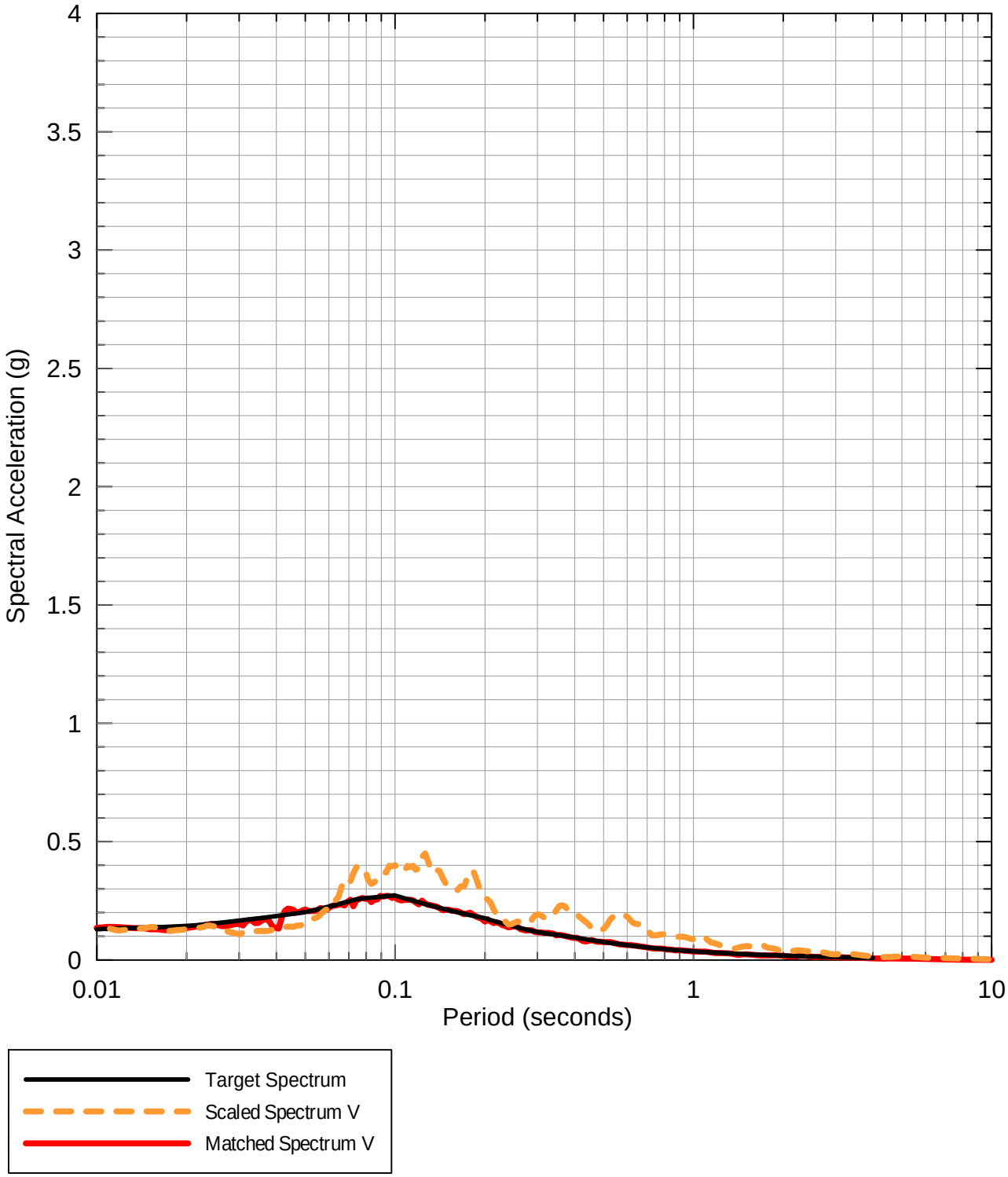

Vertical Response Spectra
1978, Tabas - Iran, Dayhook
Matched to 100-Year RP Target Spectrum
Qaraoun Dam Hazard Study
Litani River Basin, Lebanon

By: DG	Date: 9/9/2011	Project No. OD11161570
AMEC Geomatrix		Figure **B-2b**

I:\Project\16000\OD11161570 - Qaraoun Dam\12000 CALCS EVALS ANALYSIS\Figures\memo_figures\TH plots

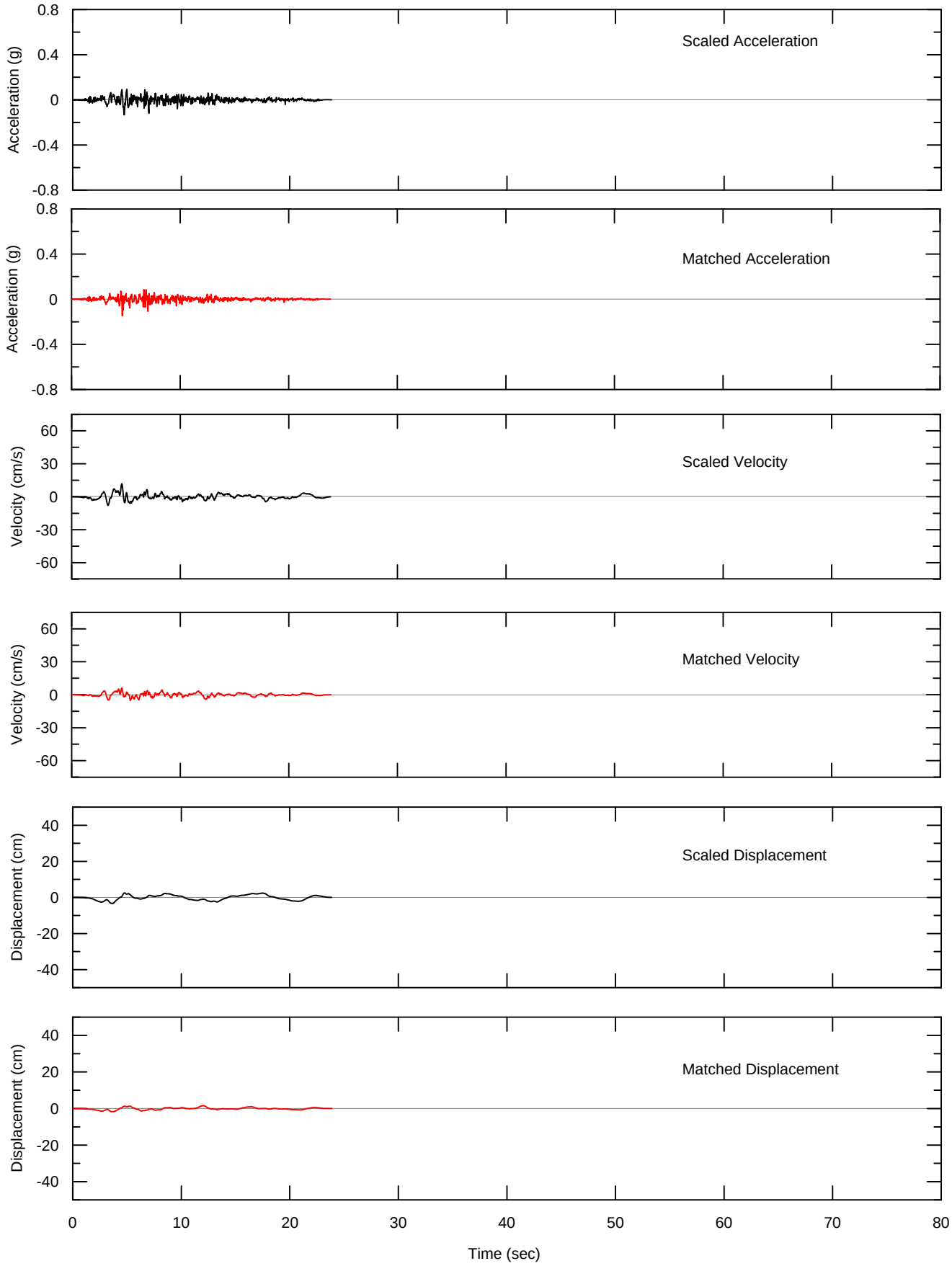

1978, Tabas - Iran, Dayhook, FP Matched to 100-Year RP Target Spectrum Qaraoun Dam Hazard Study, Lebanon	By: DG / Date: 9/9/2011 AMEC Geomatrix	Project No. OD11161570 Figure **B-2c**

I:\Project\16000\OD11161570 - Qaraoun Dam\12000 CALCS EVALS ANALYSIS\Figures\memo_figures\TH plots

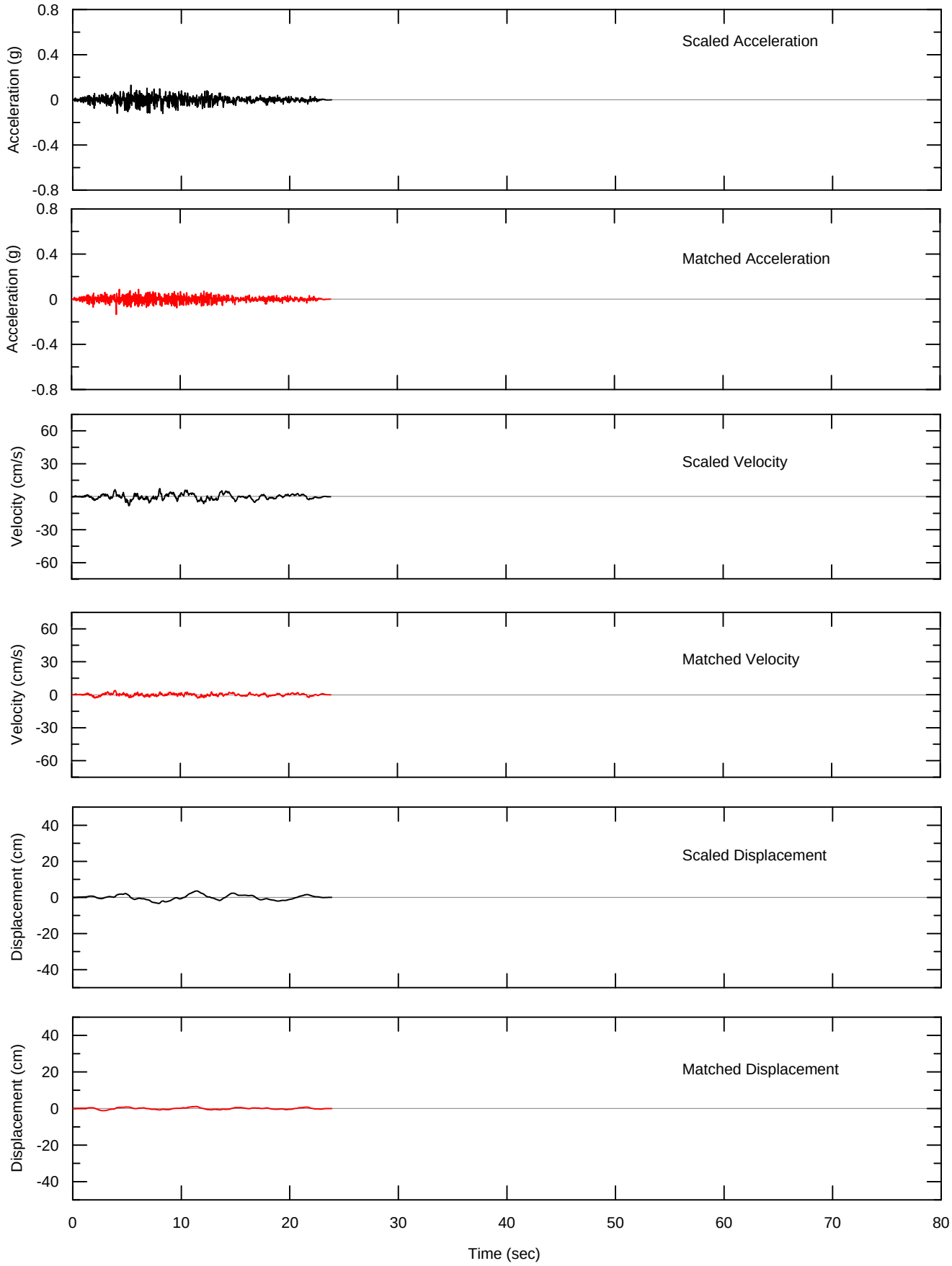

1978, Tabas - Iran, Dayhook, V Matched to 100-Year RP Target Spectrum Qaraoun Dam Hazard Study, Lebanon	By: DG	Date: 9/9/2011	Project No. OD11161570
	AMEC Geomatrix		Figure **B-2d**

I:\Project\16000\OD11161570 - Qaraoun Dam\12000 CALCS EVALS ANALYSIS\Figures\memo_figures\TH plots

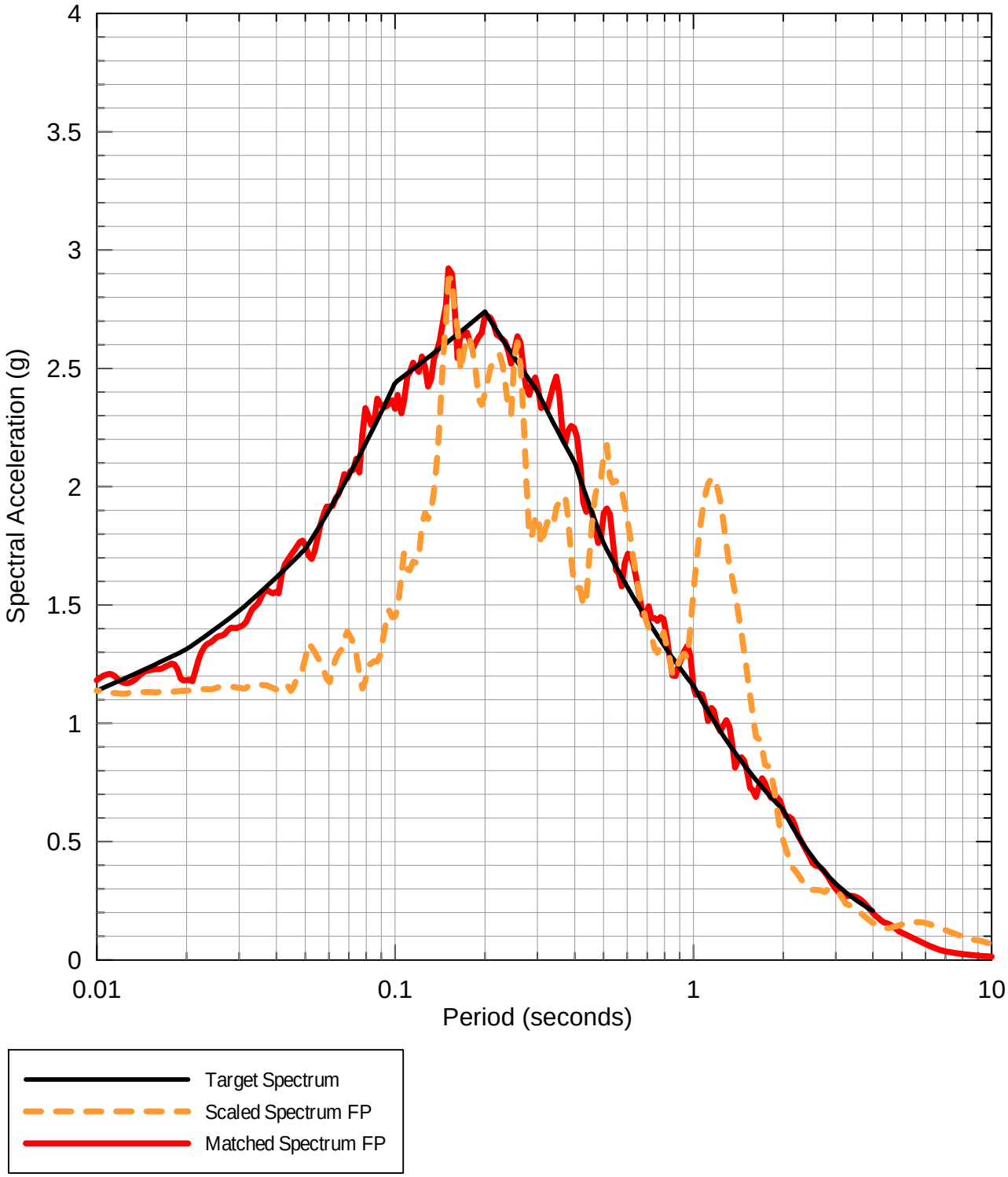

Horizontal Response Spectra
1999, Hector Mine, Hector
Matched to 10,000-Year RP Target Spectrum
Qaraoun Dam Hazard Study
Litani River Basin, Lebanon

By: DG	Date: 9/9/2011	Project No. OD11161570
AMEC Geomatrix		Figure **B-3a**

I:\Project\16000\OD11161570 - Qaraoun Dam\12000 CALCS EVALS ANALYSIS\Figures\memo_figures\TH plots

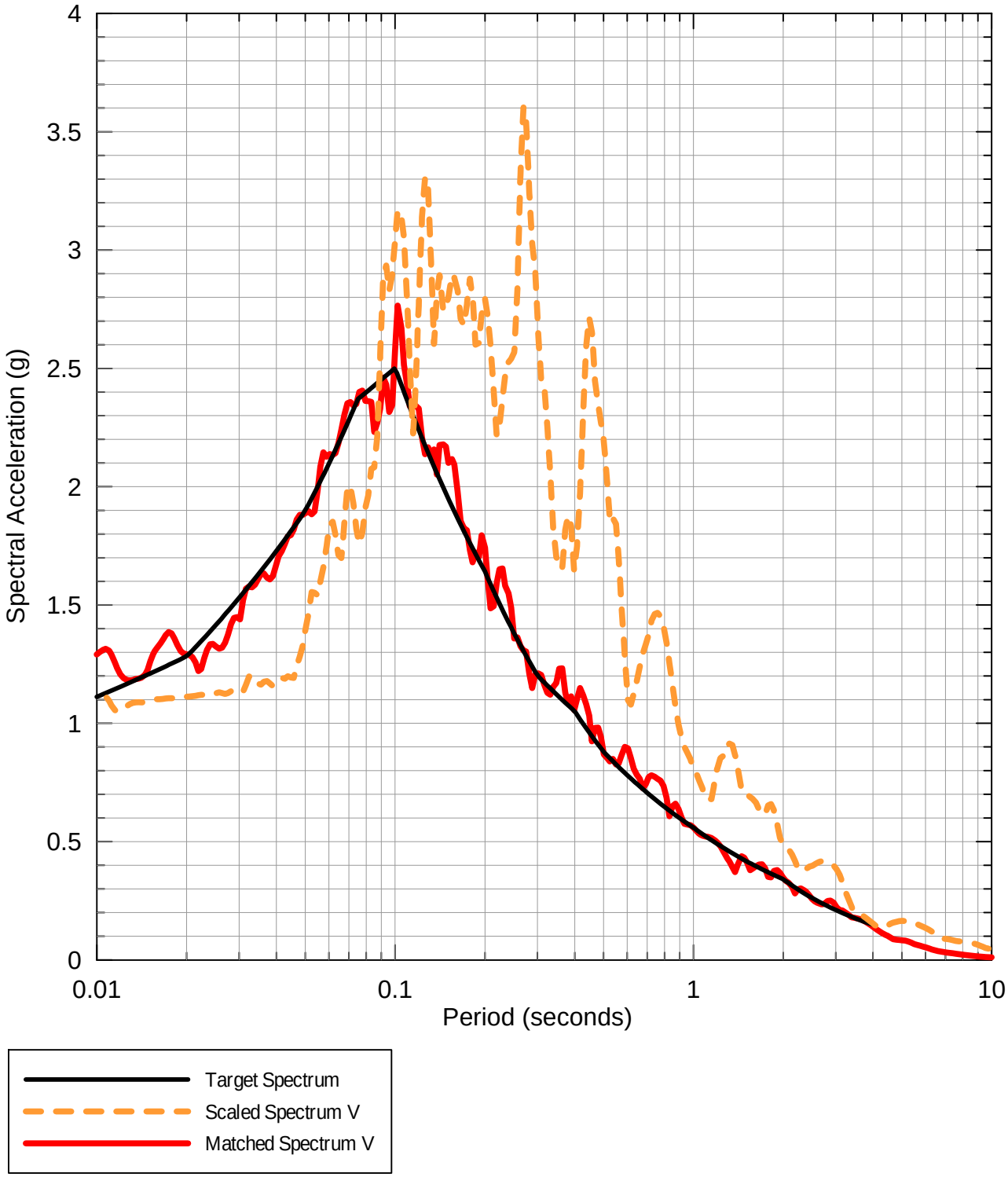

Vertical Response Spectra
1999, Hector Mine, Hector
Matched to 10,000-Year RP Target Spectrum
Qaraoun Dam Hazard Study
Litani River Basin, Lebanon

By: DG	Date: 9/9/2011	Project No. OD11161570
AMEC Geomatrix		Figure **B-3b**

I:\Project\16000\OD11161570 - Qaraoun Dam\12000 CALCS EVALS ANALYSIS\Figures\memo_figures\TH plots

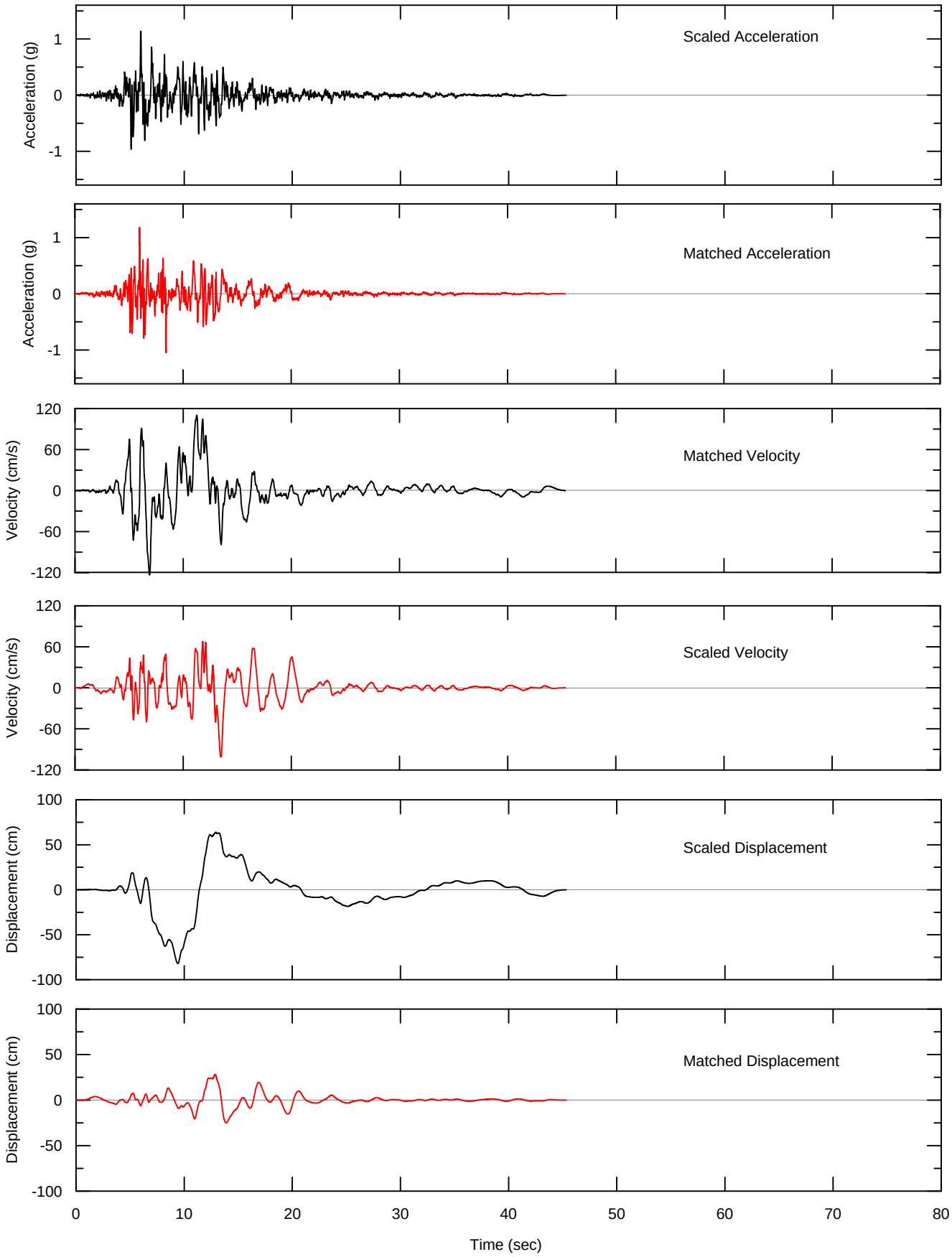

1999, Hector Mine, Hector, FP
Matched to 10,000-Year RP Target Spectrum
Qaraoun Dam Hazard Study, Lebanon

By: DG | Date: 9/9/2011 | Project No. OD11161570

AMEC Geomatrix

Figure **B-3c**

I:\Project\16000\OD11161570 - Qaraoun Dam\12000 CALCS EVALS ANALYSIS\Figures\memo_figures\TH plots

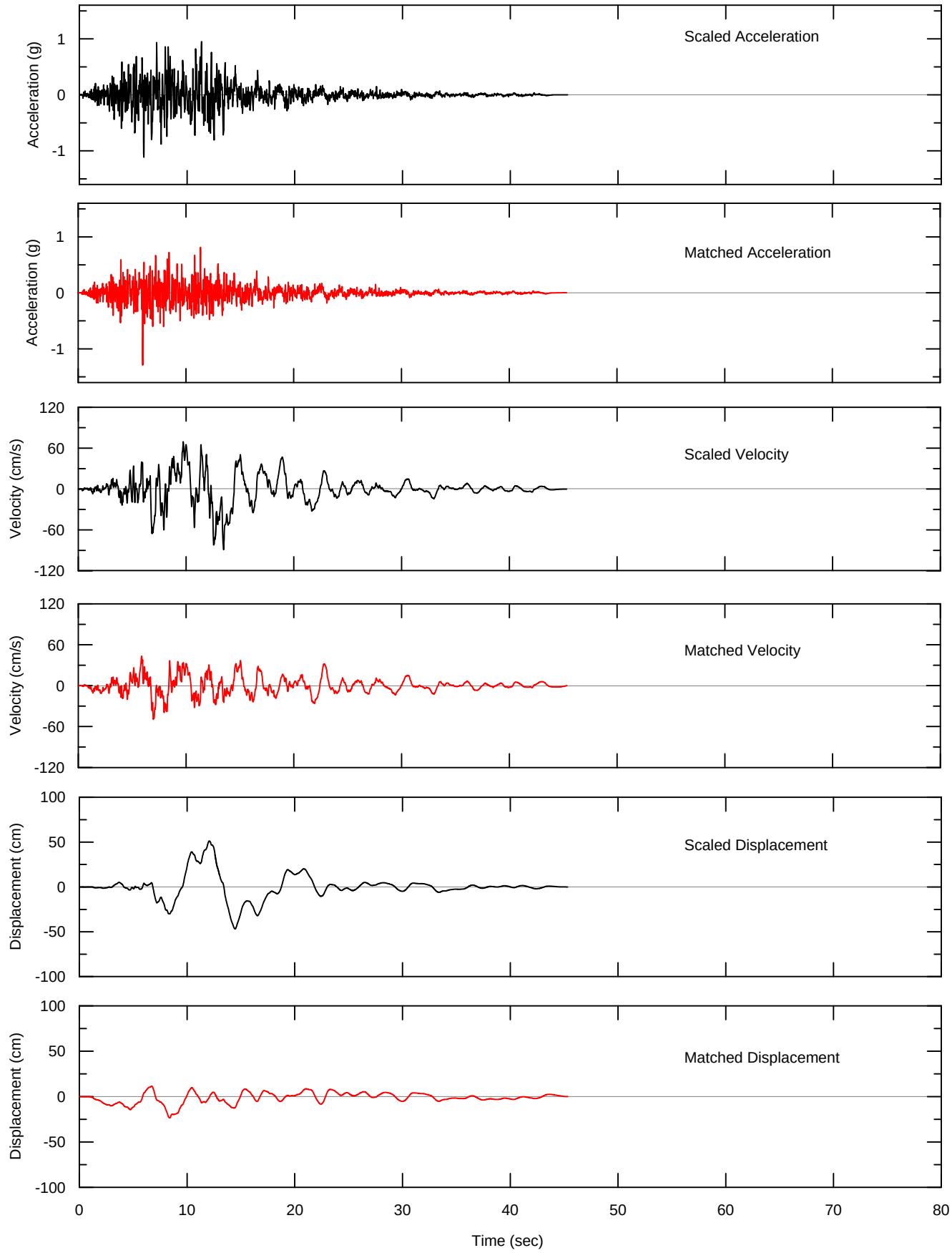

1999, Hector Mine, Hector, V Matched to 10,000-Year RP Target Spectrum Qaraoun Dam Hazard Study, Lebanon	By: DG	Date: 9/9/2011	Project No. OD11161570
	AMEC Geomatrix		Figure **B-3d**

I:\Project\16000\OD11161570 - Qaraoun Dam\12000 CALCS EVALS ANALYSIS\Figures\memo_figures\TH plots

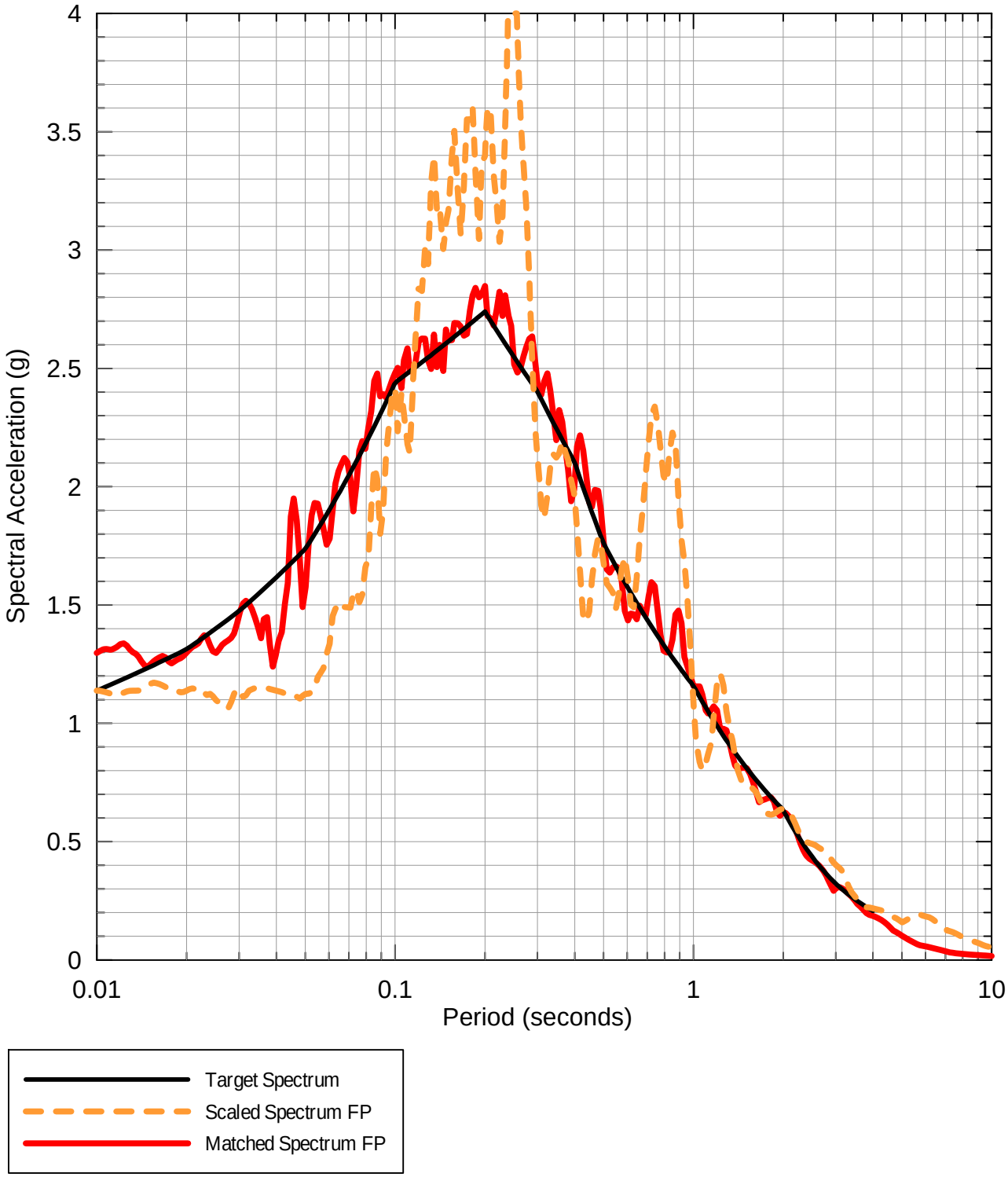

Horizontal Response Spectra
1978, Tabas - Iran, Tabas
Matched to 10,000-Year RP Target Spectrum
Qaraoun Dam Hazard Study
Litani River Basin, Lebanon

By: DG	Date: 9/9/2011	Project No. OD11161570
AMEC Geomatrix		Figure **B-4a**

I:\Project\16000\OD11161570 - Qaraoun Dam\12000 CALCS EVALS ANALYSIS\Figures\memo_figures\TH plots

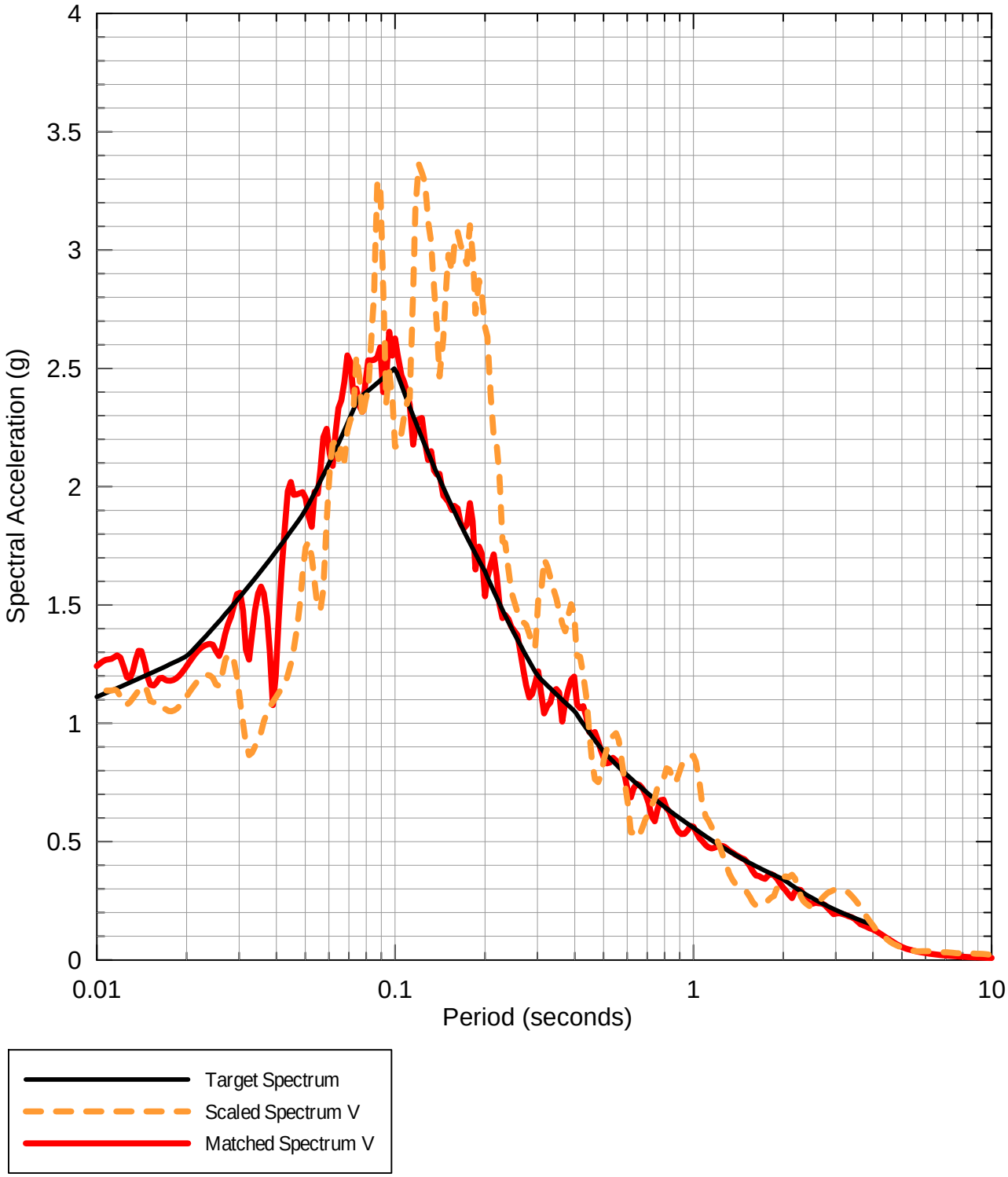

Vertical Response Spectra
1978, Tabas - Iran, Tabas
Matched to 10,000-Year RP Target Spectrum
Qaraoun Dam Hazard Study
Litani River Basin, Lebanon

By: DG	Date: 9/9/2011	Project No. OD11161570
AMEC Geomatrix		Figure **B-4b**

I:\Project\16000\OD11161570 - Qaraoun Dam\12000 CALCS EVALS ANALYSIS\Figures\memo_figures\TH plots

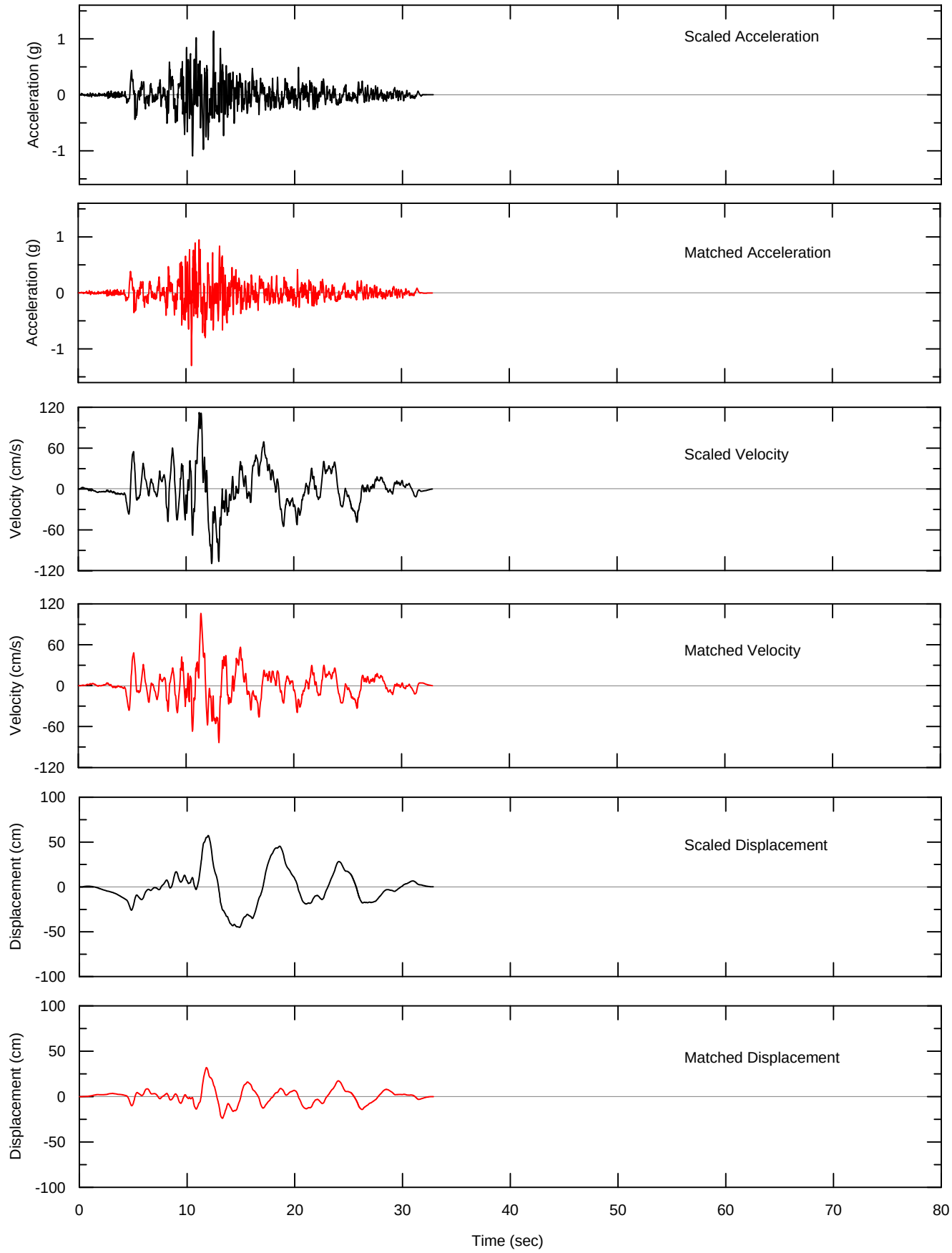

1978, Tabas - Iran, Tabas, FP Matched to 10,000-Year RP Target Spectrum Qaraoun Dam Hazard Study, Lebanon	By: DG	Date: 9/9/2011	Project No. OD11161570
	AMEC Geomatrix		Figure **B-4c**

I:\Project\16000\OD11161570 - Qaraoun Dam\12000 CALCS EVALS ANALYSIS\Figures\memo_figures\TH plots

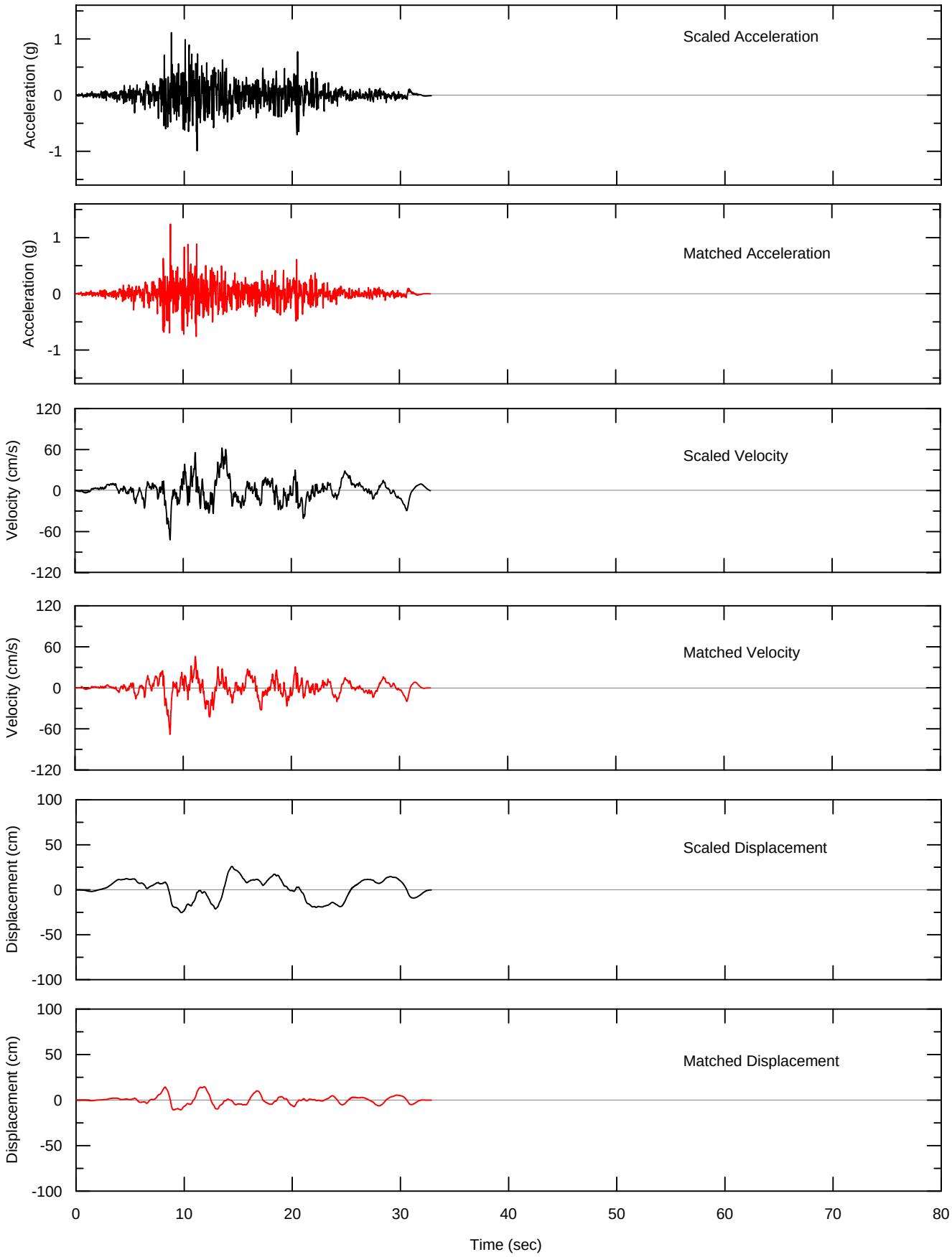

1978, Tabas - Iran, Tabas, V
Matched to 10,000-Year RP Target Spectrum
Qaraoun Dam Hazard Study, Lebanon

By: DG | Date: 9/9/2011 | Project No. OD11161570

AMEC Geomatrix

Figure **B-4d**

I:\Project\16000\OD11161570 - Qaraoun Dam\12000 CALCS EVALS ANALYSIS\Figures\memo_figures\TH plots

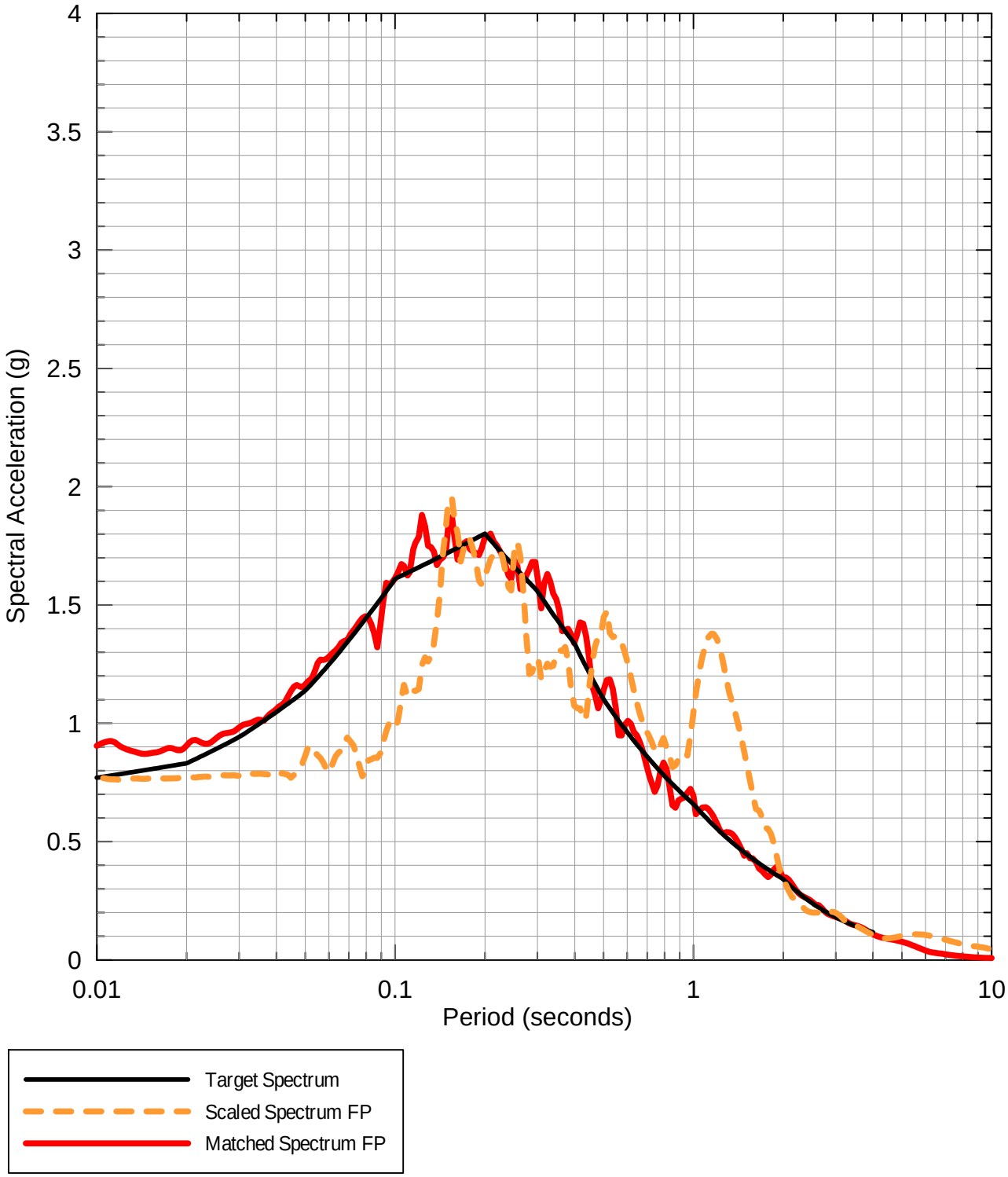

Horizontal Response Spectra
1999, Hector Mine, Hector
Matched to 2,475-Year RP Target Spectrum
Qaraoun Dam Hazard Study
Litani River Basin, Lebanon

By: DG	Date: 1/18/2012	Project No. OD11161570
AMEC Geomatrix		Figure **B-5a**

I:\Project\16000\OD11161570 - Qaraoun Dam\12000 CALCS EVALS ANALYSIS\Figures\memo_figures\TH plots

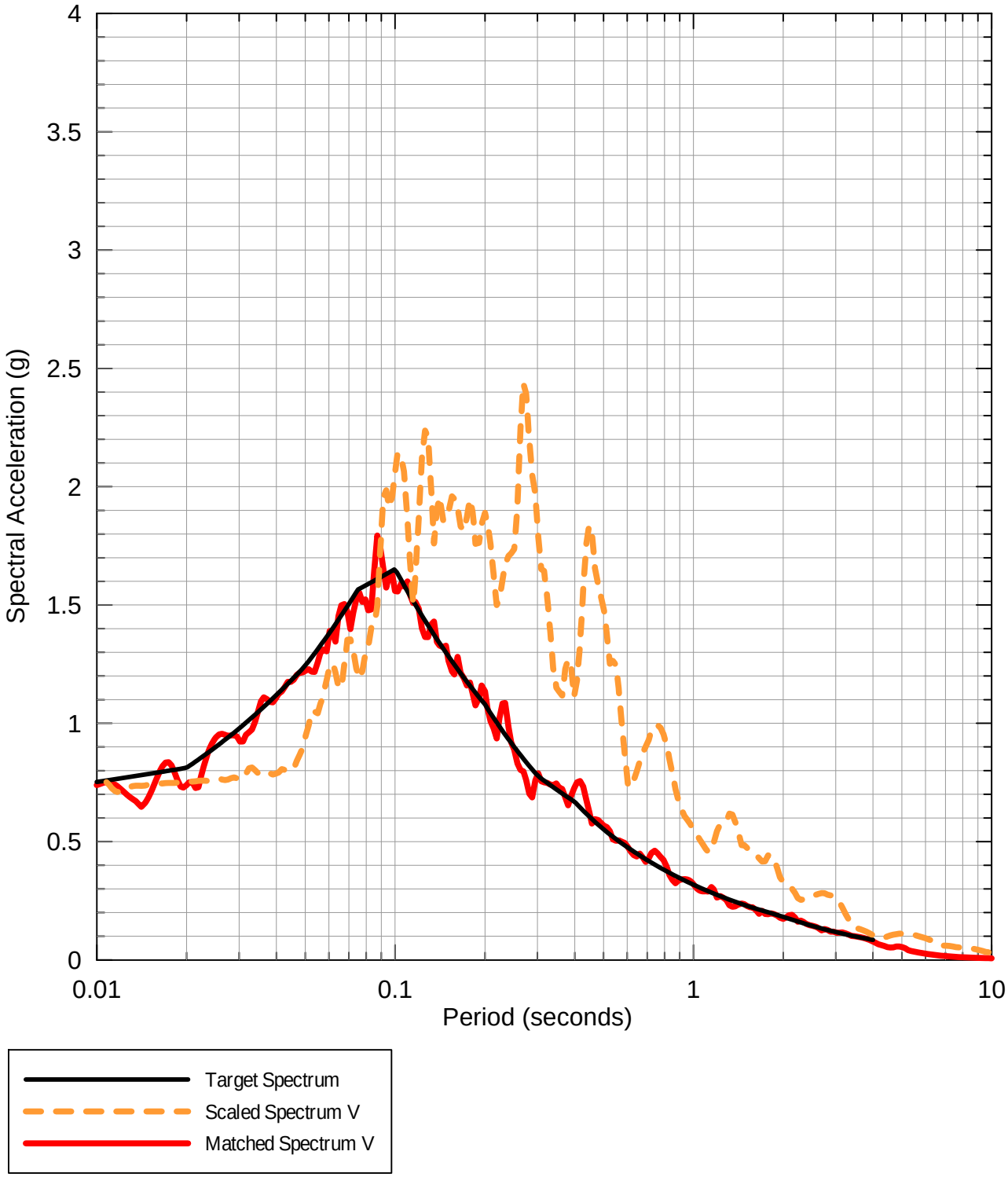

Vertical Response Spectra
1999, Hector Mine, Hector
Matched to 2,475-Year RP Target Spectrum
Qaraoun Dam Hazard Study
Litani River Basin, Lebanon

By: DG	Date: 1/18/2012	Project No. OD11161570
AMEC Geomatrix		Figure **B-5b**

I:\Project\16000\OD11161570 - Qaraoun Dam\12000 CALCS EVALS ANALYSIS\Figures\memo_figures\TH plots

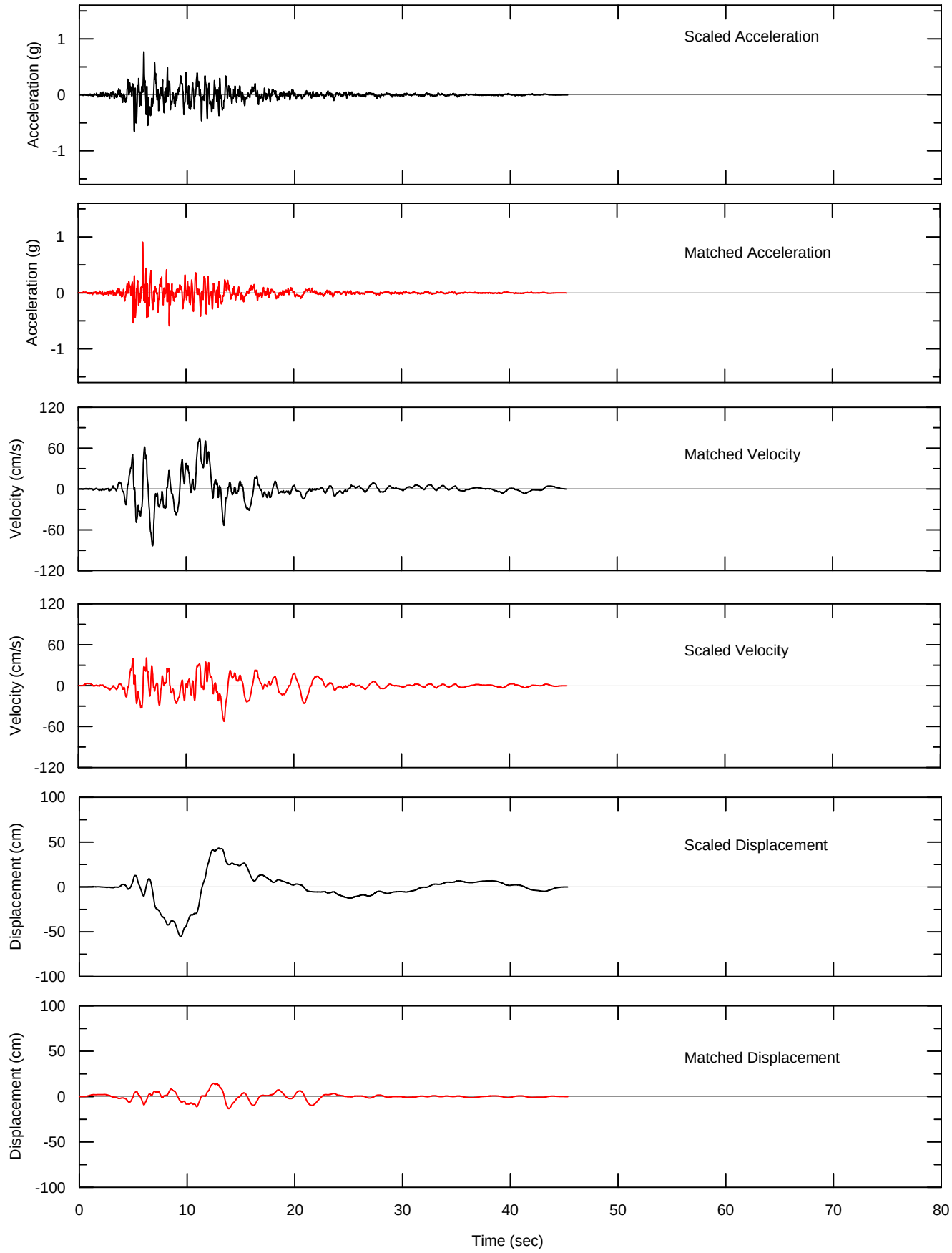

1999, Hector Mine, Hector, FP
Matched to 2,475-Year RP Target Spectrum
Qaraoun Dam Hazard Study, Lebanon

By: DG | Date: 1/18/2012 | Project No. OD11161570

AMEC Geomatrix

Figure **B-5c**

I:\Project\16000\OD11161570 - Qaraoun Dam\12000 CALCS EVALS ANALYSIS\Figures\memo_figures\TH plots

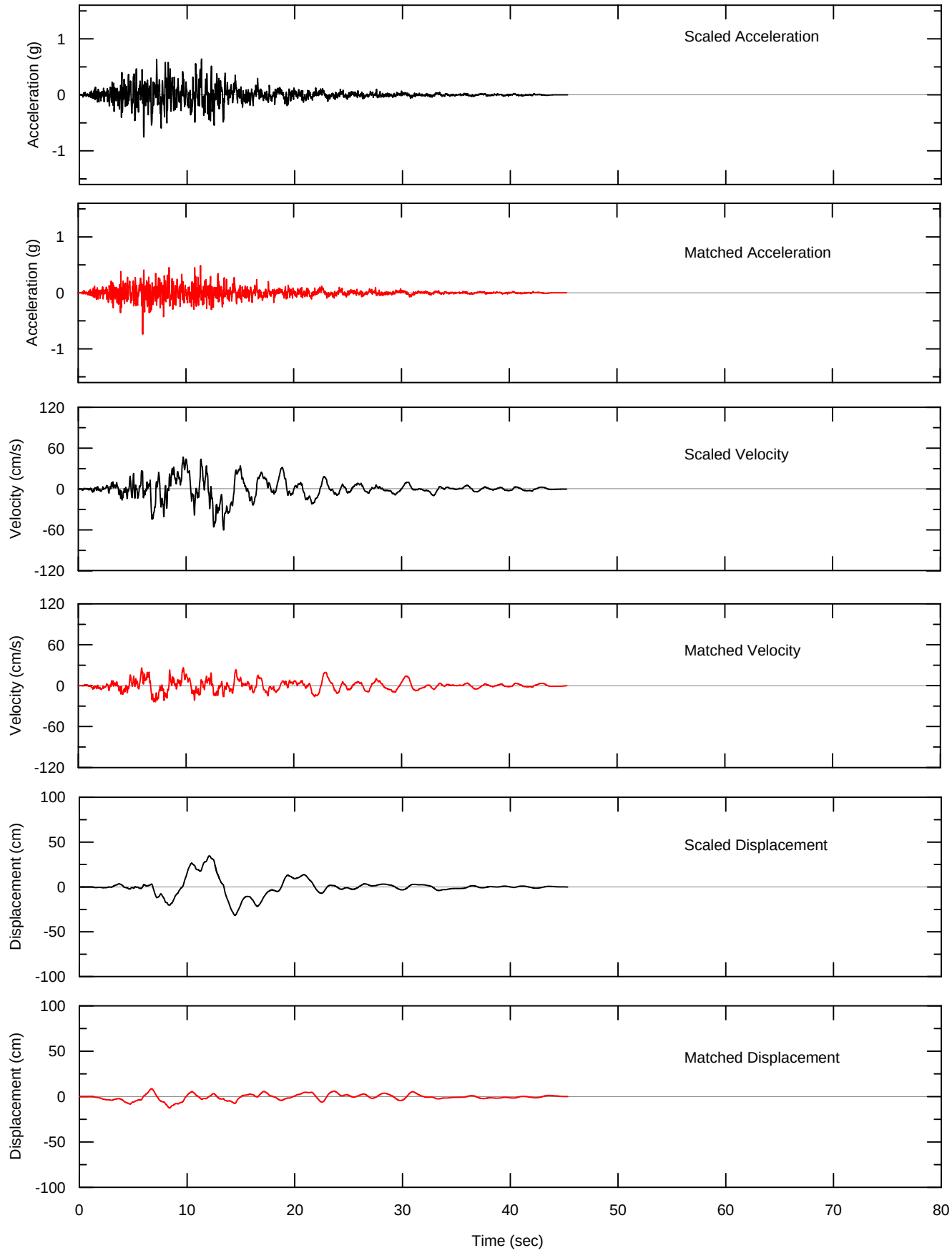

1999, Hector Mine, Hector, V
Matched to 2,475-Year RP Target Spectrum
Qaraoun Dam Hazard Study, Lebanon

By: DG | Date: 1/18/2012 | Project No. OD11161570

AMEC Geomatrix

Figure **B-5d**

I:\Project\16000\OD11161570 - Qaraoun Dam\12000 CALCS EVALS ANALYSIS\Figures\memo_figures\TH plots

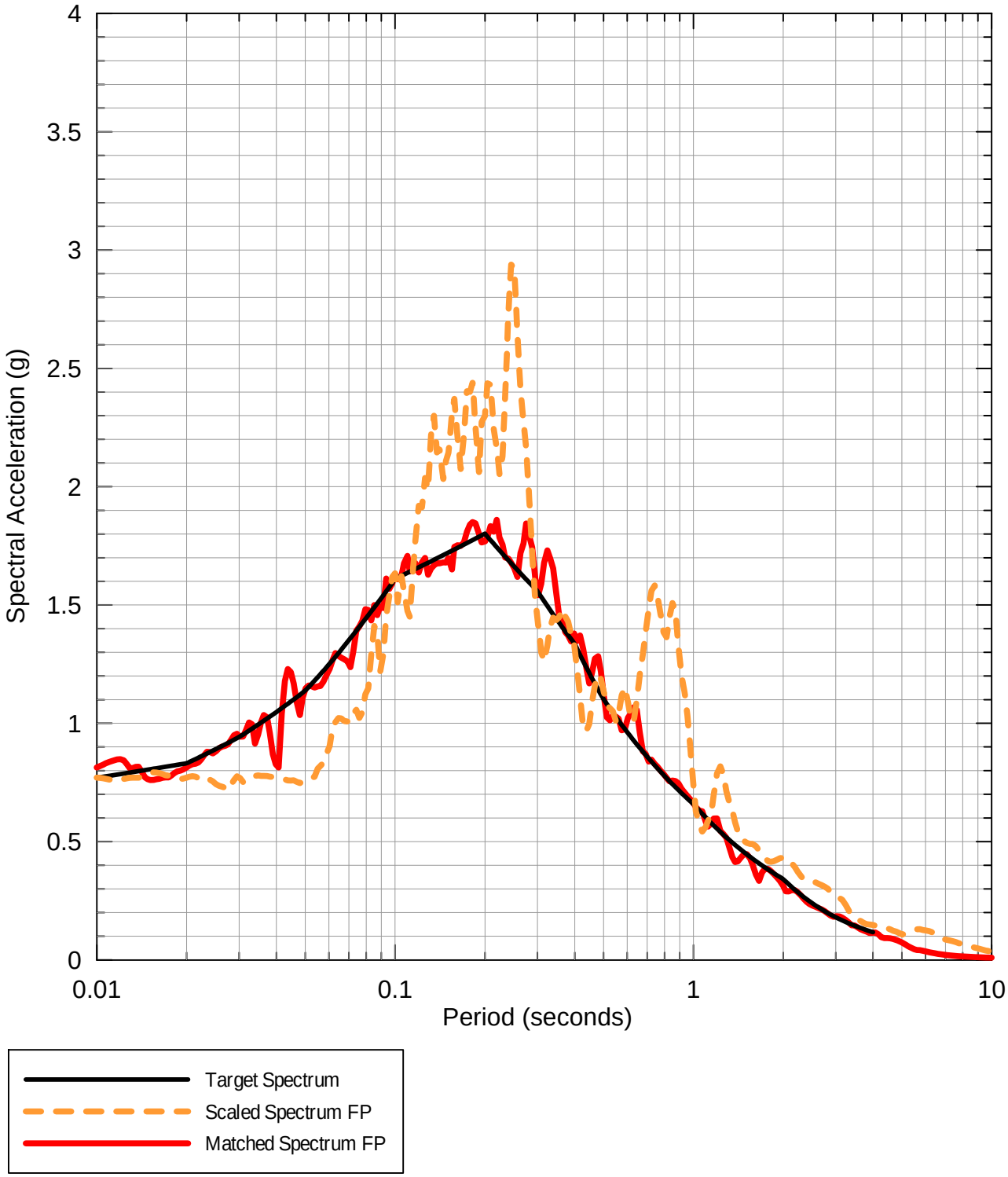

Horizontal Response Spectra
1978, Tabas - Iran, Tabas
Matched to 2,475-Year RP Target Spectrum
Qaraoun Dam Hazard Study
Litani River Basin, Lebanon

By: DG	Date: 1/18/2012	Project No. OD11161570
AMEC Geomatrix		Figure **B-6a**

I:\Project\16000\OD11161570 - Qaraoun Dam\12000 CALCS EVALS ANALYSIS\Figures\memo_figures\TH plots

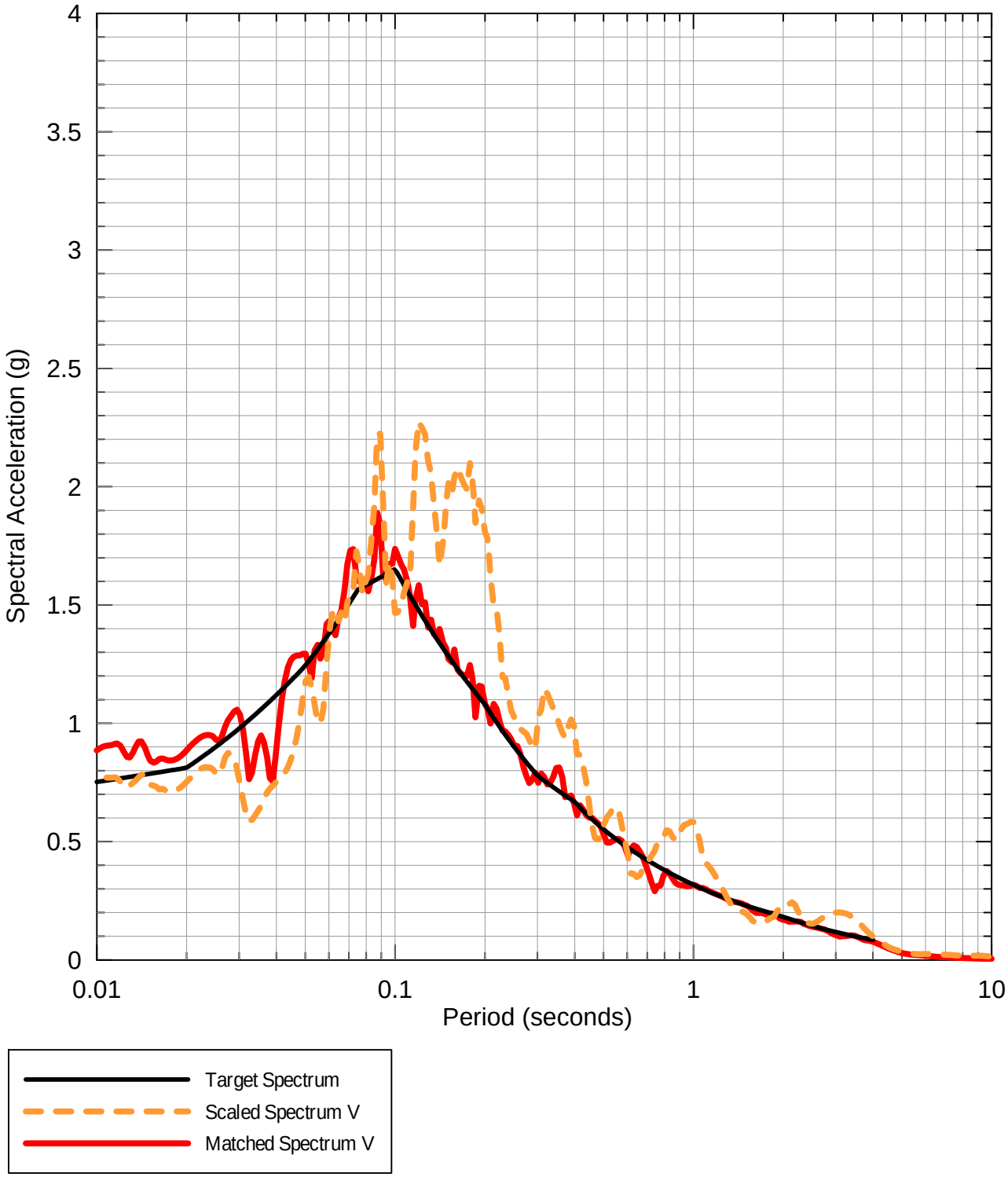

Vertical Response Spectra
1978, Tabas - Iran, Tabas
Matched to 2,475-Year RP Target Spectrum
Qaraoun Dam Hazard Study
Litani River Basin, Lebanon

By: DG	Date: 1/18/2012	Project No. OD11161570
AMEC Geomatrix		Figure **B-6b**

I:\Project\16000\OD11161570 - Qaraoun Dam\12000 CALCS EVALS ANALYSIS\Figures\memo_figures\TH plots

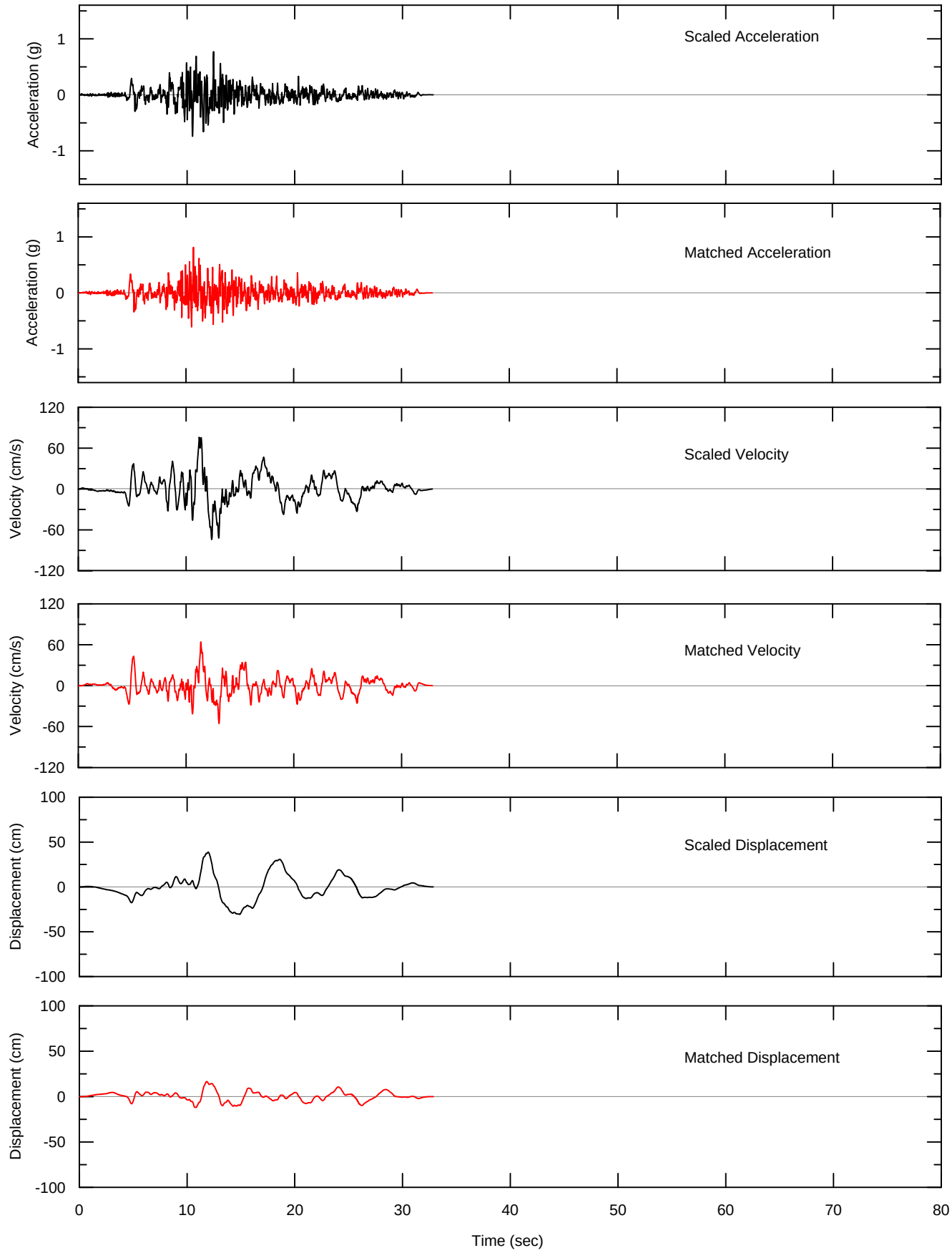

1978, Tabas - Iran, Tabas, FP
Matched to 2,475-Year RP Target Spectrum
Qaraoun Dam Hazard Study, Lebanon

By: DG | Date: 1/18/2012 | Project No. OD11161570

AMEC Geomatrix

Figure **B-6c**

I:\Project\16000\OD11161570 - Qaraoun Dam\12000 CALCS EVALS ANALYSIS\Figures\memo_figures\TH plots

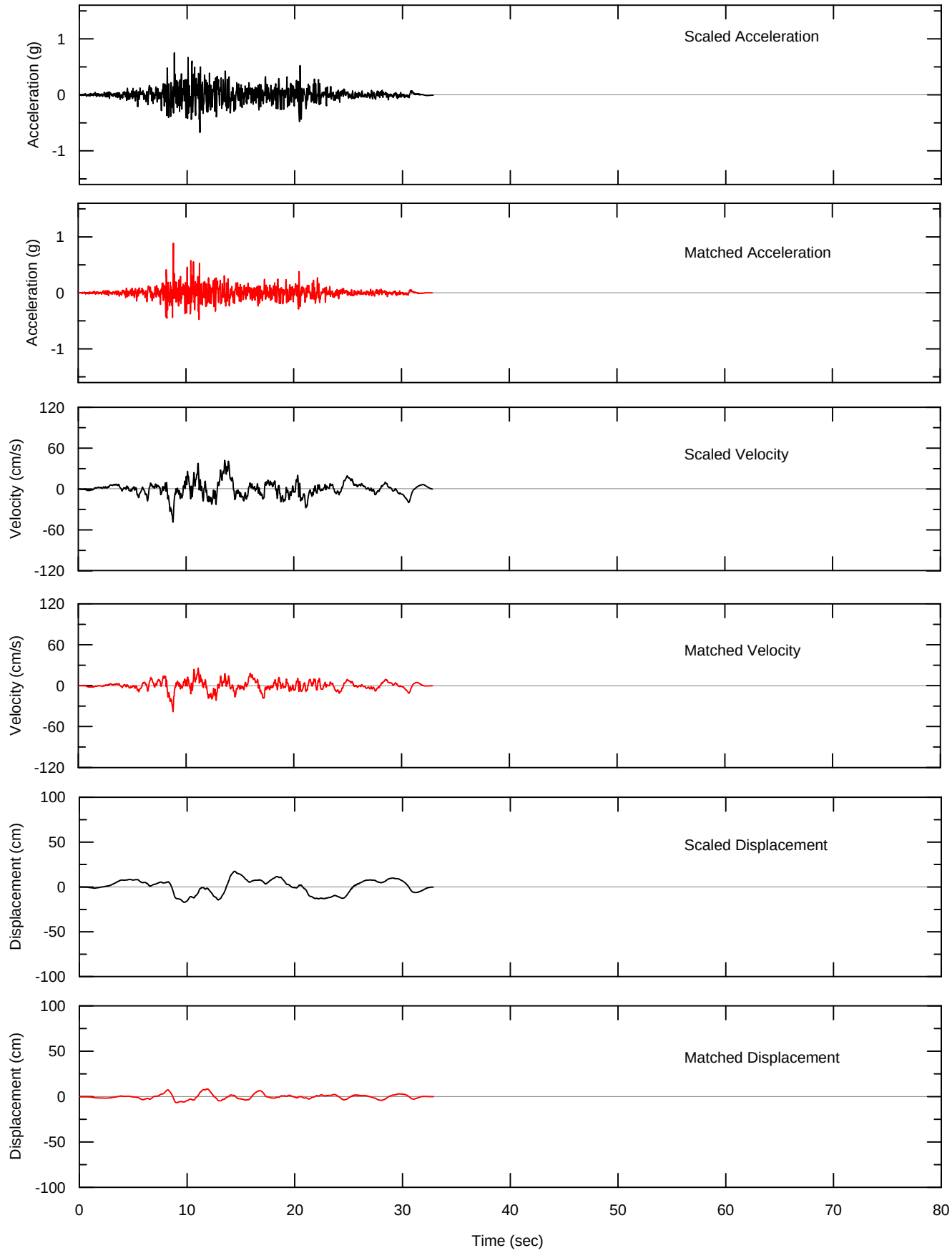

1978, Tabas - Iran, Tabas, V
Matched to 2,475-Year RP Target Spectrum
Qaraoun Dam Hazard Study, Lebanon

By: DG | Date: 1/18/2012 | Project No. OD11161570

AMEC Geomatrix

Figure **B-6d**

I:\Project\16000\OD11161570 - Qaraoun Dam\12000 CALCS EVALS ANALYSIS\Figures\memo_figures\TH plots

APPENDIX C

Electronic Files of Acceleration Time Histories [CD-ROM]

U.S. Agency for International Development
1300 Pennsylvania Avenue, NW
Washington, DC 20523
Tel: (202) 712-0000
Fax: (202) 216-3524
www.usaid.gov